NOBLE GASES DISSOLVED IN GROUNDWATERS OF THE MICHIGAN BASIN: IMPLICATIONS FOR PALEOCLIMATOLOGY, HYDROGEOLOGY, TECTONICS AND MANTLE GEOCHEMISTRY

by

Lin Ma

A dissertation submitted in partial fulfillment
of the requirements for the degree of
Doctor of Philosophy
(Geology)
in The University of Michigan
2009

Doctoral Committee:

Associate Professor Maria Clara Cruz Da Silva Castro, Chair
Professor Kyger C Lohmann
Associate Professor Avery H. Demond
Associate Research Scientist Chris M. Hall
Associate Professor Daniele L. Pinti, Université du Québec à Montréal

---

To
Lixin and our families

ACKNOWLEDGEMENTS

First of all, I am very grateful to my advisor Dr. Clara Castro, who opened the door to the noble gas geochemistry for me and guided my Ph D study with continuous support, encouragements and patience. Clara is a great mentor and is always there to help me to prepare for my future academic career. I have great respect and admiration for her enthusiasm in science, critical thinking and hard work.

My other dissertation committee members: Drs. Chris Hall, Kyger C (Kacey) Lohmann, Avery Demond, and Daniele Pinti also provided insightful comments and suggestions to this dissertation, and I benefit so much from their expertise.

I am indebted to Chris, who not only passed along knowledge in the noble gas lab, but also shared his thoughtful advice along my study. I enjoyed our discussions on many interesting topics. Special thanks go to Kacey for his advice on stable isotopes and thermal history of the Michigan Basin.

I would like to thank Dr. Avery Demond, my cognate member. I benefited tremendously from her classes in groundwater and soils, and also from her perspectives from the outside of geology. I also want to thank her for many detailed edits on this dissertation. Finally, Dr. Daniele Pinti has shared his scientific thoughts from Montreal and I also thank Daniele for his generosity with his time, arranging international trips to attend my committee meetings and defense.

I would like to thank the past and current members in our noble gas research group: Delphine Patriarche, Martin Saar, Tie Sun, Jess Malone, Brian Ellis, and Kathy Flemming. This dissertation benefited from them in many ways.

As an international student, I am grateful to the help and friendship from the faulty, staff and students in the Department of Geological Sciences. I would also like to acknowledge my friends who made my time in Ann Arbor much more enjoyable: Huaiwei Ni, Ya Gao, Wenjun Yong, Ying Zhao, Hejiu Hui, Xiaoqing Song, Yang Chen, Jing Zhou, Yuehan Lu, and many others. They are an invaluable part of my life during my tenure as a graduate student, and we have so much fun together.

Special thanks go to my wife, Lixin, and our parents for their love and support.

TABLE OF CONTENTS

LIST OF TABLES

LIST OF FIGURES

Chapter 2

Chapter 3

ABSTRACT

This dissertation uses noble gases dissolved in groundwaters of the Michigan Basin as natural tracers of crustal fluids. Noble gases are used to reconstruct paleoclimate, to study cross-formation flow, to trace the origin and evolution of deep brines, to investigate the thermal and tectonic history of this region, and to place constraints on the underlying mantle structure and convection models.

Dissolved noble gases from the shallow Marshall aquifer reveal a paleo-temperature record since the end of last glacial maximum (LGM) for southern Michigan, which suggests that groundwater recharge occurred under the Laurentide Ice Sheet. This record also identifies major global climatic oscillations such as the Bølling-Allerød warm phases in this region and suggests that an atmospheric circulation pattern distinct from today prevailed in the late Pleistocene.

Analyses of He isotopes from the Marshall aquifer show unusually high He excesses for such shallow depths and yield estimated He fluxes far greater than those reported in other sedimentary basins, suggesting the presence of a dominant vertical water flow component at greater depths. Of particular relevance is the contrast observed between high helium and low heat fluxes in this shallow aquifer leading to helium/heat flux ratios greater than the expected radiogenic production ratio in certain areas, which points to the occurrence of a major past thermal event in the basin. Subsequent analyses

of all noble gases (He, Ne, Ar, Kr, Xe) in deep Michigan Basin brines from eight different formations all confirmed the presence of a past thermal event with a mantle origin, most likely related to a recent reactivation of the Mid Continent Rift (MCR) underneath the basin. More specifically, the atmospheric component shows a strong depletion pattern resulting from subsurface boiling and steam separation. This pattern is consistent with the presence of past high temperatures in the basin. The crustal component further supports the occurrence of the upward transport of noble gases released from the Precambrian basement beneath the basin. More importantly, the mantle component clearly reveals a primordial solar-like component in this stable continental region, where the presence of mantle plumes is highly unlikely. This suggests that a deep primordial mantle reservoir is not required to explain the presence of such components. Such a finding provides new insights into the current debate of mantle structure and convection models.

CHAPTER 1

INTRODUCTION

In this introductory chapter, the first section is intended to provide a brief overview of the use of noble gases (atmospheric, crustal and mantle components) as natural tracers in subsurface fluids in a diversity of geological settings. The next section introduces the noble gas study in the Michigan Basin and illustrates the goals and scopes of the present work. A detailed structure of this dissertation is provided in the last section.

1.1. Noble gases as natural tracers in crustal fluids

Because of their stable orbital configuration with the outer shell filled with electrons, noble gases are chemically inert and stable, and thus only sensitive to physical processes [e.g., *Ozima and Podesek,* 2002]. Moreover, noble gases in subsurface fluids are derived from the atmosphere, crust and mantle, all of which show distinct isotopic and elemental signatures [*Ozima and Podesek,* 2002; *Porcelli et al.,* 2002]. This fact makes noble gases ideal natural tracers for studying the origin and evolution of crustal fluids in sedimentary basins [e.g., *Oxburgh et al.,* 1986; *Hiyagon and Kennedy,* 1992; *Pinti and Marty*, 1995; *Castro et al., 1998a,b*], and, in addition, for reconstructing past climate records archived in groundwater flow systems [e.g., *Kipfer et al.*, 2002; *Castro and Goblet*, 2003a]. Combined with other natural tracers, particularly heat flow, the study of noble gases in crustal fluids reveals new insights into the tectonic and thermal history

of continental regions, as well as the structure and convection models for the underlying mantle [*Castro et al.*, 2005].

Atmospheric noble gases are introduced into the subsurface by recharge water in solubility equilibrium with the atmosphere (Air Saturated Water - ASW). Because their solubility in water is primarily dependent on the ambient temperature at the time recharge took place, atmospheric noble gas concentrations in groundwater of known ages can be used to reconstruct the paleo-temperatures in the late Pleistocene and Holocene [e.g., *Kipfer et al.*, 2002; *Castro and Goblet*, 2003a]. Unlike many other continental climate proxies, noble gas temperatures (NGTs) are a direct measure of the ambient temperature at the water table in the recharge area. While the concentrations of atmospheric noble gases in groundwater are expected to reflect those of ASW at the time of recharge, depletion of this component, when observed in sedimentary systems, commonly suggests a loss to an oil or natural gas phase in the subsurface, which is originally free of atmospheric noble gases [*Zartman et al.*, 1961; *Bosch and Mazor*, 1988; *Zaikowski and Spangler*, 1990]. This concept has been traditionally used to identify and quantify subsurface oil, gas, and water phase interactions [*Zartman et al.*, 1961; *Bosch and Mazor*, 1988; *Zaikowski and Spangler*, 1990; *Ballentine et al.*, 1991; *Pinti and Marty*, 1995]. Alternatively, depletion of atmospheric noble gases due to subsurface boiling and steam phase separation has also been previously recorded in tectonically active areas (hydrothermal systems) [*Mazor and Truesdell*, 1984; *Kennedy*, 1988; *Winkler et al.*, 2000]. Such noble gas depletion occurs in the residual water phase as pressure decreases during hot fluid ascent, leading to a separate noble gas enriched steam (water vapor)

phase. Depletion of atmospheric noble gases in a particular region due to boiling and steam separation is thus indicative of the occurrence of a thermal event.

By contrast, concentrations of certain noble gases (e.g., ^{4}He, ^{21}Ne, ^{40}Ar) in deep groundwater frequently exceed those expected for ASW. These excesses result mainly from crustal production of noble gases, such as ^{4}He and ^{40}Ar from radioactive decay of U/Th and ^{40}K, respectively; ^{21}Ne from secondary α or n-reactions; and $^{131, 132, 134, 136}$Xe isotopes from spontaneous fission of U [e.g., *Wetherill ,* 1953, 1954; *Ballentine and Burnard,* 2002]. Crustal noble gases may be produced inside the aquifer (in-situ production) or in deeper layers (external production), and then subsequently transported to shallower levels by advection, dispersion and/or diffusion [e.g., *Castro et al.*, 1998a, b; *Castro and Goblet*, 2003b]. Although chemically inert and stable, noble gases display contrasting physical properties due to their large differences in atomic numbers. Noble gases are thus very sensitive to physical processes during subsurface transport and consequently, their concentrations and elemental ratios have been widely used as geochemical tracers of subsurface fluid movement in major sedimentary systems around the world [e.g., *Torgersen and Clarke,* 1985; *Torgersen et al.,* 1989; *Ballentine et al.*, 1991; *Pinti and Marty*, 1995; *Castro et al.*, 1998a, b; *Castro et al.*, 2005]. Furthermore, when combined with heat flow which is also produced by the radioactive decay, the study of ^{4}He in crustal fluids allows for the reconstruction of the thermal and tectonic history of continental regions [*Castro et al.*, 2005]. More specifically, *Castro et al.* [2005] have shown that the occurrence of a ^{4}He/heat flux ratio greater than the expected radiogenic production ratio can only result from a past thermal event in which most of the heat has already escaped while He is slowly making its way toward the surface. This highlights

the use of ^{4}He/heat flux ratios as a novel tracer to identify past thermal events in currently stable regions.

The Earth's mantle presents another very important noble gas reservoir. It is believed that mantle contains primordial noble gases which were trapped during the early accretion of the Earth [e.g., *Ozima and Podesek,* 2002]. Mantle noble gases which are characterized by their specific isotopic signatures (e.g., ^{3}He/^{4}He ratios) have been commonly observed in sedimentary basins both in tectonically active regions [e.g., *Oxburgh et al.*, 1986; *O'Nions and Ballentine,* 1993], and stable areas with no recent substantial magmatism and tectonism [e.g., *Hiyagon and Kennedy,* 1992; *Kennedy et al.*, 2007]. The latter regime has led to the interpretation that mantle volatiles can be released from a past mantle thermal event via deep-seated faults and fractures and subsequently trapped in shallow crust for substantial geological periods. Importantly, noble gases in mantle-derived samples have been widely used to place constraints on the structure and convection models of the inaccessible mantle [e.g., *Porcelli and Ballentine*, 2002]. For example, the presence of a primordial He and Ne signature in oceanic island basalts (OIBs) as well as the presence of a mantle He/heat flux ratio lower than the radiogenic production ratio near mid-ocean ridges have historically been used to support a two-layered mantle convection model [*O'Nions and Oxburgh*, 1983; *Porcelli and Wasserburg*, 1995; *Moreira and Allegre*, 1998]. This model comprises a lower, primordial, largely undegassed reservoir from which OIBs originate via deep mantle plumes, and a degassed upper mantle of which mid-ocean ridge basalts (MORBs) is representative. Primordial He and Ne signatures, which are commonly thought to be solar-like and representative of the Earth's early formation stages [e.g., *Honda et al.*, 1991] have thus been systematically

associated with the occurrence of mantle plumes, and the existence of a lower, largely undegassed, mantle reservoir [*Porcelli and Wasserburg*, 1995; *Moreira and Allegre*, 1998]. By contrast, low He/heat flux ratios have commonly been regarded as reflecting a He deficit in the original upper MORB degassed mantle reservoir [*O'Nions and Oxburgh*, 1983]. However, this view was recently challenged and the argument based on He and heat transport was invalidated [*Castro et al.*, 2005]. Hence, alternative mantle structures and convection models are possible for which the presence of two distinct mantle reservoirs is not required [see, *Anderson*, 1998; *Albarede*, 2005].

1.2. A noble gas study in the Michigan Basin: from shallow fresh groundwater to deep basin brines

Located within the interior of the North American craton, the Michigan Basin experienced repeated continental glaciations during the past 2 million years, with the last glacial maximum (LGM) occurring at about 21000 years ago [*Dorr and Eschamn*, 1970; *Dyke et al.*, 2002]. Advance and retreat of continental ice sheets have the potential to profoundly change local climate and alter regional-scale groundwater flow [e.g., *Alley and Clark*, 1999; *Person et al.*, 2007]. Although it is still not fully understood, the impact of glaciations on groundwater recharge and flow patterns has been the object of numerous studies in recent years [e.g., *Siegel*, 1991; *Beyerle et al.*, 1998; *Hoaglund et al.*, 2004; *Person et al.*, 2007]. More specifically, it has been proposed that local groundwater recharge in central Europe was prevented during the LGM due to permafrost formation [*Beyerle et al.*, 1998]. However, a number of studies have also indicated that, as a result of high hydraulic pressures from glacial loading, groundwater recharge rates could be dramatically enhanced and flow patterns could be reversed in many areas [*Siegel*, 1991;

Hoaglund et al., 2004; *Person et al.*, 2007]. Hence, a study of past climate through the use of noble gases in groundwater of the Michigan Basin, which was ice-covered during the LGM, is critical to assessing the impact of glaciations on groundwater recharge, flow dynamics and climate evolution, in addition to providing invaluable information for the exploration and regulation of the precious freshwater resources in this region.

In contrast to shallow freshwaters, deep formation waters (brines) with very high salinities (e.g., >450g/L) have been documented throughout the Michigan Basin [*Long et al.*, 1988; *Wilson and Long*, 1993a, b]. Studies of major elements and stable isotopes have shown that these brines originate from ancient seawater and have a complex evolution history [*Long et al.*, 1988; *Wilson and Long*, 1993a, b; *Davisson and Criss*, 1996; *Martini*, 1997; *McIntosh et al.*, 2004]. While the brines have been long recognized to play an important role in regional chemical alteration and diagenesis [*Coniglio et al.*, 1994; *Girard and Barnes*, 1995], mass and heat transport [*Long et al.*, 1988; *Vugrinovich*, 1989; *Coniglio et al.*, 1994], and deposition of petroleum and ore resources [*Budai and Wilson*, 1991], their origin and evolution history are still poorly understood. Moreover, despite a currently observed low geothermal gradient (~19°C/Km) [*Vugrinovich*, 1989], oil and natural gas reservoirs in the Michigan Basin are abundant and ubiquitously distributed within the sedimentary sequence [e.g., *Dorr and Eschman*, 1970], indicating the occurrence of higher temperatures in the past. A wealth of thermal studies in the basin based on a diversity of proxies (e.g., organic maturity data, stable isotopes, fluid inclusions, authigenic clay minerals, apatite fission track ages), all point to the occurrence of past high temperatures (up to 260°C) in the basin [*Cercone and Lohmann*, 1987; *Cercone and Pollack*, 1991; *Crowley*, 1991; *Coniglio et al.*, 1994; *Girard and Barnes*,

1995; *Luczaj et al.*, 2006]. However, the origin of such past high temperatures also remains uncertain. The application of noble gases as natural tracers in the Michigan Basin provides invaluable information to investigate the origin and subsurface movements of the brines, to clarify the origin of past high temperatures, as well as to help in the understanding of the thermal and tectonic history in this currently stable continental region. These are the goals of the present work.

This dissertation is divided into two parts. The first part (Chapters 2 and 3) is aimed at investigating the impact of LGM on groundwater recharge and local climate, as well as understanding groundwater flow dynamics through the use of noble gases dissolved in groundwaters of the shallow Marshall aquifer in the Michigan Basin. The noble gas study is also combined with a study of stable isotopes (δD, $\delta^{18}O$, and $\delta^{13}C$), radiocarbon (^{14}C) and major elements (e.g., Br, Cl, Na, Ca, and Mg). This analysis of the combined helium-heat flux ratios in this shallow aquifer also provides new insights into the thermal evolution of this currently stable region. This leads to the second part of this dissertation (Chapters 4, 5 and 6), which is focused on noble gases in deep brines of the Michigan Basin. The analysis presented here provides new insights into the origin and evolution history of these deep brines, assessing their influences on the basin thermal evolution, as well as revealing the unique nature of the underlying lithospheric mantle.

1.3. Dissertation structure

The chapters that follow either have been published or have been submitted and are currently in review [*Ma et al.*, 2004; *Ma et al.*, 2005; *Castro et al.*, 2008; *Ma et al.*, 2008a; *Ma et al.*, 2008b].

Chapter 2 presents a paleo-temperature record in southern Michigan since the LGM based on atmospheric noble gas concentrations and ^{14}C groundwater ages in the shallow Marshall aquifer. NGT records from mid-high latitude areas hold great promise not only to ascertain whether or not groundwater recharge occurs under ice-covered regions, but also to identify major global climatic oscillations and changes of atmospheric circulation patterns. This work has been published in *Ma et al.* [2004].

In Chapter 3, helium isotopes in the Marshall aquifer are systematically investigated. Helium concentrations are used to calibrate the helium fluxes entering the bottom of the Marshall aquifer from great depths with a 2-D helium advection-dispersion model. Together with major elemental data from Michigan Basin groundwaters, the analysis indicates that the upward transport of deep basinal fluids is responsible for the presence of high He excess and high salinities at shallow depths of the basin. Of particular relevance is the contrast observed between high helium and low heat fluxes, leading to helium/heat flux ratios greater than the radiogenic production ratio in certain areas. Such high helium/heat flux ratios strongly suggest the occurrence of a major past thermal event in the basin. This helium work has been published in *Ma et al.* [2005].

To confirm the presence of such a thermal event and to clarify its origin, the second part of this dissertation (Chapters 4, 5, and 6) systematically investigates the mantle, atmospheric and crustal noble gas components in 38 deep (down to ~3.6 km depth) Michigan Basin brine samples from eight different formations beneath the Marshall aquifer. Specifically, Chapter 4 is focused on the mantle noble gas signatures. The mantle noble gases reveal the presence of significant primordial solar-like He and Ne mantle components in this stable continental region, where the presence of mantle plumes

is highly unlikely, pointing to the existence of shallow refractory primordial noble gas reservoirs beneath the ancient continental crust. This study reveals not only the mantle origin of such a thermal event, but also the unique nature of the underlying lithospheric mantle, providing new insights into the current debates of mantle structure and convection models. This work has been submitted to Earth and Planetary Science Letters and is currently in review [*Castro et al.*, 2008].

Chapter 5 discusses the accompanying atmospheric noble gases in these deep brines. The concentrations of atmospheric noble gases are compared to those in ASW and the brine samples show a strong depletion pattern. To understand the mechanisms responsible for this overall atmospheric noble gas depletion, various phase interaction models are tested. This depletion pattern is best explained by a model involving subsurface boiling and steam separation, and thus, is consistent with the occurrence of a past thermal event of mantle origin as previously suggested by both the high ^{4}He/heat flux ratios and the presence of primordial mantle He and Ne signatures in the basin. This finding is also consistent with the presence of past elevated basin temperatures (~>80-260°C). This study pioneers the use of atmospheric noble gases in subsurface fluids to trace the thermal history of stable tectonic regions. Chapter 5 is now in press with Earth and Planetary Science Letters [*Ma et al.*, 2008a].

Chapter 6 presents the concentrations and isotopic ratios of the crustal noble gas components in these deep brines. The crustal noble gases within the basin are shown to originate from a deep, external source, likely the Precambrian crystalline basement beneath the Michigan Basin. Furthermore, observed elemental ratios of crustal noble gases in these brines vary over several orders of magnitude with respect to the expected

production ratios from the crystalline basement rocks and display systematic patterns within the basin. These ratios are investigated and discussed by using Rayleigh-type elemental fractionation models. The results suggest that upward transport of these deep crustal noble gases into the basin is controlled by both solubility- and diffusion-related elemental fractionation processes. The release of crustal noble gases into the basin also points to the occurrence of a past thermal event in the basin, as previously suggested through the study of heat and mantle noble gases. This study highlights the use of crustally produced noble gases to trace subsurface fluid movement and to help in understanding the role of tectonic activity in deep crustal degassing processes. Chapter 6 has been submitted to Geochemistry Geophysics Geosystems and is currently in revision [*Ma et al.*, 2008b].

The conclusions from the mantle (Chapter 4), atmospheric (Chapter 5) and crustal (Chapter 6) noble gas components in these deep basin brines are remarkably consistent, all pointing to the presence of a past thermal event in the basin, which is most likely related to the recent reactivation of the Mid Continent Rift (MCR) system underneath the Michigan Basin. The analysis of noble gases in deep Michigan basin brines provides new insights into the origin and evolution of Michigan Basin brines, the thermal and tectonic history of this currently stable basin, as well as the nature of the underlying lithospheric mantle.

A summary of the major results and conclusions of this dissertation is provided in Chapter 7. Experimental techniques used are provided in detail in the Appendix. This dissertation work has important implications for the fields of paleoclimatology, hydrogeology, tectonics, and mantle geochemistry.

References

Albarede, F. (2005), The survival of mantle geochemical heterogeneities. In: van der Hilst, R.D., Bass, J.D., Matas, J., Trampert, J. (Eds.), *Earth's Deep Mantle – Structure, Composition, and Evolution*, AGU Monograph, vol. 160, pp. 27-46.

Alley, R.B., and P.U. Clark (1999), The deglaciation of the northern hemisphere: a global perspective, *Annu. Rev. Earth Planet. Sci.*, *27*, 149-182.

Anderson, D.L. (1998), A model to explain the various paradoxes associated with mantle noble gas geochemistry, *Proc. Natl. Acad. Sci. USA*, *95*, 9087-9092.

Ballentine, C.J., R.K. O'Nions, E.R. Oxburgh, F. Horvath, and J. Deak (1991), Rare gas constraints on hydrocarbon accumulation, crustal degassing and groundwater flow in the Pannonian Basin, *Earth Planet. Sci. Lett.*, *105*, 229-246.

Ballentine, C.J., and P.G. Burnard (2002), Production, release and transport of noble gases in the continental crust, *Rev. Mineral. Geochem.*, *47*, 481-538.

Beyerle, U., R. Purtschert, W. Aeschbach-Hertig, D.M. Imboden, H.H. Loosli, R. Wieler, and R. Kipfer (1998), Climate and groundwater recharge during the last glaciation in an ice-covered region, *Science*, *282*(5389), 731-734.

Bosch, A., and E. Mazor (1988), Natural gas association with water and oil as depicted by atmospheric noble gases: case studies from the southeastern Mediterranean Coastal Plain, *Earth Planet. Sci. Lett.*, *87*, 338-346.

Budai, J.M., and J.L. Wilson (1991), Diagenesis history of the Trenton and Black River formations in the Michigan Basin, in *Early sedimentary evolution of the Michigan Basin*, edited by P.A. Catacosinos and P.A. Jr. Daniels, GSA Special Paper, *256*, pp. 73-88.

Castro, M.C., A. Jambon, G. de Marsily, and P. Schlosser (1998a), Noble gases as natural tracers of water circulation in the Paris Basin 1. Measurements and discussion of their origin and mechanisms of vertical transport in the basin, *Water Resour. Res.*, *34*, 2443-2466.

Castro, M.C., P. Goblet, E. Ledoux, S. Violette, and G. de Marsily (1998b), Noble gases as natural tracers of water circulation in the Paris Basin 2. Calibration of a groundwater flow model using noble gas isotope data, *Water Resour. Res.*, *34*, 2467-2483.

Castro, M.C., and P. Goblet (2003a), Noble gas thermometry and hydrologic ages: Evidence for late Holocene warming in Southwest Texas, *Geophys. Res. Lett.*, *30*(24), 2251, doi:10.1029/2003GL018875.

Castro, M.C., and P. Goblet (2003b), Calibration of regional groundwater flow models: working toward a better understanding of site-specific systems, *Water Resour.*

Res., *39*, 1172, doi:10.1029/2002WR001653.

Castro, M.C., D. Patriarche, and P. Goblet (2005), 2-D numerical simulations of groundwater flow, heat transfer and ^{4}He transport – implications for the He terrestrial budget and the mantle helium-heat imbalance, *Earth Planet. Sci. Lett.*, *237*, 893-910.

Castro, M.C., L. Ma, and C.M. Hall (2008), A primordial, solar He-Ne signature in crustal fluids of a stable continental region, *Earth Planet. Sci. Lett.*, in review.

Cercone, K.R., and H.N. Pollack (1991), Thermal maturity of the Michigan Basin, in *Early sedimentary evolution of the Michigan Basin*, edited by P.A. Catacosinos and P.A. Jr. Daniels, GSA Special Paper, *256*, pp. 1-11.

Cercone, K.R., and K.C. Lohmann (1987), Late burial diagenesis of Niagaran (middle Silurian) pinnacle reefs in Michigan Basin, *AAPG Bulletin*, *71*, 156-166.

Coniglio, M., R. Sherlock, A.E., Williams-Jones, K. Middleton, and S.K. Frape (1994), Burial and hydrothermal diagenesis of Ordovician carbonates from the Michigan Basin, Ontario, Canada, *Spec. Publs. Int. Ass. Sediment.*, *21*, 231-254.

Crowley, K.D. (1991), Thermal history of Michigan Basin and southern Canadian Shield from apatite fission track analysis, *Journal of Geophysical Research*, *96*, 697-711.

Davisson, M.L., and R.E. Criss (1996), Na-Ca-Cl relations in basinal fluids, *Geochim. Cosmochim. Acta*, *60*, 2743-2752.

Dorr, J.A. Jr., and D.F. Eschman (1970), *Geology of Michigan*, 1st ed. Univ. of Michigan Press, Ann Arbor, Michigan.

Dyke, A.S., J.T. Andrews, P.U. Clark, J.H. England, G.H. Miller, J. Shaw, and J.J. Veillette (2002), The Laurentide and Innuitian ice sheets during the Last Glacial Maximum, *Quat. Sci. Rev.*, *21*(1-3), 9-31.

Girard, J.-P., and D.A. Barnes (1995), Illitization and paleothermal regimes in the middle Ordovician St. Peter sandstone, central Michigan Basin: K-Ar, oxygen isotope, and fluid inclusion data, *AAPG Bulletin*, *79*, 49-69.

Hiyagon, H., and B.M. Kennedy (1992), Noble gases in CH_4-rich gas fields, Alberta, Canada, *Geochim. Cosmochim. Acta*, *56*, 1569-1589.

Hoaglund, J.R., III, J.J. Kolak, D.T. Long, and G.J. Larson (2004), Analysis of modern and Pleistocene hydrologic exchange between Saginaw Bay (Lake Huron) and the Saginaw Lowlands area, *Geol. Soc. Am. Bull.*, *116*(1-2), 3-15, doi:10.1130/B25290.1.

Honda, M., I. McDougall, D.B. Patterson, A. Doulgeris, and D.A. Clague (1991), Possible solar noble-gas component in Hawaiian basalts, *Nature*, *349*, 149-151.

Kennedy, B.M. (1988), Noble gases in vent water from the Juan de Fuca Ridge, *Geochimica et Cosmochimica Acta*, *52*, 1929-1935.

Kennedy, B.M., and M.C. van Soest (2007), Flow of mantle fluids through the ductile lower crust: helium isotope trends, *Science*, *318*, 1433-1436.

Kipfer, R., W. Aeschbach-Hertig, F. Peeters, and M. Stute (2002), Noble gases in lakes and ground waters, *Reviews in Mineralogy and Geochemistry*, *47*, 615-700.

Long, D.T., T.P. Wilson, M.J. Takacs, and D.H. Rezabek (1988), Stable-isotope geochemistry of saline near-surface ground water: east-central Michigan Basin, *Geo. Soc. Am. Bull.*, *100*, 1568-1577.

Luczaj, J.A., W.B. III Harrison, and N.S. Williams (2006), Fractured hydrothermal dolomite reservoirs in the Devonian Dundee formation of the central Michigan Basin, *AAPG Bulletin*, *90*, 1787-1801.

Ma, L., M.C. Castro, and C.M. Hall (2004), A late Pleistocene-Holocene noble gas paleotemperature record in southern Michigan, *Geophysical Research Letters*, *31*, L23204, doi:10.1029/2004GL021766.

Ma, L., M.C. Castro, C.M. Hall, and L.M. Walter (2005), Cross-formational flow and salinity sources inferred from a combined study of helium concentrations, isotopic ratios, and major elements in the Marshall aquifer, southern Michigan, *Geochem. Geophys. Geosyst.*, *6*, Q10004, doi:10.1029/2005GC001010.

Ma, L., M.C. Castro, and C.M. Hall (2008a), Atmospheric noble gas signatures in deep Michigan Basin brines as indicators of a past thermal event, *Geochem. Geophys. Geosyst.*, in revision.

Ma, L., M.C. Castro, and C.M. Hall (2008b), Crustal noble gases in deep brines as natural tracers of vertical transport processes in the Michigan Basin, *Earth Planet. Sci. Lett.*, in press.

Martini, A.M. (1997), Hydrogeochemistry of saline fluids and associated water and gas, Ph.D. dissertation, Univ. of Michigan, Ann Arbor.

Mazor, E., and A.H. Truesdell (1984), Dynamics of a geothermal field traced by noble gases: Cerro Prieto, Mexico, *Geothermics*, *13*, 91-102.

McIntosh, J.C., L.M. Walter, and A.M. Martini (2004), Extensive microbial modification of formation water geochemistry: Case study from a mid-continent sedimentary basin, United States, *Geo. Soc. Am. Bull.*, *116*, 743-759.

Moreira, M., and C.J. Allegre (1998), Helium-neon systematics and the structure of the mantle, *Chemical Geology*, *147*, 53-59.

O'Nions, R.K., and E.R. Oxburgh (1983), Heat and helium in the Earth, *Nature*, *306*, 429-431.

O'Nions, R.K., and C.J. Ballentine (1993), Rare gas studies of basin scale fluid movement, *Phil. Trans. R. Soc. Lond. A*, *344*, 141-156.

Oxburgh, E.R., R.K. O'Nions, and R.I. Hill (1986), Helium isotopes in sedimentary basins, *Nature*, *324*, 632-635.

Ozima, M., and F.A. Podosek (2002), *Noble gas geochemistry*, 2nd ed., 286 pp., Cambridge University Press, New York.

Person, M., J. McIntosh, V. Bense, and V.H. Remenda (2007), Pleistocene hydrology of North America: the role of ice sheets in reorganizing groundwater flow systems, *Reviews of Geophysics*, *45*, RG3007, doi:10.1029/2006RG000206.

Pinti, D.L., and B. Marty (1995), Noble gases in crude oils from the Paris Basin, France: implications for the origin of fluids and constraints on oil-water-gas interactions, *Geochim. Cosmochim. Acta*, *59*, 3389-3404.

Porcelli, D., and G.J. Wasserburg (1995), Mass transfer of helium, neon, argon, and xenon through a steady-state upper mantle, *Geochimica et Cosmochimica Acta*, *59*, 4921-4937.

Porcelli, D., and C.J. Balllentine (2002), Models for the distribution of terrestrial noble gases and the evolution of atmosphere, *Reviews in Mineralogy and Geochemistry*, *47*, 411-480.

Porcelli, D., C.J. Ballentine, and R. Wieler (2002), *Noble gases in geochemistry and cosmochemistry*, 844 pp., Reviews in Mineralogy and Geochemistry, volume 47.

Siegel, D.I. (1991), Evidence for dilute of deep, confined ground water by vertical recharge of isotopically heavy Pleistocene water, *Geology*, 19, 433-436.

Torgersen, T., and W.B. Clarke (1985), Helium accumulation in groundwater; I. an evaluation of sources and the continental flux of crustal ^{4}He in the Great Artesian Basin, Australia, *Geochim. Cosmochim. Acta*, *49*, 2445-2452.

Torgersen, T., B.M. Kennedy, H. Hiyagon, K. Y. Chiou, J.H. Reynolds, and W.B. Clarke (1989), Argon accumulation and the crustal degassing flux of ^{40}Ar in the Great Artesian Basin, Australia, *Earth Planet. Sci. Lett.*, *92*, 43-56.

Vugrinovich, R. (1989), Subsurface temperatures and surface heat flow in the Michigan Basin and their relationships to regional subsurface fluid movement, *Marine and Petroleum Geology*, *6*, 60-70.

Wetherill, G.W. (1953), Spontaneous fission yields from uranium and thorium, *Physical Review*, *92*, 907-912.

Wetherill, G.W. (1954), Variations in the isotopic abundances of neon and argon extracted from radioactive minerals, *Physical Review*, *96*, 679-683.

Wilson, T.P., and D.T. Long, (1993a), Geochemistry and isotope chemistry of Michigan Basin brines: Devonian formations, *Applied Geochemistry*, *8*, 81-100.

Wilson, T.P., and D.T. Long (1993b), Geochemistry and isotope chemistry of Ca-Na-Cl brines in Silurian strata, Michigan Basin, *Applied Geochemistry*, *8*, 507-524.

Winckler, G., R. Kipfer, W. Aeschbach-Hertig, R. Botz, M. Schmidt, S. Schuler, and R. Bayer (2000), Sub sea floor boiling of Red Sea brines: new indication from noble gas data, *Geochimica et Cosmochimica Acta*, *64*, 1567-1575.

Zaikowski, A., B.J. Kosanke, and N. Hubbard (1987), Noble gas composition of deep brines from the Palo Duro Basin, Texas, *Geochim. Cosmochim. Acta*, *51*, 73-84.

Zartman, R.E., G.J. Wasserburg, and J.H. Reynolds (1961), Helium, argon, and carbon in some natural gases, *J. Geophys. Res.*, *66*, 277-306.

CHAPTER 2

A LATE PLEISTOCENE - HOLOCENE NOBLE GAS PALEOTEMPERATURE RECORD IN SOUTHERN MICHIGAN

Abstract

Noble gas temperatures (NGTs) and ^{14}C derived ages in groundwaters of the Michigan Basin reveal a ground temperature of ~1ºC toward the end of the Last Glacial Maximum (LGM), suggesting that groundwater recharge occurred under the Laurentide Ice Sheet (LIS) cover. In addition to the general warming observed since the LGM, the NGT record indicates an abrupt warming event between ~12.8 and 11.1kyrs BP, correlative to the Bølling-Allerød (BOA) warm phases. Ice-sheet-linked changes in freshwater delivery to the North Atlantic, together with changes in the North Atlantic Deep Water (NADW) circulation are possible causes of such abrupt climate shifts in northeastern US. Pleistocene waters yielding the lowest NGTs have the highest $\delta^{18}O$ and δD values, suggesting an atmospheric circulation pattern distinct from today, with a stronger moisture component from the Gulf of Mexico, possibly due to the presence of the LIS which weakened the Pacific westerly flow.

2.1. Introduction

Late Pleistocene and Holocene paleoclimatic reconstructions through the use of noble gases dissolved in groundwater have been the object of numerous studies in recent years [e.g., *Kipfer et al.*, 2002; *Castro and Goblet*, 2003]. Unlike many other continental proxies, noble gas temperatures (NGTs) are a direct measure of the temperature at which groundwater equilibrated with the atmosphere during infiltration. This results from the fact that the solubility of noble gases in water, especially those of Ar, Kr and Xe is primarily dependent on the mean local atmospheric pressure (altitude of the recharge area) and temperature of the water at the time recharge took place [*Kipfer et al.*, 2002].

With the exception of *Beyerle et al.* [1998], who conducted a paleoclimatic reconstruction using NGTs in a mid-latitude region that experienced ice-cover during the Last Glacial Maximum (LGM), all other available climate records based on NGTs come from permanently ice-free regions. In addition to providing a much improved understanding of past climate evolution and atmospheric circulation patterns, such paleoclimatic reconstructions in ice-covered regions during the LGM are critical to assess the impact of glaciation on groundwater recharge and dynamics.

Here, we present a ~17kyrs (^{14}C derived ages) NGT and stable isotope record derived mostly from the Marshall aquifer in southern Michigan, a region covered by the Laurentide Ice Sheet (LIS) during the LGM and early deglaciation periods. Our NGT record reveals new aspects of late Pleistocene climate change in southern Michigan and provides new information on the occurrence of groundwater recharge under ice-sheet cover. The combined analysis of NGTs and δD and $\delta^{18}O$ shed new light into atmospheric circulation patterns in place during the early stages of deglaciation in this region.

2.2. Regional Setting

The Marshall aquifer, a major groundwater flow system composed mostly of sandstones is located in the central portion of the Michigan Basin, a basin with an ovate shape occupying the Lower Peninsula of Michigan (Fig. 2.1). The Bayport-Michigan confining units which are composed mostly of shale, overly the Marshall aquifer and are in turn overlain by the Saginaw aquifer, which mainly consists of sandstone [*Mandle and Westjohn*, 1989]. These formations subcrop at an altitude of ~300m and are overlain by glacial deposits from the Wisconsinan and possibly older Pleistocene ages. In the Marshall aquifer in southern Michigan, groundwater flows gravitationally to the NE and NW (Fig. 2.1), and groundwater discharges into Lake Huron and Lake Michigan, in the Saginaw and Michigan Lowlands area, respectively [*Vugrinovich*, 1986]. Flow in the Saginaw aquifer is toward the NE.

2.3. Sample collection and measurements

Water samples were collected from thirteen wells in the Marshall and one well in the Saginaw (sample 11) aquifers (cf. Fig. 2.1) for measurement of noble gases (Ne, Ar, Kr and Xe) (Table 2.1), major elements (Tables 2.2), stable isotope ratios (δD and $\delta^{18}O$) and carbon isotopes ($\delta^{13}C$ and ^{14}C activities) (Table 2.3).

Noble gas samples were collected in copper tubes (i.e., standard refrigeration grade 3/8" Cu tubing) and water was allowed to flow through for ~10 minutes. While the water flushed through the system, the absence of gas bubbles that could potentially contaminate or phase fractionate the samples was checked through a transparent plastic tube mounted at the end of the Cu tube. The Cu tubes were then sealed by stainless steel

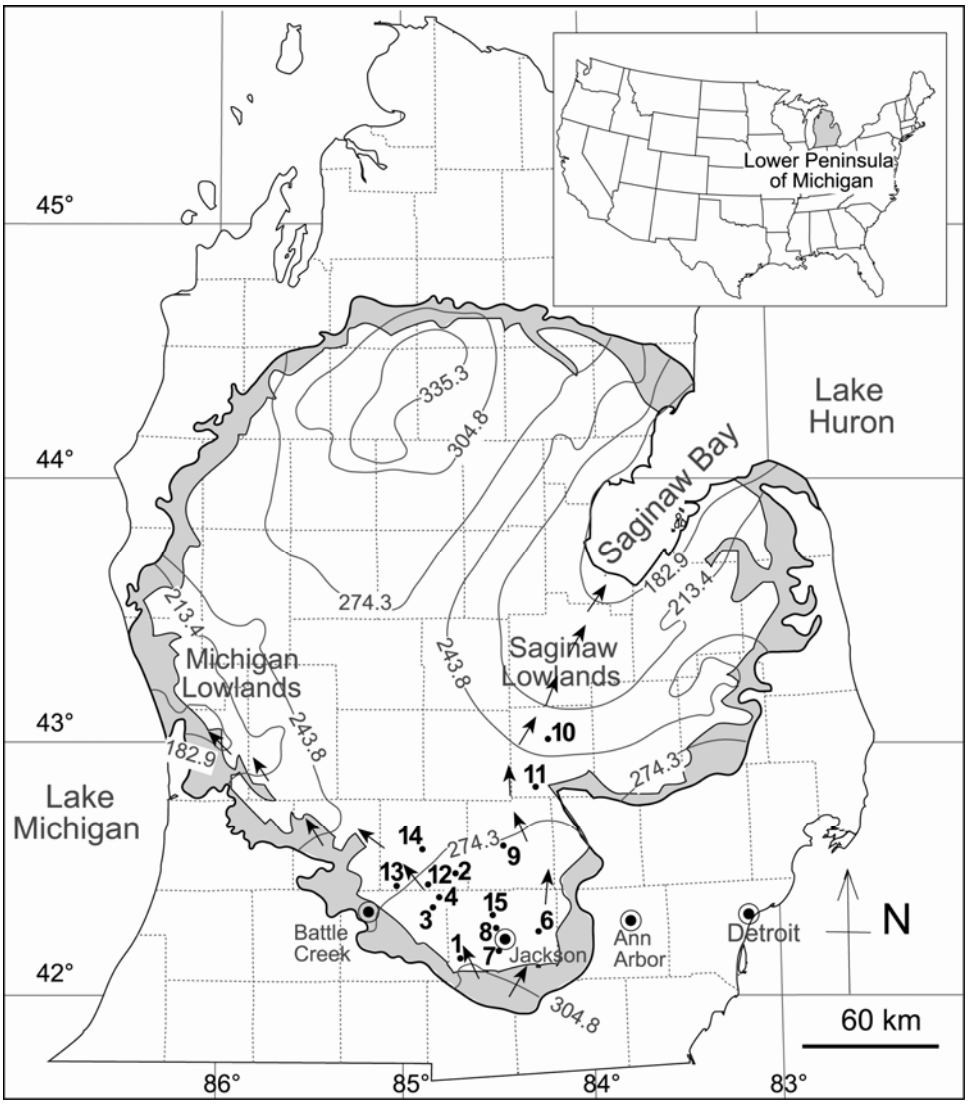

Fig. 2.1. Study area and sample locations in southern Michigan [adapted from *Mandle and Westjohn*, 1989]. The Marshall aquifer subcrop (shaded area), equipotentials (m, contour lines), and direction of groundwater flow (arrows) are indicated. Sample numbers are in bold

Table 2.1. Sample locations, noble gas concentrations, as well as fitted NGTs and excess air components.

Sample Number	Latitude (N, degree)	Longitude (W, degree)	Depth (m)	Ne[(a)] ($\times10^{-7}$, cm^3STP/g)	Ar ($\times10^{-4}$, cm^3STP/g)	Kr ($\times10^{-8}$, cm^3STP/g)	Xe ($\times10^{-8}$, cm^3STP/g)	NGT[(b)] (°C)	± (°C)	Excess Air ($\times10^{-3}$, cm^3STP/g)	± ($\times10^{-3}$, cm^3STP/g)	χ^2
MI-1	42.175	84.644	82	3.68	4.72	10.7	1.59	6.78	0.89	9.01	0.62	10.3
MI-2a	42.483	84.671	110	3.76	5.07	12.1	1.71	3.45	0.82	9.06	0.63	10
MI-2b				2.49	4.50	11.2	1.71	3.14	0.55	2.10	0.32	5.6
MI-3	42.365	84.796	73	2.16	4.06	10.0	1.60	5.78	0.91	0.65	0.45	14.6
MI-4a	42.414	84.750	85	2.62	4.68	11.4	1.66	2.98	0.33	2.90	0.20	1.7
MI-4b				2.54	4.81	11.1	1.71	2.50	0.46	2.42	0.28	4.1
MI-6	42.250	84.217	111	2.20	4.04	10.3	1.42	6.46	0.93	0.98	0.46	14.7
MI-7	42.243	84.393	117	2.23	4.01	9.7	1.52	7.05	0.80	1.18	0.39	10.6
MI-8	42.275	84.383	122	4.27	5.37	11.6	1.64	4.98	0.39	12.20	0.31	0.1
MI-9	42.606	84.417	171	2.44	4.46	10.6	1.59	4.48	0.33	2.07	0.19	0.1
MI-10a	42.982	84.200	110	2.62	4.40	10.8	1.29	6.96	1.96	3.52	1.10	61.3
MI-10b				2.69	4.93	12.0	1.35	4.16	2.79	3.71	1.69	139.2
MI-11	42.806	84.251	73	2.62	4.62	11.0	1.58	4.02	0.34	3.03	0.20	2
MI-12a	42.451	84.882	88	2.64	4.84	10.7	1.58	3.92	0.94	3.22	0.56	15.8
MI-12b				2.67	4.64	10.6	1.53	4.91	0.51	3.46	0.30	4.4
MI-13	42.444	85.017	86	2.46	4.54	11.7	1.63	2.78	0.88	1.96	0.51	14.9
MI-14a	42.575	84.896	107	2.90	5.15	12.6	1.68	1.11	1.10	4.28	0.75	23.7
MI-14b				3.01	5.14	12.2	1.75	1.31	0.48	4.86	0.33	4.3
MI-15	42.354	84.372	107	2.76	4.83	11.7	1.72	2.30	0.33	3.57	0.21	0.7

a. Uncertainties (±1σ) for Ne, Ar, Kr and Xe are 1.3%, 1.3%, 1.5% and 2.2%, respectively.

b. NGTs, excess air components and χ^2 fitted after *Ballentine and Hall* [1999]. χ^2 represents the sum of squared error-weighted misfits (goodness of fitting).

Table 2.2. Major element data for samples from the Marshall and Saginaw aquifers

Sample Number	Temperature(°C)	pH	Alk (meq/kg)	Ca^{2+} (mM/kg)	Mg^{2+} (mM/kg)	Na^{+} (mM/kg)	K^{+} (mM/kg)	Cl^{-} (mM/kg)	NO_3^{-} (mM/kg)	SO_4^{2-} (mM/kg)
MI-1	11.3	7.0	5.91	2.15	1.03	0.33	0.02	0.5	0	0.3
MI-2	10.4	7.3	6.49	1.69	1.21	0.81	0.24	0.07	0.01	0.24
MI-4	9.8	7.0	6.07	8.9	1.33	2.49	0.7	0.69	0.89	7.58
MI-6	11.1	7.7	5.39	1.73	0.84	0.67	0.07	0.46	0	0.1
MI-7	11.3	7.4	6.30	2.75	1.24	2.14	0.07	1.75	0	1.01
MI-8	11.7	7.1	7.11	3.45	1.30	0.36	0.04	1.02	0	1.25
MI-9	10.8	7.3	6.26	2.39	1.30	0.72	0.08	0.71	0	0.62
MI-10	11.8	7.7	6.43	1.09	0.67	8.99	0.1	1.42	0	2.4
MI-11	11.4	7.8	3.98	1.13	0.76	0.02	0.02	0.03	0	0.05
MI-12	11.5	8.0	6.86	1.65	1.00	8.1	0.16	2.69	0.01	2.59
MI-13	11.2	8.2	6.86	3.05	1.25	6.4	0.25	5.8	0	0.69
MI-14	12.2	8.1	5.13	3.21	1.60	13.44	0.29	15.21	0.01	1.71
MI-15	12.0	7.4	7.65	3.13	1.46	11.48	0.36	8.6	0	1.46

Table 2.3. Stable isotopes (H,O, and C), ^{14}C activities and calculated ^{14}C ages.

Sample Number	NOSAMS references	δD[(a)] (per mil)	$\delta^{18}O$ (per mil)	$\delta^{13}C$ (per mil)	^{14}C (%)	± (%)	^{14}C age (year)	± (year)	TDIC[(b)] (mM/kg)	H_2CO_3 (mM/kg)	HCO_3^- (mM/kg)	$\log(pCO_2)$ (atm)
MI-1	OS-41508	-62.8	-9.1	-11.9	64	0.3	modern	null	7.38	1.47	5.9	-1.5
MI-2	OS-41509	-61.9	-9	-13.5	31.8	0.2	6046	674	7.3	0.82	6.46	-1.8
MI-3	OS-41510	-63.1	-9.6	-12.1	49.6	0.3	780	800	null	null	null	Null
MI-4	OS-41511	-61.6	-9.3	-13.6	36.1	0.1	4726	699	7.08	1.35	5.72	-1.6
MI-6	OS-41512	-63.4	-9.1	-10.2	61.1	0.2	modern	null	5.63	0.27	5.33	-2.2
MI-7	OS-41513	-61.8	-9.1	-11.7	61.6	0.3	modern	null	6.89	0.61	6.26	-1.9
MI-8	OS-41514	-62.4	-9.3	-10	56.1	0.2	modern	null	8.46	1.36	7.09	-1.5
MI-9	OS-41515	-62.1	-9	-12.6	59.4	0.2	modern	null	7.03	0.78	6.23	-1.8
MI-10	OS-41516	-77.3	-10.8	-13.2	30.4	0.1	6377	663	6.72	0.31	6.39	-2.2
MI-11	OS-41517	-67.2	-9.8	-11.8	52.4	0.2	432	780	4.11	0.16	6.73	-2.5
MI-12	OS-41641	-58	-8.8	-13.4	17.8	0.1	11142	658	6.96	0.16	6.73	-2.5
MI-13	OS-41642	-56.7	-8.6	-13.5	21.8	0.2	9558	667	6.82	0.1	6.58	-2.7
MI-14	OS-41643	-56.3	-8.7	-14.3	9.3	0.1	17384	655	5.12	0.09	4.95	-2.7
MI-15	OS-41644	-61.1	-8.8	-12.5	12.5	0.1	12778	784	8.33	0.7	7.6	-1.8

a. Uncertainties (1σ) for δD, $\delta^{18}O$, $\delta^{13}C$ are 1.0 per mil, 0.1 per mil and 0.4 per mil, respectively.
b. Calculated using Solminq 88 [*Kharaka et al.*, 1988].

pinch-off clamps [*Weiss*, 1968]. Noble gas concentrations and isotopic ratios were analyzed at the Noble Gas Laboratory at the University of Michigan. Details on measurements for noble gases are given in the appendix. Excess air, air saturated water (ASW) components and NGTs were determined following *Ballentine and Hall* [1999].

Major element samples were filtered with a 0.45 μm Gelman Laboratory AquaPrep filter, and subsequently preserved in high-density polyethylene bottles with no head space before analyses. Samples for cation analyses were acidified to pH<2 by using nitric acid. Major ion chemistry of these samples was determined in the Experimental and Aqueous Geochemistry Laboratory at the University of Michigan. Alkalinity was measured by the Gran-Alkalinity titration method [*Gieskes and Rogers*, 1973] with a precision of ±0.4%. Cation chemistry was determined by inductively coupled plasma-atomic emission spectrometry with a Leeman Labs PlasmaSpec III system (precision, ±2%). Anions were analyzed by ion chromatograpgy (IC) with a Dionex 4000I series (precision, ±1%).

Water samples for analysis of δD and $\delta^{18}O$ were collected in 60-mL glass bottles with polyethylene seal caps and were measured at the University of Michigan Stable Isotope Laboratory. For analysis of δD, a capillary tube containing 3 μL of water is loaded into a quartz tube containing 100mg of Indiana zinc [*Kendall and Coplen*, 1985]. Samples are reacted at 800°C for 4 minutes, and analyzed in a Delta S Finnigan MAT dual-inlet gas source mass spectrometer. Data are normalized to VSMOW and VSLAP, and precision and accuracy for the technique is maintained at ±1‰. For analysis of $\delta^{18}O$, waters are equilibrated with CO_2 for a minimum of 14 hours in an oscillating water bath maintained at 25°C [*Socki et al.*, 1992]. The resultant CO_2 is subsequently cryogenically

separated from the water and analyzed on a Finnigan MAT Delta S dual-inlet gas source mass spectrometer. Water $\delta^{18}O$ is calculated based on the fractionation of CO_2 and water at 25°C. Data is normalized relative to VSMOW and VSLAP, and overall analytical precision is better than 0.1‰ for $\delta^{18}O$.

Samples for carbon isotope (^{13}C and ^{14}C) measurements were collected in 500-mL glass bottles. To avoid alteration of the carbonate system due to biological activity during storage in the glass bottles, the ^{14}C samples were poisoned with 0.3 cm^3 of saturated $HgCl_2$ solution. ^{14}C concentrations and $^{13}C/^{12}C$ ratios were determined at the NOSAMS facility at Woods Hole Oceanographic Institution using the procedures outlined in *Jones et al.* [1990].

2.4. Groundwater ^{14}C dating

2.4.1 ^{14}C age calculation

^{14}C ages were calculated by a multi-model approach to estimate the effect of carbonate dissolution on the initial ^{14}C activity. Except for sample 3, for which we have no major element data, five conventional correction models were applied to all other samples [*Pearson and White*, 1967; *Tamers*, 1967; *Fontes and Garnier*, 1979; *Evans et al.*, 1979; *Eichinger*, 1983] using chemical and isotopic balances to convert activity values into ^{14}C ages. They all yielded consistent results. For sample 3, the Pearson's correction model was applied. Application of more sophisticated correction models [e.g., *Plummer et al.*, 1994] is not appropriate, because the complexity of the flow in the study area renders difficult an exact definition of distinct flow paths along which geochemical evolution of groundwater occurs.

Conversion of ^{14}C activity values into ^{14}C ages presented here (Table 2.3) are those following the *Fontes and Garnier* [1979] correction. The parameters used in this model are presented as follows. ^{14}C activities of soil CO_2 and solid carbonates are set up as 100% and 0%, respectively. $\delta^{13}C$ of soil CO_2 (average soil CO_2 value in Michigan) is ~-22‰ [*Ku*, 2001] and $\delta^{13}C$ of solid carbonates is 0 ‰. For each sample, fractionation factors used for soil CO_2-bicarbonate, bicarbonate-solid carbonate, and aqueous CO_2-soil CO_2, were calculated following the temperature-fractionation factor relationships given by *Fontes and Garnier* [1979]. Aqueous carbonate speciation and pCO_2 were calculated with the code Solmineq. 88 [*Kharaka et al.*, 1988], which accounts for major elements (Ca^{2+}, Mg^{2+}, Na^{+}, K^{+}, Cl^{-}, SO_4^{2-}, NO_3^{-}), alkalinity (HCO_3^{-}), pH, and temperature (Table 2.2). Calculated values for pCO_2, H_2CO_3 and HCO_3^{-} from the Solmineq.88 output are presented in Table 2.3. Concentration of dissolved carbon from solid carbonates was calculated from both major elements and carbonate alkalinity data (Table 2.2), and the average of these two values was used in the age calculation (Table 2.3).

For the purposes of error calculation, we assume an error of 5% for the percent modern carbon factor used to convert activity values to ^{14}C ages. This error estimate encompasses the range of values produced by the above correction techniques and is therefore a conservative error estimate. Age errors are then determined using a standard propagation of errors technique.

2.4.2. Interpretation of ^{14}C age for sample 14

Except for sample 3, all ^{14}C ages here presented are those obtained using the *Fontes and Garnier* [1979] correction (Table 2.3). Sample 14 yielded the oldest ^{14}C age

and coldest NGT. The sample belongs to a time period during which the recharge area is believed to have been under glacial cover (see next section). Under such conditions, the potential for difficulties in the ^{14}C age interpretation is possible. The *Fontes and Garnier* [1979] model requires a soil CO_2 source with plant signature ($\delta^{13}C$=-22‰, ^{14}C activity = 100%). It is likely that a soil CO_2 (or subglacial CO_2) source with plant signature exists under glacial cover due to bacteria activity even though root respiration is limited or non-existent. The decay of organic matter (by aerobic bacteria) is very likely since the interpretation of NGTs indicates clearly that there is communication with the atmosphere under the glaciers, and the temperature of the soil is above the melting point. So, although that it is true that plant activity may be limited under the glaciers due to the harsh environment, bacteria could still play an important role in converting organic matter into CO_2 under these conditions. Recent studies have found widespread bacterial populations at glacier beds [e.g., *Sharp et al.*, 1999] in addition to a high CO_2 production rate [e.g., *Souchez and Lemmens*, 1995]. pCO_2 calculated from sample 14 is ~$10^{-2.7}$atm, which is consistent with soil CO_2 values measured in high latitude areas [*Brook et al.*, 1983]. Recent field studies in a forested watershed in northern Michigan found that a similar soil pCO_2 level (~$10^{-2.6}$atm) can build up during winter time due to the thick snow cover [*Ku*, 2001].

Although the impact of glaciers on soil CO_2 is not yet fully understood, it is likely that a soil/subglacial CO_2 source with plant signature exists under glaciers due to bacteria activity. Having a similar CO_2 source, ^{14}C correction models should apply to recharge beneath an ice sheet. This was the assumption made for this particular sample.

2.5. Results and discussion

Samples range in age from modern to ~17.4kyrs BP and yield NGTs between 7.05±0.80ºC (sample 7) and 1.28±0.44ºC (samples 14a,b) (Fig. 2.2). Samples close to the recharge area (samples 1, 6, 7, 8; Fig. 2.1), displaying negative corrected ^{14}C "apparent" ages, yield an average NGT of 6.3±0.8ºC. This value is ~3ºC lower than the average annual air temperature of 9.1±0.8ºC for Jackson (1931-2002) (Fig. 2.1). Although ^{14}C ages indicate that samples 1, 6, 7, and 8 are "modern", these waters could possibly be hundreds of years old and representative of a cooler period instead. NGTs over several degrees cooler than present were recorded elsewhere (e.g., in the Carrizo aquifer of Texas) at the beginning of the last millennium [*Castro and Goblet*, 2003]. Samples close to the recharge area together with samples 3, 9 and 11 indicate similar NGT variations, up to ~3ºC within the last thousand years (Fig. 2.2). Lack of age resolution through ^{14}C, however, does not allow for a detailed paleoclimatic reconstruction within this period. Estimation of NGTs in the recharge area will be needed to assess the present ground temperature and determine if such a value is higher and closer to the mean annual air temperature (MAAT). In the discussion that follows and for comparative purposes, "modern" recharge temperature potentially representative of an average for the last millennium is taken as 6.3±0.8ºC.

Our NGT record displays a smooth general warming trend between the late stages of the LGM at ~17.4kyrs BP and present time (Fig. 2.2), interrupted by an abrupt warming event between ~12.8 and 11.1kyrs BP. Of particular interest is the NGT record representative of the late stages of the LGM (sample 14a, b; Fig. 2.2), a period during which the LIS reached its maximum extent, penetrating into central Indiana and Ohio, far

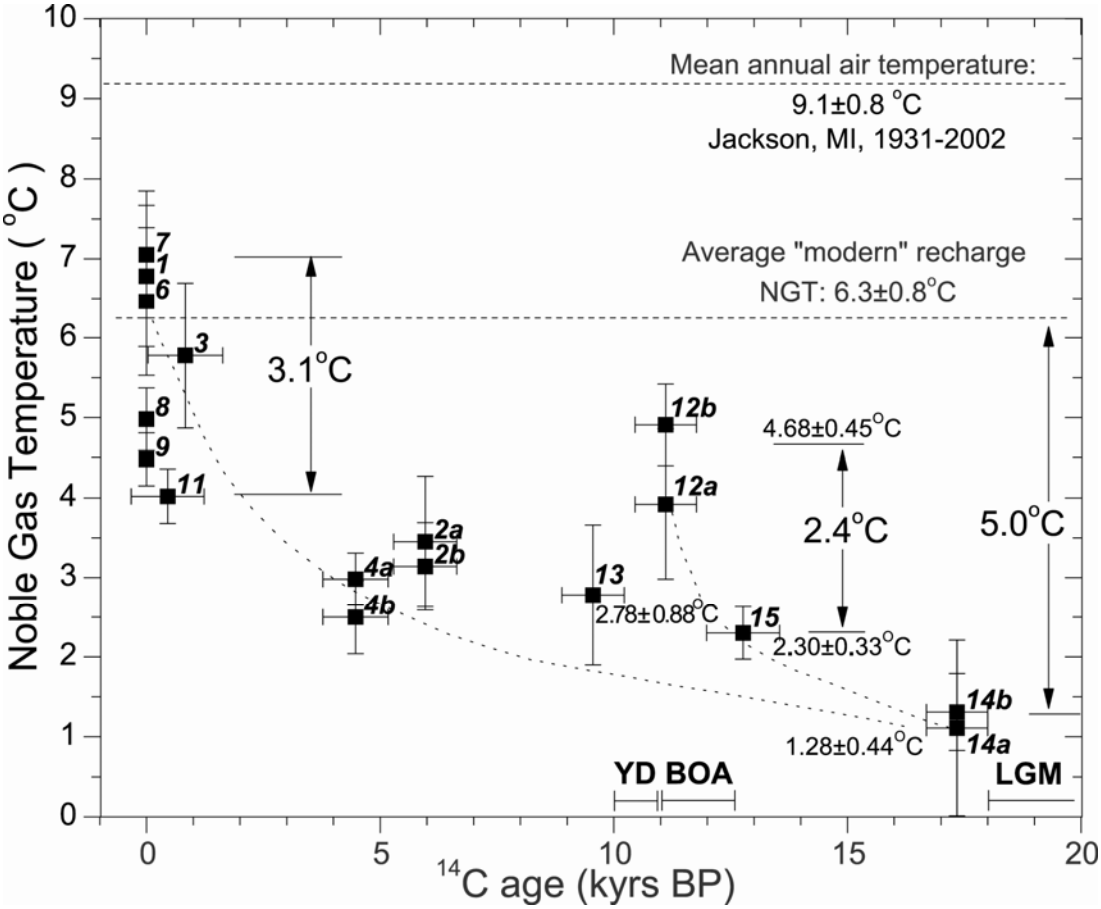

Fig. 2.2. Noble gas temperatures (ºC) versus ^{14}C ages. Mean annual air temperature is from http://lwf.ncdc.noaa.gov/oa/climate/stationlocator.html; BOA: Bølling-Allerød warm phases; YD: Younger Dryas; LGM: Last Glacial Maximum [after *Yu and Eicher*, 1998].

south of the Marshall subcrop (Fig. 2.3). The LIS experienced several subsequent fluctuations near its maximum extent and retreated rapidly at a later time into the Great Lakes basins, at ~14kyrs BP [*Dyke et al.*, 2002]. Chronology of the LIS suggests that the Marshall recharge area was under glacial cover until ~15.5kyrs BP. Our NGT record indicates an average recharge temperature of 1.28±0.44ºC (sample 14a, b; Fig. 2.2) at an earlier time, strongly suggesting the occurrence of subglacial groundwater recharge. Our results support the findings of *Hoaglund et al.* [2004] in which numerical groundwater flow simulations (and $\delta^{18}O$ anomalies) in the Michigan Basin suggest a reversal in the direction of the groundwater flow in the Saginaw Lowlands area due to ice-induced hydraulic loading and the resultant occurrence of subglacial recharge. By contrast, based on a calculated groundwater age gap between ~17 and 25kyrs BP, *Beyerle et al.* [1998] concluded that local groundwater recharge in the Glatt Valley aquifer, Switzerland, was prevented by overlying glaciers during the LGM. Although the impact of glaciation on groundwater flow behavior is not fully understood, a number of studies have shown that glaciers can dramatically change groundwater flow patterns [e.g., *Siegel*, 1991]. Such impact might be of a different nature depending on the geological/tectonic history, and thus, the hydrogeological system of the region under consideration. Our NGT record provides important direct support for the existence of subglacial recharge in Michigan and indicates a temperature underneath glaciers of ~1ºC. It further suggests a ground temperature at the late stages of the LGM 5ºC cooler than that of "modern" recharge (Fig. 2.2). Temperature differences between the ground and the atmosphere, however, have the potential to be much greater due to a possible insulation effect of the ground from colder air temperatures by glacier cover. Such effect has been observed in snow covered regions

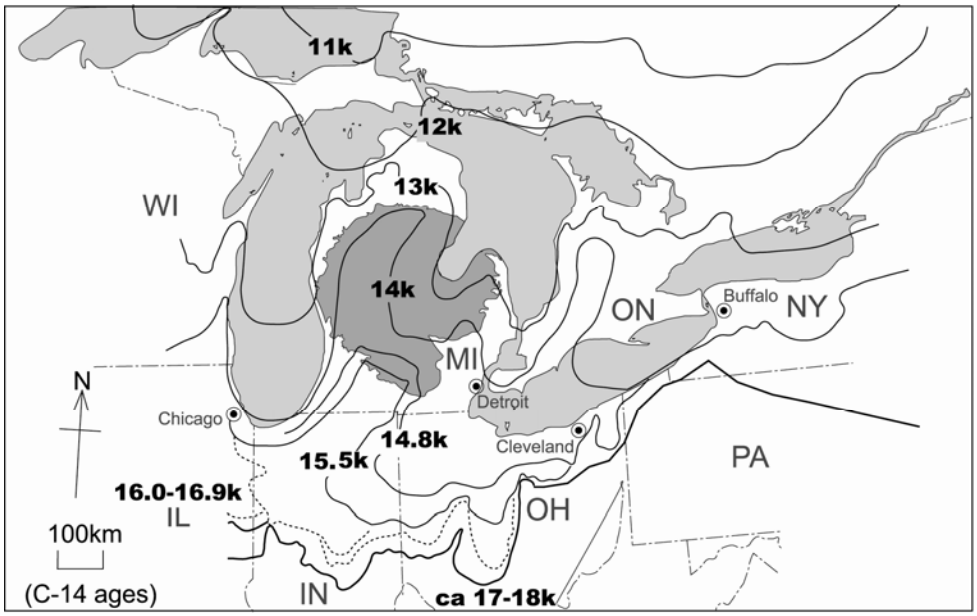

Fig. 2.3. Laurentide Ice Sheet extent and deglaciation history (^{14}C ages) in the Great Lakes region since the Last Glacial Maximum [after *Prest*, 1969; *Fullerton*, 1986]. The Marshall aquifer is indicated (dark shaded area) as well as present Great Lakes locations (light shaded areas).

[*Pollack and Huang*, 2000]. Beetle assemblages during the LGM from regions south of the LIS suggest mean January and July temperatures 10-19ºC and 11-12ºC cooler than present, respectively [*Elias et al.*, 1996]. Additional NGTs that span the full interval of the LGM will be needed to assess whether or not groundwater recharge occurred continuously during this time period.

Another important aspect of our NGT record is the observed abrupt warming between ~12.8 (sample 15) and 11.1kyrs BP (sample 12a,b) of ~2.4ºC (Fig. 2.2) immediately following deglaciation in the region (Fig. 2.3). Taking into account the general warming trend between the LGM and present time, as well as the trend suggested by sample 13 at ~9.6kyrs BP (Fig. 2.2), such a warming period seems to be followed by a rapid climate reversal. Similar broad-scale climate oscillations within the North Atlantic region were observed within the same time period (~13-10kyrs BP). Here, an initial general warming corresponding to the Bølling-Allerød (BOA) warm phases (~13-11kyrs BP) was found. This event is contemporaneous with global deglaciation and was followed by a climate reversal correlative to the Younger Dryas (YD) at ~11.0-10.0kyrs BP, prior to a return to warmer conditions [*Alley and Clark*, 1999]. In northeastern US, such abrupt warming began at ~12.4kyrs BP to peak at ~11kyrs, followed by a cold phase (YD) from ~10.8-10kyrs BP [*Peteet et al.*, 1993]. In the Great Lakes region, similar paleoclimatic oscillations have been identified based on a variety of proxies. Pollen records in northern Ohio indicate a mean annual temperature increase of 8ºC at ~13-11kyrs BP, followed by a cold period with a temperature decrease of 2-5ºC and 1-2ºC in January and July, respectively, suggesting the possible westward extension of the YD into the Great Lake regions [*Shane and Anderson*, 1993]. Based on stable isotopes, pollen

records, and plant macrofossils from lake sediments in Ontario, *Yu and Eicher* [1998] further demonstrate that late glacial-to-early Holocene climate oscillations occurred in the Great Lakes region with the onset of BOA at ~12.5kyrs BP down to 11.0kyrs. Although our NGT increase of ~2.4ºC is not as pronounced as the one suggested by pollen records, the NGT record has undoubtedly captured the occurrence of climatic oscillations during the late glacial period, in particular, the BOA warm phases.

Ice-sheet-linked changes in freshwater delivery to the North Atlantic, as well as changes in the North Atlantic Deep Water (NADW) circulation are possibly at the origin of such abrupt climate shifts in the northeastern US. BOA warming was accompanied by an increase of NADW formation, suggesting a link between heat transport to the North Atlantic region and NADW production. A decrease of continental freshwater fluxes to the North Atlantic and a diversion of fresh water to the Gulf of Mexico via the Mississippi River due to fluctuations of the southern LIS margin could generate more vigorous deep water circulation, and lead to the BOA warm phases [*Clark et al.*, 2001].

Samples 2a,b and 4a,b follow the general warming trend, with a possible slight temperature increase of ~0.7ºC at ~6kyrs BP (sample 2a,b), relative to the long-term warming.

Stable isotope analyses for all samples yield δD and $\delta^{18}O$ varying between -56.3 and -77.3‰, and -8.6 and -10.8‰, respectively (Fig. 2.4a). All δD and $\delta^{18}O$ lie close to both the global [*Craig*, 1961] and local (Simcoe, Ontario, Canada) meteoric water lines (Fig. 2.4a), indicating that δD and $\delta^{18}O$ were not significantly modified by isotope exchange within the aquifer.

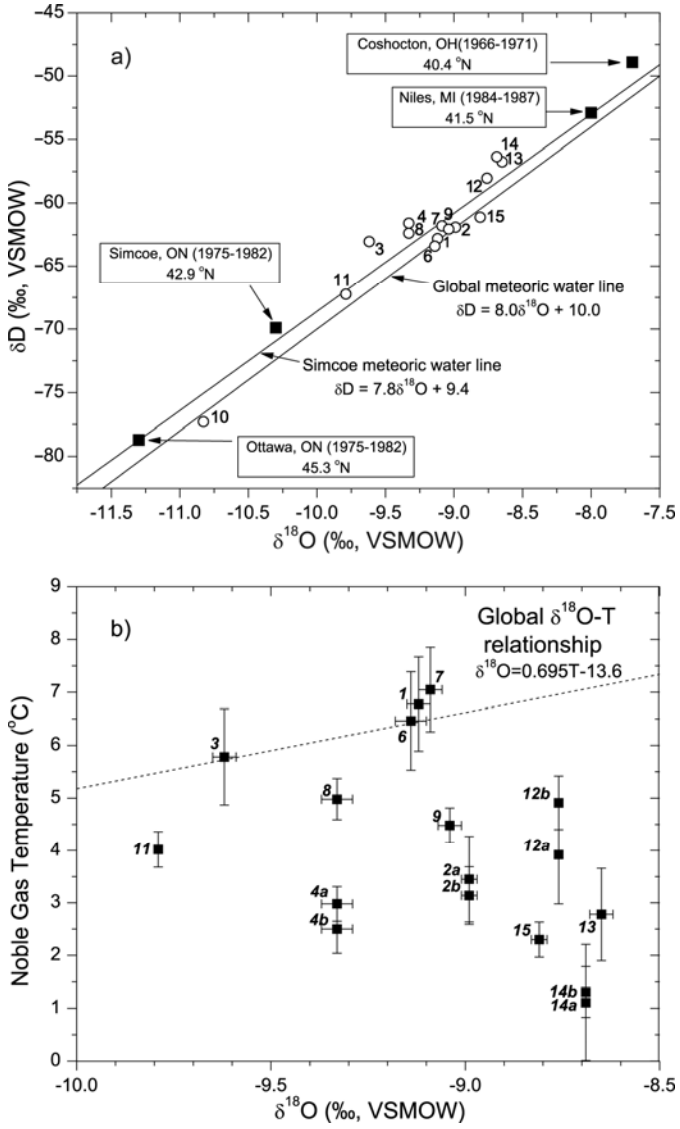

Fig. 2.4. a) δD vs. $\delta^{18}O$ in Michigan groundwaters; mean annual values for Ottawa, Simcoe, Niles and Coshocton, as well as the Simcoe meteoric water line from http://isohis.iaea.org. Global water meteoric line from *Craig* [1961]. **b)** Noble Gas Temperatures versus $\delta^{18}O$ values; global $\delta^{18}O$-T relationship from *Dansgaard* [1964].

In eastern and central North America, mean annual δD and $\delta^{18}O$ precipitation values have a pronounced latitude effect, with a depletion of $\delta^{18}O$ and δD with increased latitude (Fig. 2.4a), a depletion that is likely related to a decrease in the mean annual air temperature [*Dansgaard*, 1964]. Surprisingly, and unlike most of our "modern" samples, early Holocene and late Pleistocene waters follow no particular relationship with temperature (Fig. 2.4b). Importantly, late Pleistocene samples (samples 12-15) with some of the lowest NGT temperatures, yield the highest δD and $\delta^{18}O$ values, and thus present an opposite trend to that normally expected (Fig. 2.4b). Such a decoupling between $\delta^{18}O$ and local temperature precipitation was previously found in Pleistocene waters and attributed, respectively, to a milder climate [*Siegel*, 1991] and to prevailing atmospheric circulation patterns distinct from those in place today [*Plummer*, 1993].

Precipitation in southern Michigan is currently controlled by two distinct moisture sources [*Bryson and Hare*, 1974]: a depleted Pacific source from the west, as well as a more enriched Gulf of Mexico source from the south, reaching the Midwest with a $\delta^{18}O$ value of -10.8‰ and -7.2‰, respectively [*Simpkins*, 1995]. Thus, both an increase in the contribution from the Gulf of Mexico moisture and/or a decrease of contribution from Pacific moisture have the potential to generate precipitation with enriched $\delta^{18}O$ values in southern Michigan, masking the local precipitation temperature effect. This suggests that during the LGM and early deglaciation periods, a different atmospheric circulation pattern was in place in southern Michigan, with a dominant moisture source originating in the Gulf of Mexico. Possible causes for this distinct pattern might be related to the presence of the LIS, which could deflect the Pacific westerly flow, thus, weakening its influence on local Michigan precipitation [*Amundson et al.*, 1996].

2.6. Concluding remarks

Noble gases hold great potential at identifying with relative accuracy major global climatic oscillations, at least since the LGM. Here, the BOA warm phases are recognized for the first time through NGT records. Such records hold also great promise for ascertaining whether or not groundwater recharge occurs under ice-covered regions. Together with stable isotope analysis, they allow for a better understanding of past atmospheric circulation patterns.

Acknowledgments

We thank J.E. Saiers and L.M. Walter for their thoughtful comments, J.R. Hoaglund and an anonymous reviewer for their insightful reviews, and D. Westjohn for his assistance at providing well information. Financial support by the Petroleum Research Fund/American Chemical Society award PRF# 38175-G8 is greatly appreciated.

References

Alley, R.B., and P.U. Clark (1999), The deglaciation of the northern hemisphere: a global perspective, *Annu. Rev. Earth Planet. Sci.*, *27*, 149-182.

Amundson, R.G., O.A. Chadwick, C. Kendall, Y. Wang, and M.J. DeNiro (1996), Isotopic evidence for shifts in atmospheric circulation patterns during the late Quaternary in mid-North America, *Geology*, *24*(1), 23-26.

Ballentine, C.J., and C.M. Hall (1999), Determining paleotemperature and other variables by using an error-weighted nonlinear inversion of noble gas concentrations in water, *Geochim. Cosmochim. Acta*, *63*(16), 2315-2336.

Beyerle, U., R. Purtschert, W. Aeschbach-Hertig, D.M. Imboden, H.H. Loosli, R. Wieler, and R. Kipfer (1998), Climate and groundwater recharge during the last glaciation in an ice-covered region, *Science*, *282*(5389), 731-734.

Brook, G.A., M.E. Folkoff, and E.O. Box (1983), A world model of soil carbon dioxide, *Earth Surf. Proc.*, *8*, 79-88.

Bryson, R.A., and F.K. Hare (1974), The Climate of North America, in *Climate of North* America, World Survey of Climatology, *11*, edited by R.A. Bryson, and F.K. Hare, 1-47.

Castro, M.C., and P. Goblet (2003), Noble gas thermometry and hydrologic ages: Evidence for late Holocene warming in Southwest Texas, *Geophys. Res. Lett.*, *30*(24), 2251, doi:10.1029/2003GL018875.

Clark, P.U., S.J. Marshall, G.K.C. Clarke, S.W. Hostetler, J.M. Licciardi, and J.T. Teller (2001), Freshwater forcing of abrupt climate change during the last glaciation, *Science*, *293*(5528), 283-287, doi:10.1126/science.1062517.

Craig, H. (1961), Isotopic variations in meteoric waters, *Science*, *133*(3465), 1702-1703.

Dansgaard, W. (1964), Stable isotopes in precipitation, *Tellus*, *16*, 436-468.

Dyke, A.S., J.T. Andrews, P.U. Clark, J.H. England, G.H. Miller, J. Shaw, and J.J. Veillette (2002), The Laurentide and Innuitian ice sheets during the Last Glacial Maximum, *Quat. Sci. Rev.*, *21*(1-3), 9-31.

Eichinger, L. (1983), A contribution to the interpretation of 14C groundwater ages considering the example of a partially confined sandstone aquifer, In Proceedings of the 11th International 14C Conference, *Radiocarbon*, *25(2)*, 347-356.

Elias, S.A., K.H. Anderson, and J.T. Andrews (1996), Late Wisconsin climate in northeastern USA and southeastern Canada, reconstructed from fossil beetle

assemblages, *J. Quat. Sci.*, *11*(5), 417-421.

Evans, G.V., R.L. Otlet, A. Downing, R.A. Monkhouse and G. Rae (1979), Some problems in the interpretation of isotope measurements in United Kingdom aquifers, In *Isotope Hydrogeology* II. Vienna, IAEA, 679-708.

Fontes, J.-C., and J.-M. Garnier (1979), Determination of the Initial ^{14}C Activity of the Total Dissolved Carbon: A Review of the Existing Models and a New Approach, *Water Resour. Res.*, *15*(2), 399-413.

Fullerton, D.S. (1986), Stratigraphy and correlation of glacial deposits from Indiana to New York and New Jersey, *Quat. Sci. Rev*, *5*, 23-37.

Gieskes, J. M., and W. C. Rogers (1973), Alkalinity Determination in Interstitial Waters of Marine Sediments, *Journal of Sedimentary Petrology*, *43*(1), 272-277.

Hoaglund, J.R., III, J.J. Kolak, D.T. Long, and G.J. Larson (2004), Analysis of modern and Pleistocene hydrologic exchange between Saginaw Bay (Lake Huron) and the Saginaw Lowlands area, *Geol. Soc. Am. Bull.*, *116*(1-2), 3-15, doi:10.1130/B25290.1.

Jones, G.A., A.P. McNichol, and K.F. VonReden (1990), The National Ocean Sciences AMS facility at Woods Hole Oceanographic Institiution, *Nucl. Inst. Meth. Phys. Res.*, *52*, 278-284.

Kendall, C., and T.B. Coplen (1985), Multisample Conversion of Water to Hydrogen by Zinc for Stable Isotope Determination, *57* (7), 1437-1440.

Kharaka, Y.K., W.D. Gunter, P.K. Aggarwal, E.H. Perkins, and J.D. DeBraal(1988), SOLMINEQ.88: A computer program for geochemical modeling of water-rock interactions: U.S. Geological Survey.

Kipfer, R., W. Aeschbach-Hertig, F. Peeters, and M. Stute (2002), Noble gases in lakes and ground waters, in *Reviews in Mineralogy and Geochemistry*, *47*, 615-700.

Ku, T.C.W. (2001), Organic Carbon-Mineral Interactions in Terrestrial and Shallow Marine Environments, *Ph.D. Dissertation*, University of Michigan, 318pp.

Mandle, R.J., and D.B. Westjohn (1989), Geohydrologic framework and ground-water flow in the Michigan Basin, in *Regional aquifer systems of the United States: aquifers of the Midwestern area, AWRA Monograph Series*, *13*, 83-109.

Pearson, F.J., Jr., and D.E. White (1967), Carbon-14 ages and flow rates of water in the Carrizo Sand, Atascosa County,Texas, *Water Resour. Res.*, *3*, 251-261.

Peteet, D.M., R.A. Daniels, L.E. Heusser, J.S. Vogel, J.R. Southon, and D.E. Nelson (1993), Late-glacial pollen, macrofossils and fish remains in northeastern U.S.A.-The Younger Dryas oscillation, *Quat. Sci. Rev.*, *12*, 597-612.

Plummer, L.N. (1993), Stable isotope enrichment in paleowaters of the southeast Atlantic Coastal Plain, United States, *Science*, *262*(5142), 2016-2020.

Plummer, L.N., E.C. Prestemon, and D.L. Parkhurst (1994), An interactive code (NETPATH) for modeling NET geochemical reactions along a flow PATH-Version 2.0, Water-Resources Investigations Rep 94-4169, USGS, Washington DC.

Pollack, H.N., and S. Huang (2000), Climate reconstruction from subsurface temperatures, *Annu. Rev. Earth Planet. Sci.*, *28*, 339-365.

Prest, V.K. (1969), Retreat of Wisconsin and recent ice in North America, *Geological Survey of Canada Map 1257A.*

Shane, L.C.K., and K.H. Anderson (1993), Intensity, gradients and reversals in late glacial environmental change in East-Central North America, *Quat. Sci. Rev.*, *12*, 307-320.

Sharp, M., J. Parkes, B. Cragg, I.J. Fairchild, H. Lamb, and M. Tranter (1999), Widespread bacterial populations at glacier beds and their relationship to rock weathering and carbon cycling, *Geology*, *27*, 107-110.

Siegel, D.I. (1991), Evidence for dilute of deep, confined ground water by vertical recharge of isotopically heavy Pleistocene water, *Geology*, 19, 433-436.

Simpkins, W.W. (1995), Isotopic composition of precipitation in central Iowa, *J. Hydrol.*, *172*(1-4), 185-207.

Socki, R.A., H.R. Karlsson, and E.K. Gibson (1992), Extraction Technique for the Determination of O-18 in Water Using Preevacuated Glass Vials, *64* (7), 829-831.

Souchez, R., and M. Lemmens (1995), Flow-induced mixing in the GRIP basal ice induced from the CO2 and CH4 records, *Geophysical Research Letters*, *22*, 41-44.

Tamers, M.A. (1967), Radiocarbon ages of groundwater in an arid zone unconfined aquifer, In Isotope Techniques in the Hydrological Cycle, *American Geophysical Union Monograph 11*, 143-152.

Vugrinovich, R. (1986), Patterns of Regional Subsurface Fluid Movement in the Michigan Basin, *Michigan Geological Survey Division Open-File Report 86-6*, 28pp.

Weiss, R.F. (1968), Piggyback sampler for dissolved gas studies on sealed water samples, *Deep Sea Res.*, *15*, 695-699.

Yu, Z., and U. Eicher (1998), Abrupt climate oscillations during the last deglaciation in central North America, *Science*, *282*(5397), 2235-2238.

CHAPTER 3

CROSS-FORMATIONAL FLOW AND SALINITY SOURCES INFERRED FROM A COMBINED STUDY OF HELIUM CONCENTRATIONS, ISOTOPIC RATIOS AND MAJOR ELEMENTS IN THE MARSHALL AQUIFER, SOUTHERN MICHIGAN

Abstract

Helium data and major ion chemistry are presented for the shallow Marshall aquifer in southern Michigan. This data set is subsequently analyzed in conjunction with major element data sets from deeper and shallower water levels previously collected in this area. He excesses and isotopic ratios suggest the presence of tritiogenic ^{3}He in young waters in the Marshall aquifer. He excesses in old groundwater samples are mostly of crustal origin although the presence of a significant mantle He component in some samples cannot be ruled out. He excesses in the Marshall aquifer are unusually high for such shallow depths (≤300m), and reach over two and three orders of magnitude above those of air-saturated water (ASW) for ^{3}He and ^{4}He, respectively. The latter require a He source external to the aquifer, partly supplied by underlying formations within the sedimentary sequence, partly from the crystalline basement. Calibration of He concentrations observed in the Marshall aquifer require He fluxes of 1×10^{-13} and 1.6×10^{-6} cm^{3} STP $cm^{-2}yr^{-1}$ for ^{3}He and ^{4}He, respectively. The latter are far greater than He

fluxes reported in other sedimentary basins around the world (e.g., Paris Basin, Gulf Coast Basin) at similar and far greater depths. Such high He fluxes present at such shallow depths within the Michigan Basin strongly suggest the presence of a dominant vertical water flow component, and further indicate that impact of recharge water at depth is minor. Upward cross-formational flow is also likely responsible for the extremely high salinities present in the shallow sub-surface of the Michigan Basin. The observed positive correlation between helium and bromide concentrations strongly suggests that these two very distinct conservative tracers originate both at greater depths, and further suggests that advection is the dominant transport mechanism within the basin. The occurrence of large-scale cross-formational flow is also consistent with the evolution displayed by the major ion chemistry throughout most of the sedimentary sequence, indicating that solutes from shallow levels carry the signature of deep formation brines.

3.1. Introduction

Subsurface fluids presenting high salinities are a common occurrence in sedimentary basins at great depths (e.g., Gulf Coast Basin, Illinois Basin, Paris Basin) [*Carpenter*, 1978; *Stueber and Walter*, 1991; *Fontes and Matray*, 1993]. By contrast, high salinity fluids are found at all depths in the Michigan Basin, from the deep Ordovician St. Peters Sandstone up to the very shallowest sub-surface levels (Glacial Drift) [*Long et al.*, 1988; *Wilson*, 1989]. In addition to its ubiquitous distribution, some of these high salinity fluids in the Michigan Basin also present some rather unusual characteristics. For example, fluids from the Lower Devonian-Silurian formations (1Km $\leq$ depth $\leq$ 2Km) yield some of the highest salinities (total dissolved solids: TDS > 450

g/L) reported in sedimentary basins around the world, and contain high concentrations of Ca^{2+}, Br^- and Cl^-, as well as low Mg^{2+}, SO_4^{2-}, and HCO_3^- [*Wilson and Long*, 1993a]. Salinities up to 200 g/L are also found in aquifers and aquitards of the Carboniferous-Upper Devonian formations at shallow depths (< 300 m) [*Martini*, 1997]. The origin of such high salinities, however, remains uncertain and has been the focus of numerous studies [e.g., *Long et al.*, 1988; *Wilson*, 1989; *Wilson and Long*, 1993a, b; *Ging et al.*, 1996; *Martini*, 1997; *McIntosh et al.*, 2004]. Indeed, while Lower Devonian-Silurian brines (e.g., Detroit River Group, Niagara/Salina Formation) evolved most likely from evaporated concentrated seawater subsequently modified by water-rock interactions [*Wilson and Long*, 1993a], the evolution of shallow Carboniferous-Upper Devonian formation fluids (e.g. Marshall Sandstone, Antrim Shale, Traverse Formation) does not appear to support extreme seawater evaporation [*Long et al.*, 1988; *Wilson and Long*, 1993b; *Ging et al.*, 1996; *McIntosh et al.*, 2004]. Although the dissolution of evaporites in neighboring formations may explain some of the high salinities observed locally in some shallow formations (e.g., Antrim Formation waters in the northern marginal basin; *McIntosh et al.* [2004]), such a process, however, cannot account for the high Br^- concentrations commonly found in these waters [e.g. *Long et al.*, 1988; *Ging et al.*, 1996].

Upward transport of deep basinal brines and subsequent mixing with meteoric water has been previously proposed to account for the presence of such high salinity waters in near-surface environments in the Michigan Basin [*Long et al.*, 1988; *Mandle and Westjohn*, 1989; *Weaver et al.*, 1995; *Kolak et al.*, 1999; *McIntosh et al.*, 2004]. Such upward transport, however, has not been confirmed.

The study of helium isotopes in large-scale groundwater flow systems offers a powerful tool to investigate cross-formational flow within sedimentary basins [see, e.g., *Castro et al.*, 1998a, b; *Castro and Goblet*, 2003; *Patriarche et al.*, 2004]. Helium isotopes can thus be used to ascertain whether or not cross-formational flow, i.e., upward leakage, is occurring through the entire sedimentary sequence in the Michigan Basin, therefore, better constraining the origin of the very high salinities present at all depths, and, more specifically, in shallow groundwater systems.

Because of its conservative nature, helium is transported in and by the water without reacting with the reservoir rocks. Typically, helium is present in the mantle (e.g., primordial origin), in the crust (nucleogenic and radiogenic origin), and in the atmosphere (as a consequence of the degassing of the Earth). Depending on its origin, helium presents specific characteristics, which allow the identification of its sources and sinks [e.g., *Stute et al.*, 1992; *Hilton and Porcelli*, 2003; *Castro*, 2004; *Saar et al.*, 2005]. Concentrations of He isotopes (^{3}He, ^{4}He) in groundwater frequently exceed those expected for water in solubility equilibrium with the atmosphere (air-saturated water: ASW). These excesses can result from different sources: 1) an excess air component resulting from dissolution of small air bubbles caused by fluctuations of the groundwater table [*Heaton and Vogel*, 1981]; 2) the β-decay of natural and bomb tritium (tritiogenic ^{3}He); 3) the ^{6}Li(n, α)^{3}H (^{3}He) reaction [*Morrison and Pine*, 1955] (nucleogenic ^{3}He); 4) the α-decay of the natural U and Th decay series elements (radiogenic ^{4}He), and; 5) mantle contributions to both ^{3}He and ^{4}He.

In this contribution, helium data and major ion chemistry are presented for the Marshall aquifer in southern Michigan. This shallow groundwater data set is

subsequently analyzed in conjunction with major element data sets from deeper and shallower water levels previously acquired in this area [*Dannemiller and Baltusis*, 1990; *Wilson and Long*, 1993a,b; *McIntosh et al.*, 2004]. In a similar manner to that of observed high salinities, it will be shown that He excesses in the Marshall aquifer are unusually high for such shallow depths. Such high excesses require a helium source external to the aquifer, partly supplied by underlying formations within the sedimentary sequence, partly from the crystalline basement. The positive correlation observed between helium and bromide strongly suggests that these two very distinct conservative tracers both originate at greater depths, and further suggests that advection is the dominant transport mechanism within the basin. Our findings reinforce the notion that upward leakage is the main process responsible for the presence of such high salinities at shallow depths. The latter is also consistent with the evolution displayed by the major ion chemistry through most of the sedimentary sequence, indicating that solutes from shallow levels carry the signature of deep formation brines.

This study aims at illustrating the practical gains achieved in clarifying the nature of cross-formational flow as well as the origin of high salinity fluids through the combined use of helium isotopes and major ion chemistry.

3.2. Geological and Hydrogeologic Background

Located in the northeastern United States, the Michigan Basin is a concentric intracratonic depression floored by crystalline Precambrian basement (Fig. 3.1a, b, c), and consists of a succession of sedimentary rocks from Precambrian to Jurassic that reaches depths over 5Km [*Dorr and Eschman*, 1970; *Catacosinos and Daniels*, 1991].

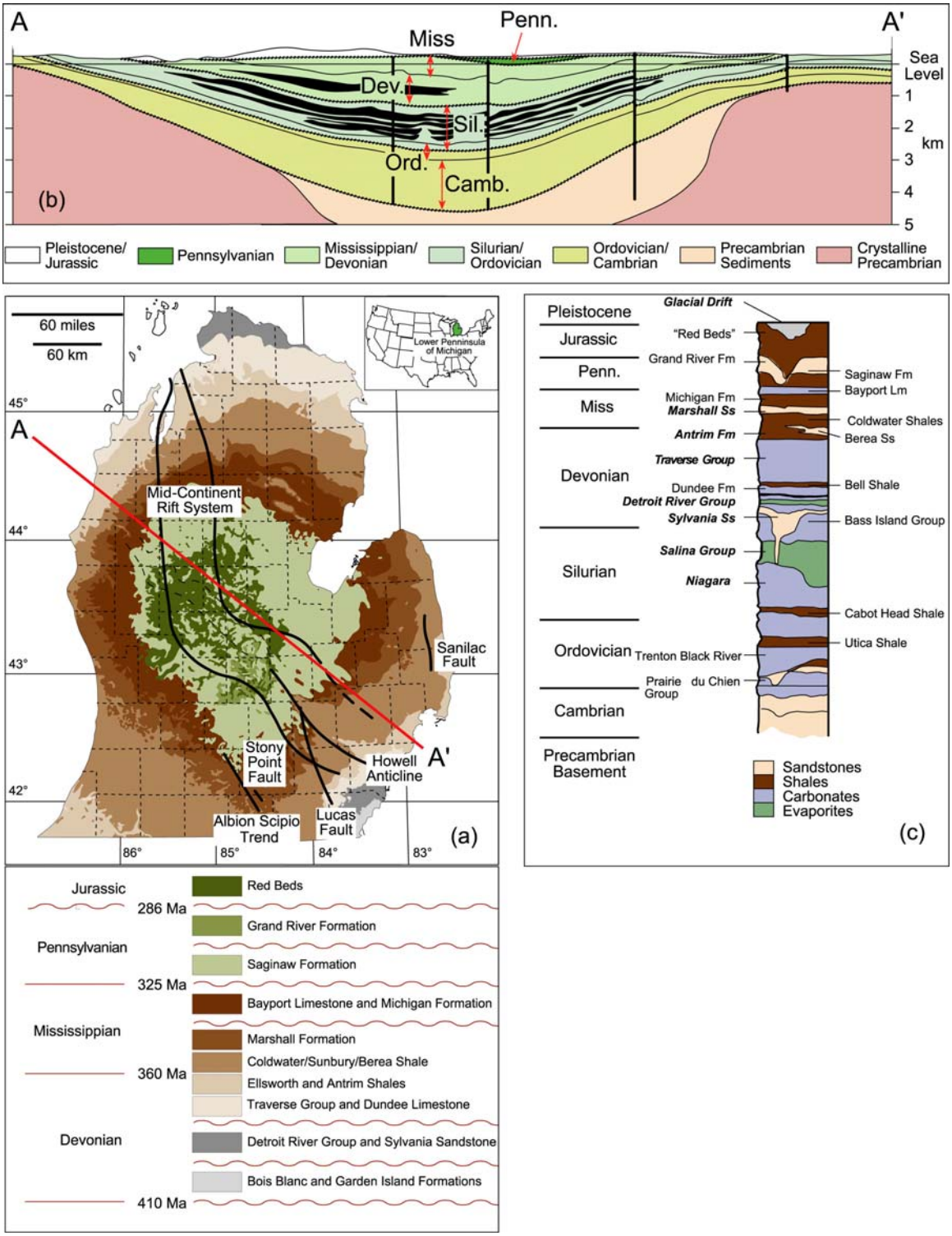

Fig. 3.1. a) Sub-crop formations and major structures present in the Michigan Basin - Lower Peninsula of Michigan [after *Dorr and Eschman*, 1970; *Fisher et al.*, 1988]; **b)** General schematic geologic representation along cross section A-A'; **c)** Stratigraphic succession through the Michigan Basin in which major lithologies present in the basin are identified; units for which chemistry of formation waters is discussed in this study are indicated (bold italic).

The entire sedimentary strata are covered by thick Pleistocene Glacial Drift sediments and are composed mainly of evaporites (e.g., Salina Group), carbonates (e.g., Traverse Formation), shales (e.g., Antrim and Coldwater Formations), and sandstones (e.g., Marshall Formation) (Fig. 3.1c). Depending on their nature, these sedimentary rocks constitute either aquitards (e.g., shale, evaporites) or aquifers (mostly sandstones and reefal and dolomitized limestones), giving rise to a multi-layered aquifer system [*Vugrinovich*, 1986; *Westjohn and Weaver*, 1996].

Major tectonic structures such as the Albion-Scipio Fault, the Lucas Fault, and the Howell Anticline (Fig. 3.1a) are present in southern Michigan and penetrate also the Precambrian crystalline basement [*Fisher et al.*, 1988]. The latter belongs to the Eastern Granite and Rhyolite Province (EGRP), and displays an age of ~ 1.5 Ga [*Hinze et al.*, 1975; *Van Schmus*, 1992; *Menuge et al.*, 2002].

The Marshall aquifer, a major groundwater flow system composed mostly of sandstones of Mississippian age, is located in the central portion of the Michigan Basin (Figs. 3.1a,c, 3.2). The Bayport-Michigan confining units which are composed mostly of shale and limestone overlie the Marshall aquifer, which, in turn, overlies the Coldwater and Antrim Shale confining units (Fig. 3.1c). These formations subcrop at an altitude of ~300m. In the Marshall aquifer in southern Michigan, groundwater flows gravitationally to the NE and NW (Fig. 3.2), and groundwater discharges into Lake Huron and Lake Michigan, in the Saginaw and Michigan Lowlands area, respectively [*Vugrinovich*, 1986; *Mandle and Westjohn*, 1989]. Salinities increase from the recharge (TDS≤0.5 g/L) toward the discharge areas (TDS≥200 g/L).

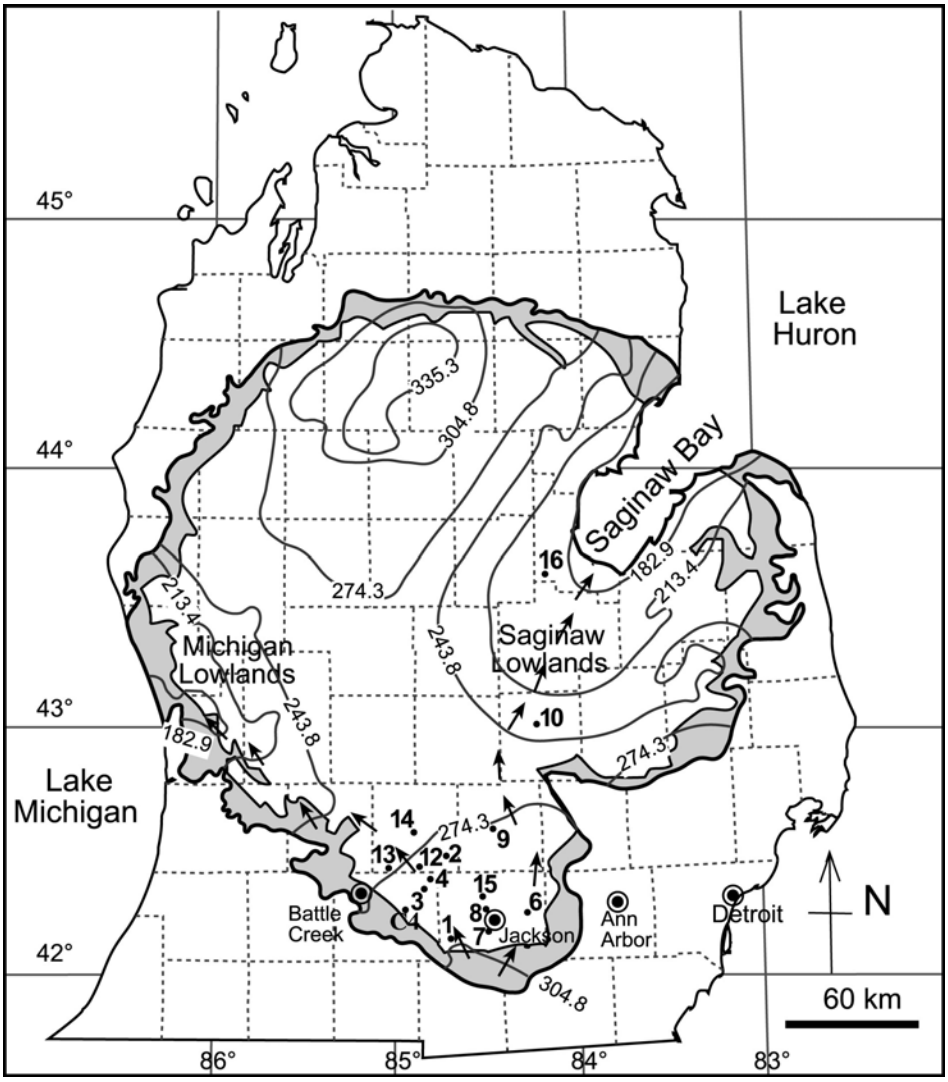

Fig. 3.2. Detailed study area and sample locations for the Marshall aquifer in southern Michigan [adapted from *Mandle and Westjohn*, 1989]. The Marshall aquifer subcrop (shaded area), equipotentials (m, contour lines), and direction of water flow (arrows) are indicated, as well as the location of a groundwater sample for which tritium measurements are available (C4, cf. *Dannemiller and Baltusis* [1990]). Sample numbers are in bold.

3.3. Sampling Techniques and Experimental Methods

Water samples for analysis of noble gases (He, Ne, Ar, Kr and Xe) were collected from 14 wells in the Marshall aquifer (Fig. 3.2) after temperature and pH reached equilibrium. Samples were collected in copper tubes (i.e., standard refrigeration grade 3/8" Cu tubing) and water was allowed to flow through the tubing for ~10 minutes prior to collection. While the water flushed through the system, the absence of gas bubbles that could potentially contaminate or phase fractionate the samples was checked through a transparent plastic tube mounted at the end of the Cu tube. The Cu tubes were then sealed by stainless steel pinch-off clamps [*Weiss*, 1968]. Noble gases were analyzed at the Noble Gas Laboratory at the University of Michigan as described briefly below and in detail by *Ma et al.* [2004], and *Saar et al.* [2005].

Water samples in Cu tubes were attached to a vacuum extraction system and noble gases were quantitatively extracted for inletting into a MAP-215 mass spectrometer. Noble gases were transported using water vapor as a carrier gas through two constrictions in the vacuum system, purified, and sequentially allowed to enter a MAP-215 mass spectrometer using a cryo-separator. The complete measurement procedure comprises estimation of He, Ne, Ar, Kr, and Xe concentrations, and their respective isotopic ratios, with standard errors for volume estimates of 1.5, 1.3, 1.3, 1.5 and 2.2%, respectively. When replicate analyses are available, an error-weighted average is reported.

Water samples collected for analyses of major elements were filtered with a 0.45 μm Gelman Laboratory AquaPrep filter, and subsequently preserved in high-density polyethylene bottles with no head space before analyses. Samples for cation analyses

were acidified to pH<2 by using nitric acid. Major ion chemistry of these samples was determined in the Experimental and Aqueous Geochemistry Laboratory at the University of Michigan. Alkalinity was measured by the Gran-Alkalinity titration method [*Gieskes and Rogers*, 1973] with a precision of ±0.4%. Cation chemistry was determined by inductively coupled plasma-atomic emission spectrometry with a Leeman Labs PlasmaSpec III system (precision, ±2%). Anions were analyzed by ion chromatograpgy (IC) with a Dionex 4000I series (precision, ±1%).

3.4. Helium Systematics

Excess He (He_{exc}) is calculated by removing the ASW (He_{eq}) and excess air (He_{ea}) components from total measured He concentrations (He_{meas}) in water samples [cf., *Stute et al.*, 1992; *Castro et al.*, 2000]. He_{eq} and He_{ea} are estimated based on recharge temperatures derived from Ne, Ar, Kr, and Xe concentrations previously reported by *Ma et al.* [2004], and following *Ballentine and Hall* [1999]. He_{exc} comprises both mantle (He_m) and crustal ($He_c = He_{cin} + He_{cext}$) components, where He_{cin} and He_{cext} are produced in situ within the aquifer and externally at greater depths, respectively, and ^3He_t is the tritiogenic ^{3}He, so that:

$$\begin{aligned} {}^3He_{exc} &= {}^3He_{meas} - {}^3He_{eq} - {}^3He_{ea} \\ &= {}^3He_{cin} + {}^3He_{cext} + {}^3He_m + {}^3He_t \end{aligned} \tag{3.1}$$

and

$$
\begin{aligned}
{}^4He_{exc} &= {}^4He_{meas} - {}^4He_{eq} - {}^4He_{ea} \\
&= {}^4He_{cin} + {}^4He_{cext} + {}^4He_m
\end{aligned}
\tag{3.2}
$$

Concentrations of ^{3}He in equation (3.1) are given by ${}^3He_{eq} = {}^4He_{eq} \times R_{eq}$, ${}^3He_{ea} = {}^4He_{ea} \times R_a$, and ${}^3He_{meas} = {}^4He_{meas} \times R_{meas}$, where $R_{eq} = (1.360 \pm 0.006) \times 10^{-6}$ is the ^{3}He/^{4}He ratio for ASW [*Benson and Krause*, 1980], $R_a = (1.384 \pm 0.013) \times 10^{-6}$ is the atmospheric ^{3}He/^{4}He ratio [*Clarke et al.*, 1976], and R_{meas} is the total measured ^{3}He/^{4}He ratio. We also define the ratios for excess, crustal and mantle helium as:

$$
R_{exc} = \frac{{}^3He_{exc}}{{}^4He_{exc}} \qquad R_c = \frac{{}^3He_{cin} + {}^3He_{cext}}{{}^4He_{cin} + {}^4He_{cext}} \qquad R_m = \frac{{}^3He_m}{{}^4He_m} \tag{3.3}
$$

A schematic diagram (Fig. 3.3) shows the main components of He which may be found in sedimentary fluid as discussed above.

3.5. Marshall Aquifer - Results and Discussion

3.5.1 General data overview

He concentrations and isotopic ratios, ^{14}C and calendar ages, pH, temperature, major element data, as well as sample names, locations, and well depths are given in Tables 3.1 and 3.2, respectively. ^{14}C ages were estimated according to *Fontes and Garnier* [1979]'s correction model and a half-life value of 5730 yrs was used as suggested by these authors. ^{14}C ages were subsequently converted into calendar ages using CALIB Rev4.4.1 [*Stuiver and Reimer, 1993*]. Additional details on ^{14}C age estimation can be found in *Ma et al.* [2004].

Table 3.1. Sample locations, He concentrations and isotopic ratios as well as groundwater ages

Sample Number	County	Latitude	Longitude	Depth (m)	$^4He_{meas}$ (cm^3 STP/g)	+/- 1σ	R_{meas}/R_a	+/- 1σ	$^4He_{exc}$ (cm^3 STP/g)	+/- 1σ	$^3He_{exc}$ (cm^3 STP/g)	+/- 1σ
1	Jackson	42.175	-84.644	82	1.38E-07	2.07E-09	0.886	0.020	4.56E-08	2.49E-09	4.20E-14	8.13E-15
2	Eaton	42.483	-84.671	110	4.28E-07	6.42E-09	0.256	0.006	3.35E-07	6.57E-09	2.29E-14	
3	Calhoun	42.365	-84.796	73	6.86E-08	1.03E-09	0.857	0.025	1.95E-08	1.27E-09	1.45E-14	5.42E-15
4a	Calhoun	42.414	-84.750	85	2.07E-05	3.11E-07	0.161	0.005	2.07E-05	3.11E-07	4.53E-12	1.60E-13
4b					2.28E-05	3.42E-07	0.144	0.006	2.27E-05	3.42E-07	4.46E-12	2.02E-13
6	Jackson	42.250	-84.217	111	1.72E-07	2.58E-09	0.439	0.015	1.21E-07	2.69E-09	3.54E-14	6.19E-15
7	Jackson	42.243	-84.393	117	3.49E-07	5.24E-09	0.394	0.011	2.98E-07	5.29E-09	1.20E-13	7.37E-15
8	Jackson	42.275	-84.383	122	1.20E-07	1.80E-09	1.383	0.042	9.81E-09	2.44E-09	7.85E-14	8.85E-15
9	Ingham	42.606	-84.417	171	1.87E-07	2.81E-09	0.564	0.016	1.31E-07	2.93E-09	6.83E-14	5.23E-15
10a	Shiawassee	42.982	-84.200	110	1.64E-06	2.46E-08	0.082	0.009	1.58E-06	2.46E-08	9.88E-14	2.35E-14
10b					1.62E-06	2.43E-08	0.121	0.018	1.55E-06	2.43E-08	1.82E-13	4.41E-14
12a	Eaton	42.451	-84.882	88	4.61E-06	6.92E-08	0.066	0.012	4.54E-06	6.92E-08	3.35E-13	7.71E-14
12b					4.33E-06	6.50E-08	0.040	0.007	4.27E-06	6.50E-08	1.52E-13	4.22E-14
13	Eaton	42.444	-85.017	86	3.44E-06	5.16E-08	0.051	0.008	3.39E-06	5.16E-08	1.65E-13	3.86E-14
14a	Eaton	42.575	-84.896	107	9.59E-06	1.44E-07	0.081	0.024	9.52E-06	1.44E-07	9.80E-13	3.19E-13
14b					1.11E-05	1.67E-07	0.033	0.008	1.10E-05	1.67E-07	4.08E-13	1.23E-13
15	Jackson	42.354	-84.372	107	5.83E-06	8.75E-08	0.052	0.012	5.76E-06	8.75E-08	3.30E-13	9.71E-14
16	Bay	43.635	-84.129	313	3.35E-04	5.03E-06	0.036	0.004	3.35E-04	5.03E-06	1.66E-11	1.87E-12
ASW [c]					4.76E-08		1.000					

[a] *Ma et al.* [2004].
[b] Calendar ages calculated from ^{14}C ages after *Stuiver and Reimer* [1993].
[c] Air-saturated water (ASW) for a pressure of 1 atm and a temperature of 5°C [*Ozima and Podosek*, 2002].

Table 3.1.(continued)

Sample Number	R_{exc}/R_a	+/- 1σ	^{14}C age[a] (yr)	+/- 1σ	Calendar age[b] (yr)
1	0.665	0.134	"modern"		0
2	0.049	0.017	6046	674	6883
3	0.537	0.204	780	800	790
4a	0.158	0.006	4726	699	5362
4b	0.142	0.007			
6	0.211	0.037	"modern"		0
7	0.291	0.019	"modern"		0
8	5.784	1.581	"modern"		0
9	0.377	0.030	"modern"		0
10a	0.045	0.011	6377	663	7169
10b	0.085	0.021			
12a	0.053	0.012	11142	658	13080
12b	0.026	0.007			
13	0.035	0.008	9558	667	10946
14a	0.074	0.024	17348	655	20684
14b	0.027	0.008			
15	0.041	0.012	12778	784	15134
16	0.036	0.004			
ASW [c]					

Table 3.2. Major element data for samples from the Marshall aquifer

Sample number	pH	T (^{o}C)	TDS (mg/L)	Alkalinity (meq/kg)	Cl^- (mM)	Br^- (mM)	SO_4^{2+} (mM)	Na^+ (mM)	Ca^{2+} (mM)	Mg^{2+} (mM)	K^+ (mM)	Sr^{2+} (mM)	CB[a] %
1	7.0	11.3	541.0	5.914	0.496	0.0000	0.303	0.335	2.147	1.028	0.023	0.0014	-2.2
2	7.3	10.4	560.1	6.486	0.074	0.0000	0.245	0.812	1.688	1.208	0.238	0.0260	-1.5
4	7.0	9.8	1707	6.068	0.689	0.0000	7.579	2.489	8.895	1.332	0.698	0.1157	1.8
6	7.7	11.1	499.7	5.386	0.462	0.0005	0.098	0.665	1.728	0.843	0.065	0.0258	-1.0
7	7.4	11.3	756.3	6.297	1.748	0.0018	1.008	2.140	2.747	1.243	0.074	0.0103	0.8
8	7.1	11.7	789.5	7.113	1.021	0.0010	1.247	0.364	3.450	1.297	0.036	0.0021	-3.6
9	7.3	10.8	626.5	6.258	0.708	0.0000	0.620	0.717	2.385	1.297	0.076	0.0096	-0.3
10	7.7	11.8	958.2	6.435	1.418	0.0023	2.398	8.994	1.086	0.672	0.100	0.0324	-0.2
12	8.0	11.5	1062	6.861	2.692	0.0106	2.590	8.099	1.654	0.999	0.158	0.0208	-4.2
13	8.2	11.2	1020	6.863	5.797	0.0511	0.694	6.399	3.048	1.251	0.249	0.0436	3.9
14	8.1	12.2	1530	5.128	15.21	0.0499	1.714	13.44	3.206	1.597	0.287	0.0551	-1.0
15	7.4	12.0	1376	7.646	8.600	0.0739	1.464	11.48	3.126	1.460	0.357	0.0531	4.4
16	5.4	16.9	217105	0.286	4711	21.536	0.479	3164	708.4	310.2	19.10	7.2209	4.9

[a] Charge balance in %.

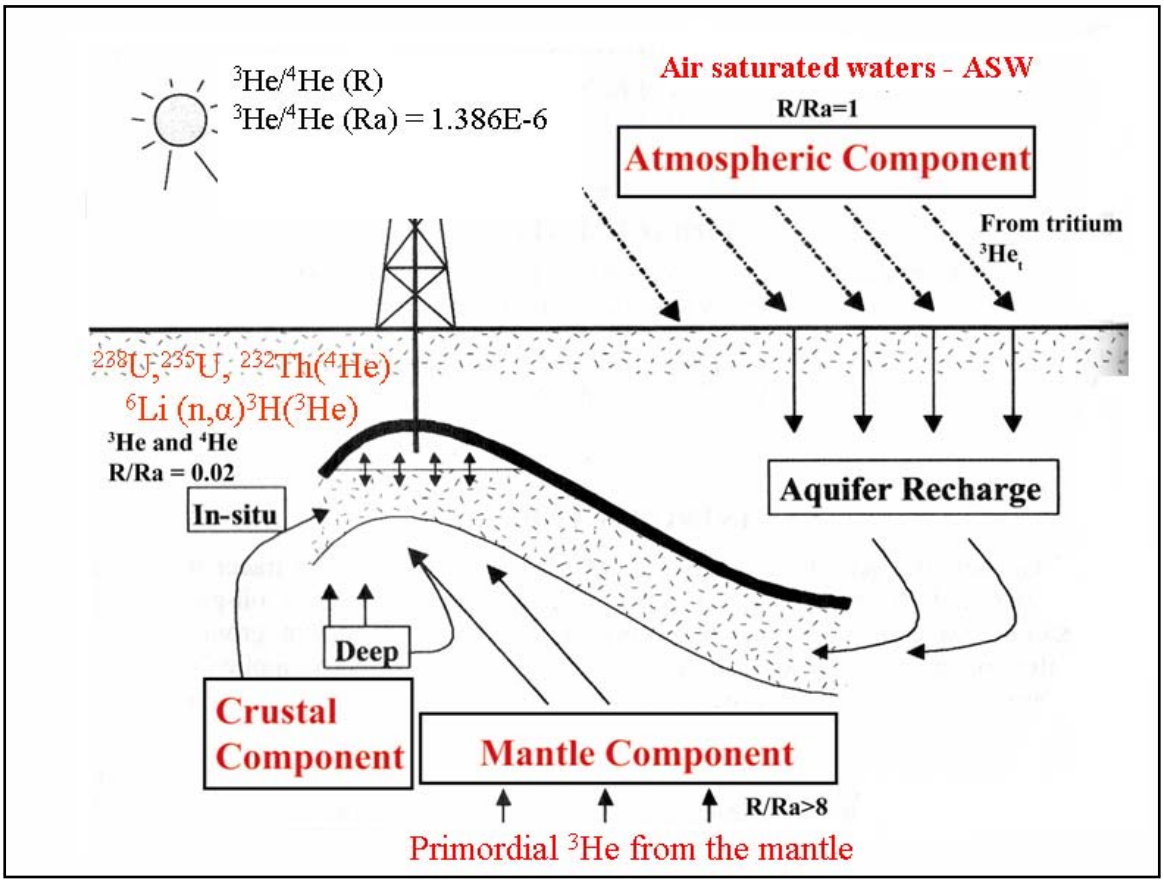

Fig. 3.3. Schematic diagram showing the main components of He which may be found in sedimentary fluids. The typical He isotopic ratios are reported for each component. [*modified after Ballentine et al.*, 2002]

For most of the Marshall groundwater samples, ^{3}He and ^{4}He concentrations are found in excess of those expected for water in solubility equilibrium with the atmosphere (Table 3.1). He excesses vary and are greater for ^{4}He than for ^{3}He. These excesses reach values of over two and three orders of magnitude above those of ASW for ^{3}He and ^{4}He, respectively, and are particularly high for sample 16, located in the Saginaw Lowland discharge area in the central portion of the basin (Fig. 3.2). Similarly, R_{exc}/R_a values vary from 5.78 to 0.03, and are far greater for "modern waters" (samples 1, 3, 6-9, Table 3.1) than older ones (e.g., samples 14a,b, 16, Table 3.1). The observed decrease in R_{exc}/R_a values is accompanied by an increase in $^{3}He_{exc}$ and $^{4}He_{exc}$ (Figs. 3.4a, b).

^{3}He and ^{4}He excesses increase both with groundwater age and TDS (Tables 3.1, 3.2). With the exception of samples 4a,b, $^{3}He_{exc}$ and $^{4}He_{exc}$ increase almost linearly with groundwater age (Fig. 3.4c), and indicate a progressive accumulation of He isotopes in the Marshall aquifer over time. Approximate regional flow paths are indicated in Figure 3.2. Note, however, that distance from recharge areas to the different sample locations are highly variable due to the concentric shape of the Marshall subcrop (Fig. 3.2). As a result, groundwater ages and corresponding He excesses of the different water samples reflect this variability. TDS values increase from ~ 0.5g/L for samples located at the proximity of recharge areas ("modern waters") up to 217 g/L for sample 16, located in the Saginaw Lowland discharge area (Fig. 3.2, Table 3.2). This progressive increase of He excess components as well as TDS is also accompanied by a marked evolution in water chemistry (Fig. 3.4c). Specifically, young ("modern") waters display major-ion compositions dominated by a calcium-bicarbonate ($Ca\text{-}HCO_3$) facies, and evolve progressively into a dominantly sodium-bicarbonate ($Na\text{-}HCO_3$) facies. As groundwater

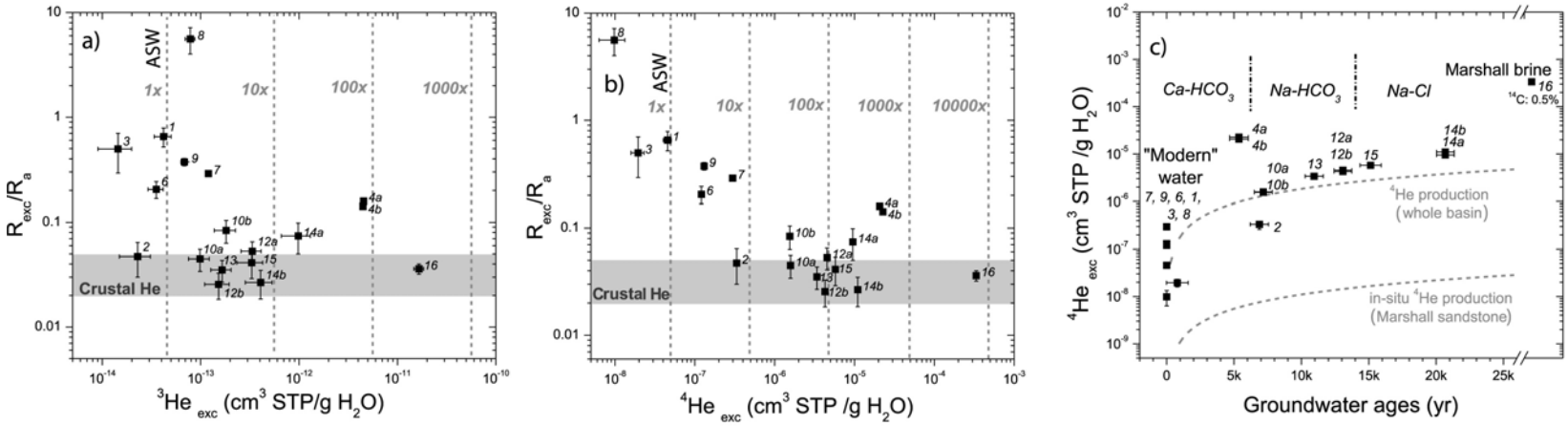

Fig. 3.4. a), b) R_{exc}/R_a values versus ^{3}He and ^{4}He excess concentrations for samples from the Marshall aquifer, respectively; Vertical dashed lines indicate 1×, 10×, 100×, 1000× the ASW value at 1 atm pressure and 5°C; shaded areas indicate typical crustal R_c/R_a values (0.02-0.05); **c)** ^{4}He excess versus groundwater (calendar) ages; dashed lines indicate He accumulation resulting both from in-situ production in the Marshall sandstone, and from the sedimentary sequence underlying the Marshall aquifer ("whole basin"), respectively; groundwater hydrochemical facies are also indicated; "Modern" water refers to samples for which the water age ≤1000 years (Table 3.1; see *Ma et al.* [2004]); sample 16 corresponds to a Marshall brine sample with TDS~217g/L for which it was not possible to fit a ^{14}C model age due to its high salinity; 0.5% corresponds to the ^{14}C activity measured.

ages become older and salinity increases (e.g., samples 14, 15, 16), the groundwater chemistry shifts progressively into a dominantly sodium-chloride (Na-Cl) facies. Samples 4a,b, with an unusual chemistry type and unusually high He excesses and R_{exc}/R_a value as compared to its groundwater age are an exception to this pattern, and suggest a very distinct origin to these specific waters. This is discussed below.

3.5.2 Excess ^{3}He – tritiogenic versus mantle and crustal components

While $^4He_{exc}$ present in most groundwaters has a dominant crustal origin [e.g., *Castro et al.*, 1998a,b; *Castro et al.*, 2000], $^3He_{exc}$ can result from three distinct sources: from natural and/or bomb ^{3}H decay, in addition to a mantle and/or crustal origin. These three different ^{3}He sources can be identified partly based on R_{exc}/R_a values, ^{3}He and ^{4}He excesses, as well as on groundwater age considerations [e.g., see *Saar et al.*, 2005]. For example, mantle-derived He is characterized by $8 \leq R_m/R_a \leq 30$ [e.g., *Graham*, 2002; *Hilton and Porcelli*, 2003] while very young waters carrying an important ^{3}He tritiogenic component can also yield $R_{exc}/R_a > 1$ [*Schlosser et al.*, 1989] (atmospheric ratio $R/R_a=1$). By contrast, He produced in the crystalline crust as well as in shale dominated formations results in $0.02 \leq R_c/R_a \leq 0.05$ while typical in situ production in aquifers (e.g., sandstones, limestones) yields values of about one order of magnitude lower, with $0.001 \leq R_c/R_a \leq 0.005$ [e.g., *Castro*, 2004]. In the analysis that follows we adopt $0.02 \leq R_{exc}/R_a \leq 0.05$ as our "reference" crustal value (Figs. 3.4a,b). Thus, R_{exc}/R_a values greater than the latter strongly suggest the presence of a significant mantle or tritiogenic ^{3}He contribution. We attempt to identify these two distinct sources below.

"Modern" water samples (1, 3, 6-9, cf. Table 3.1; see discussion by *Ma et al.* [2004]), i.e., samples at the proximity of recharge areas display small He excesses (<10 times that of ASW; Figs. 3.4a,b) and $0.21 \leq R_{exc}/R_a \leq 5.78$, the latter being far greater than typical crustal He values (0.02-0.05). Thus, these result either from natural or bomb ^3H decay or the addition of a mantle He component. Although no tritium measurements are available for our groundwater samples, tritium analysis performed in 1986 on one groundwater sample from the Marshall aquifer in our study area with similar ^{14}C activity and chemical composition to that of our young samples yielded 22TU [*Dannemiller and Baltusis*, 1990]. This value is well above the natural ^3H background in precipitations (usually ≤5 TU, e.g. *Roether* [1967]) and therefore indicates the addition of bomb test ^3H to this groundwater. Between 1963 (time of the bomb ^3H peak, e.g., *IAEA/WMO* [1998]) and 1986, about two ^3H half lives have elapsed. A rough estimation was performed for the amount of ^3H that would be present in the recharge waters of this aquifer when the bomb tests reached their maximum. This simple calculation yields a value of ~94 TU. Therefore between 1963 and 2003 (date of our sampling campaign), a maximum of 85 TU have decayed into ^3He in these groundwaters, equivalent to the addition of 2.1×10^{-13} cm^3 ^3He STP/g in water (1 TU = 2.5×10^{-15} cm^3 ^3He STP/g). This amount of anthropogenic ^3He is capable of explaining the ^3He excess observed in our young samples (^3He excess: 1.5×10^{-14} to 1.2×10^{-13} cm^3 STP/g). Although we cannot be certain that most $^3He_{exc}$ in these samples results from bomb tritium decay due to water age uncertainties associated with these samples (see discussion by *Ma et al.* [2004]), the observed high R_{exc}/R_a values associated with these young water ages strongly suggests that most $^3He_{exc}$ in these samples are the result of anthropogenic tritium decay. The

simultaneous presence of a small amount of $^{4}He_{exc}$ indicates a mixture between this young water component and an older one. The observed decrease of R_{exc}/R_a values with increased $^{3}He_{exc}$ and $^{4}He_{exc}$ and increased groundwater ages further supports this hypothesis. The presence of a small mantle He component in these samples although less likely, cannot be excluded completely.

With the exception of "modern" water samples as well as sample 4, all other samples (ages>5kyrs, cf. Table 3.1, Figs. 3.4a,b) present lower R_{exc}/R_a ratios, ranging from 0.09 (10b) to 0.03 (12b, 14b), indicative of an increasing dominance of crustally produced ^{3}He and ^{4}He in these waters. Although most of these R_{exc}/R_a values fall into the typical crustally produced He values ($0.02 \leq R_c/R_a \leq 0.05$), it is important to note that the presence of a significant mantle component that is potentially masked by dilution of the original signal by crustally produced He cannot be excluded (e.g., see discussion by *Castro* [2004]).

As previously mentioned, samples 4a,b present an unusual He signature, with unusually high He excesses (~ up to and above 2 orders of magnitude that of the ASW for ^{3}He and ^{4}He, respectively) and high R_{exc}/R_a values (~0.16) as compared to its groundwater age (~5 kyrs). In addition, and as discussed above, the amount of tritiogenic He that is potentially present is these waters is negligible with respect to its $^{3}He_{exc}$. Thus, this high R_{exc}/R_a value is clearly indicative of the presence of a mantle He component. If one assumes a simple binary mixture between a typical mantle component with $R_m/R_a = 8$ and a crustal component with $R_c/R_a=0.02$, the corresponding mantle contribution is ~2%. Significant mantle He contributions in groundwaters are commonly found in active tectonic geological settings [e.g., *Stute et al.*, 1992; *Hilton et al.*, 2002; *Saar et al.*, 2005].

However, mantle He signatures in groundwater from stable tectonic settings have also been documented [*Torgersen et al.*, 1995; *Siegel et al.*, 2004; *Castro*, 2004]. The mantle signature found in samples 4a,b together with the observed high ^{3}He and ^{4}He excesses, strongly suggests a deeper origin for these water samples and the potential presence of a local deep permeable fault.

On the basis of the R_{exc}/R_a values and $^3He_{exc}$ values from the Marshall aquifer, it is clear that the addition of tritiogenic ^{3}He can account for most of the observed ^{3}He excess in "modern" water samples, while the older water samples are largely dominated by crustal (nucleogenic) ^{3}He. A smaller mantle contribution is also present in at least some of the older samples.

3.5.3 Crustal ^{3}He and ^{4}He components: external versus in-situ production origin

From the above discussion, it is clear that, with the exception of tritiogenic ^{3}He in young waters and the presence of a small mantle component in older samples, most of the excess ^{3}He and ^{4}He in the groundwaters of the Marshall aquifer is of crustal origin. Here, we discuss the origin of the crustally produced ^{3}He and ^{4}He, in order to ascertain whether or not $^3He_{exc}$ and $^4He_{exc}$ present in the Marshall waters result mostly from in-situ production within the aquifer, or if instead, it has an external deeper origin. With regard to the latter, it is also important to ascertain whether or not the sedimentary sequence underlying the Marshall is the main contributor or if the crystalline basement is providing most of the He present in the Marshall groundwaters.

To answer to this question, production rates of ^{3}He and ^{4}He were calculated for the Marshall Sandstone, the sedimentary formations underlying the Marshall aquifer, as well as the crystalline basement, as follows [e.g. *Ballentine*, 1991]:

$$P(^3He) = (6.035[U] + 1.434[Th]) \times [Li] \times 10^{-23} cm^3 STP g_{rock}^{-1} yr^{-1} \quad (3.4)$$

$$P(^4He) = 1.207 \times 10^{-13}[U] + 2.867 \times 10^{-14}[Th] cm^3 STP g_{rock}^{-1} yr^{-1} \quad (3.5)$$

where $[Li]$, $[U]$, and $[Th]$ represent the Li, U, and Th concentrations (ppm), respectively (Table 3.3). The accumulation rate of He isotopes in the water was then estimated according to the expression:

$$[P_{He}^i]_{H_2O} = P(^iHe) \times \rho_r \times \Lambda \times ((1-\omega)/\omega) \times \rho_w cm^3 STP g_{H2O}^{-1} yr^{-1} \quad (3.6)$$

where i represents ^{3}He or ^{4}He, ρ_r is the mass density of the rock in gcm^{-3}, ρ_w is the density of the water in gcm^{-3}, ω is the porosity of the reservoir rock and Λ is the transfer efficiency of He from the rock matrix to the water. For sediments, it can be assumed that Λ=1 [e.g., *Torgersen*, 1980; *Torgersen and Clarke*, 1985]. Table 3.3 lists the ^{3}He and ^{4}He in-situ production rates calculated using Eqn. 3.6, thickness and porosity values for the Marshall aquifer, and the whole sedimentary sequence underlying the Marshall in the study area. Corresponding R/R_a production values as well as ^{3}He and ^{4}He accumulation rates in the water for the Marshall and underlying sedimentary sequences are also indicated. ^{4}He production rates for the crystalline basement are also given.

Table 3.3. Calculated ^{3}He and ^{4}He production rates and corresponding $^{3}He/^{4}He$ and R_{in}/R_{a} ratios in the Michigan Basin, as well as ^{4}He production rates in the crystalline basement

Lithology	Thickness (m)	Porosity (%)	Th (ppm)	U (ppm)	Li (ppm)	Density[d] (g cm^{-3})	P[^{4}He] (cm^{3} STP g$^{-1}_{rock}$ yr^{-1})	P[^{3}He] (cm^{3} STP g$^{-1}_{rock}$ yr^{-1})	$^{3}He/^{4}He$	R_{in}/R_{a}	P[^{4}He] (cm^{3} STP g$^{-1}_{H2O}$ yr^{-1})	P[^{3}He] (cm^{3} STP g$^{-1}_{H2O}$ yr^{-1})
Marshall sandstone[a]	90	20	1.7	0.45	15	2.6	1.03E-13	7.73E-22	7.50E-09	0.005	1.07E-12	8.04E-21
Sedimentary sequence underlying Marshall[b]	2400		7.4	2.7	32	2.5	5.38E-13	8.61E-21	1.60E-08	0.012	1.83E-10	4.03E-18
Crystalline basement[c]			12	4			8.27E-13					

[a] U, Th, and Li estimated from average lithological composition after *Parker* [1967]; thickness and porosity values after *Westjohn and Weaver* [1996].
[b] Based on average lithological composition: shale (40%), limestone (20%), dolomite (20%), evaporites (10%), and sandstone (10%) [after *Speece et al.*, 1985]; values of U, Th, and Li estimated from average lithological composition after *Parker* [1967] and *Tolstikhin et al.* [1996].
[c] U and Th estimated from outcrop area for the crystalline basement [*Menuge et al.*, 2002].
[d] Density of rocks estimated after *Handbook of Physical Constants*, Volume II, CRC Press, Florida, 1966.

If it is assumed that all ^{3}He and ^{4}He excesses in the Marshall groundwaters results from in-situ production and if one excludes all "modern" samples, under such accumulation rates (Table 3.3) it would take between 2.3 and 1700Myrs, and 0.2 and 300Myrs to produce the observed $^{3}He_{exc}$ and $^{4}He_{exc}$, time periods that would correspond to the required age of these groundwaters. Such groundwater ages seem to be far too high for most samples, and are clearly in contradiction with estimated ^{14}C ages (Table 3.2). In addition, the accumulation time required for the observed $^{3}He_{exc}$ in sample 16 (1700Myrs) is far greater than the age of the Marshall Sandstone itself, clearly indicating that most of the excess He has an external origin to the aquifer. Similarly, the contrast between R_{exc}/R_a ratios in the Marshall aquifer (0.03-0.15) for samples with water ages ≥5kyrs and that of in-situ produced ratios (0.005) strongly suggests that He excesses in the Marshall aquifer have an external origin, with potentially some mantle contribution [e.g., see *Castro*, 2004]. Taking into account groundwater ages as well as in-situ production rates, the expected He accumulation in the water resulting solely from in-situ production within this sandstone aquifer is ~2-3 orders of magnitude lower than the observed excess He (Fig. 3.4c). It is thus concluded that in-situ production is a negligible He source in the Marshall sandstone relative to an external contribution. Such external He sources to aquifers have been documented in a diversity of sedimentary basins around the world [e.g., *Torgersen and Clarke*, 1985; *Stute et al.*, 1992; *Castro et al.*, 1998a, b; *Castro et al.*, 2000; *Castro*, 2004]. The occurrence of an external He flux has been widely accepted as the main He excess source in multilayered aquifer systems. Alternatively, *Solomon et al.* [1996] have proposed that diffusion of inherited ^{4}He could become the

dominant external He source under specific conditions (e.g., shallow aquifers, <~20m in depth with high water velocities). Such conditions, however, do not apply to our system.

External sources can be provided either by the underlying sedimentary sequence or by the crystalline basement, or both. We now attempt to quantify these. The whole sedimentary sequence underneath the study area is ~2.4 km thick and contains mainly carbonates, shales, sandstones, and evaporites [e.g., *Fisher et al.*, 1988; *Speece et al.*, 1985]. Taking into account these different lithological compositions, thickness, and respective production rates, it is estimated that the entire sedimentary sequence is capable of producing ~20 and ~50% of $^{3}He_{exc}$ and $^{4}He_{exc}$ in the Marshall aquifer (Fig. 3.4c), respectively, if one excludes "modern" samples as well as sample 4. Indeed, production within the sedimentary sequence remains negligible for the latter (0.5 and 4% for $^{3}He_{exc}$ and $^{4}He_{exc}$, respectively). The estimated contributions represent maximum bounds with respect to the observed He excesses. Thus, while ^{3}He production within the sedimentary sequence is a relatively marginal source for ^{3}He in the Marshall (≤20%), production of ^{4}He within the basin underlying the Marshall has the potential to account for a non-negligible amount (≤50%) of the total observed $^{4}He_{exc}$ in this aquifer.

From the above discussion it is clear that an external source dominates both, $^{3}He_{exc}$ and $^{4}He_{exc}$ in the Marshall aquifer. While the sedimentary sequence underlying the Marshall aquifer has the potential to play an important role at providing ^{4}He concentrations, most of the $^{3}He_{exc}$ appears to have its source in the crystalline basement. In the following section, we estimate the external vertical ^{3}He and ^{4}He fluxes entering the Marshall aquifer from the combined underlying sedimentary sequence and crystalline

basement, and attempt at better constraining the He provided by each one of these sources.

3.5.4 He transport simulations – estimation of ^{3}He and ^{4}He external fluxes

3.5.4.1. Conceptual model

In order to quantify the transfer of He to, and its accumulation in, a confined aquifer, *Torgersen and Ivey* [1985] proposed a simple model assuming that steady-state for flow and transport is reached in the system. Here, a similar procedure is adopted to quantify the ^{3}He and ^{4}He upward fluxes entering the bottom of the Marshall aquifer. The advection-dispersion equation governing the model is given by:

$$v_x \frac{\partial C}{\partial x} + D_T \frac{\partial^2 C}{\partial z^2} = P \tag{3.7}$$

where v_x is the advective pore velocity in the x (horizontal) direction, x is the distance from the recharge area of the aquifer, z is the relative vertical position inside the aquifer, C corresponds to the $^3He_{exc}$ or $^4He_{exc}$ concentrations, D_T is the coefficient of hydrodynamic transverse dispersion given by $D_T = \alpha_z v_x + d$ (see, for example, *Freeze and Cherry* [1979]). Thus, it includes both vertical dispersion, expressed as a function of transverse dispersivity (α_z), and diffusion expressed by the molecular diffusion coefficient for the solute in the porous medium d. P is a source term, and in our case, it represents the accumulation of ^{3}He and ^{4}He in the water resulting from in-situ production, as calculated from equation (3.6). The prescribed boundary conditions for this model are: 1) a ^{3}He or ^{4}He concentration that initially is zero for all depths in the aquifer; 2) a flux J_0

of ^{3}He or ^{4}He entering the aquifer across the bottom boundary z_0, assumed to be constant; 3) a no-flux ^{3}He and ^{4}He boundary condition at the top of the aquifer, i. e., no He losses occurring through the top of the aquifer are allowed. He studies in multi-layered aquifer systems in which the advective, dispersive and diffusive fluxes were quantified [see, *Castro et al.*, 1998b] show a very important reduction of these losses of up to 30 times the (total vertical flux) flux J_0 entering at the bottom of the aquifer. In view of such results, the prescribed zero He flux boundary condition at the top of the aquifer seems to be reasonable as compared to the J_0 flux entering the bottom of the aquifer [see also *Castro et al.*, 2000].

The analytical solution to this problem is given by [*Torgersen and Ivey*, 1985]:

$$C = Pt + \frac{J_0 t}{z_0 \rho \omega} + \frac{J_0 z_0}{D_T \rho \omega}\left[\frac{3\left(\frac{z}{z_0}\right)^2 - 1}{6} - \frac{2}{\pi^2}\sum_{m=1}^{\infty}\frac{(-1)^m}{m^2}\exp\left(-\frac{D_T m^2 \pi^2 t}{z_0^2}\right)\cos\left(\frac{m\pi z}{z_0}\right)\right] \quad (3.8)$$

where z_0 is the thickness of the aquifer (m), ρ is the water density (1 gcm^{-3}), ω is the porosity, J_0 is the upward ^{3}He or ^{4}He flux (cm^3 STP cm$^{-2}_{\text{rock}}$ yr^{-1}) entering the bottom of the confined aquifer, and t is the groundwater age (yr). Because an exact recharge distance (x) for all samples is difficult to estimate due to the concentric shape of the Marshall subcrop (Fig. 3.2), excess He concentrations (C) were calculated and are presented as a function of groundwater age (t) (Table 3.1).

This analytical model used an average thickness of the Marshall aquifer in the study area of ~90 m, and a constant value of D_T = 0.13 m^{2}yr^{-1} chosen based on

measurements of transverse dispersion performed in a homogeneous sandstone at various flow rates (0.32 to 16 m yr^{-1}; *Freeze and Cherry* [1979], see also *Castro et al.* [2000]). In-situ production accumulation rates (P) in the Marshall aquifer for ^{3}He and ^{4}He are 8.0 $\times 10^{-21}$ and 1.1 $\times 10^{-12}$ $cm^3STPg^{-1}_{H2O}yr^{-1}$, respectively (as calculated in Table 3.3).

Except for sample 16 for which no groundwater age is available as it was not possible to fit a ^{14}C model age for a fluid with such high salinities, all other samples were used for calibration of the transport model.

3.5.4.2. Results and discussion

Figures 3.5a and b show the calculated $^{3}He_{exc}$ and $^{4}He_{exc}$ from the bottom (z/z_0=1) to the top of the aquifer (z/z_0=0) at constant intervals of 0.2 (z/z_0) (plain lines) as a function of the groundwater ages for our calibrated model. Contributions of ^{3}He and ^{4}He in-situ accumulation in the water are also shown (dashed lines). Calculated $^{3}He_{exc}$ and $^{4}He_{exc}$ concentrations increase with increased groundwater ages as well as with increased relative depth (z/z_0). Most of our samples with groundwater ages ≥5kyrs are located in the upper portion of the aquifer ($z/z_0 \leq 0.4$) and it is apparent that, except for sample 4, our calibrated model reproduces reasonably well the observed He excesses. The best fit obtained indicates that the high $^{3}He_{exc}$ and $^{4}He_{exc}$ observed in the Marshall aquifer require He flux values of 1 $\times 10^{-13}$ and 1.6 $\times 10^{-6}$ cm^3 STP $cm^{-2}yr^{-1}$ for ^{3}He and ^{4}He, respectively (Figs. 3.5a, b). Estimated He fluxes yield a R_{exc}/R_a = 0.045 entering the bottom of the aquifer, a value that is consistent with the observed average R_{exc}/R_a value of 0.047 of all samples with groundwater ages ≥5kyrs, with the exception of sample 4. The model also indicates, as previously concluded (section 3.5.3) that in-situ production from the

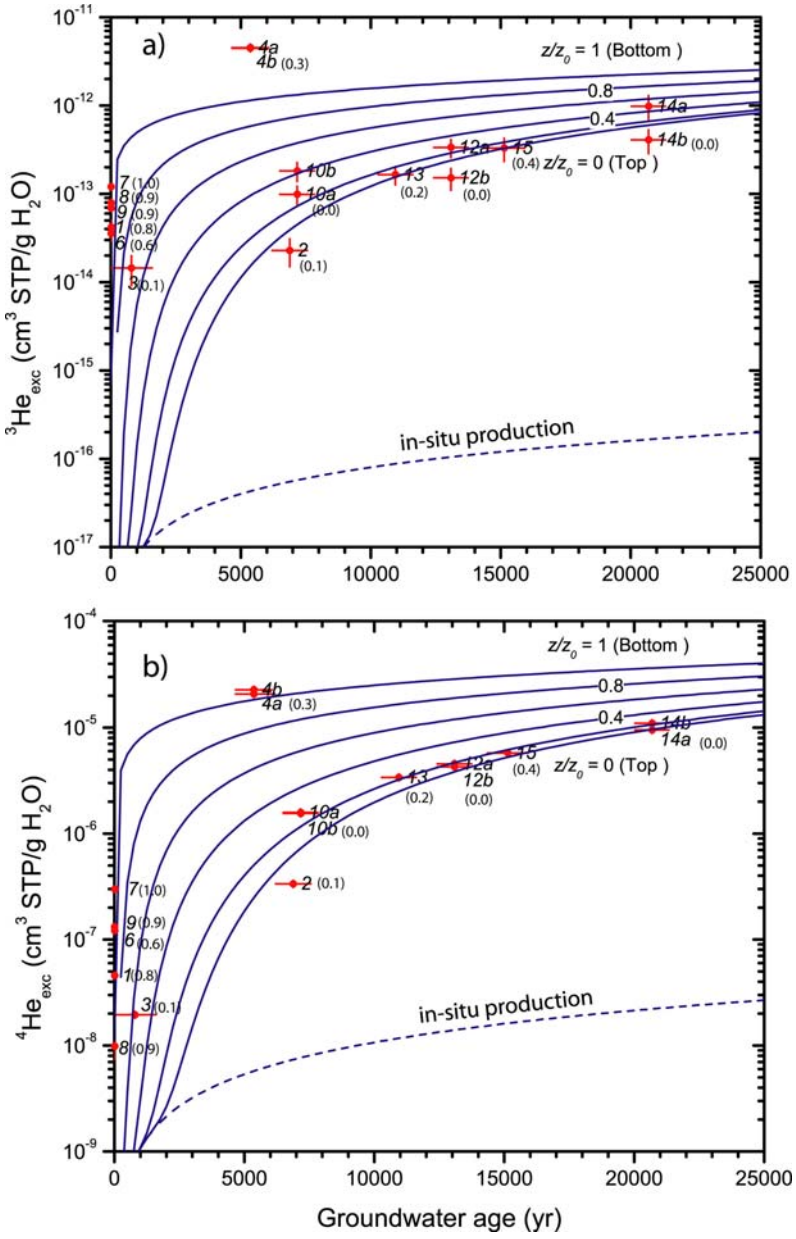

Fig. 3.5. a), b) Calculated $^3He_{exc}$ and $^4He_{exc}$ concentration curves from the bottom (z/z_0 =1) to the top of the aquifer (z/z_0 =0) at constant intervals of 0.2 (z/z_0) as a function of the groundwater (calendar) ages for the calibrated model in the Marshall aquifer, respectively. $^3He_{exc}$ and $^4He_{exc}$ values are also shown as well as the calculated $^3He_{exc}$ and $^4He_{exc}$ concentration curves resulting from in-situ production alone (dashed line). Relative depths (z/z_0) are indicated for all wells in parentheses.

Marshall sandstone is negligible, yielding concentrations that are ~2-3 orders of magnitude lower than the observed excess He in the Marshall aquifer (dashed lines, Figs. 3.5a, b).

Although these fluxes should be taken as a first order approximation due to the simplifications implemented in the model, it is clear that He fluxes entering the Marshall aquifer are far greater than He fluxes reported in other sedimentary basins at similar (≤300 m), and far greater depths (Fig. 3.6). For example, the upward ^{4}He flux entering the Marshall aquifer is over an order of magnitude greater than the one entering the Carrizo aquifer (46 times, average depth 1000m; cf. *Castro and Goblet* [2003]) in the Gulf Coast Basin, and presents an intermediate value between fluxes entering the Albian (depth ~600m) and Lusitanian aquifers (depth ~1600 m) at the center of the Paris Basin [*Castro et al.*, 1998b]. This flux is also significantly higher than those estimated in the Great Hungarian Plain [*Stute et al.*, 1992], and close to that estimated in the Great Artesian Basin [*Torgersen and Ivey*, 1985]. A similar pattern is observed for ^{3}He fluxes. Such high He fluxes present at such shallow depths within the Michigan Basin strongly suggest the existence of a deep groundwater flow system in place distinct from many other multi-layered sedimentary systems around the world, in which an horizontal component of groundwater flow plays an important role. Indeed, *Castro et al.* [1998b] have shown that ^{4}He fluxes decrease rapidly toward the surface (e.g., see Fig. 3.6) as a result of a progressive dilution by recharge water carrying a small atmospheric He component present in deeper aquifers/formations. Such a steep flux decrease does not appear to occur in the Michigan Basin, suggesting that the impact of the horizontal flow component (e.g., recharge water) at depth is minor. The presence of a dominant vertical

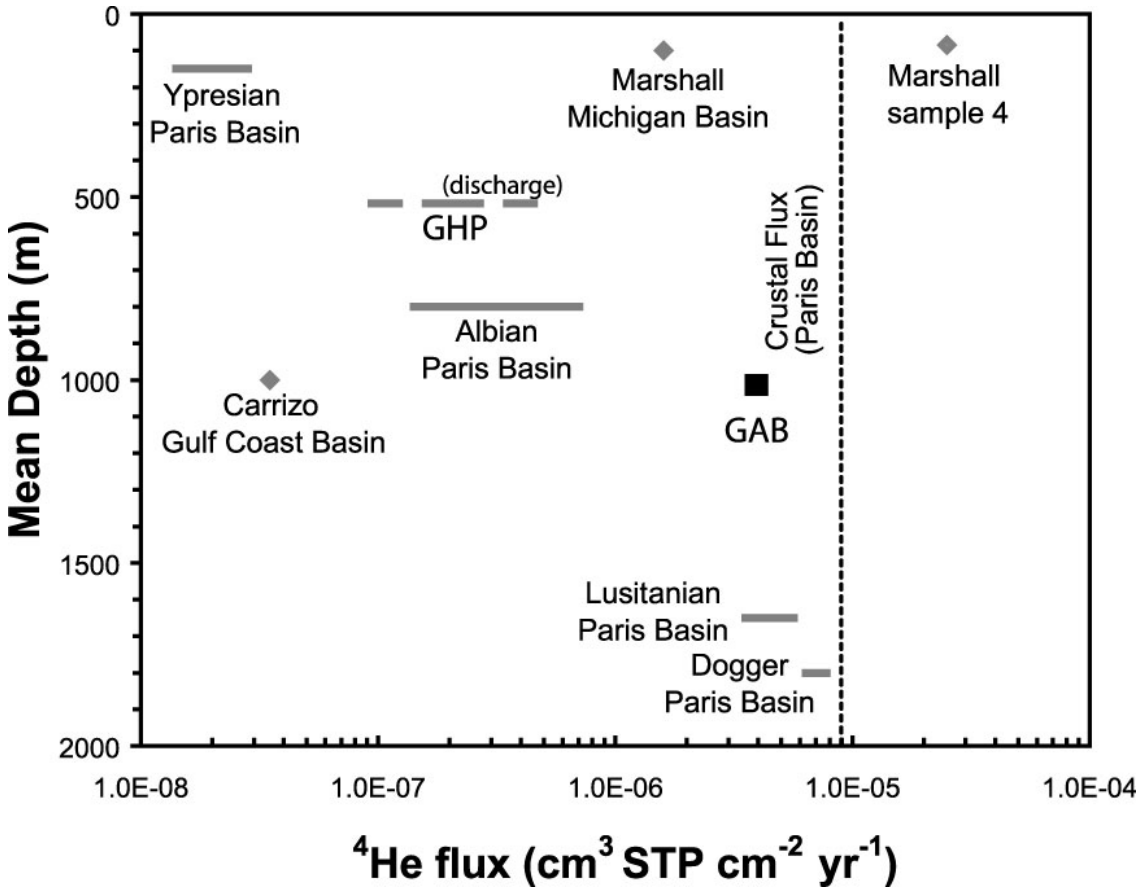

Fig. 3.6. Estimated ^{4}He fluxes entering the Marshall aquifer as compared to ^{4}He fluxes entering aquifers in other multi-layered sedimentary basins: the Carrizo aquifer in the Gulf Coast Basin [*Castro and Goblet*, 2003], the Ypresian, Albian, Lusitanian, and Dogger aquifers in the central portion of the Paris Basin [*Castro et al.*, 1998b], and the Great Artesian Basin [*Torgersen and Ivey,* 1985]; although not a multi-layered system, ^{4}He fluxes estimated in the Great Hungarian Plain [*Stute et al.,* 1992] are also indicated for comparison; the crustal flux entering the Paris Basin is also indicated [*Castro et al.*, 1998b].

flow component (upward leakage) with respect to a horizontal one is also likely responsible for the extremely high salinities in the shallow sub-surface of the Michigan Basin.

Based on measured U and Th concentrations in the Precambrian crystalline basement of our study area (Table 3.3), it is estimated that, in addition to production within the sedimentary sequence (~2.4km), at least ~6km of crystalline basement would be required to produce the ^{4}He flux underneath the Marshall aquifer. This rough estimation indicates that about 20% of $^4He_{exc}$ in the Marshall could result from the sedimentary sequence while ~80% might originate in the basement. Li concentrations are not available for the Precambrian crystalline basement, thus, such estimations for $^3He_{exc}$ cannot be made. However, as previously discussed, it is expected that the crystalline basement is by far the most important source of $^3He_{exc}$ observed in the Marshall. The basement underneath the study area is highly fractured (Fig. 3.1a) and it is likely that the faults act as conduits for groundwater flow, thereby enhancing vertical He transport within the crystalline basement, at great depths.

Such high fluxes entering the Marshall aquifer, cannot, however, explain the high $^3He_{exc}$ and $^4He_{exc}$ observed in samples 4a,b, which were collected from the upper portion of the aquifer ($z/z_0 = 0.3$). In order to fit such He excesses, fluxes of 5×10^{-12} and 2×10^{-5} cm^3 STPcm^{-2}yr^{-1}, for $^3He_{exc}$ and $^4He_{exc}$ are required, respectively. These yield R_{exc}/R_a~0.18, a value that is consistent with our observed R_{exc}/R_a of 0.15 (average for samples 4a,b), strongly suggesting the presence of a more significant and local mantle component in this area. Comparison between ^{4}He flux values required to fit samples 4a,b and the crustal flux value determined underneath the Paris Basin (Fig. 3.6) further

supports the notion that a mantle flux is partly responsible for the total local He flux in this area.

3.5.4.3. High helium/heat flux ratios in shallow groundwaters of the Marshall aquifer

The Michigan Basin has a low geothermal gradient (~19-22 °C/Km) and low surface heat flow (~44 mWm^{-2}) [*Combs and Simmons*, 1973; *Speece et al.*, 1985; *Vugrinovich*, 1989]. The first order estimated ^4He fluxes (1.6×10^{-6} cm^3 STP cm^{-2} yr^{-1}) and corresponding ^4He/heat flux ratios ($5.2*10^{-13}$ mol J^{-1}) of the shallow (<100 m) Marshall aquifer are far greater than those reported in other multi-layered basins around the world which are at far greater depths. At certain locations, however, where the presence of mantle He is apparent from R/Ra ~ 0.15 (sample 4a,b), ^4He fluxes are even greater (~2×10^{-5} cm^3 STPcm^{-2} yr^{-1}) and lead to an estimated ^4He/heat flux ratio of 5.8×10^{-12} mol J^{-1}, far higher than the crustal production ratio [*Castro et al.*, 2005]. This estimated ^4He flux corresponds to a heat flux of ~199 mWm^{-2}. Removing the present heat flux (~44 mWm^{-2}), which results partly from radiogenic production (~16 mWm^{-2}), partly from the background component (~28 mWm^{-2}) [see, *Pollack*, 1980] yields a minimum heat flux estimate of ~155 mWm^{-2}. Such heat flux could only have been supplied by a past thermal event of mantle or magmatic nature, suggesting that, while the released heat has already escaped, at least part of the released mantle He remains in the system [*Castro et al.*, 2005].

Overall, these results indicate that He has an origin external to the aquifer, from deeper sources, strongly supporting the presence of cross-formational flow (upward leakage) throughout most of the sedimentary sequence within the Michigan Basin. Our

results also suggest that the impact of a horizontal flow component (e.g., recharge water) at depth is minor. This dominant vertical water component with respect to the horizontal one can explain the observed major ions vertical patterns within the Michigan Basin as well as the extremely high salinities observed at the shallow sub-surface. These are analyzed below.

3.6. Origin of high salinity in the shallow sub-surface of the Michigan Basin

In a similar manner to the observed unusually high He excesses, high salinity values have been widely documented in both aquifers and aquitards at the shallow sub-surface in the Michigan Basin [e.g., *Long et al.*, 1988; *Weaver et al.*, 1995; *Ging et al.*, 1996]. The origin of solutes in these shallow groundwaters remains uncertain and upward transport of underlying basinal brines into shallow depths and subsequent mixing with recently recharged meteoric water has been suggested to explain the observed salinity distributions [*Long et al.*, 1988; *Ging et al.*, 1996; *Weaver et al.*, 1995; *Kolak et al.*, 1999]. The results presented above clearly indicate that the main source of He in the Marshall is external to the aquifer, partly from the underlying sedimentary sequence, partly from the crystalline basement, and strongly support the presence of large scale cross-formational flow within the Michigan Basin.

If our hypothesis based on He isotopes is correct and upward leakage indeed occurs throughout most of the sedimentary sequence, its vertical impact on major ion chemistry evolution should be equally and clearly observed. Thus, we now analyze the major ion chemistry systematics not only within the Marshall aquifer, but also, from the deeper Silurian up to the shallowest sub-surface levels (Glacial Drift sediments; Fig. 3.1c).

3.6.1 General data overview

Because bromide remains in solution during seawater evaporation and is not modified by diagenetic processes [e.g., *Carpenter*, 1978; *Stueber and Walter*, 1991], in a similar manner to He, Br^- behaves as a conservative tracer. Thus, the latter is also an ideal element to trace groundwater circulation and to identify the origin of solutes. Consequently, in order to discuss the chemistry evolution within the Michigan Basin, all other ions are plotted as a function of Br^- concentrations.

Figures 3.7 and 3.8 show the concentrations of Cl^-, Na^+, as well as Ca^{2+}, Mg^{2+}, Sr^{2+}, and K^+ plotted as a function of Br^-, respectively, for the Marshall aquifer in southern Michigan (this study; *Dannemiller and Baltusis* [1990]), the overlying Glacial Drift [*Dannemiller and Baltusis*, 1990], the underlying Upper-Devonian Antrim shale [*McIntosh et al.*, 2004] and Traverse carbonate formations [*Wilson and Long*, 1993b], as well as the evaporite-carbonate Lower-Devonian and Silurian formations [*Wilson and Long*, 1993a]. Results indicate that major ion concentrations vary between 4 (Mg^{2+} and Ca^{2+}) and 6 (Br^-, Cl^-, Na^+, and Sr^{2+}) orders of magnitude from shallow fresh groundwater to deep brines in the Michigan Basin. K^+ concentrations display an intermediate variation, up to 5 orders of magnitude. Due to these high variations in concentrations, element relationship plots are presented both in log-log and linear scale to allow for a detailed analysis of these distinct chemistry waters (Figs. 3.7, 3.8).

In the sections that follow we first discuss the origin of salinity at the shallower levels, i.e., Glacial Drift through Traverse Formation (section 3.6.2.). We then proceed to discuss how these shallower brines relate to those of deeper formations (Traverse-

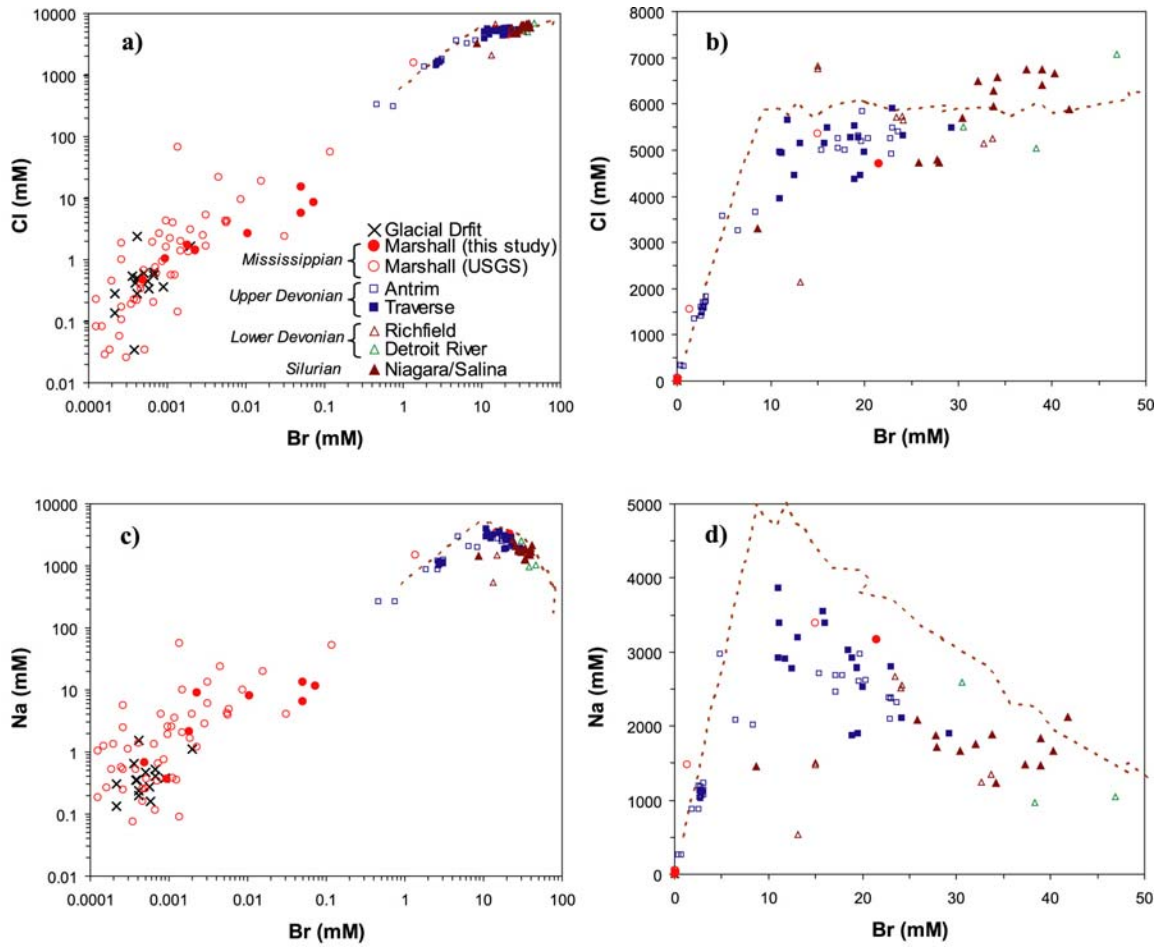

Fig. 3.7. Cl^- and Na^+ versus Br^- concentrations, respectively, for the Marshall aquifer (closed red circles, this study; open red circles, *Dannemiller and Baltusis* [1990]), the Glacial Drift (black crosses, *Dannemiller and Baltusis* [1990]), the Antrim Shale formation (open blue squares, *McIntosh et al.* [2004]), the Traverse formation (closed blue squares), the Richfield (open brown triangles), the Detroit River Group (open green triangles), and the Niagara/Salina formation (closed brown triangles) [*Wilson and Long*, 1993a,b]; both log-log (a, c) and linear scales (b, d) are shown.; seawater-evaporation curves from *McCaffrey et al.* [1987] are also shown (brown dashed line).

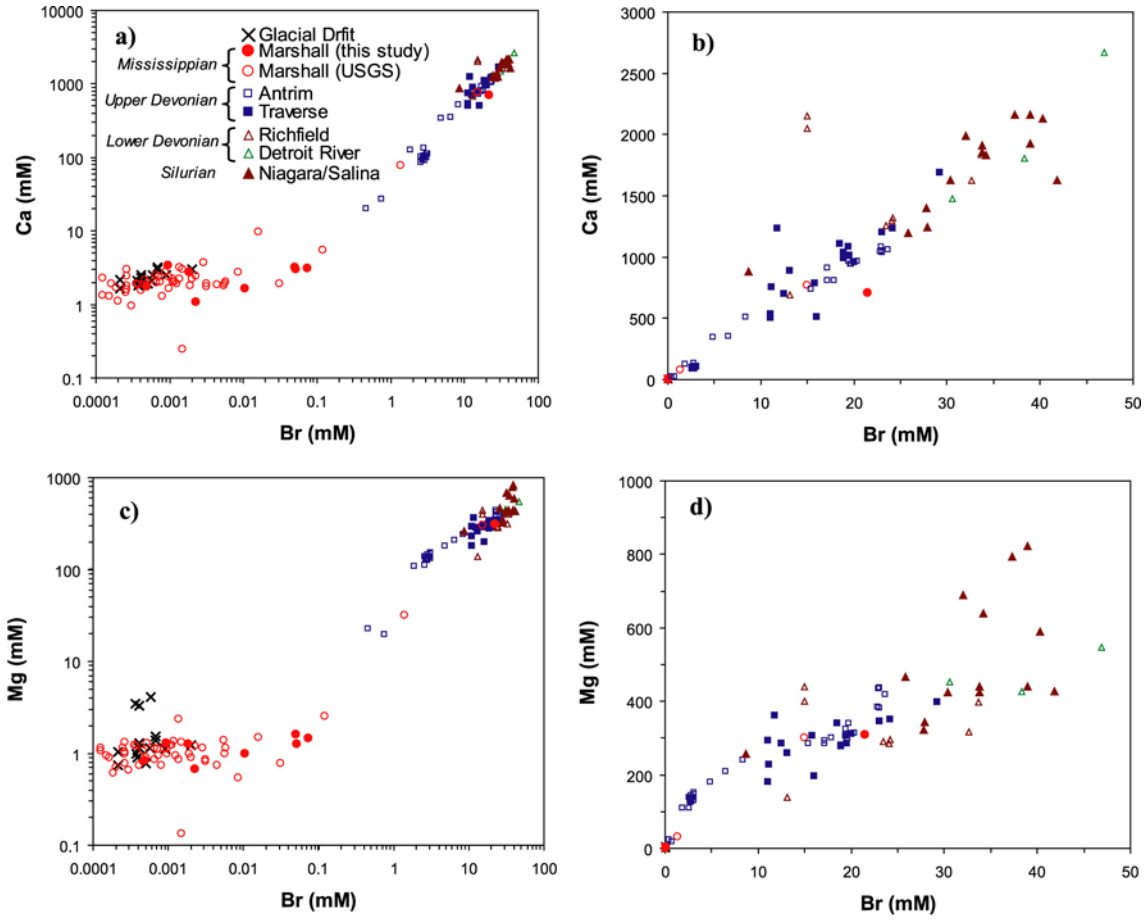

Fig. 3.8. a), b), c), d) Ca^{2+} and Mg^{2+} versus Br^{-} concentrations for the Marshall aquifer (closed red circles, this study; open red circles, Dannemiller and Baltusis, 1990), the Glacial Drift (black crosses, *Dannemiller and Baltusis* [1990]), the Antrim Shale formation (open blue squares, *McIntosh et al.* [2004]), the Traverse formation (closed blue squares), the Richfield (open brown triangles), the Detroit River Group (open green triangles), and the Niagara/Salina formation (closed brown triangles) [*Wilson and Long*, 1993a,b]; both log-log (a, c) and linear scales (b,d) are shown.

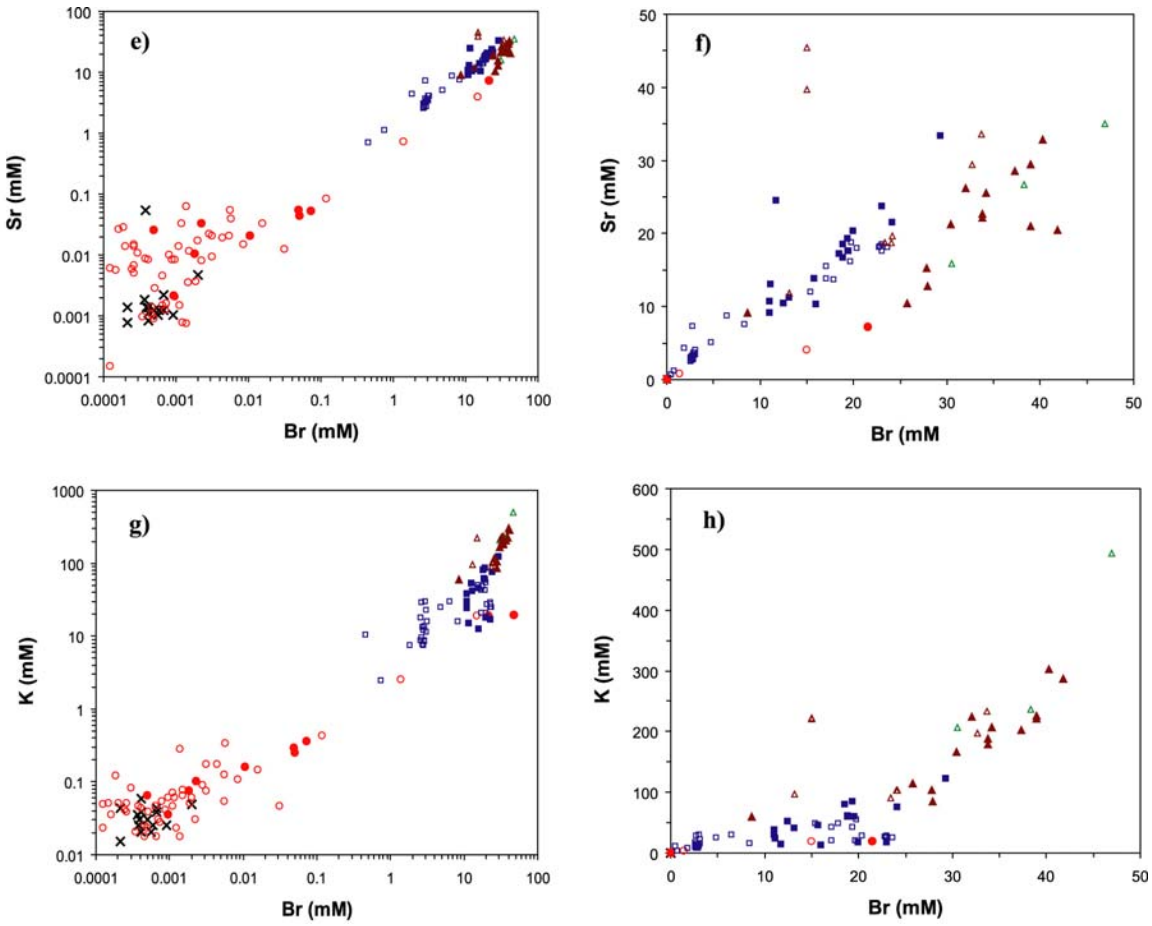

Fig. 3.8. e), f), g), h) Sr^{2+} and K^{+} versus Br^{-} concentrations for the Marshall aquifer (closed red circles, this study; open red circles, Dannemiller and Baltusis, 1990), the Glacial Drift (black crosses, *Dannemiller and Baltusis* [1990]), the Antrim Shale formation (open blue squares, *McIntosh et al.* [2004]), the Traverse formation (closed blue squares), the Richfield (open brown triangles), the Detroit River Group (open green triangles), and the Niagara/Salina formation (closed brown triangles) [*Wilson and Long*, 1993a,b]; both log-log (e, g) and linear scales (f, h) are shown.

Silurian, section 3.6.3), and present then a brief overview of the observed vertical facies evolution and He-Br^- positive correlation (section 3.6.4).

3.6.2 Origin of salinities in the shallow sub-surface of the Michigan Basin

Groundwater samples from the Marshall aquifer yield variable Cl^- and Br^- concentrations and display a positive correlation between these two elements (Fig. 3.7a). Low Cl^- and Br^- concentrations are found close to the recharge area and are indistinguishable to the composition of fresh water in the overlying Glacial Drift. By contrast, samples close to the discharge area display high Cl^- and Br^- concentrations, with a signature similar to those of the most diluted underlying Antrim Formation brines (Figs. 3.7a, b). While the dissolution of evaporites in neighboring formations may explain some of the high Cl^-concentrations observed locally in Antrim formation waters in the northern marginal basin [*McIntosh et al.*, 2004], such a process, however, cannot account for the high Br^- concentrations found in the Marshall and Antrim formation waters in our study area (southern portion of the basin). Indeed, Br^- content is negligible in evaporites. High Br^- concentrations are the result of sea water evaporation and are thus expected to have its original source in underlying Br^--enriched basinal brines [e.g. *Ging et al.*, 1996; *McIntosh et al.*, 2004]. Indeed, brines from the Traverse formation (Figs. 3.7a,b), a major carbonate aquifer underlying the Antrim shale have higher Br^- and Cl^- concentrations and plot along the seawater-evaporation curve (dashed line, Fig. 3.7b; *McCaffrey et al.* [1987]), past halite saturation, indicating that their evolution is related to evaporated seawater [*Wilson and Long*, 1993b]. Samples from the Marshall and Antrim formations also plot along the seawater-evaporation curve (Figs. 3.7a,b) and connect the fresh water

and brine end-members, suggesting a mixing of upwelling deep brines with recharge water within these shallower levels (Fig. 3.7b). High Cl^- and Br^- contents in shallow waters (e.g., Glacial Drift and Marshall aquifer) are thus most likely derived from cross-formational flow from the underlying Traverse formation brines.

As also previously suggested through estimation of He fluxes (section 3.5.4.2.), mixing of deep brines with recharge fresh water seems to be absent at lower levels as indicated by the high Cl^- concentrations in place in these formations (e.g., Traverse Formation, Silurian) as well as its observed small variability range.

Na^+ concentrations within the Marshall aquifer show a similar trend to Cl^- concentrations (Figs. 3.7c, d), and is also likely the result of upwelling basinal brines from the Traverse Formation. An almost linear trend is also observed between Ca^{2+}, Mg^{2+}, Sr^{2+}, and K^+ and Br^- in the most concentrated brines within the Marshall aquifer and those of deeper formations (Fig. 3.8), a further indication of a progressive evolution from the deepest brines (e.g., Silurian) into shallower ones (Marshall).

In fresh and less concentrated waters (e.g, Glacial Drift and Marshall), Ca^{2+}, Mg^{2+}, Sr^{2+}, and K^+ concentrations remain relatively constant with increasing Br^- contents (Br^-<0.1mM). Indeed, and unlike Na^+ and Cl^-, which are directly related to Br^- through formation of basinal brines, Ca^{2+}, Mg^{2+}, Sr^{2+}, and K^+ in diluted waters are buffered by water-rock interactions [e.g. *Szramek and Walter*, 2004].

3.6.3 Deeper brine signatures in shallow formation waters

It has just been shown that Glacial Drift and Marshall groundwaters carry the signature of the deeper Traverse brines. In earlier sections (e.g., section 3.5.4.2), it has

also been shown that the observed He excess in the Marshall aquifer originates from sources deeper than the Traverse formation, and suggested that high salinities observed in the Marshall are also likely to have a deeper origin.

Because the environmental conditions required for such extreme seawater evaporation to take place during Late Devonian (e.g., Traverse Formation) are unlikely, *Wilson and Long* [1993a,b] suggested that the latter might have been affected by the underlying Silurian brines. Indeed, such influence can be clearly observed between a diversity of ions and Br^- (Figs. 3.7, 3.8). For example, Lower Devonian and Silurian brines present the highest Cl^- and Br^- concentrations and plot further along the seawater-evaporation curve, close to K-salt saturation, indicating more extreme sea water evaporation. It is clear that Silurian and Traverse brines are not plotted as two isolated groups, but instead, Silurian brines evolve into the chemical composition of those of the Traverse group (Fig. 3.7b). Major cations (Na^+, K^+, Ca^{2+}, Mg^{2+}, and Sr^{2+}) show a similar trend. This signature of deep Silurian brines into the Traverse Formation reinforces, once again, the presence of deep cross-formational flow derived from He considerations.

Michigan Basin brines have significantly enriched Ca^{2+}, and depleted Mg^{2+}, Na^+, and K^+ concentrations (Figs. 3.7d, 3.8b, d, h) with respect to modern seawater-evaporation curves [*McCaffrey et al.*, 1987]. Extensive water-rock interactions have been proposed to explain these elemental differences from modern evaporated seawater (e.g., dolomitization for Ca^{2+}-excess and Mg^{2+}-deficit; albitization for Ca^{2+}-excess and Na^+-deficit; formation of new K-minerals for K^+-deficit, e.g., *Wilson and Long et al.* [1993a,b]; *Davisson and Criss* [1996]; *Duffin* [1989]). However these elemental differences could also be interpreted as the result of fundamentally different chemical

compositions in ancient Silurian seawaters (e.g., seawater with higher Ca^{2+}, lower Mg^{2+} and Na^{+} concentrations; *Brennan and Lowenstein* [2002]). Although no single process alone can account for the observed chemical compositions of these brines, such elemental differences with respect to modern evaporated seawater are found at almost all depths in the Michigan Basin, e.g., from Silurian to Mississippian formations. This suggests that brines at all depths may be genetically related as a result of upward cross-formational flow.

3.6.4 Vertical chemical water facies evolution and He-Br relationship in the Marshall aquifer

Overall, diluted waters in the Glacial Drift and Marshall aquifers are mostly Ca-Mg-HCO_3 dominated and represent recharge water in which water-rock interactions with carbonates have occurred over time, while highly saline waters have evolved into Na-Cl facies due to the incorporation of deeper brines (Trend 1, Fig. 3.9). Upper Devonian strata are mostly Na-Cl dominated and evolve progressively into Na-Ca-Cl facies (Devonian). The latter subsequently evolves into a dominant Ca-Na-Cl facies (Lower Devonian-Silurian; Trend 2, Fig. 3.9).

Although the Michigan Basin brines are geochemically compartmentalized [e.g., *Martini*, 1997], the above observations clearly show the influence of deep Silurian brines on the overlying strata, which likely results from upward cross-formational flow. The positive correlation observed in the Marshall aquifer between excess He and Br^{-} (Fig. 3.10), two very distinct conservative tracers, further reinforces this concept.

3.7. Conclusions

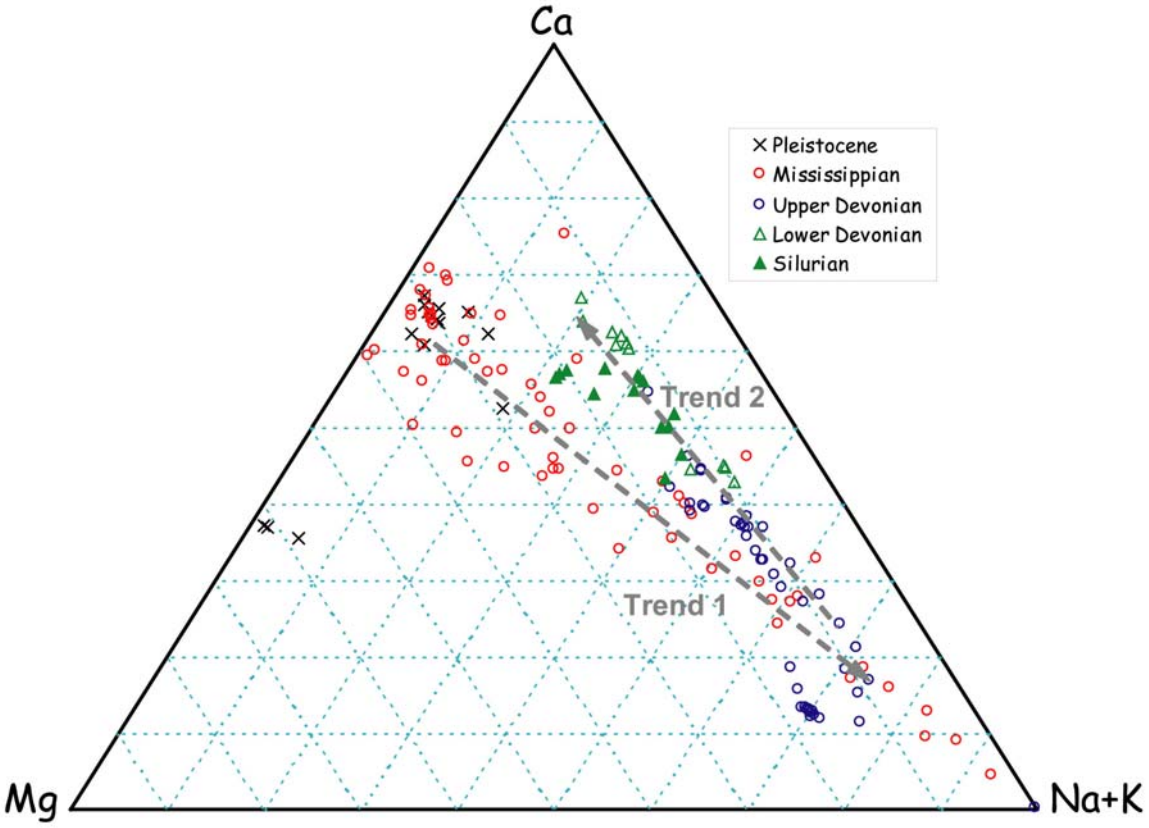

Fig. 3.9. Ternary diagram showing mole percentage of Ca, Mg, and Na+K in Michigan Basin formation waters: Pleistocene (Glacial Drift, black crosses), Mississippian (Marshall sandstone, open red circles), Upper Devonian (Antrim and Traverse formations, open blue circles), Lower Devonian (Richfield and Detroit River Group, open green triangles), Silurian (Niagara/Salina formations, closed green triangle). Trends indicating evolution of chemical facies from fresh groundwater (Trend 1) to deeper brines (Trend 2) are also indicated.

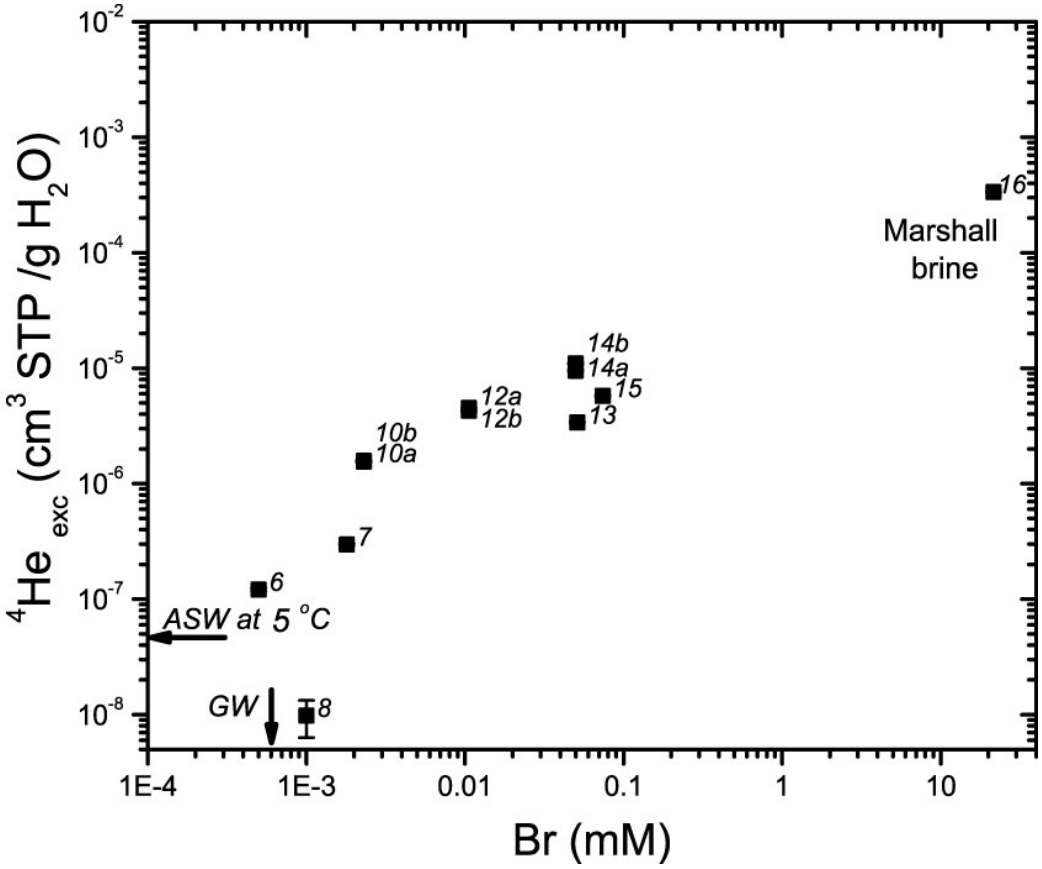

Fig. 3.10. $^4He_{exc}$ versus Br^- concentrations in the Marshall aquifer (this study); ASW ^4He concentration at 5 °C [*Ozima and Podosek*, 2002] and average Br^- concentration in shallow fresh groundwaters [*Dannemiller and Baltusis*, 1990] are indicated.

Helium data and major ion chemistry are presented for the Marshall aquifer in southern Michigan. This shallow groundwater data set is subsequently interpreted in conjunction with major element data sets from deeper and shallower water levels previously analyzed in this area [*Dannemiller and Baltusis*, 1990; *Wilson and Long*, 1993a,b; *McIntosh et al.*, 2004].

He excesses and isotopic ratios suggest the presence of tritiogenic ^{3}He in young waters in the Marshall aquifer. High He excesses in old groundwater samples are mostly of crustal origin (nucleogenic ^{3}He and radiogenic ^{4}He) with the presence of a significant mantle He component in some samples. He excesses in the Marshall aquifer are unusually high for such shallow depths, and require a source external to the aquifer, partly supplied by underlying formations within the sedimentary sequence, partly from the crystalline basement. Calibration of He concentrations through an analytical model indicate that the high $^{3}He_{exc}$ and $^{4}He_{exc}$ observed in the Marshall require He fluxes of 1×10^{-13} and 1.6×10^{-6} cm^{3} STP cm^{-2}yr^{-1} for ^{3}He and ^{4}He, respectively. The latter are far greater than He fluxes reported in other sedimentary basins around the world at similar and far greater depths (e.g., Paris Basin, Gulf Coast Basin; *Castro et al.* [1998b]; *Castro* [2004]). Such high He fluxes present at such shallow depths within the Michigan Basin strongly suggest the presence of a dominant vertical water flow component, i.e., upward leakage, and further indicate that the impact of the horizontal flow component (e.g., recharge water) at depth is minor. Cross-formational flow is also likely responsible for the extremely high salinities present in the shallow sub-surface of the Michigan Basin. The observed positive correlation between helium and bromide strongly suggests that these two very distinct conservative tracers both originate at greater depths, and further

suggests that advection is the dominant transport mechanism within the basin. The occurrence of large-scale cross-formational flow is also consistent with the evolution displayed by the major ion chemistry throughout most of the sedimentary sequence (e.g., Silurian through Glacial Drift Sediments), indicating that solutes from shallow levels carry the signature of deep formation brines. Of particular relevance is the contrast observed between high helium and low heat fluxes in the shallow Marshall aquifer, leading to helium/heat flux ratios greater than that of the radiogenic production ratio. Such high helium/heat flux ratios strongly suggest the occurrence of a major past thermal event in the basin.

Acknowledgments

The authors thank W.M. White and D.R. Hilton for the editorial handling of this manuscript, W. Aeschbach-Hertig and an anonymous reviewer for their reviews, David Westjohn for his assistance at providing well information, and Kathy Flemming for her assistance in the field. We also thank the numerous private and public well owners for having provided access to the wells for sampling. Acknowledgement is made to the Donors of the American Chemical Society Petroleum Research Fund for support of this research (PRF# 38175-G8).

References

Ballentine, C. J. (1991), He, Ne and Ar isotopes as tracers in crustal fluids, 216pp, University of Cambridge, Cambridge, UK.

Ballentine, C. J., and C. M. Hall (1999), Determining paleotemperature and other variables by using an error-weighted nonlinear inversion of noble gas concentrations in water, *Geochimica et Cosmochimica Acta*, *63*(16), 2315-2336.

Ballentine, C.J., R. Burgess, and B. Marty (2002), Tracing fluid origin, transport and interaction in the crust. *Rev. Mineral. Geochem.* 47, 539-614.

Benson, B. B., and D. Krause (1980), Isotopic Fractionation of Helium during Solution - A Probe for the Liquid-State, *Journal of Solution Chemistry*, *9*(12), 895-909.

Brennan, S. T., and T. K. Lowenstein (2002), The major-ion composition of Silurian seawater, *Geochimica et Cosmochimica Acta*, *66*(15), 2683-2700.

Carpenter, A. B. (1978), Origin and chemical evolution of brines in sedimentary basins, *Oklahoma Geological Survey Circular*, *79,* 60-77.

Castro, M. C., A. Jambon, G. de Marsily, and P. Schlosser (1998a), Noble gases as natural tracers of water circulation in the Paris Basin; 1, Measurements and discussion of their origin and mechanisms of vertical transport in the basin, *Water Resources Research*, *34*(10), 2443-2466.

Castro, M. C., P. Goblet, E. Ledoux, S. Violette, and G. de Marsily (1998b), Noble gases as natural tracers of water circulation in the Paris Basin; 2, Calibration of a groundwater flow model using noble gas isotope data, *Water Resources Research*, *34*(10), 2467-2483.

Castro, M. C., M. Stute, and P. Schlosser (2000), Comparison of ^{4}He ages and ^{14}C ages in simple aquifer systems; implications for groundwater flow and chronologies, *Applied Geochemistry*, *15*(8), 1137-1167.

Castro, M. C., and P. Goblet (2003), Calibration of regional groundwater flow models: Working toward a better understanding of site-specific systems, *Water Resources Research*, *39*(6), 1172.

Castro, M. C. (2004), Helium sources in passive margin aquifers - new evidence for a significant mantle ^{3}He source in aquifers with unexpectedly low in situ ^{3}He/^{4}He production, *Earth and Planetary Science Letters*, *222*(3-4), 897-913.

Castro, M.C., D. Patriarche, and P. Goblet (2005), 2-D numerical simulations of groundwater flow, heat transfer and ^{4}He transport – implications for the He terrestrial budget and the mantle helium-heat imbalance, *Earth Planet. Sci. Lett.*, *237*, 893-910.

Catacosinos, P. A., and P. A. J. Daniels (1991), Stratigraphy of Middle Proterozoic to Middle Ordovician formations of the Michigan Basin, *Special Paper - Geological Society of America*, *256,* 53-71.

Combs, J., and G. Simmons (1973), Terrestrial heat flow determinations in the north

central United States, *Journal of Geophysical Research*, *78*, 441-461.

Clarke, W. B., W. J. Jenkins, and Z. Top (1976), Determination of Tritium by Mass-Spectrometric Measurement of ^{3}He, *International Journal Of Applied Radiation And Isotopes*, *27*(9), 515-522.

Dannemiller, G. T., and M. A. Baltusis, Jr. (1990), Physical and chemical data for ground water in the Michigan Basin, 1986-1989, 155pp, U.S. Geological Survey Open-File Report 90-368, Boulder, CO.

Davisson, M. L., and R. E. Criss (1996), Na-Ca-Cl relations in basinal fluids, *Geochimica et Cosmochimica Acta*, *60*(15), 2743-2752.

Dorr, J. A., Jr., and D. F. Eschman (1970), *Geology of Michigan*, 476pp., University of Michigan Press, Ann Arbor, MI.

Duffin, M. E. (1989), Nature and Origin of Authigenic K-Feldspar in Precambrian Basement Rocks of the North-American Midcontinent, *Geology*, *17*(8), 765-768.

Fisher, J. H., M. W. Barratt, J. B. Droste, and R. H. Shaver (1988), Michigan Basin, in *Sedimentary Cover - North American Craton*, edited by L. L. Sloss, pp. 361-382, Geological Society of America, Boulder, CO.

Fontes, J. C., and J. M. Garnier (1979), Determination of the Initial C-14 Activity of the Total Dissolved Carbon - Review of the Existing Models and a New Approach, *Water Resour. Res.*, *15*(2), 399-413.

Fontes, J. C., and J. M. Matray (1993), Geochemistry And Origin Of Formation Brines From The Paris Basin, France.1. Brines Associated With Triassic Salts, *Chemical Geology*, *109*(1-4), 149-175.

Freeze, R. A., and J. A. Cherry (1979), *Groundwater*, 604pp, Prentice Hall, Upper Saddle River, NJ.

Gieskes, J. M., and W. C. Rogers (1973), Alkalinity Determination in Interstitial Waters of Marine Sediments, *Journal of Sedimentary Petrology*, *43*(1), 272-277.

Ging, P. B., D. T. Long, and R. W. Lee (1996), Selected geochemical characteristics of ground Water from the Marshall aquifer in the central Lower Peninsula of Michigan, 19pp, Lansing, MI.

Graham, D. (2002), Noble gas isotope geochemistry of mid-ocean ridge and ocean island basalts: Characterization of mantle source reservoirs, *Reviews in Mineralogy and Geochemistry*, *47*, 247-317.

Heaton, T. H. E., and J. C. Vogel (1981), Excess Air in Groundwater, *Journal of Hydrology*, *50*(1-3), 201-216.

Hilton, D. R., T. P. Fischer, and B. Marty (2002), Noble gases and volatile recycling at subduction zones, *Reviews in Mineralogy and Geochemistry*, 47, 319-370.

Hilton, D. R., and D. Porcelli (2003), Noble gases as mantle tracers, in: *The Mantle and Core* (ed. Carlson, R.W.) Vol. 2 Treatise on Geochemistry (eds. Holland, H.D. and Turekian, K.K.) pp 277-318, Elsevier-Pergamon, Oxford, UK.

Hinze, W. J., R. L. Kellogg, and N. W. O'Hara (1975), Geophysical studies of basement

geology of Southern Peninsula of Michigan, *AAPG Bulletin*, *59*(9), 1562-1584.

IAEA/WMO (1998), *Global network for isotopes in precipitation*.

Kolak, J. J., D. T. Long, J. M. Matty, G. J. Larson, D. F. Sibley, and T. B. Councell (1999), Ground-water, large-lake interactions in Saginaw Bay, Lake Huron; a geochemical and isotopic approach, *Geological Society of America Bulletin*, *111*(2), 177-188.

Long, D. T., T. P. Wilson, M. J. Takacs, and D. H. Rezabek (1988), Stable-isotope geochemistry of saline near-surface ground water; east-central Michigan Basin, *Geological Society of America Bulletin*, *100*(10), 1568-1577.

Ma, L., M. C. Castro, and C. M. Hall (2004), A late Pleistocene–Holocene noble gas paleotemperature record in southern Michigan, *Geophys. Res. Lett.*, *31,*L23204, doi:23210.21029/22004GL021766.

Mandle, R. J., and D. B. Westjohn (1989), Geohydrologic framework and ground-water flow in the Michigan Basin, *AWRA Monograph Series*, *13,* 83-109.

Martini, A. M. (1997), Hydrogeochemistry of saline fluids and associated water and gas, 237pp, University of Michigan, Ann Arbor.

McCaffrey, M. A., B. Lazar, and H. D. Holland (1987), The evaporation path of seawater and the coprecipitation of Br^- and K^+ with halite, *Journal of Sedimentary Petrology*, *57*(5), 928-937.

McIntosh, J. C., L. M. Walter, and A. M. Martini (2004), Extensive microbial modification of formation water geochemistry; case study from a Midcontinent sedimentary basin, United States, *Geological Society of America Bulletin*, *116*(5-6), 743-759.

Menuge, J. F., T. S. Brewer, and C. M. Seeger (2002), Petrogenesis of metaluminous A-type rhyolites from the St Francois Mountains, Missouri and the Mesoproterozoic evolution of the southern Laurentian margin, *Precambrian Research*, *113*(3-4), 269-291.

Morrison, P., and J. Pine (1955), Radiogenic Origin of the Helium Isotopes in Rock, *Annals of the New York Academy of Sciences*, *62*(3), 71-92.

Ozima, M., and F. A. Podosek (2002), *Noble gas Geochemistry*, 2nd ed., 286pp., Cambridge Univ. Press, New York.

Parker, R. L. (1967), Composition of Earth's crust, data of geochemistry, pp. 1-19, U.S. Geol. Surv. Prof. Pap. 440-D.

Patriarche, D., M. C. Castro, and P. Goblet (2004), Large-scale hydraulic conductivities inferred from three-dimensional groundwater flow and He-4 transport modeling in the Carrizo aquifer, Texas, *Journal of Geophysical Research-Solid Earth*, *109*(B11), B11202.

Pollack, P.N. (1980), The heat flow from the earth: a review, in *Mechanisms of continental drift and plate tectonics*, edited by P.A. Davies and S.K. Runcorn, pp. 183-192, Academic Press, London.

Roether, W. (1967), Estimating the tritium input to groundwater from wine samples: groundwater and direct run-off contribution to central European surface waters, in *Isotopes in Hydrology*, edited, IAEA, Vienna.

Saar, M. O., M. C. Castro, C. M. Hall, M. Manga, and T. P. Rose (2005), Quantifying magmatic, crustal, and atmospheric helium contributions to volcanic aquifers using all stable noble gases: Implications for magmatism and groundwater flow, *Geochemistry, Geophysics, Geosystems*, *6*(3), 18pp. doi:10.1029/2004GC000828.

Schlosser, P., M. Stute, C. Sonntag, and K. O. Munnich (1989), Tritiogenic ^{3}He in Shallow Groundwater, *Earth And Planetary Science Letters*, *94*(3-4), 245-256.

Siegel, D. I., K. A. Lesniak, M. Stute, and S. Frape (2004), Isotopic geochemistry of the Saratoga springs; implications for the origin of solutes and source of carbon dioxide, *Geology*, *32*(3), 257-260.

Soloman, D. K., A. Hunt, and R. J. Poreda (1996), Source of radiogenic helium 4 in shallow aquifers: implications for dating young groundwater, *Water Resour. Res.*, *32*, 1805-1813.

Speece, M. A., T. D. Bowen, J. L. Folcik, and H. N. Pollack (1985), Analysis of temperatures in sedimentary basins; the Michigan Basin, *Geophysics*, *50*(8), 1318-1334.

Stueber, A. M., and L. M. Walter (1991), Origin and chemical evolution of formation waters from Silurian-Devonian strata in the Illinois Basin, USA, *Geochimica et Cosmochimica Acta*, *55*(1), 309-325.

Stuiver, M., and P. J. Reimer (1993), Extended ^{14}C Data-Base And Revised Calib 3.0 ^{14}C Age Calibration Program, *Radiocarbon*, *35*(1), 215-230.

Stute, M., C. Sonntag, J. Deak, and P. Schlosser (1992), Helium in deep circulating groundwater in the Great Hungarian Plain; flow dynamics and crustal and mantle helium fluxes, *Geochimica et Cosmochimica Acta*, *56*(5), 2051-2067.

Szramek, K., and L. M. Walter (2004), Impact of carbonate precipitation on riverine inorganic carbon mass transport from a mid-continent, forested watershed, *Aquatic Geochemistry*, *10*(1-2), 99-137.

Tolstikhin, I., B. E. Lehmann, H. H. Loosli, and A. Gautschi (1996), Helium and argon isotopes in rocks, minerals, and related groundwaters: A case study in northern Switzerland, *Geochimica et Cosmochimica Acta*, *60*(9), 1497-1514.

Torgersen, T. (1980), Controls on Pore-Fluid Concentration of ^{4}He and ^{222}Rn and the Calculation of ^{4}He-^{222}Rn Ages, *Journal of Geochemical Exploration*, *13*(1), 57-75.

Torgersen, T., and W. B. Clarke (1985), Helium accumulation in groundwater; I, An evaluation of sources and the continental flux of crustal ^{4}He in the Great Artesian Basin, Australia, *Geochimica et Cosmochimica Acta*, *49*(5), 1211-1218.

Torgersen, T., and G. N. Ivey (1985), Helium accumulation in groundwater; II, A model for the accumulation of the crustal ^{4}He degassing flux, *Geochimica et Cosmochimica Acta*, *49*(11), 2445-2452.

Torgersen, T., S. Drenkard, M. Stute, P. Schlosser, and A. M. Shapiro (1995), Mantle helium in ground waters of eastern North America; time and space constraints on sources, *Geology*, *23*(8), 675-678.

Van Schmus, W. R. (1992), Tectonic setting of the Midcontinent Rift system, *Tectonophysics*, *213*, 1-15.

Vugrinovich, R. (1986), Patterns of regional subsurface fluid movement in the Michigan Basin, 27pp, Michigan Geological Survey.

Vugrinovich, R. (1989), Subsurface temperatures and surface heat flow in the Michigan Basin and their relationships to regional subsurface fluid movement, *Marine and Petroleum Geology*, *6*, 60-70.

Weaver, T. R., S. K. Frape, and J. A. Cherry (1995), Recent cross-formational fluid flow and mixing in the shallow Michigan Basin, *Geological Society of America Bulletin*, *107*(6), 697-707.

Weiss, R. F. (1968), Piggyback Sampler for Dissolved Gas Studies on Sealed Water Samples, *Deep-Sea Research*, *15*(6), 695-699.

Westjohn, D. B., and T. L. Weaver (1996), Hydrogeologic framework of Mississippian rocks in the central Lower Peninsula of Michigan, 46pp, USGS Water-Resources Investigations Report 94-4246, Lansing, MI.

Wilson, T. P. (1989), Origin and geochemical evolution of the Michigan Basin brine, 272pp, Michigan State University, East Lansing.

Wilson, T. P., and D. T. Long (1993a), Geochemistry and isotope chemistry of Ca-Na-Cl brines in Silurian strata, Michigan Basin, U.S.A, *Applied Geochemistry*, *8*(5), 507-524.

Wilson, T. P., and D. T. Long (1993b), Geochemistry and isotope chemistry of Michigan Basin brines; Devonian formations, *Applied Geochemistry*, *8*(2), 81-100.

CHAPTER 4

A PRIMORDIAL, SOLAR HE-NE SIGNATURE IN CRUSTAL FLUIDS OF A STABLE CONTINENTAL REGION

Abstract

Primordial He and Ne have been historically regarded as signatures of mantle plumes that are expressions of a largely undegassed lower mantle. A complementary degassed upper mantle is widely invoked to explain low He with high heat flow at mid-ocean ridges, but recent work demonstrates that this is not required. Here, we report He and Ne data from deep Michigan Basin brines that clearly reveal a primordial solar-like component in this stable continental region, where the presence of mantle plumes is highly unlikely. It is suggested here that this primordial signature can be accounted for by a shallow refractory reservoir in the subcontinental lithospheric mantle and that primordial He and Ne does not necessarily reflect the presence of mantle plumes, with their associated undegassed lower mantle reservoir.

4.1. Introduction

The presence of a primordial He and Ne signature in ocean island basalts (OIBs) as well as the presence of a mantle He/heat flux ratio lower than the radiogenic

production ratio near mid-ocean ridges have historically been used to support a two-layered mantle convection model [*O'Nions and Oxburgh*, 1983; *Porcelli and Wasserburg*, 1995; *Moreira and Allegre*, 1998]. This model comprises a lower, primordial, largely undegassed reservoir from which OIBs originate via deep mantle plumes, and a degassed upper mantle of which mid-ocean ridge basalts (MORBs) are representative. Primordial He and Ne signatures, which are commonly thought to be solar-like and representative of the Earth's early formation stages [e.g., *Honda et al.*, 1991] have thus been systematically associated with the occurrence of mantle plumes, and the existence of a lower, largely undegassed, mantle reservoir [*Porcelli and Wasserburg*, 1995; *Moreira and Allegre*, 1998]. By contrast, low He/heat flux ratios have commonly been regarded as reflecting a He deficit in the original upper MORB degassed mantle reservoir [*O'Nions and Oxburgh*, 1983]. However, this view was recently challenged and arguments based on He and heat transport invalidated [*Castro et al.*, 2005]. It was also shown that the occurrence of a He/heat flux ratio greater than the radiogenic production ratio can only result from a past mantle event [*Castro et al.*, 2005]. Such a high He/heat flux ratio was recently identified in shallow (<100 m) groundwaters of the Michigan Basin [*Ma et al*., 2005; *Castro et al.*, 2007]. To confirm the presence of this mantle component in the basin and to clarify its origin, 38 deep (0.5-3.6Km) brine samples were collected and analyzed for noble gas concentrations and isotopic ratios. While both He and Ne isotopic ratios clearly indicate the presence of a mantle component, Ne isotopic compositions point unequivocally to the presence of a primordial, solar-like signature in this continental region where the presence of a mantle plume is highly unlikely. A combined He and Ne isotopic analysis further reinforces

these findings. Here, we report our He and Ne results in the Michigan Basin and argue that the presence of primordial noble gas signatures do not necessarily indicate the presence of mantle plumes and thus, the existence of a deep, largely undegassed, OIB-type reservoir.

4.2. Geological and hydrogeological background

Located in the northeastern United States, the Michigan Basin is a concentric intracratonic depression floored by crystalline Precambrian basement (Fig. 4.1a, b, c) and consists of a succession of sedimentary rocks from the Precambrian to Jurassic that reaches depths over 5Km [*Dorr and Eschman*, 1970; *Catacosinos et al.*, 1991]. The entire sedimentary strata (Fig. 4.1b) are composed mainly of evaporites (e.g., Salina Group), carbonates (e.g., Traverse Formation, Niagaran), shales (e.g., Antrim and Coldwater Formations), and sandstones (e.g., Marshall Formation). Depending on their nature, these sedimentary rocks constitute either aquitards (e.g., shale, evaporites) or aquifers (mostly sandstones and reefal and dolomitized limestones), giving rise to a multi-layered aquifer system [*Vugrinovich*, 1986; *Westjohn and Weaver*, 1996]. The rift zone, which transects the entire crystalline basement (Fig. 4.1a) is believed to be part of the Mid-Continent Rift (MCR) system [*Hinze et al.*, 1975; *Van Schmus*, 1992]. Other major tectonic structures such as the Albion-Scipio Fault, the Lucas Fault, and the Howell Anticline are also present in southern Michigan and penetrate the Precambrian crystalline basement. This basin presents a very low geothermal gradient (average ~19ºC/Km) [*Vugrinovich*, 1989], the highest He fluxes ever recorded in a shallow, fast flowing groundwater flow environment [*Ma et al.*, 2005], in addition to some of the

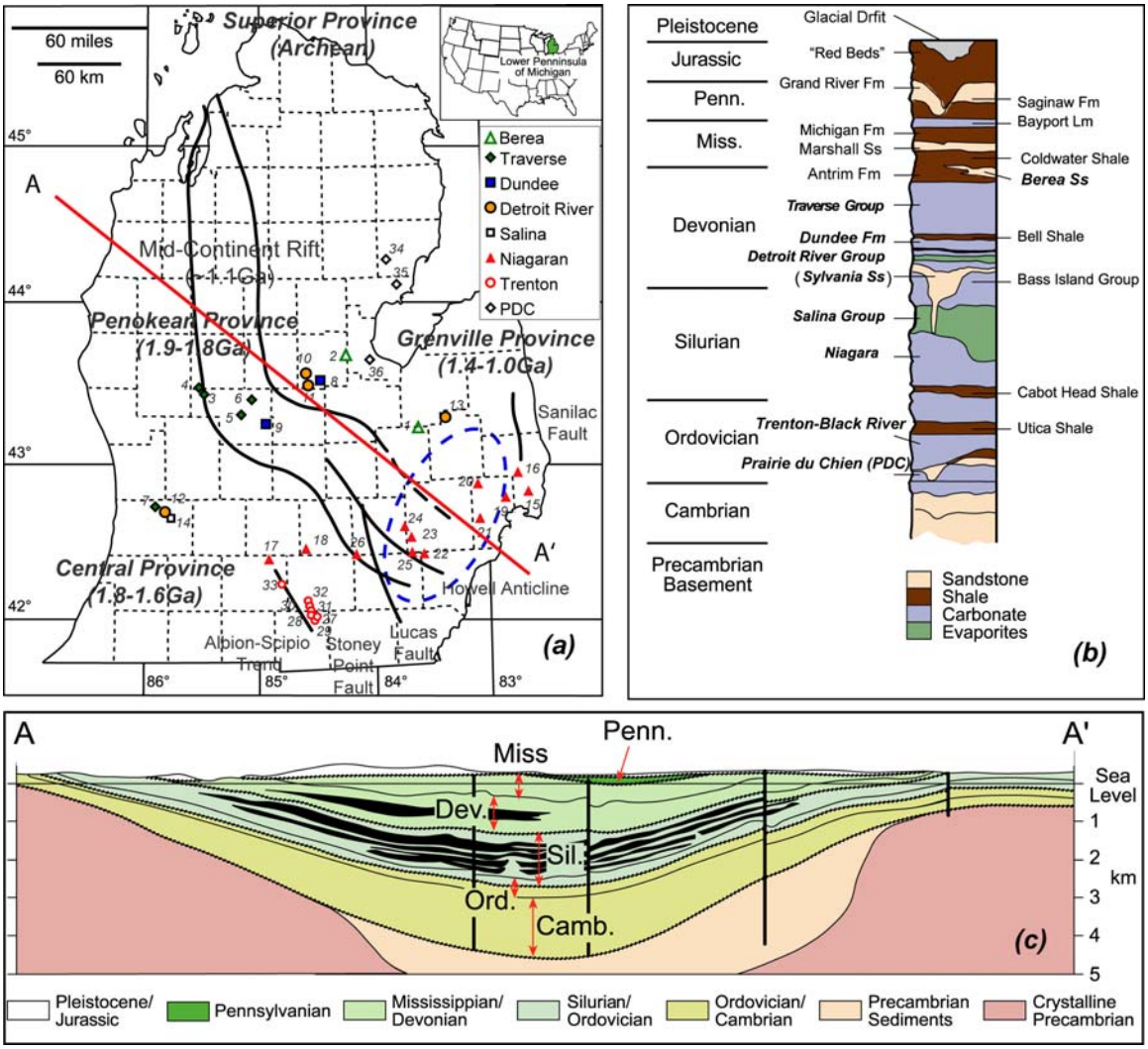

Fig. 4.1 a. Central portion of the Michigan Basin (Lower Peninsula of Michigan). Major tectonic structures (e.g., Mid Continental Rift - MCR) are indicated, as well as basement provinces [after *Dorr and Eschman*, 1970; *Catacosinos et al.*, 1991; *Fisher et al.*, 1988] and sample location; dashed blue line indicates the approximate location of apatite fission track samples revealing thermal activity in the Cretaceous; **b.** Stratigraphic succession of the Michigan Basin. Major lithologies present in the basin are identified; units for which formation brines were sampled in this study are highlighted in bold. **c.** General schematic geologic representation along cross section A–A.

highest salinities (up to 600 g/L) ever reported in sedimentary basins around the world [*Case*, 1945; *Wilson and Long*, 1993a,b]. Such high He fluxes in shallow aquifers suggest the presence of a dominant vertical water flow component and a minor impact of recharge water at depth [*Ma et al.*, 2005]. Both extremely high salinities and high He fluxes at shallow depths point to the absence of significant groundwater flow in the deeper portions of the basin and thus, to the presence of extremely old groundwater, possibly millions of years old. This is also consistent with major element and stable isotope data, which show that these brines originate from ancient seawater [e.g., *Wilson and Long*, 1993a,b].

4.3. Sampling techniques and experimental methods

Brine samples for noble gas analyses were collected from eight formations (carbonates and sandstones) in the Michigan Basin (Fig. 4.1a,b). Brines were sampled from actively pumping wells in standard refrigeration grade 3/8" Cu tubes (~14 ml) that were sealed by stainless steel pinch-off clamps [*Weiss*, 1968] at well head pressures after water was allowed to flow through the tubing for ~10 minutes to avoid atmospheric contamination and to ensure that the temperature had reached equilibrium. Elemental and isotopic noble gas measurements were performed at the University of Michigan as described below. Additional detail on noble gas measurements can be found elsewhere [*Ma et al.*, 2004; *Saar et al.*, 2005]. He and Ne results are presented in Table 4.1.

Brine samples were attached to a vacuum extraction system and noble gases were quantitatively extracted for inletting into a MAP-215 mass spectrometer. Noble gases were transported using water vapor as a carrier gas through two constrictions in the

Table 4.1. He and Ne elemental and isotopic compositions (±1σ uncertainties) with well idenfication number, formation, lithology, and well depths.

Sample Number	Formation	Lithology	Depth (m)	^{4}He ($cm^{3}STP/g$)	+/-	$^{3}He/^{4}He$ (R/Ra)	+/-	^{22}Ne ($cm^{3}STP/g$)	+/-	$^{20}Ne/^{22}Ne$	+/-	$^{21}Ne/^{22}Ne$	+/-
	Devonian												
1	Berea	Sandstone	1005	8.37E-07	1.26E-08	0.251	0.044	4.50E-11	5.85E-13	10.04	0.26	0.0312	0.0010
2	Berea	Sandstone	780	5.35E-06	8.03E-08	0.414	0.110	5.17E-11	6.72E-13	9.94	0.16	0.0298	0.0006
3	Traverse	Carbonate	1014	5.03E-07	7.54E-09	0.104	0.014	4.68E-11	6.09E-13	10.45	0.11	0.0301	0.0005
4	Traverse	Carbonate	1015	5.99E-06	9.80E-07	0.110	0.022	1.05E-10	1.36E-12	10.08	0.05	0.0304	0.0003
5	Traverse	Carbonate	909	3.00E-05	4.51E-07	0.071	0.010	1.24E-10	1.61E-12	10.00	0.05	0.0393	0.0003
6	Traverse	Carbonate	1072	1.82E-05	2.72E-07	0.073	0.009	1.56E-10	2.03E-12	10.32	0.10	0.0325	0.0005
7	Traverse	Carbonate	546	1.57E-07	2.36E-09	1.216	0.328	1.48E-10	1.93E-12	10.05	0.12	0.0291	0.0004
8	Dundee	Carbonate	1036	1.76E-04	2.64E-06	0.213	0.032	2.90E-09	3.78E-11	9.64	0.06	0.0299	0.0002
9	Dundee	Carbonate	1090	9.68E-06	1.45E-07	0.059	0.015	6.74E-10	8.76E-12	9.85	0.05	0.0306	0.0002
10	Detroit River	Carbonate	1378	9.26E-05	1.39E-06	0.053	0.009	2.85E-10	3.71E-12	9.90	0.04	0.0392	0.0003
11	Detroit River	Sandstone	1480	4.69E-04	7.03E-06	0.063	0.015	3.68E-09	4.78E-11	9.76	0.08	0.0337	0.0004
12	Detroit River	Carbonate	572	1.49E-05	2.23E-07	0.184	0.027	9.14E-10	1.19E-11	9.93	0.07	0.0290	0.0002
13	Detroit River	Sandstone	1070	3.72E-04	5.57E-06	0.131	0.030	9.25E-10	1.20E-11	9.70	0.08	0.0340	0.0004
	Silurian												
14	Salina	Carbonate	699	6.13E-07	9.20E-09	0.099	0.013	4.04E-10	5.25E-12	10.09	0.06	0.0294	0.0002
15	Niagaran	Carbonate	830	2.16E-07	3.24E-09	1.290	0.266	1.63E-10	2.12E-12	10.54	0.20	0.0303	0.0010
16	Niagaran	Carbonate	1022	2.35E-05	3.53E-07	0.105	0.026	9.92E-11	1.29E-12	9.88	0.16	0.0344	0.0006
17	Niagaran	Carbonate	1096	1.33E-05	1.99E-07	0.055	0.009	3.52E-10	4.58E-12	9.86	0.05	0.0319	0.0002
18	Niagaran	Carbonate	1168	1.70E-03	2.55E-05	0.101	0.020	3.57E-09	4.64E-11	9.49	0.07	0.0337	0.0004
19	Niagaran	Carbonate	887	8.67E-06	1.30E-07	0.679	0.148	5.24E-11	6.82E-13	10.23	0.28	0.0336	0.0012
20	Niagaran	Carbonate	1143	3.66E-06	5.49E-08	0.143	0.021	5.48E-11	7.13E-13	9.83	0.30	0.0315	0.0010
21	Niagaran	Carbonate	915	7.01E-06	1.05E-07	0.109	0.014	2.04E-10	2.66E-12	10.42	0.11	0.0327	0.0005
22a	Niagaran	Carbonate	941	1.42E-07	2.14E-09	0.396	0.055	4.68E-11	6.08E-13	10.74	0.13	0.0301	0.0005
22b	Niagaran	Carbonate	941	1.92E-07	2.88E-09	0.691	0.104	4.91E-11	6.39E-13	10.78	0.12	0.0305	0.0005
23	Niagaran	Carbonate	1138	1.33E-05	1.99E-07	0.113	0.020	1.08E-10	1.41E-12	10.31	0.08	0.0346	0.0005
24	Niagaran	Carbonate	1259	1.45E-06	2.17E-08	0.064	0.012	4.44E-11	5.78E-13	10.33	0.13	0.0314	0.0005
25a	Niagaran	Carbonate	996	4.27E-07	6.41E-09	0.405	0.039	5.63E-11	7.32E-13	10.78	0.10	0.0294	0.0006
25b	Niagaran	Carbonate	996	6.55E-07	9.82E-09	0.153	0.017	6.19E-11	8.05E-13	10.76	0.16	0.0293	0.0005
26	Niagaran	Carbonate	937	1.53E-03	2.29E-05	0.133	0.030	5.83E-09	7.57E-11	9.61	0.06	0.0336	0.0002
	Ordovician												
27	Trenton	Carbonate	1330	5.39E-06	8.08E-08	0.068	0.010	8.67E-11	1.13E-12	10.18	0.06	0.0329	0.0004
28	Trenton	Carbonate	1332	3.53E-06	5.29E-08	0.089	0.013	7.49E-11	9.74E-13	10.40	0.08	0.0326	0.0004
29	Trenton	Carbonate	1301	4.62E-06	6.93E-08	0.059	0.008	8.24E-11	1.07E-12	10.06	0.07	0.0331	0.0004
30	Trenton	Carbonate	1302	1.91E-05	2.86E-07	0.082	0.008	1.09E-10	1.42E-12	10.09	0.07	0.0348	0.0004
31	Trenton	Carbonate	1302	1.09E-04	1.63E-06	0.076	0.007	3.01E-10	3.91E-12	9.75	0.04	0.0410	0.0002
32	Trenton	Carbonate	1233	8.87E-05	1.33E-06	0.058	0.009	1.94E-10	2.52E-12	9.74	0.06	0.0432	0.0004
33	Trenton	Carbonate	1283	1.17E-06	1.75E-08	0.059	0.007	5.95E-11	7.73E-13	10.24	0.09	0.0312	0.0003
34	PDC	Carbonate	3595	3.33E-06	4.99E-08	0.133	0.015	5.03E-11	6.55E-13	10.65	0.48	0.0314	0.0011
35	PDC	Carbonate	3621	3.66E-05	5.49E-07	0.057	0.006	1.29E-10	1.68E-12	9.86	0.08	0.0395	0.0004
36	PDC	Carbonate	3196	2.50E-06	3.75E-08	0.098	0.014	5.55E-11	7.21E-13	10.42	0.10	0.0324	0.0004
ASW(5M NaCl solution) at 25°C [(1)]				1.3E-08		1.0		4.1E-09		9.80		0.029	

1. ASW concentrations calculated from *Crovetto et al.* [1982], *Smith* [1985], and *Smith and Kennedy* [1983]. Isotopic ratios as given by *Ozima and Podosek* [2002]

vacuum system, purified by two Ti sponge getters, and sequentially allowed to enter a MAP-215 mass spectrometer using a cryo-separator. Release temperatures for He, Ne, Ar, Kr, and Xe from the cryo-separator were 30K, 60K, 180K, 215K, and 270K, respectively. ^{4}He and ^{20}Ne were measured using a Faraday detector and ^{3}He, ^{21}Ne, and ^{22}Ne were measured using an electron multiplier in ion counting mode. During neon isotope analysis, a liquid N_2 cold trap equipped with sintered steel was used to minimize peak interferences and appropriate mass peaks were monitored to correct for interferences due to doubly charged ions $^{40}Ar^{2+}$ on ^{20}Ne, CO_2^{2+} on ^{22}Ne and interfering contaminant $H_2{}^{18}O^{+}$ on ^{20}Ne. The correction factor for $^{40}Ar^{2+}/^{40}Ar^{+}$ is 0.247, previously measured by cryo-separated Ar without the presence of Ne. The correction factor for $^{44}CO_2^{2+}/^{44}CO_2^{+}$ is 0.007, measured with the presence of CO_2 in the mass spectrometer. The correction factor for $H_2{}^{18}O^{+}/H_2{}^{16}O^{+}$ is 0.002, the ^{18}O fraction in the oxygen isotopes. The correction for interferences at mass 20 (from $^{40}Ar^{2+}$ and $H_2{}^{18}O^{+}$) ranges from 0.13%-4.38% of the total mass 20 signal for all water samples, averaging 1.07%. The correction for interference at mass 22 (from $^{44}CO_2^{2+}$) ranges from 0.01%-1.56% for all samples, averaging 0.17%. These corrections are small and comparable to those where the presence of a primordial/solar-like Ne component was previously identified in OIBs [see, e.g., *Sarda et al.*, 1988; *Honda et al.*, 1993].

Before each sample analysis, a calibrated amount of air standard and a procedural blank were performed exactly in the same manner as the sample measurement. The blank correction was applied to all measured peaks. The typical ^{4}He Blank level during these experiments was 2.1×10^{-7} cm^{3}STP. ^{3}He and ^{4}He blank corrections were negligible due to the large sample signal sizes. The typical ^{22}Ne blank level was 4.2×10^{-10} cm^{3}STP and the

average measured sample/blank signal size ratio for ^{22}Ne is about 15. The ^{4}He and ^{22}Ne elemental abundances and $^{3}He/^{4}He$, $^{20}Ne/^{22}Ne$, $^{21}Ne/^{22}Ne$ isotopic ratios for each sample were normalized to the air standard after blank correction. ^{4}He and ^{20}Ne abundances have typical uncertainties of 1.5 and 1.3%, respectively. All uncertainties are at $\pm 1\sigma$ level of confidence. The above procedure was tested and calibrated with synthetic laboratory fresh water samples produced at a known temperature.

4.4. Helium and neon systematics

The concentrations of helium isotopes (^{3}He, ^{4}He) in old groundwater flow systems frequently exceed those expected for water in solubility equilibrium with the atmosphere (Air Saturated Water: ASW). In these systems, excesses result mainly from the $^{6}Li(n, \alpha)^{3}H$ (^{3}He) reaction [*Morrison and Pine*, 1955] (nucleogenic ^{3}He), the α-decay of the natural U and Th decay series elements in common rocks (radiogenic ^{4}He), and mantle contributions to both ^{3}He and ^{4}He [*Oxburgh et al.*, 1986].

In these same systems, crustal Ne is generally dominant due to the production of nucleogenic ^{21}Ne, which results mainly from reactions between α particles from U-Th decay and O and Mg atoms in the crust [*Wetherill*, 1954]. The production of nucleogenic ^{20}Ne and ^{22}Ne in the crust which occurs mostly through nuclear reactions $^{17}O(\alpha, n)^{20}Ne$ and $^{23}Na(n,\alpha)^{20}Ne$ for ^{20}Ne and $^{19}F(\alpha, n)^{22}Na(\beta^{+})^{22}Ne$, $^{19}F(\alpha, p)^{22}Ne$, and $^{25}Mg(n, \alpha)^{22}Ne$ for ^{22}Ne [*Wetherill*, 1954] is typically negligible (see also Appendix 4A). When present in excess with respect to ASW values, ^{20}Ne typically has a mantle origin. Because the ^{22}Ne nuclear production rate is far more pronounced in the crust than that of ^{20}Ne [*Wetherill*, 1954; *Ballentine and Burnard*, 2002], when crustal production of these two

isotopes takes place, it leads to an extremely small $^{20}Ne/^{22}Ne$ ratio of ~0.05, a value that is far smaller than that of air (9.8, Table 4.2).

Radiogenic and nucleogenic He and Ne production is assumed here to represent the crustal composition of these two isotopes.

4.5. Results and discussion

$^{3}He/^{4}He$ (R) ratios in Michigan brines vary from 0.053±0.009 times the atmospheric ratio Ra, a typical crustal production value (≤0.05, Table 4.2), to 1.29±0.27 (Table 4.1). Because atmospheric He contributions are negligible for all samples (Table 4.3), measured R/Ra ratios above the crustal production value represent simply a binary mixture between a crustal and mantle components (e.g., 8.5 for MORB and 120 for Primordial Solar-like, Table 4.2). Originally high R/Ra mantle values in these samples will be quickly lowered by low crustal production ratios [*Castro*, 2004], i.e., predominantly radiogenic ^{4}He production. Despite this crustal masking effect, a total He mantle contribution of up to 15% is readily identifiable in these samples.

$^{20}Ne/^{22}Ne$ ratios greater than the atmospheric ratio (9.8, Table 4.2) are observed for a large subset of samples and reach values of up to 10.78±0.10 (Table 4.1). Because the production of nucleogenic ^{20}Ne as well as the occurrence of mass dependent fractionation were excluded as potential sources of such high $^{20}Ne/^{22}Ne$ values (see Appendixes 4A and 4B, respectively), it is clear that these high $^{20}Ne/^{22}Ne$ ratios largely reflect the addition of mantle ($^{20}Ne/^{22}Ne$ =13.8, Table 4.2) ^{20}Ne, with contributions of up to 32% of the total measured Ne. By contrast, $^{21}Ne/^{22}Ne$ ratios greater than the atmospheric value of 0.0290 (Table 4.2), up to 0.0432±0.0004 (Table 4.1), reflect the

Table 4.2. End-member isotopic and elemental ratios of distinct Earth reservoirs.

	Isotopic ratios				*Elemental ratios*		
	$^{3}He/^{4}He$ (R/Ra)	$^{20}Ne/^{22}Ne$	$^{21}Ne/^{22}Ne$	$^{4}He/^{20}Ne$	$^{3}He/^{22}Ne$	$^{4}He/^{22}Ne$	$K = (^{4}He/^{22}Ne)_{crust}/(^{4}He/^{22}Ne)_{mantle}$
Air [1]	1	9.8	0.029				
Crust [2]	0.05	0.3	0.33			7.90E+07	
Crust [3]			0.47				
			0.1				
Mantle							
Primordial (primitive solar nebula) [4]	120	13.8	0.0328	850		1.17E+04	6735
OIB mantle (Iceland) [5]	35	13.8	0.035		6	1.24E+05	636
OIB mantle (Hawaii) [5]		13.8	0.039				
OIB mantle(Reunion) [5]		13.8	0.043				
OIB mantle (Kerguelen) [5]		13.8	0.053				
MORB mantle [5]	8.5	13.8	0.075		8.8	7.50E+05	105

1. From *Ozima and Podosek* [2002].
2. $^{3}He/^{4}He$ ratio after *Oxburgh et al.* [1986]; $^{20}Ne/^{22}Ne$ and $^{21}Ne/^{22}Ne$ ratios constrained by our χ^2 fitting procedure. $^{4}He/^{22}Ne$ ratio after *Yatsevich and Honda* [1997].
3. After *Kennedy et al.* [1990].
4. $^{3}He/^{4}He$ ratio after *Mahaffy et al.* [2000]; $^{20}Ne/^{22}Ne$ and $^{21}Ne/^{22}Ne$ ratios after *Benkert et al.* [1993]; $^{4}He/^{20}Ne$ ratio after *Anders and Grevesse* [1989]; $^{4}He/^{22}Ne$ ratio calculated from $^{4}He/^{20}Ne$ and $^{20}Ne/^{22}Ne$ ratios.
5. Summarized by *Graham* [2002]; Iceland - *Dixon et al.* [2000], Hawaii - *Honda et al.* [1991], Reunion - *Hanyu et al.* [2001], Kerguelen - *Valbratch et al.* [1996], MORB - *Moreira et al.* [1998]; $^{4}He/^{22}Ne$ ratios calculated from $^{3}He/^{22}Ne$ and $^{3}He/^{4}He$ ratios.

Table 4.3. He and Ne $_{(crust+mantle)}$ isotopic compositions after atmospheric component removal.

Sample Number	$(^3He/^4He)_{crust+mantle}$* (R/Ra)	+/-	$(^{20}Ne/^{22}Ne)_{crust+mantle}$	+/-	$(^{21}Ne/^{22}Ne)_{crust+mantle}$	+/-
1	0.251	0.045	12.73	0.99	0.056	0.022
2	0.414	0.110	13.08	0.88	0.049	0.019
3	0.104	0.014	13.67	0.12	0.036	0.003
4	0.110	0.028	13.18	0.13	0.047	0.003
5	0.071	0.010	11.07	0.23	0.093	0.005
6	0.073	0.009	13.00	0.16	0.050	0.004
7	1.216	0.329	13.93	0.26	0.030	0.006
8	0.213	0.032				
9	0.059	0.015	11.53	0.90	0.083	0.020
10	0.053	0.009	10.52	0.24	0.105	0.005
11	0.063	0.015	8.82	2.48	0.142	0.055
12	0.184	0.027	13.95	0.34	0.030	0.008
13	0.131	0.030				
14	0.097	0.013	13.73	0.11	0.034	0.002
15	1.291	0.267	13.68	0.23	0.036	0.005
16	0.105	0.026	10.78	1.54	0.099	0.034
17	0.055	0.009	11.10	0.68	0.092	0.015
18	0.101	0.020				
19	0.679	0.149	12.62	0.60	0.059	0.013
20	0.143	0.021				
21	0.109	0.014	13.10	0.13	0.048	0.003
22a	0.396	0.055	13.77	0.09	0.033	0.002
22b	0.691	0.105	13.71	0.09	0.035	0.002
23	0.113	0.020	12.58	0.15	0.060	0.003
24	0.064	0.012	13.26	0.15	0.045	0.003
25a	0.404	0.040	13.89	0.11	0.031	0.002
25b	0.152	0.017	13.92	0.10	0.030	0.002
26	0.133	0.030				
27	0.068	0.010	12.63	0.15	0.059	0.003
28	0.089	0.013	13.07	0.10	0.049	0.002
29	0.059	0.008	12.24	0.26	0.067	0.006
30	0.082	0.008	12.00	0.22	0.073	0.005
31	0.076	0.008	9.39	0.35	0.130	0.008
32	0.058	0.009	9.33	0.44	0.131	0.010
33	0.059	0.007	13.22	0.12	0.046	0.003
34	0.133	0.015	13.51	0.30	0.039	0.007
35	0.057	0.006	10.25	0.53	0.111	0.012
36	0.098	0.014	13.14	0.11	0.047	0.002

* Estimated after removal of the atmospheric component using the atmosphere-derived ^{22}Ne concentrations following *Craig et al.* [1978]. $(^3He/^4He)_{crust+mantle}$ ratios are indistinguishable from the measured $^3He/^4He$ ratios (Table 1) due to the extremely high measured $^4He/^{22}Ne$ ratios of the brine samples (1.1×10^3 - 4.8×10^5), 350-154000 times the atmospheric value (3.12) [*Ozima and Podosek*, 2002].

addition of crustally produced nucleogenic ^{21}Ne. $^{20}Ne/^{22}Ne$ and $^{21}Ne/^{22}Ne$ ratios of Michigan brines (Fig. 4.2, Table 4.1) reflect a three-component mixing between the atmosphere, the crust, and the mantle, and provide clarification on the nature of this mantle component. Specifically, 22 out of 38 samples plot within the area defined by the Air-MORB-Solar end-members (Fig. 4.2). Of greater significance is the fact that, 14 samples plot well above the well established MORB line [*Moreira et al.*, 1998], falling into the domain of multiple OIB lines (e.g., Kerguelen, Reunion, Hawaii, Iceland, Fig. 4.2, Table 4.2), thus pointing strongly to the presence of a primordial Ne component. This primordial Ne component can be traced to a pristine solar-like origin as shown by samples 22 and 25 (Fig. 4.2) which fall on the Solar line (Table 4.2). Duplicates were run for these two samples and this primordial, solar-like component was confirmed (Table 4.1, Fig. 4.2). Direct identification of such a primordial, solar-like Ne component in crustal fluids is remarkable taking into account both atmospheric Ne addition through groundwater (ASW) and continuous ^{21}Ne production in the crust leading, over time, to progressively higher $^{21}Ne/^{22}Ne$ ratios (Fig. 4.2). This addition and production will move samples with original primordial signatures plotting along the Air-Solar line to different OIB lines, from Iceland toward Kerguelen, as nucleogenic ^{21}Ne increases. Over time, due to the combined effect of ASW incorporation and nucleogenic production, samples will move from the Air-MORB-Solar domain into the Air-MORB-Crustal domain and, subsequently, into the Air-Crustal domain (defined by the different Air-Crust mixing lines with low $^{20}Ne/^{22}Ne$ and variable $^{21}Ne/^{22}Ne$ ratios, depending on local production rates, e.g., samples 8, 13, 26, Fig. 4.2), eventually completely masking the presence of a primordial, solar component. The preservation of a solar component in these brines is

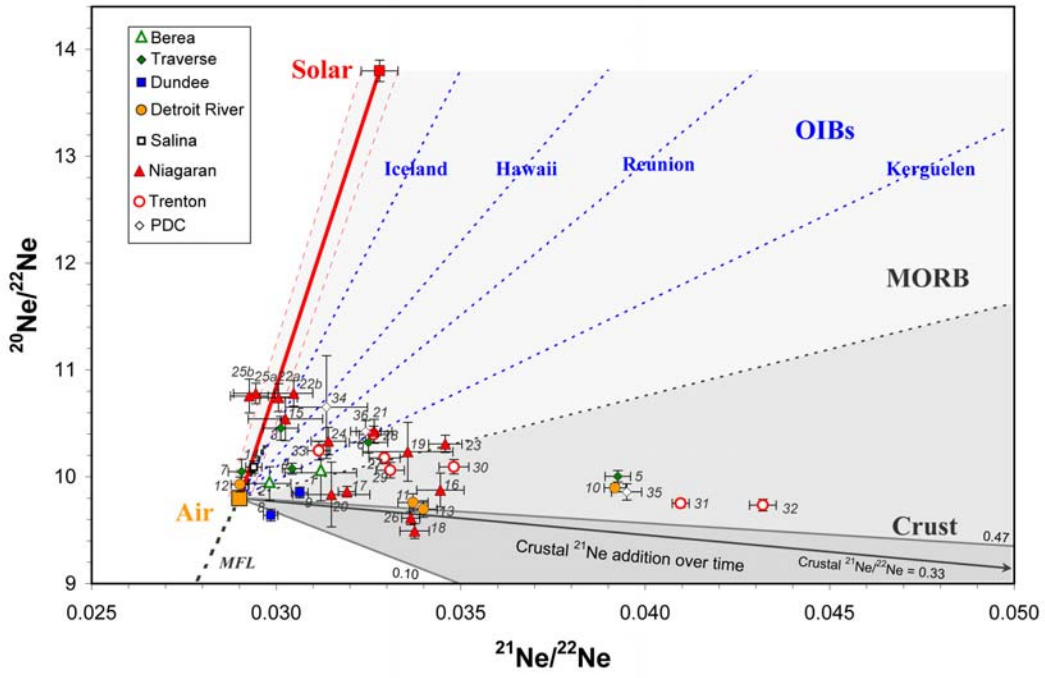

Fig. 4.2. Measured $^{20}Ne/^{22}Ne$ vs. $^{21}Ne/^{22}Ne$ ratios for Michigan Basin brines. Three components are presented in this diagram: Air, Mantle (MORB, OIBs, Solar), and Crust. Mixing lines between Air-Solar, Air-MORB as well as Air-OIBs (Iceland, Hawaii, Reunion, Kerguelen) are indicated. Air-Crust mixing lines with $^{21}Ne/^{22}Ne$ ratios of 0.1, 0.47 (Table 4.2), and 0.33 (this study) are also shown. Triangular grey areas, from lighter to darker indicate the Air-Solar-MORB, Air-MORB-Crust, and Air-Crust domains, respectively. End-member values are provided in Table 4.2. MFL represents the mass-fractionation line. Dashed lines along the Air-Solar line provide uncertainty associated with measurements.

thus dependent on the rate of nucleogenic and atmospheric additions for each sample as well as on the time elapsed since this solar component was introduced into the basin at a particular location. Evolution of isotopic ratios in these brines is thus similar in nature to that proposed to explain the highly variable measured R/Ra ratios in OIBs around the world [*Anderson*, 1998].

In Michigan brines, the existence of a solar-like component for samples lying below the MORB line (Fig. 4.2) can also be traced through the combined analysis of He and Ne isotopic ratios. Here, a primordial component is commonly characterized by directly correlated $^{20}Ne/^{22}Ne$ and inversely correlated $^{21}Ne/^{22}Ne$ with R/Ra ratios, respectively [*Moreira and Allegre*, 1998; *Graham*, 2002]. This combined analysis in our brines requires removal of the atmospheric Ne component so that, like R/Ra ratios, Ne isotopic ratios will represent solely a binary mixture between crust and mantle (MORB, OIB, or Solar) end-members ($^{20}Ne/^{22}Ne_{crust+mantle}$ and $^{21}Ne/^{22}Ne_{crust+mantle}$). Removal of atmospheric Ne was achieved following previously developed procedures [*Ballentine and O'Nions*, 1992; *Ballentine*, 1997; Appendix 4C]. Mixing lines between the crust and mantle (MORB, OIB, and Solar, respectively) in these two-element isotope plots (Figs. 4.3a,b) are defined by their respective isotopic ratio end-members (Table 4.2). The curvature of each hyperbola is defined by $K_{crust\text{-}mantle} = (^4He/^{22}Ne)_{crust}/(^4He/^{22}Ne)_{mantle}$, where $(^4He/^{22}Ne)_{crust}$ and $(^4He/^{22}Ne)_{mantle}$ are the crustal and mantle (MORB, OIB, Solar) $^4He/^{22}Ne$ elemental ratios, respectively (Table 4.2). If no uncertainty were associated with the crustal and mantle He and Ne end-members, and if, prior to mixing, all end-members had a spatially constant crustal and mantle $^4He/^{22}Ne$ ratio, all samples should fall along a single mixing line within error. Under these same assumptions, Michigan brines would be

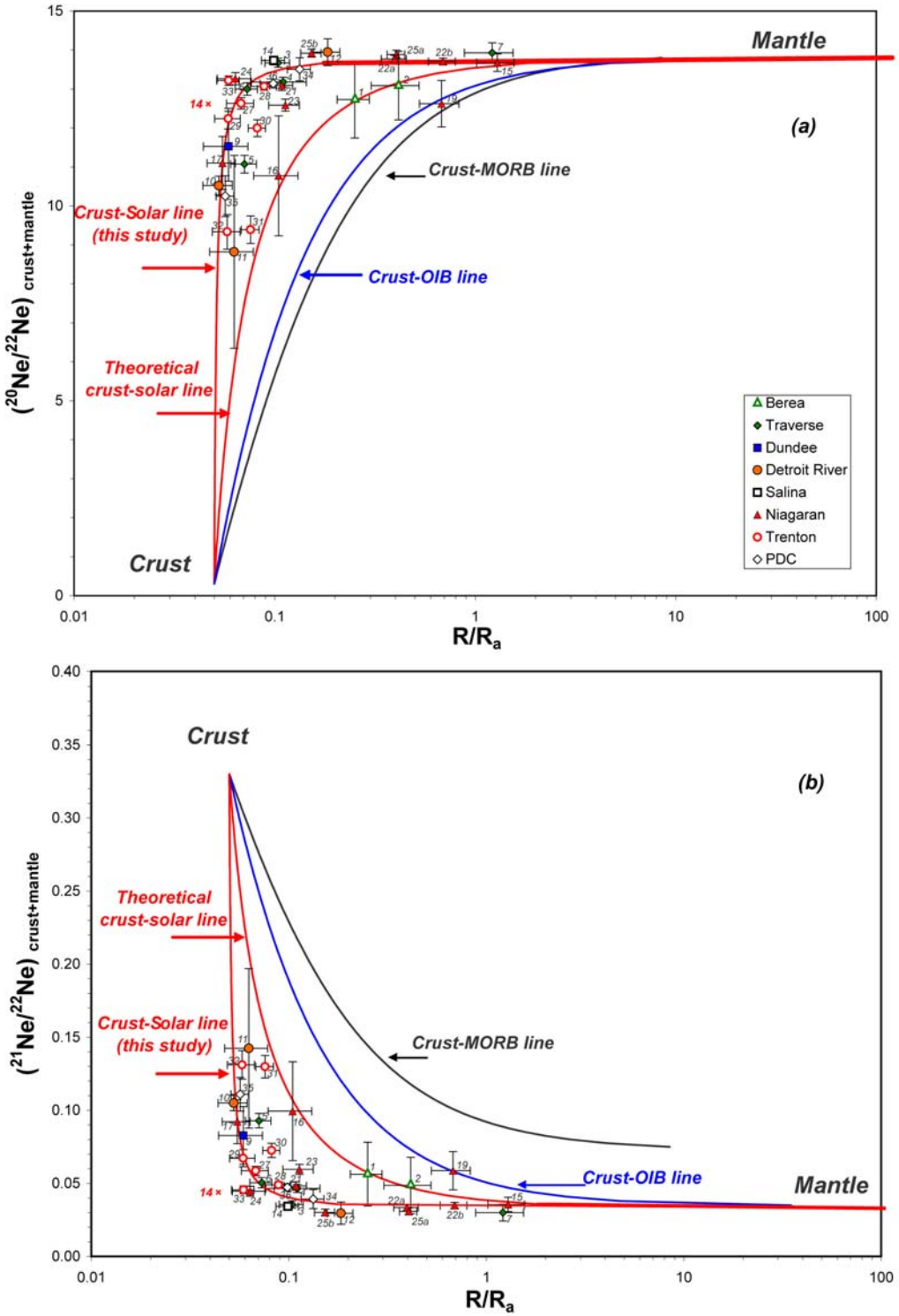

Fig. 4.3. Two-component mixing plots for $^{20}Ne/^{22}Ne_{crust+mantle}$ (a) and $^{21}Ne/^{22}Ne_{crust+mantle}$ (b) vs. R/Ra ratios for Michigan Basin brines. Crust-MORB, Crust-OIB and theoretical Crust-solar mixing lines are shown (see also Table 4.2 for end-member values). Crust-Solar mixing line (this study) from estimated optimal values for $K_{crust-solar}$ and crustal $^{21}Ne/^{22}Ne$ end-member is also shown (see also Appendix 4C).

expected to fall along the theoretically defined Crust-Solar line (Figs. 4.3a,b, Table 4.2). With the exception of $K_{crust\text{-}solar}$ and crustal $^{21}Ne/^{22}Ne$ ratios, all other end-members used to construct both, the mixing lines as well as to calculate $^{20}Ne/^{22}Ne_{crust+mantle}$ and $^{21}Ne/^{22}Ne_{crust+mantle}$ for all samples were those previously reported in the literature (Table 4.2). The solar-like $^{4}He/^{22}Ne$ elemental ratio used to build the theoretical Crust-Solar mixing line is representative of the primitive solar nebula, and assumes that no significant He/Ne elemental fractionation occurred during the early stages of the Earth's formation (Fig. 4.3a,b, $K_{crust\text{-}solar}$ = 6700, Table 4.2, Mizuno et al, 1980). Optimal values for $K_{crust\text{-}solar}$ and the crustal $^{21}Ne/^{22}Ne$ end-member were obtained using a χ^2 minimization procedure (Appendix 4C). For most samples, calculated $^{20}Ne/^{22}Ne_{crust+mantle}$ ratios (Table 4.3, Fig. 4.3a) display an overwhelming dominance of a primordial component with values up to 13.8 (e.g., samples 22, 25, 15, 7), indicating the presence of a pristine solar component as previously discussed (see also Fig. 4.2). Calculated $(^{21}Ne/^{22}Ne)_{crust+mantle}$ ratios (Table 4.3, Fig. 4.3b) reflect, as expected, an almost complete absence of nucleogenic ^{21}Ne for some samples (e.g., 15, 22), as opposed to a significant crustal ^{21}Ne component in others (e.g., 31, 32). Significantly, these two-element isotopic plots display the expected direct correlation between $^{20}Ne/^{22}Ne$ and R/Ra ratios (Fig. 4.3a) as well as inversely correlated $^{21}Ne/^{22}Ne$ vs. R/Ra values (Fig. 4.3b). It is clear that none of the samples fall on or close to the Crust-MORB line. While a small subset of samples fall along the theoretical Crust-Solar line previously discussed, it is apparent that most of our brine samples fall to the left, along a line defined by our optimized $K_{crust\text{-}solar}$ value (Figs. 4.3a,b), 14 times the theoretical one. This discrepancy is expected taking into account uncertainties associated with the estimation of the theoretical solar value, and the

occurrence of He-Ne fractionation from a variety of sources (e.g., equilibrium partitioning of He and Ne between a melt and gas phase). Similar discrepancies between optimized and theoretical $K_{crust\text{-}MORB}$ were also found and attributed to different He-Ne fractionation sources [*Ballentine*, 1997]. In a data set that includes samples with such distinct depths (Table 4.1), geographic locations (Fig. 4.1), and consequently contrasting ages, distinct $K_{crust\text{-}solar}$ values are a reflection of each sample's individual history which will compound multiple sources and degrees of He-Ne fractionation.

4.6. A primordial noble gas signature in a shallow refractory reservoir – discussion and implications

While the existence of a primordial, solar-like Ne component is unequivocal, its connection to a lower, largely undegassed mantle reservoir via a mantle plume is highly unlikely. Indeed, in addition to a lack of evidence for mantle or magmatic activity within the Michigan Basin [*Catacosinos et al.*, 1991] throughout its entire history (>0.5Ga), no hotspots or hotspot tracks are known in the area [*Heaman et al.*, 2004; *Anderson and Schram*, 2005]. Mantle activity was last recorded during an episode of crustal extension at ~1.1Ga, leading to the emplacement of a rift believed to be part of the Mid-Continent Rift (MCR) system, which transects the old Archean-Proterozoic (~1.2->2.5Ga) [*Bickford*, 1986] crystalline basement throughout the entire basin (Fig. 4.1). Underneath the basement is a 200-Km thick [*Griffin et al.*, 2004] subcontinental lithospheric mantle (SCLM). The upper part is rich in depleted lherzolites and harzburgites, a feature that increases with decreasing depth. These account for up to 30% of the SCLM material at the top [*Griffin et al.*, 2004] and suggest a highly depleted U and Th environment [*Anderson*, 1998]. This upper section is similar to many other modified Archean SCLM

sections [*Griffin et al.*, 2004]. For example, studies based on peridotite xenoliths as well as surface heat flow estimations point also to an almost completely depleted U-Th-K environment in the SCLM of the Canadian Shield [*Rudnick and Nyblade*, 1999], just north of our study area. Overall, Archean SCLM is depleted, refractory, and buoyant relative to the asthenosphere, which greatly limits its potential for recycling, thus enhancing its preservation over time, in particular, underneath Archean cratons [*Menzies*, 1990; *Griffin et al.*, 1999]. In addition to a highly depleted U and Th environment, such a high concentration of depleted lherzolites and harzburgites at the top of the SCLM underneath the Michigan Basin suggests the presence, at very shallow depths, of potential He and Ne reservoirs [*Graham et al.*, 1990; *Anderson*, 1998; *Coltice and Ricard*, 2002; *Meibom et al.*, 2005]. Indeed, it was suggested that high R/Ra ratios commonly observed in OIBs could signal residues from ancient differentiation of the primitive mantle that was outgassed during an early stage of the Earth's history [*Graham et al.*, 1990]. It was argued that He might be more compatible than U and Th, leaving olivine-rich partial melt residues such as harzburgites with high He/(U+Th) ratios and thus, over time, greater than expected R/Ra ratios in OIBs [*Graham et al.*, 1990]. Recent experimental work [*Parman et al.*, 2005] supports this prediction. *Anderson* [1998] subsequently argued for the presence of shallow refractory (low U and Th) reservoirs potentially created through a mechanism similar to that suggested by *Graham et al.* [1990] to account for high R/Ra ratios in OIBs as opposed to a deep primitive source. Fluid inclusions in olivine with high He/(U+Th) ratios formed during shallow crystallization of the melt would be a good candidate for such a reservoir. Alternatively, mantle degassing at shallow depths might occur, leading to He release into a CO_2-rich gas phase, separation from MORBs, and

subsequent storage in a refractory reservoir [*Anderson*, 1998]. Similar mechanisms leading to primordial Ne signatures were subsequently extended to Ne [*Meibom et al.*, 2005]. More recently, early diffusion of solar-like He and Ne isotopes from primitive material into a residual refractory reservoir such as dunites during the early Earth's history stages was proposed [*Albarede*, 2008]. Here, it is argued that the source of such a primordial signature in our brines is likely the shallow refractory reservoir of the Michigan Basin SCLM, possibly created by one of the mechanisms similar to that proposed by *Anderson* [1998], or that more recently proposed by *Albarede* [2008] for oceanic regions. It is further suggested that recent reactivation of the old MCR system (Fig. 4.1) transecting the crystalline basement is responsible for the release of a gas phase carrying this primordial noble gas signature into the basin. Indeed, its reactivation during the Late Devonian-Mississippian (370-323Ma) period was previously suggested based on authigenic illite, which yields the youngest ages (323Ma) and highest temperatures (~170°C) in the vicinity of the MCR [*Girard and Barnes*, 1995]. Such temperatures cannot be explained by the current geothermal gradient in the basin. A major upflit of the basin fault blocks in southern Michigan also occurred at the end of the Mississipian period [*Fisher et al.*, 1988], further suggesting a reactivation of the MCR. Importantly, apatite fission track ages from basement samples further indicate two additional, more recent periods of thermal activity, during the Triassic and Cretaceous, respectively [*Crowley*, 1991]. Of particular relevance are the apatite fission track samples revealing thermal activity in the Cretaceous. Indeed, their locations correspond to that of our brine samples displaying the strongest primordial Ne signatures (Niagaran Reef in southern Michigan, Fig. 4.1), and strongly suggest simultaneous release of heat and primordial

noble gases (likely in a gas phase) into the basin during that period (~111Ma). Our two most pristine solar Ne isotopic signatures (samples 22, 25) are located in this same area, precisely above the MCR (Fig. 4.1). It is noted that there are high R/Ra ratios (~30) found in Archean komatites (2.7Ga) in Ontario, Canada, just north of our study area [*Matsumoto et al.*, 2002]. Original R/Ra values were reconstructed by correcting for radiogenic crustal ^{4}He production and found to be $67.5 \leq R/Ra \leq 80.8$. Such primordial He isotopic signatures, potentially representative of the Archean convecting mantle [*Matsumoto et al.*, 2002], are consistent with our observed solar-like He and Ne signatures.

4.7. Concluding remarks

Overall, the primordial solar-like He and Ne signatures present in the Michigan Basin brines not only suggest that a deep primordial mantle reservoir is not required to explain the presence of such components, but also point to a very heterogeneous mantle as previously suggested [*Anderson*, 1998; *Coltice and Ricard*, 2002; *Meibom et al.*, 2005; *Albarede*, 2005, 2008]. Consequently, the presence of a primordial noble gas signature does not necessarily fingerprint the existence of a deep mantle plume. The SCLM underneath ancient cratons is a great candidate for hosting primitive ancient mantle reservoirs. Our study provides a strong observational case for long-term primordial lithospheric storage of noble gases.

Appendix 4A: **Ne crustal production from natural nuclear reactions cannot account for the observed ^{20}Ne excess in the Michigan Basin brines and corresponding high ^{20}Ne/^{22}Ne ratios**

Production of ^{20}Ne in the crust is due to the nuclear reactions $^{17}O(\alpha, n)^{20}Ne$ and $^{23}Na(n,\alpha)^{20}Ne$ (Wetherill, 1954), where the α and n particles are derived from the natural decay of U and Th. ^{20}Ne production rates can be estimated for variable U and Th compositions in the crust following *Ballentine and Burnard* [2002]. For an average upper crust composition (U = 2.8ppm and Th = 10.7ppm) [*Rudnick and Fountain*, 1995], the ^{20}Ne production rate is 2.8×10^{-21} cm^3STP/g. Thus, considering an average porosity of 10%, it would take up to ~2Ga to produce the amounts of excess ^{20}Ne observed in these brines. This age is significantly older than the formation ages of the sedimentary rocks that host these brines (~360-480 Ma). Alternatively, if one would consider production of ^{20}Ne in the rocks that host these brines, i.e., carbonates (U=2.2ppm, Th=1.7ppm) [*Parker*, 1967] and sandstones (U=0.45ppm and Th=1.7 ppm) [*Parker*, 1967], which have significantly lower U and Th concentrations compared to the average crust, it would take up to 3.2Ga and 11Ga, respectively, to produce the observed ^{20}Ne anomalies in these brines.

Of greater significance is the fact that the ^{22}Ne nuclear production rate is far more pronounced in the crust than that of ^{20}Ne [*Wetherill*, 1954; *Ballentine and Burnard*, 2002], thus leading to an extremely small ^{20}Ne/^{22}Ne crustal production ratio of ~0.05. Consequently, in the event that the ^{20}Ne anomalies in these brines were the result from crustal production, an extremely low ^{20}Ne/^{22}Ne ratio of 1.8 would be observed, far lower than the atmospheric ratio of ~9.8, as opposed to our observed higher than atmospheric ^{20}Ne/^{22}Ne ratio value. Crustal nuclear reactions can therefore be ruled out to explain the observed ^{20}Ne excesses in the Michigan Basin brines and corresponding high ^{20}Ne/^{22}Ne values.

Appendix 4B: Mass-dependent fractionation (MDF)

Mass dependent fractionation can be ruled out as the source for the higher measured $^{20}Ne/^{22}Ne$ ratios in the Michigan brine samples. Indeed, samples with the highest $^{20}Ne/^{22}Ne$ ratios (e.g., 22ab, 25ab, 3, 24, 28) have $^{38}Ar/^{36}Ar$ ratios similar to the air value (0.188) and plot straight above the MDF line (Fig. 4.B1), ruling out the possibility of single or multiple stages of MDF. Furthermore, ^{22}Ne concentrations show that these brines have lost a significant amount of atmosphere-derived noble gases and represent a residual phase from an original reservoir (Table 4.1) [*Ma et al.*, 2008]. Mass-dependent fractionation (MDF) generates higher $^{20}Ne/^{22}Ne$ ratios in an escaped phase from a reservoir and complementary lower $^{20}Ne/^{22}Ne$ ratios in the residual phase [see, e.g., *Matsumoto et al.*, 2004]. Thus, if mass-dependent fractionation had occurred at the time the Michigan brines underwent degassing, this process would have led to lower $^{20}Ne/^{22}Ne$ ratios in the brines (residual phase), as opposed to higher $^{20}Ne/^{22}Ne$ ratios. Such a trend is opposite to what is observed in Michigan brine samples displaying high $^{20}Ne/^{22}Ne$ ratios. In turn, this could also lead to higher than atmospheric $^{38}Ar/^{36}Ar$ ratios, which is observed in some samples (Fig. 4.B1). Degassing can thus also be ruled out as a possible process capable of explaining the observed high $^{20}Ne/^{22}Ne$ ratios.

Because molecular diffusion is the mechanism with the greatest potential to create fractionation between the different isotopes, when referring to mass fractionation above, we implicitly refer to fractionation due to molecular diffusion. Two other mechanisms capable of creating fractionation are mutual and thermal diffusion [see, e.g., *Marty*, 1984]. Mutual diffusion yields a trend of $^{38}Ar/^{36}Ar$ vs. $^{20}Ne/^{22}Ne$ ratios similar to that of molecular diffusion (see MFL line, Fig. 4.B1) and thus can, for the reasons already pointed above, also be ruled out as a mechanism capable of producing the highest $^{20}Ne/^{22}Ne$ ratios in these brines. Thermal diffusion can also occur in certain systems. In order for thermal diffusion to occur and lead to significant fractionation, extreme temperature differences in the system are required between the two ends of a diffusion column. For example, a temperature difference of 340°C between two poles could only account for ~2.4% enrichment of ^{20}Ne over ^{22}Ne [e.g., *Marty*, 1984], a value that is much smaller than some of the observed ^{20}Ne anomalies in our brines. Under these conditions, lighter isotopes will concentrate in the hot pole leading to high $^{20}Ne/^{22}Ne$ ratios, while heavier isotopes will concentrate in the colder pole leading to lower $^{20}Ne/^{22}Ne$ ratios. If fractionation due to thermal diffusion had occurred in the Michigan Basin, this would lead to high $^{20}Ne/^{22}Ne$ ratios in the deepest (and warmest) areas of the basin and lower $^{20}Ne/^{22}Ne$ ratios in the shallower (and cooler) formations, a pattern that is not observed in the basin. Absence of such a pattern rules out the presence of any significant impact of thermal diffusion as a viable process to create isotopic fractionation in the Michigan Basin.

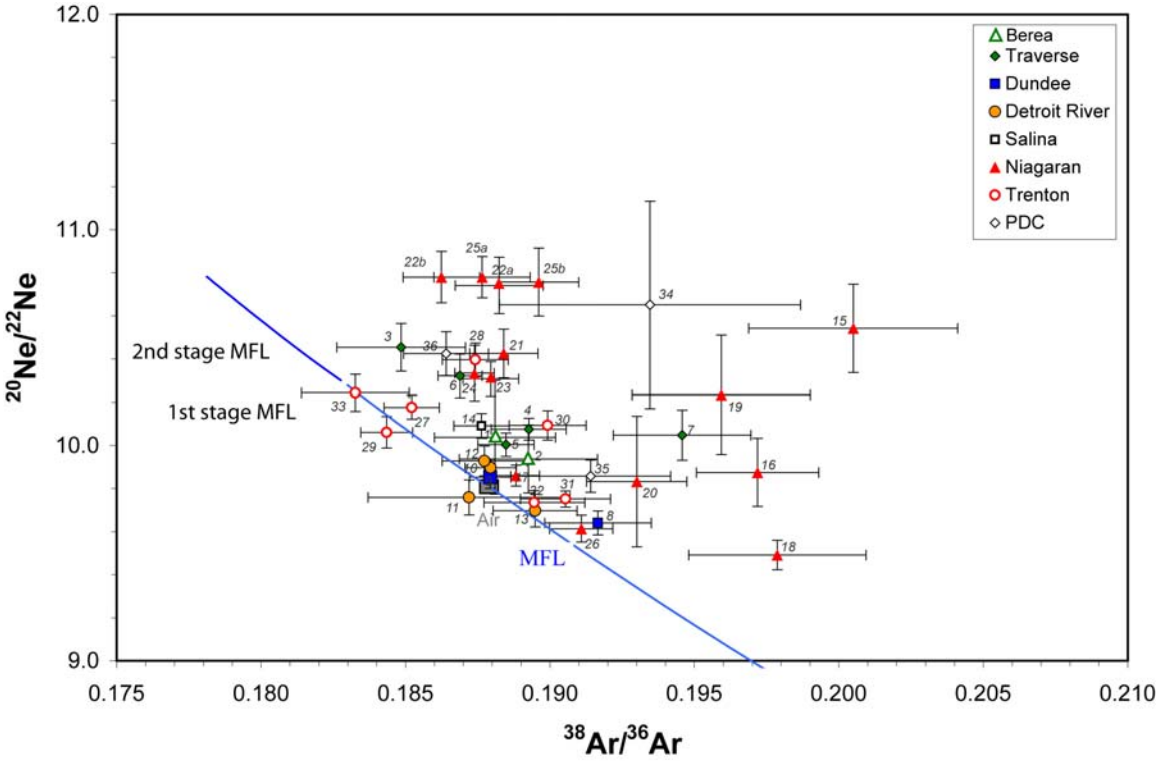

Fig. 4.B1. Measured $^{20}Ne/^{22}Ne$ vs. $^{38}Ar/^{36}Ar$ ratios. The mass-dependent fractionation line (MFL, blue line) from the air value is calculated after *Matsumoto et al.* [2004]. The upper limit of the single stage MFL is indicated, as well as the second MFL stage. The air value is also indicated.

Appendix 4C: Atmospheric Ne separation and optimized Crust-Solar mixing line

The procedure followed for separation of the atmospheric Ne component was essentially similar to that described in detail by *Ballentine and O'Nions* [1992] and *Ballentine* [1997]. Significant differences concern the use in this study of our entire data set (all 38 samples, without exception) as opposed to *Ballentine* [1997], as well as incorporating the R/Ra error into our calculations as explained below.

Optimal values for $K_{crust+mantle}$ and for $^{21}Ne/^{22}Ne_{crust}$ were obtained using a χ^2 minimization procedure similar to that used in *Ballentine* [1997]. In that study, the sum of squared error-weighted misfits of air corrected Ne ratios to a He-Ne mixing curve was plotted as a function of $K_{crust+mantle}$ and the crustal $^{21}Ne/^{22}Ne$ ratio. We have extended that technique by also taking into account the error in the measured R/Ra. For a given He-Ne mixing curve, let x be the R/Ra ratio and let y be the air corrected Ne isotopic ratio (i.e., either $^{20}Ne/^{22}Ne$ or $^{21}Ne/^{22}Ne$). The contribution of a single data point to the total χ^2 value is given by:

$$S_i = \left(\frac{x_i - x_{Ti}}{\sigma_{xi}} \right)^2 + \left(\frac{y_i - y_{Ti}}{\sigma_{yi}} \right)^2$$

where S_i is minimized for each point by adjusting x_{Ti} and y_{Ti} subject to the constraint that these values fall exactly along the He-Ne mixing line and σ_{xi} and σ_{yi} are the error estimates for x_i and y_i respectively. Then the χ^2 statistic is given by:

$$\chi^2 = \sum S_i$$

Figure 4.C1 shows χ^2 as a function of $K_{crust+solar}$ and $^{21}Ne/^{22}Ne_{crust}$ for the entire suite of 38 samples.

The minimum χ^2 value gives the best estimate of both $K_{crust+solar}$ and crustal $^{21}Ne/^{22}Ne$ values for this data set (Fig. 4.C1). The best estimated crustal $^{21}Ne/^{22}Ne$ ratio (0.33) is used to calculate the $^{20}Ne/^{22}Ne_{crust+mantle}$ and $^{21}Ne/^{22}Ne_{crust+mantle}$ ratios (Table 4.3). All the Ne end-member isotopic ratios used in the calculation are listed in Table 4.2. A crustal $^{20}Ne/^{22}Ne$ value of 0.3 is used throughout the study as our analyses show that the calculated $^{20}Ne/^{22}Ne_{crust+mantle}$ and $^{21}Ne/^{22}Ne_{crust+mantle}$ ratios are insensitive to the choice of crustal $^{20}Ne/^{22}Ne$ value.

Calculated $^{20}Ne/^{22}Ne_{crust+mantle}$ and $^{21}Ne/^{22}Ne_{crust+mantle}$ ratios of samples 20, 26, 13 are associated with very large propagated errors. For clarity, samples 20, 26, and 13 are

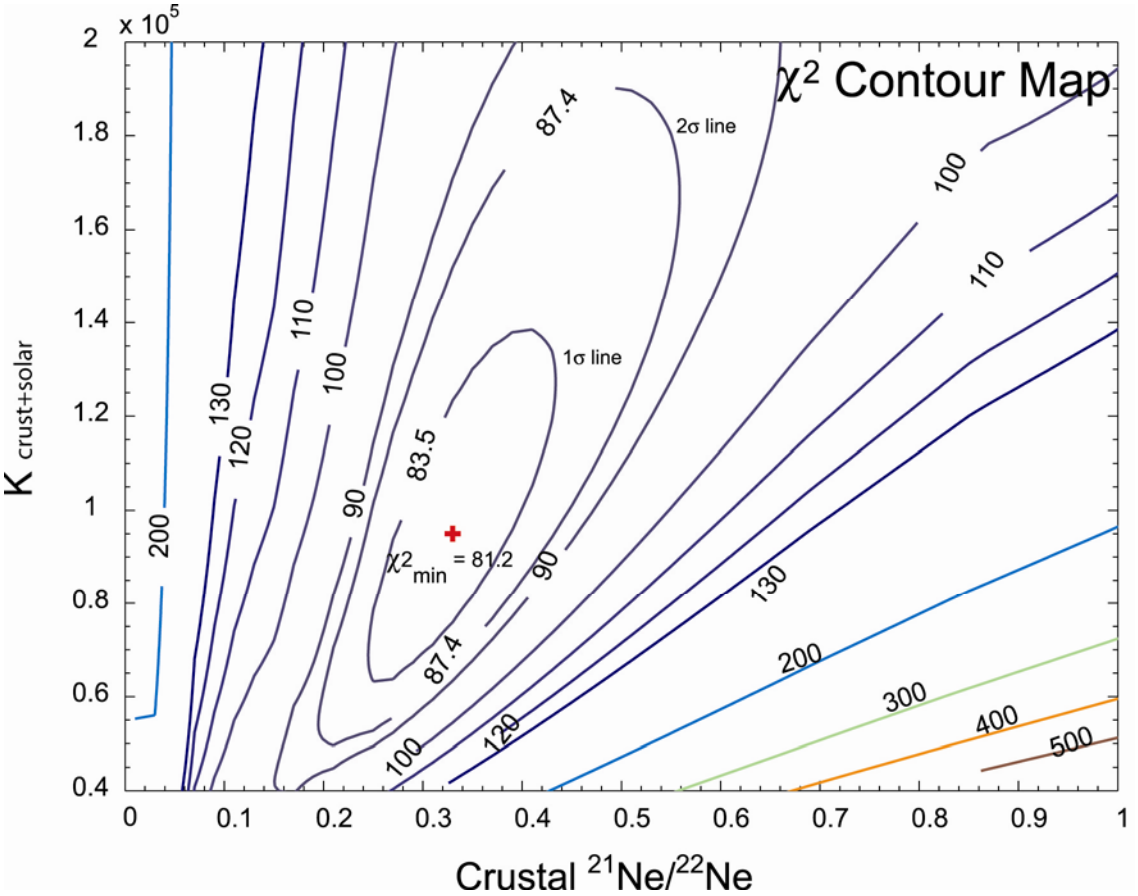

Fig. 4.C1. χ^2 contours for all our data set (38 samples) are plotted as a function of $K_{crust+solar}$ and crustal $^{21}Ne/^{22}Ne$. $K_{crust+solar}$ is the hyperbolic constant for the crust-solar mixing line and crustal $^{21}Ne/^{22}Ne$ is the nucleogenic crustal end-member value. The minimum χ^2 value, χ^2_{min}, gives the best estimate for both $K_{crust+solar}$ and crustal $^{21}Ne/^{22}Ne$ values for this data set. Contour lines with χ^2 values of 90, 100, 110, 120, 130, 200, 300, 400, and 500 are shown. For a data set with two variables, the contour lines representing the 1σ confidence region (contour $\chi^2 = \chi^2_{min}+2.30$) and the 2σ confidence region (contour $\chi^2 = \chi^2_{min}+6.17$) are also shown.

not plotted in Fig. 4.3a, b. Samples 8 and 18 yield $^{20}Ne/^{22}Ne_{crust+mantle}$ and $^{21}Ne/^{22}Ne_{crust+mantle}$ ratios beyond the ranges defined by the Ne end-member isotopic ratios as they both plot below the best estimated air-crust line (0.33) (Fig. 4.2), indicating possibly different crustal $^{21}Ne/^{22}Ne$ ratios for these two samples, and they are therefore not shown in Fig. 4.3a, b. All these five samples, however, were taken into account in the χ^2 minimization procedure; they are simply not graphically shown for clarity purposes.

References

Albarede, F., 2005. The survival of mantle geochemical heterogeneities. In: van der Hilst, R.D., Bass, J.D., Matas, J., Trampert, J. (Eds.), *Earth's Deep Mantle – Structure, Composition, and Evolution*, AGU Monograph, vol. 160, pp. 27-46.

Albarede, F., 2008. Rogue mantle helium and neon. *Science* 319, 943-945.

Anders, E., Grevesse, N., 1989. Abundance of the elements: meteoritic and solar. *Geochimica et Cosmochimica Acta* 53, 197-214.

Anderson, D.L., 1998. A model to explain the various paradoxes associated with mantle noble gas geochemistry. *Proc. Natl. Acad. Sci. USA* 95, 9087-9092.

Anderson, D.L., Schramm, K.A., 2005. Global hotspot maps. In: Foulger, G.R., Natland, J.H., Presnall, D.C., Anderson, D.L. (Eds.), *Plates, Plumes, and Paradigms*, GSA Special Paper, vol. 388, pp.19-29.

Ballentine, C.J., 1997. Resolving the mantle He/Ne and crustal $^{21}Ne/^{22}Ne$ in well gases. *Earth and Planetary Science Letters* 152, 233-249.

Ballentine, C.J., O'Nions, R.K., 1992. The nature of mantle neon contributions to Vienna Basin hydrocarbon reservoirs. *Earth and Planetary Science Letters* 113, 553-567.

Ballentine, C.J., Burnard, P.G., 2002. Production, release and transport of noble gases in the continental crust. *Rev. Mineral. Geochem.* 47, 481-538.

Benkert, J.-P., Baur, H., Signer, P., Wieler, R., 1993. He, Ne, and Ar from the solar wind and solar energetic particles in Lunar ilmenties and pyroxenes. *Journal of Geophysical Research* 98, 13147-13162.

Bickford, M.E., van Schmus, W.R., Zietz, I., 1986. Proterozoic history of the midcontinent region of North America. *Geology* 14, 492-496.

Case, L.C., 1945. Exceptional Silurian brine near Bay City, Michigan. *Bull. Am. Assoc. Petrol. Geol.* 29, 567-570.

Castro, M.C., 2004. Helium sources in passive margin aquifers – new evidence for a significant mantle ^{3}He source in aquifers with unexpectedly low in situ $^{3}He/^{4}He$ production. *Earth and Planetary Science Letters* 222, 897-913.

Castro, M.C., Patriarche, D., Goblet, P., 2005. 2-D numerical simulations of groundwater flow, heat transfer and ^{4}He transport – implications for the He terrestrial budget and the mantle helium-heat imbalance, *Earth and Planetary Science Letters* 237, 893-910.

Castro, M.C., Patriarche, D., Goblet, P., Ma, L., Hall, C.M., 2007. ^{4}He/heat flux ratios as new indicators of past thermal and tectonic events – new constrains on the

tectonothermal history of the Michigan Basin, *the 4th Mini Conference on Noble Gases in the Hydrosphere and in Natural Gas Reservoirs*, GFZ Potsdam.

Catacosinos, P.A., Daniel, P.A. Jr., Harrison, W.B. III, 1991. Structure, stratigraphy, and petroleum geology of the Michigan Basin. In: Leighton, M.W., Kolata, D.R., Oltz, D.F., Eidel, J.J. (Eds.), *Interior cratonic basins*, AAPG Memoir, vol. 51, pp. 561-601.

Coltice, N., Ricard, Y., 2002. On the origin of noble gases in mantle plumes. *Phil. Trans. R. Soc. Lond. A* 360, 2633-2648.

Craig, H., Lupton, J.E., Horibe, Y., 1978. A mantle helium component in circum Pacific volcanic gases: Hakone, the Marianas, and Mt Lassen. In: Alexander, E.C., Ozima M. (Eds.), *Terrestrial Rare Gases*, Japan Sci Societies Press, Tokyo, pp.3-16.

Crovetto, R. Fernandez-Prini, R., Japas, M.L., 1982. Solubilities of inert gases and methane in H_2O and in D_2O in the temperature range of 300 to 600K, *J. Chem. Phys.* 76, 1077-1086.

Crowley, K.D., 1991. Thermal history of Michigan Basin and southern Canadian Shield from apatite fission track analysis, *Journal of Geophysical Research* 96, 697-711.

Dixon, E.T., Honda, M., McDougall, I., Campbell, I.H., Sigurdsson, I., 2000. Preservation of near-solar neon isotopic ratios in Icelandic basalts. *Earth and Planetary Science Letters* 180, 309-324.

Dorr, J.A. Jr., Eschman, D.F., 1970. *Geology of Michigan*, first ed. Univ. of Michigan Press, Ann Arbor, Michigan.

Fisher, J.H., Barratt, M.W., Droste, J.B., Shaver, R.H., 1988. Michigan Basin. In: Sloss, L.L. (Ed.), *Sedimentary Cover – North America Craton*, Geological Society of America, vol. D-2, pp. 361-382.

Girard, J.-P., Barnes, D.A., 1995. Illitization and paleothermal regimes in the middle Ordovician St. Peter sandstone, central Michigan Basin: K-Ar, oxygen isotope, and fluid inclusion data, *AAPG Bulletin* 79, 49-69.

Graham, D., Lupton, J., Albarede, F., Condomines, M., 1990. Extreme temporal homogeneity of helium isotopes at Piton de la Fournaise, Reunion Island. *Nature* 347, 545-548.

Graham, D.W., 2002. Nobel gas isotope geochemistry of mid-ocean ridge and ocean island basalts: characterization of mantle source reservoirs. *Reviews in Mineralogy and Geochemistry* 47, 247-318.

Griffin, W.L., O'Reilly, S.Y., Ryan, C.G., 1999. The composition and origin of sub-continental lithosphere mantle. In: Fei, Y., Bertka, C.M., Mysen, B.O. (Eds.),

Mantle Petrology: Field Observations and High Pressure Experiments, Geochemical Society, pp. 13-45.

Griffin, W.L., O'Reilly, S.Y., Doyle, B.J., Pearson, N.J., Coopersmith, H., Kivi, K., Malkovets, V., Pokhilenko, N., 2004. Lithosphere mapping beneath the North American plate. *Lithos* 77, 873-922.

Hanyu, T., Dunai, T.J., Davies, G.R., Kaneoka, I., Nohda, S., Uto, K., 2001. Noble gas study of the Reunion hotspot: evidence for distinct less-degassed mantle sources. *Earth and Planetary Science Letters* 193, 83-98.

Heaman, L.M., Kjarsgaard, B.A., Creaser, R.A., 2004. The temporal evolution of North American kimberlites. *Lithos* 76, 377-397.

Hinze, W.J., Kellogg, R.L., O'Hara, N.W., 1975. Geophysical studies of basement geology of Southern Peninsula of Michigan, *AAPG Bulletin* 59, 1562-1584.

Honda, M., McDougall, I., Patterson, D.B., Doulgeris, A., Clague, D.A., 1991. Possible solar noble-gas component in Hawaiian basalts. *Nature* 349, 149-151.

Honda, M., McDougall, I., Patterson, D.B., Doulgeris, A., Clague, D.A., 1993. Noble gases in submarine pillow basalt glasses from Loihi and Kilauea, Hawaii: a solar component in the Earth. *Geochimica et Cosmochimica Acta* 57, 859-874.

Kennedy, B.M., Hiyagon, H., Reynolds, J.H., 1990. Crustal neon: a striking uniformity. *Earth and Planetary Science Letters* 98, 277-286.

Ma, L., Castro, M.C., Hall, C.M., 2004. A late Pleistocene-Holocene noble gas paleotemperature record in southern Michigan, *Geophysical Research Letters* 31, L23204, doi:10.1029/2004GL021766.

Ma, L., Castro, M.C., Hall, C.M., Walter, L.M., 2005. Cross-formational flow and salinity sources inferred from a combined study of helium concentrations, isotopic ratios, and major elements in the Marshall aquifer, southern Michigan, *Geochemistry Geophysics Geosystems* 6, Q10004, doi:10.1029/2005GC001010.

Ma, L., Castro M.C., Hall, C.M., 2008. Atmospheric noble gas signatures in deep Michigan Basin brines as indicators of a past thermal event. *Earth and Planetary Science Letters*, in press.

Mahaffy, P.R., Niemann, H.B., Alpert, A., Atreya, S.K., Demick, J., Donahue, T.M., Harpold, D.N., Owen, T.C., 2000. Noble gas abundance and isotope ratios in the atmosphere of Jupiter from the Galileo Probe Mass Spectrometer. *Journal of Geophysical Research* 105, 15061-15071.

Marty, B., 1984. On the noble gas isotopic fractionation in naturally occurring gases. *Geochemical Journal* 18, 157-162.

Matsumoto, T., Seta, A., Matsuda, J.-i., Takebe, M., Chen, Y., Arai, S., 2002. Helium in the Archean komatiites revisited: significantly high $^{3}He/^{4}He$ ratios revealed by fractional crushing gas extraction. *Earth and Planetary Science Letters* 196, 213-225.

Matsumoto, T., Honda, M., McDougall, I., Yatsevich, I., O'Reilly, S.Y., 2004. Isotope fractionation of neon during stepheating extraction?: a comment on 'Re-interpretation of the existence of a primitive plume under Australia based on neon isotope fractionation during step heating' by Gautheron and Moreira (2003). *Terra Nova* 16, 23-26.

Meibom, A., Sleep, N.H., Zahnle, K., Anderson, D.L., 2005. Models for noble gases in mantle geochemistry: some observations and alternatives. In: Foulger, G.R., Natland, J.H., Presnall, D.C., Anderson, D.L. (Eds.), *Plates, Plumes, and Paradigms*, GSA Special Paper, vol. 388, pp.347-363.

Menzies, M.A., 1990. Archaean, Proterozoic, and Phanerozoic lithospheres. In Menzies, M.A. (Ed.), *Continental Mantle*, Clarendon Press, pp.67-86.

Mizuno, H., Nakazawa, K., Hayashi, C., 1980. Dissolution of the primordial rare gases into the molten Earth's material. *Earth and Planetary Science Letters* 50, 202-210.

Moreira, M., Allegre, C.J., 1998. Helium-neon systematics and the structure of the mantle. *Chemical Geology* 147, 53-59.

Moreira, M., Kunz, J., Allegre, C., 1998. Rare gas systematics in popping rock: isotopic and elemental compositions in the upper mantle. *Science* 279, 1178-1181.

Morrison, P., Pine, J., 1955. Radiogenic origin of the helium isotopes in rocks. *Ann. N.Y. Acad. Sci.* 62, 69-92.

O'Nions, R.K., Oxburgh, E.R., 1983. Heat and helium in the Earth. *Nature* 306, 429-431.

Oxburgh, E.R., O'Nions, R.K., Hill, R.I., 1986. Helium isotopes in sedimentary basins. *Nature* 324, 632-635.

Ozima, M., Podosek, F.A., 2002. *Noble gas geochemistry*, second ed. Cambridge University Press, New York.

Parker, R.L., 1967. *Composition of Earth's crust, Data of Geochemistry*. U. S. Geol. Surv. Prof. Pap. 440-D, 19pp.

Parman, S.W., Kurz, M.D., Hart, S.R., Grove, T.L., 2005. Helium solubility in olivine and implications for high $^{3}He/^{4}He$ in ocean island basalts. *Nature* 437, 1140-1143.

Porcelli, D. Wasserburg, G.J., 1995. Mass transfer of helium, neon, argon, and xenon through a steady-state upper mantle. *Geochimica et Cosmochimica Acta* 59, 4921-4937.

Rudnick, R.L., Fountain, D.M., 1995. Nature and compostion of the continental crust: a lower crustal perspective. *Reviews of Geophysics* 33, 267-309.

Rudnick, R.L., Nyblade, A.A., 1999. The thickness and heat production of Archean lithosphere: constrains from xenolith thermobarometry and surface heat flow. In: Fei, Y., Bertka, C.M., Mysen, B.O. (Eds.), *Mantle Petrology: Field Observations and High Pressure Experiments*, Geochemical Society, pp. 3-12.

Saar, M.O., Castro, M.C., Hall, C.M., Manga, M., Rose, T.P., 2005. Quantifying magmatic, crustal, and atmospheric helium contributions to volcanic aquifers using all stable noble gases: implications for magmatism and groundwater flow, *Geochemistry Geophysics Geosystems* 6, Q03008, doi:10.1029/2004GC000828.

Sarda, P., Staudacher, T., Allegre, C.J., 1988. Neon isotopes in submarine basalts. *Earth and Planetary Science Letters* 91, 73-88.

Smith, S.P., 1985. Noble gas solubility in water at high temperatures, *Eos Trans.* AGU 66, 397.

Smith, S.P., Kennedy, B.M., 1983. The solubility of noble gases in water and in NaCl brine, *Geochimica et Cosmochimica Acta* 47, 503-515.

Valbracht, P.J., Honda, M., Matsumoto, T., Mattielli, N., McDougall, I., Ragettli, R., Weis, D., 1996. Helium, neon and argon isotope systematics in Kerguelen ultramafic xenoliths: implications for mantle source signatures. *Earth and Planetary Science Letters* 138, 29-38.

Van Schmus, W.R., 1992. Tectonic setting of the Midcontinent Rift system, *Tectonophysics* 213, 1-15.

Vugrinovich, R., 1986. *Patterns of regional subsurface fluid movement in the Michigan Basin*, Open File Rep. 86-6, Geol. Surv. Div. Mich. Dep. of Nat. Resour., Lansing.

Vugrinovich, R., 1989. Subsurface temperatures and surface heat flow in the Michigan Basin and their relationships to regional subsurface fluid movement. *Marine and Petroleum Geology* 6, 60-70.

Weiss, R.F., 1968. Piggyback sampler for dissolved gas studies on sealed water samples, *Deep Sea Res. Oceanogr. Abstr.* 15, 695-699.

Westjohn, D.B., Weaver, T.L., 1996. *Hydrogeologic framework of Mississippian rocks in the central Lower Peninsula of Michigan*. U.S. Geol. Surv. Water Resour. Invest. Report 94-4246, 46pp.

Wetherill, G.W., 1954. Variations in the isotopic abundances of neon and argon extracted from radioactive minerals. *Physical Review* 96, 679-683.

Wilson, T.P., Long, D.T., 1993a. Geochemistry and isotope chemistry of Michigan Basin brines: Devonian formations, *Applied Geochemistry* 8, 81-100.

Wilson, T.P., Long, D.T., 1993b. Geochemistry and isotope chemistry of Ca-Na-Cl brines in Silurian strata, Michigan Basin, *Applied Geochemistry* 8, 507-524.

Yatsevich, I., Honda, M., 1997. Production of nucleogenic neon in the Earth from natural radioactive decay. *Journal of Geophysical Research* 102, 10291-10298.

CHAPTER 5

ATMOSPHERIC NOBLE GAS SIGNATURES IN DEEP MICHIGAN BASIN BRINES AS INDICATORS OF A PAST THERMAL EVENT

Abstract

Atmospheric noble gases (e.g., ^{22}Ne, ^{36}Ar, ^{84}Kr, ^{130}Xe) in crustal fluids are only sensitive to subsurface physical processes. In particular, depletion of atmospheric noble gases in groundwater due to boiling and steam separation is indicative of the occurrence of a thermal event and can thus be used to trace the thermal history of stable tectonic regions. We present noble gas concentrations of 38 deep brines (~0.5-3.6km) from the Michigan Basin. The atmospheric noble gas component shows a strong depletion pattern with respect to air saturated water. Depletion of lighter gases (^{22}Ne and ^{36}Ar) is stronger compared to the heavier ones (^{84}Kr and ^{130}Xe). To understand the mechanisms responsible for this overall atmospheric noble gas depletion, phase interaction models were tested. It is shown that this atmospheric noble gas depletion pattern is best explained by a model involving subsurface boiling and steam separation, and thus, consistent with the occurrence of a past thermal event of mantle origin as previously indicated by both high ^{4}He/heat flux ratios and the presence of primordial mantle He and Ne signatures in the basin. Such a conceptual model is also consistent with the presence of past elevated temperatures in the Michigan Basin (e.g., ~80-260°C) at shallow depths as suggested by

previous thermal studies in the basin. It is suggested here that a recent reactivation of the ancient mid-continent rift system underneath the Michigan Basin is likely responsible for the release of both heat and mantle noble gases into the basin via deep-seated faults and fracture zones. Relative enrichment of atmospheric Kr and Xe with respect to Ar is also observed, and is interpreted as reflecting the addition of sedimentary Kr and Xe from associated hydrocarbons, following the hydrothermal event. This study pioneers the use of atmospheric noble gases in subsurface fluids to trace the thermal history of stable tectonic regions.

5.1. Introduction

Because of their conservative nature and because of their specific characteristics depending on their origin (atmosphere, crust or mantle), the study of noble gases (He, Ne, Ar, Kr, and Xe) in sedimentary basins has proved to be a powerful tool to investigate the origin and history of crustal fluids [e.g., *Pinti and Marty*, 1995; *Castro et al.*, 1998a, b; *Lippmann et al.*, 2003; *Prinzhofer and Battani*, 2003; *Patriarche et al.*, 2004]. More specifically, the atmospheric component of noble gases (^{22}Ne, ^{36}Ar, ^{84}Kr and ^{130}Xe) dissolved in deep groundwaters that is introduced into the subsurface by recharge water in solubility equilibrium with the atmosphere (Air Saturated Water - ASW) has been traditionally used to identify and quantify oil, gas, and water phase interactions [*Zartman et al.*, 1961; *Bosch and Mazor*, 1988; *Zaikowski and Spangler*, 1990; *Ballentine et al.*, 1991; *Pinti and Marty*, 1995]. Indeed, while atmospheric noble gas concentrations in deep waters are expected to reflect those of ASW, depletion of this component in sedimentary systems commonly suggests loss of this atmospheric component to an oil or

natural gas phase, which is originally free of atmospheric noble gases [*Zartman et al.*, 1961; *Bosch and Mazor*, 1988; *Zaikowski and Spangler*, 1990]. By contrast, and although never previously reported in stable continental regions, depletion of atmospheric noble gases due to boiling and steam separation was previously recorded in tectonically active areas (hydrothermal systems), more specifically, the Cerro Pietro in Mexico [*Mazor and Truesdell*, 1984], the Juan de Fuca Ridge in Pacific Ocean [*Kennedy*, 1988], and the Red Sea Basin [*Winkler et al.*, 2000]. Such noble gas depletion in the residual water phase occurs as pressure decreases during fluid ascent leading to a separate steam (water vapor) enriched noble gas phase. The depletion of atmospheric noble gases in a particular region due to boiling and steam separation is thus indicative of the occurrence of a thermal event.

In addition to atmospheric noble gases, the study of ^{4}He in crustal fluids of mantle and/or crustal origin, which is due to radioactive decay of naturally occurring U and Th, has also proven to be an invaluable tracer of subsurface fluids [*Torgersen and Clark*, 1985; *Castro et al.*, 1998a, b; *Castro et al.*, 2000; *Castro and Goblet*, 2003]. In particular, when combined with heat flow, it allows for the reconstruction of the thermal and tectonic history of continental regions [*Castro et al.*, 2005]. More specifically, *Castro et al.* [2005] have shown that the occurrence of a ^{4}He/heat flux ratio greater than the radiogenic production ratio can only result from a past thermal event of mantle origin. Such a high ^{4}He/heat flux ratio was recently identified in shallow (<100 m) groundwaters of the Marshall aquifer in the Michigan Basin [*Ma et al.*, 2005; *Castro et al.*, 2007]. To confirm the occurrence of such a thermal event and to clarify its origin, 38 deep (0.5-3.6Km) brine samples were collected and analyzed for noble gas concentrations and isotopic ratios in the Michigan Basin [*Castro et al*., 2008; this study]. While both He and

Ne isotopic ratios clearly indicate the presence of a mantle component, the Ne isotopic composition points unequivocally to the presence of a primordial, solar-like signature in this continental region, thus, confirming the mantle origin of this past thermal event [*Castro et al.*, 2008].

Here, we present a companion study that focuses on the atmospheric noble gases in these same deep Michigan Basin brines. This component displays a strong depletion pattern with respect to ASW. It is shown that this atmospheric noble gas depletion pattern is best explained by a model involving subsurface boiling and steam separation, and thus, is consistent with the occurrence of a past thermal event of mantle origin as previously indicated by both high ^{4}He/heat flux ratios and the presence of a primordial mantle He and Ne signature in the basin [*Castro et al.*, 2008]. This study pioneers the use of atmospheric noble gases in subsurface fluids to trace the thermal history of stable tectonic regions.

5.2. Geological and Hydrogeologic Background

The Michigan Basin is a concentric intracratonic depression floored by crystalline Precambrian basement, and consists of a succession of sedimentary rocks with ages from Precambrian to Jurassic that reaches depths over 5Km (Fig. 5.1) [*Dorr and Eschman*, 1970; *Catacosinos et al.*, 1991]. The entire sedimentary strata are composed mainly of evaporites, carbonates, shale, and sandstone underneath a thick layer of Pleistocene glacial deposits (Fig. 5.1b). Depending on their nature, these sedimentary rocks constitute either aquitards (e.g., shale, evaporites) or aquifers (mostly sandstones and reefal and

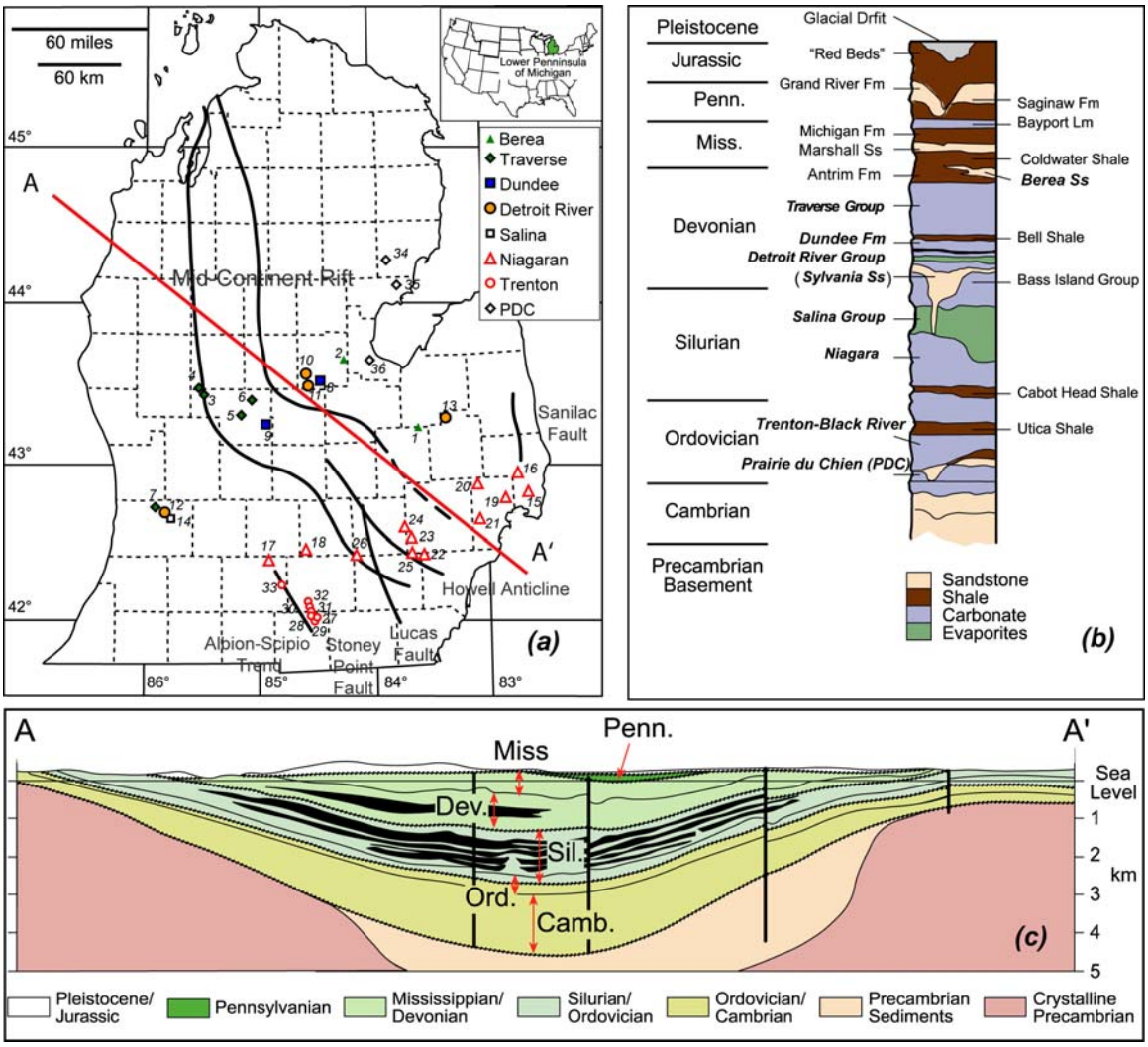

Figure 5.1. a) Central portion of the Michigan Basin (Lower Peninsula of Michigan). Major tectonic structures (e.g., Mid Continental Rift - MCR) and sample locations are indicated [after *Dorr and Eschman*, 1970; *Fisher et al.*, 1988; *Catacosinos et al.*, 1991]; **b)** Stratigraphic succession of the Michigan Basin. Major lithologies present in the basin are identified; units for which formation brines were sampled in this study are highlighted in bold; **c)** general schematic geological representation along cross section A-A'.

dolomitized limestones), giving rise to a multi-layered aquifer system [*Vugrinovich*, 1986].

Major tectonic structures such as the Albion-Scipio Fault, the Lucas Fault, and the Howell Anticline are present in southern Michigan and penetrate the crystalline basement which is mainly composed of Precambrian (~1.1->2.5Ga) igneous-metamorphic rocks (Fig. 5.1a). The basement is believed to have a well-developed pattern of jointing and faulting, similar to the highly fractured neighboring Canadian Shield outcrop [*Sanford et al.*, 1985; *Fisher et al.*, 1988]. A rift zone which formed during an episode of crustal extension at ~1.1 Ga transects the entire crystalline basement of the Michigan Basin (Fig. 5.1a), and is believed to be part of the Mid-Continent Rift (MCR) system [*Hinze et al.*, 1975; *Van Schmus*, 1992]. Repeated movements along major faults in southern Michigan prevailed throughout the early part of the Paleozoic and a major uplift of most of the basin fault blocks occurred at the end of the Mississippian Period (~320 Ma) [*Fisher et al.*, 1988].

Despite its present low geothermal gradient (~19°C/Km) [*Vugrinovich*, 1989], oil and gas reservoirs in southern Michigan are abundant and ubiquitously distributed throughout most of the sedimentary sequence, from the deep Ordovician to the shallow Mississipian (Fig. 5.1b) [*Dorr and Eschman*, 1970; *Catacosinos et al.*, 1991; *Dolton*, 1995], indicating the occurrence of higher temperatures in the past. A wealth of thermal studies in the basin based on a diversity of proxies (e.g., organic maturity data, stable isotopes, fluid inclusions, authigenic clay minerals, apatite fission track ages) all point to the occurrence of high temperatures (up to 260°C) in the past [*Cercone and Lohmann*, 1987; *Cercone and Pollack*, 1991; *Crowley*, 1991; *Coniglio et al.*, 1994; *Girard and*

Barnes, 1995; *Luczaj et al.*, 2006]. The origin and formation period of such reservoirs, however, remains uncertain. Because these high temperatures cannot be easily explained by long-term deep burial [e.g, *Cercone*, 1984; *Vugrinovich*, 1988; *Luczaj et al.*, 2006], models involving transport of heat and fluids from deeper parts of the basin along major faults and fracture zones connected to the Precambrian basement structures have been proposed [*Sanford et al.*, 1985; *Budai and Wilson*, 1991; *Coniglio et al.*, 1994; *Girard and Barnes*, 1995; *Luczaj et al.*, 2006].

In addition to oil and natural gases, formation waters (brines) with very high salinities (e.g., >~450g/L of total dissolved solids - TDS) ubiquitously distributed throughout the basin have also been documented [*Long et al.*, 1988; *Wilson and Long*, 1993a, b; *Martini*, 1997; *McIntosh et al.*, 2004]. Studies of major elements and stable isotopes suggest that these deep basinal brines originate from ancient seawater with a complicated evapo-concentration evolution history involving intensive water-rock interactions, dissolution of evaporites, as well as mixing with meteoric and seawater [*Long et al.*, 1988; *Wilson and Long*, 1993a, b; *Davisson and Criss*, 1996; *Martini*, 1997; *McIntosh et al.*, 2004). Upward transport has also been suggested to account for the presence of extremely high salinity waters [*Long et al.*, 1988] as well as unusually high ^{4}He excesses and fluxes [*Ma et al.*, 2005] at shallow depths.

5.3. Sampling Techniques and Experimental Methods

A total of 38 brine samples were collected from eight formations in the Michigan Basin for noble gas analysis (Fig. 5.1a,b). Brines were sampled from actively pumping wells in copper tubes (i.e. standard refrigeration grade 3/8" Cu tubing) that were sealed

by stainless steel pinch-off clamps [*Weiss*, 1968] at well head pressures after water was allowed to flow for ~10 minutes to avoid atmospheric contamination and to ensure that temperature had reached equilibrium. Elemental and isotopic noble gas measurements were performed at the University of Michigan as described briefly below and in detail elsewhere [*Ma et al.*, 2004; *Saar et al.*, 2005].

Brine samples (~14 ml) were attached to a vacuum extraction system and noble gases were quantitatively extracted for inletting into a MAP-215 mass spectrometer. Noble gases were transported using water vapor as a carrier gas through two constrictions in the vacuum system, purified by two Ti sponge getters, and sequentially allowed to enter the MAP-215 mass spectrometer using a cryo-separator. The cryo-separator temperatures were set at 30, 60, 180, 215, and 270K for analysis of He, Ne, Ar, Kr, and Xe, respectively. ^{4}He was measured using a Faraday detector and ^{22}Ne, ^{36}Ar, ^{84}Kr, and ^{130}Xe isotopes were measured using an electron multiplier in ion counting mode. During the neon isotope analysis, a liquid N_2 cold trap was applied to minimize peak interferences and appropriate mass peaks were monitored to correct for interferences of $^{40}Ar^{2+}$ on ^{20}Ne, CO_2^{2+} on ^{22}Ne and $H_2{}^{18}O^{+}$ on ^{20}Ne. The interference corrections for ^{20}Ne and ^{22}Ne were typically ~1.1% and 0.17%, respectively. Before each sample analysis, a calibrated amount of air standard and a procedural blank were performed following the same procedure of the sample measurement. The blank correction was applied to all measured peaks. ^{4}He, ^{22}Ne, ^{36}Ar, ^{84}Kr, and ^{130}Xe elemental abundances for each sample were normalized to the air standard after blank correction. Blank correction for ^{4}He, ^{36}Ar, ^{84}Kr, and ^{130}Xe is negligible. The average measured sample/blank signal size ratio for ^{22}Ne is about 15. ^{4}He, ^{22}Ne, ^{36}Ar, ^{84}Kr, and ^{130}Xe abundances have typical uncertainties

of 1.5, 1.3, 1.3, 1.5 and 2.2%, respectively. All uncertainties are at ±1σ level of confidence.

5.4. Results and Discussion

5.4.1. Depletion of atmospheric noble gases

Noble gas concentrations, sample number, formation, lithology as well as depth are given in Table 5.1. The concentration of ASW at 0°C and 30°C for both 0M and 5M NaCl solution as well as seawater at 25°C (0.6M NaCl solution, addition of 0.1% excess air) are also indicated for reference (Table 5.1). He and Ne isotopic ratios have been previously reported and discussed [*Castro et al.*, 2008].

^{4}He concentrations for all samples are found in excess of those expected for ASW, reaching values of over four orders of magnitude above that of ASW (0-30°C, 0-5M, Table 5.1, Fig. 5.2). ^{4}He in these brines has a dominant crustal origin (~85%), with a mantle contribution of ~15% [*Castro et al.*, 2008]. Because atmospheric ^{4}He is negligible in these samples, He will not be the object of further discussion in the present study.

Unlike He isotopes, ^{22}Ne, ^{36}Ar, ^{84}Kr, and ^{130}Xe in subsurface fluids are dominantly atmospheric. Previous analysis of Ne isotopic ratios [*Castro et al.*, 2008] indicate a dominant atmospheric ^{22}Ne component ($^{22}Ne_{atm}$) for all samples, with contributions varying between 75% and 95% with respect to the total measured ^{22}Ne (Table 5.1). For simplicity, in the discussion that follows, the atmospheric ^{22}Ne component ($^{22}Ne_{atm}$) is referred as ^{22}Ne. ^{38}Ar/^{36}Ar, ^{80}Kr/^{84}Kr, and ^{128}Xe/^{130}Xe ratio values are indistinguishable from that of air and indicate an almost entirely atmospheric component for ^{36}Ar, ^{84}Kr and ^{130}Xe isotopes. In this study we thus assume a 100%

Table 5.1. He, Ne, Ar, Kr, and Xe elemental concentrations (±1σ uncertainties) with well identification number, formation, lithology, and depth.

Sample Number	Formation	Lithology	Depth (m)	^{4}He (cm^3STP/g)	+/-	^{22}Ne (cm^3STP/g)	+/-	^{36}Ar (cm^3STP/g)	+/-	^{84}Kr (cm^3STP/g)	+/-	^{130}Xe (cm^3STP/g)	+/-
	Devonian												
1	Berea	Sandstone	1005	8.37E-07	1.26E-08	4.50E-11	5.85E-13	1.11E-08	1.45E-10	1.27E-09	1.90E-11	3.59E-11	7.90E-13
2	Berea	Sandstone	780	5.35E-06	8.03E-08	5.17E-11	6.72E-13	2.98E-09	3.88E-11	1.50E-10	2.24E-12	9.20E-12	2.02E-13
3	Traverse	Carbonate	1014	5.03E-07	7.54E-09	4.68E-11	6.09E-13	3.34E-09	4.35E-11	2.97E-10	4.45E-12	2.40E-11	5.27E-13
4	Traverse	Carbonate	1015	5.99E-06	9.80E-07	1.05E-10	1.36E-12	5.82E-09	7.56E-11	2.38E-10	3.58E-12	5.54E-12	1.22E-13
5	Traverse	Carbonate	909	3.00E-05	4.51E-07	1.24E-10	1.61E-12	1.86E-08	2.42E-10	8.80E-10	1.32E-11	2.09E-11	4.60E-13
6	Traverse	Carbonate	1072	1.82E-05	2.72E-07	1.56E-10	2.03E-12	2.64E-08	3.43E-10	1.23E-09	1.85E-11	8.01E-11	1.76E-12
7	Traverse	Carbonate	546	1.57E-07	2.36E-09	1.48E-10	1.93E-12	6.65E-09	8.64E-11	1.97E-10	2.95E-12	1.42E-11	3.13E-13
8	Dundee	Carbonate	1036	1.76E-04	2.64E-06	2.90E-09	3.78E-11	5.27E-08	6.85E-10	1.30E-09	1.96E-11	1.23E-11	2.70E-13
9	Dundee	Carbonate	1090	9.68E-06	1.45E-07	6.74E-10	8.76E-12	4.38E-08	5.69E-10	1.65E-09	2.47E-11	2.26E-11	4.97E-13
10	Detroit River	Carbonate	1378	9.26E-05	1.39E-06	2.85E-10	3.71E-12	2.12E-08	2.75E-10	6.80E-10	1.02E-11	7.32E-12	1.61E-13
11	Detroit River	Sandstone	1480	4.69E-04	7.03E-06	3.68E-09	4.78E-11	1.65E-07	2.14E-09	6.82E-09	1.02E-10	8.09E-11	1.78E-12
12	Detroit River	Carbonate	572	1.49E-05	2.23E-07	9.14E-10	1.19E-11	4.51E-08	5.86E-10	1.40E-09	2.10E-11	2.06E-11	4.53E-13
13	Detroit River	Sandstone	1070	3.72E-04	5.57E-06	9.25E-10	1.20E-11	3.96E-08	5.14E-10	1.84E-09	2.77E-11	2.40E-11	5.28E-13
	Silurian												
14	Salina	Carbonate	699	6.13E-07	9.20E-09	4.04E-10	5.25E-12	6.40E-08	8.32E-10	2.53E-09	3.80E-11	5.22E-11	1.15E-12
15	Niagaran	Carbonate	830	2.16E-07	3.24E-09	1.63E-10	2.12E-12	1.00E-08	1.30E-10	4.09E-10	6.13E-12	7.12E-11	1.57E-12
16	Niagaran	Carbonate	1022	2.35E-05	3.53E-07	9.92E-11	1.29E-12	5.77E-09	7.50E-11	2.85E-10	4.28E-12	6.89E-12	1.51E-13
17	Niagaran	Carbonate	1096	1.33E-05	1.99E-07	3.52E-10	4.58E-12	2.28E-08	2.97E-10	1.15E-09	1.73E-11	1.47E-11	3.24E-13
18	Niagaran	Carbonate	1168	1.70E-03	2.55E-05	3.57E-09	4.64E-11	5.44E-08	7.07E-10	8.85E-10	1.33E-11	1.51E-11	3.33E-13
19	Niagaran	Carbonate	887	8.67E-06	1.30E-07	5.24E-11	6.82E-13	1.12E-08	1.45E-10	1.23E-09	1.85E-11	7.42E-11	1.63E-12
20	Niagaran	Carbonate	1143	3.66E-06	5.49E-08	5.48E-11	7.13E-13	1.19E-08	1.55E-10	1.12E-09	1.68E-11	7.20E-11	1.58E-12
21	Niagaran	Carbonate	915	7.01E-06	1.05E-07	2.04E-10	2.66E-12	4.09E-08	5.32E-10	2.31E-09	3.47E-11	3.81E-11	8.39E-13
22a	Niagaran	Carbonate	941	1.42E-07	2.14E-09	4.68E-11	6.08E-13	5.12E-09	6.65E-11	9.12E-10	1.37E-11	6.41E-11	1.41E-12
22b	Niagaran	Carbonate	941	1.92E-07	2.88E-09	4.91E-11	6.39E-13	7.97E-09	1.04E-10	2.12E-09	3.18E-11	1.43E-10	3.14E-12
23	Niagaran	Carbonate	1138	1.33E-05	1.99E-07	1.08E-10	1.41E-12	2.05E-08	2.67E-10	1.55E-09	2.32E-11	1.76E-11	3.87E-13
24	Niagaran	Carbonate	1259	1.45E-06	2.17E-08	4.44E-11	5.78E-13	1.51E-08	1.96E-10	1.07E-09	1.61E-11	5.37E-11	1.18E-12
25a	Niagaran	Carbonate	996	4.27E-07	6.41E-09	5.63E-11	7.32E-13	5.70E-09	7.42E-11	1.13E-09	1.70E-11	7.60E-11	1.67E-12
25b	Niagaran	Carbonate	996	6.55E-07	9.82E-09	6.19E-11	8.05E-13	6.95E-09	9.04E-11	1.11E-09	1.67E-11	9.42E-11	2.07E-12
26	Niagaran	Carbonate	937	1.53E-03	2.29E-05	5.83E-09	7.57E-11	2.08E-07	2.70E-09	8.78E-09	1.32E-10	7.03E-11	1.55E-12
	Ordovician												
27	Trenton	Carbonate	1330	5.39E-06	8.08E-08	8.67E-11	1.13E-12	1.55E-08	2.01E-10	7.78E-10	1.17E-11	2.48E-11	5.47E-13
28	Trenton	Carbonate	1332	3.53E-06	5.29E-08	7.49E-11	9.74E-13	1.57E-08	2.04E-10	1.33E-09	2.00E-11	5.51E-11	1.21E-12
29	Trenton	Carbonate	1301	4.62E-06	6.93E-08	8.24E-11	1.07E-12	1.25E-08	1.62E-10	7.78E-10	1.17E-11	3.01E-11	6.62E-13
30	Trenton	Carbonate	1302	1.91E-05	2.86E-07	1.09E-10	1.42E-12	9.28E-09	1.21E-10	6.81E-10	1.02E-11	1.06E-11	2.32E-13
31	Trenton	Carbonate	1302	1.09E-04	1.63E-06	3.01E-10	3.91E-12	3.26E-08	4.24E-10	2.11E-09	3.17E-11	2.77E-11	6.10E-13
32	Trenton	Carbonate	1233	8.87E-05	1.33E-06	1.94E-10	2.52E-12	1.42E-08	1.84E-10	6.26E-10	9.39E-12	1.16E-11	2.55E-13
33	Trenton	Carbonate	1283	1.17E-06	1.75E-08	5.95E-11	7.73E-13	5.21E-09	6.77E-11	3.79E-10	5.69E-12	2.16E-11	4.76E-13
34	PDC	Carbonate	3595	3.33E-06	4.99E-08	5.03E-11	6.55E-13	1.83E-08	3.54E-10	1.76E-09	2.64E-11	8.14E-11	1.79E-12
35	PDC	Carbonate	3621	3.66E-05	5.49E-07	1.29E-10	1.68E-12	1.96E-08	2.54E-10	6.28E-10	9.43E-12	6.88E-12	1.51E-13
36	PDC	Carbonate	3196	2.50E-06	3.75E-08	5.55E-11	7.21E-13	9.81E-09	1.28E-10	3.71E-10	5.57E-12	1.26E-11	2.76E-13
	ASW (0M NaCl solution) at 0°C[b]			5.1E-08		2.1E-08		1.7E-06		7.4E-08		8.4E-10	
	ASW (5M NaCl solution) at 0°C			1.2E-08		3.6E-09		2.2E-07		8.5E-09		7.7E-11	
	ASW (0M NaCl solution) at 30°C			4.3E-08		1.6E-08		8.6E-07		3.2E-08		2.8E-10	
	ASW (5M NaCl solution) at 30°C			1.3E-08		4.1E-09		1.7E-07		5.7E-09		4.5E-11	
	Seawater (0.6M NaCl solution, 0.1% excess air) at 25°C[c]			4.3E-08		1.6E-08		8.0E-07		2.9E-08		2.6E-10	

a. Atmospheric ^{22}Ne contribution was calculated based on Ne isotopic analysis after correcting for the mantle and crustal components [*Castro et al.*, 2008].

b. ASW concentrations calculated from *Crovetto et al.* [1982], *Smith* [1985], and *Smith and Kennedy* [1983].

c. Addition of 0.1% excess air (volume ratio) is a typical value due to air injection into seawater [see, e.g., *Ozima and Podosek*, 2002].

Table 5.1. (continued)

Sample Number	Atmospheric $^{22}Ne^{(a)}$(%)	$^{22}Ne_{atm}$ (cm^3STP/g)
1	91.9%	4.13E-11
2	95.8%	4.95E-11
3	83.2%	3.90E-11
4	91.8%	9.59E-11
5	84.0%	1.04E-10
6	83.7%	1.31E-10
7	93.9%	1.39E-10
8		
9	97.1%	6.54E-10
10	86.5%	2.47E-10
11	95.8%	3.53E-09
12	96.9%	8.86E-10
13		
14	92.6%	3.74E-10
15	80.9%	1.32E-10
16	92.2%	9.15E-11
17	95.4%	3.36E-10
18		
19	84.7%	4.44E-11
20	96.6%	5.29E-11
21	81.1%	1.66E-10
22a	76.3%	3.57E-11
22b	74.9%	3.68E-11
23	81.7%	8.85E-11
24	84.7%	3.76E-11
25a	76.1%	4.29E-11
25b	76.7%	4.75E-11
26		
27	86.6%	7.51E-11
28	81.7%	6.12E-11
29	89.3%	7.36E-11
30	86.7%	9.47E-11
31	88.1%	2.65E-10
32	86.0%	1.67E-10
33	87.1%	5.18E-11
34	77.0%	3.88E-11
35	87.1%	1.13E-10
36	81.4%	4.52E-11

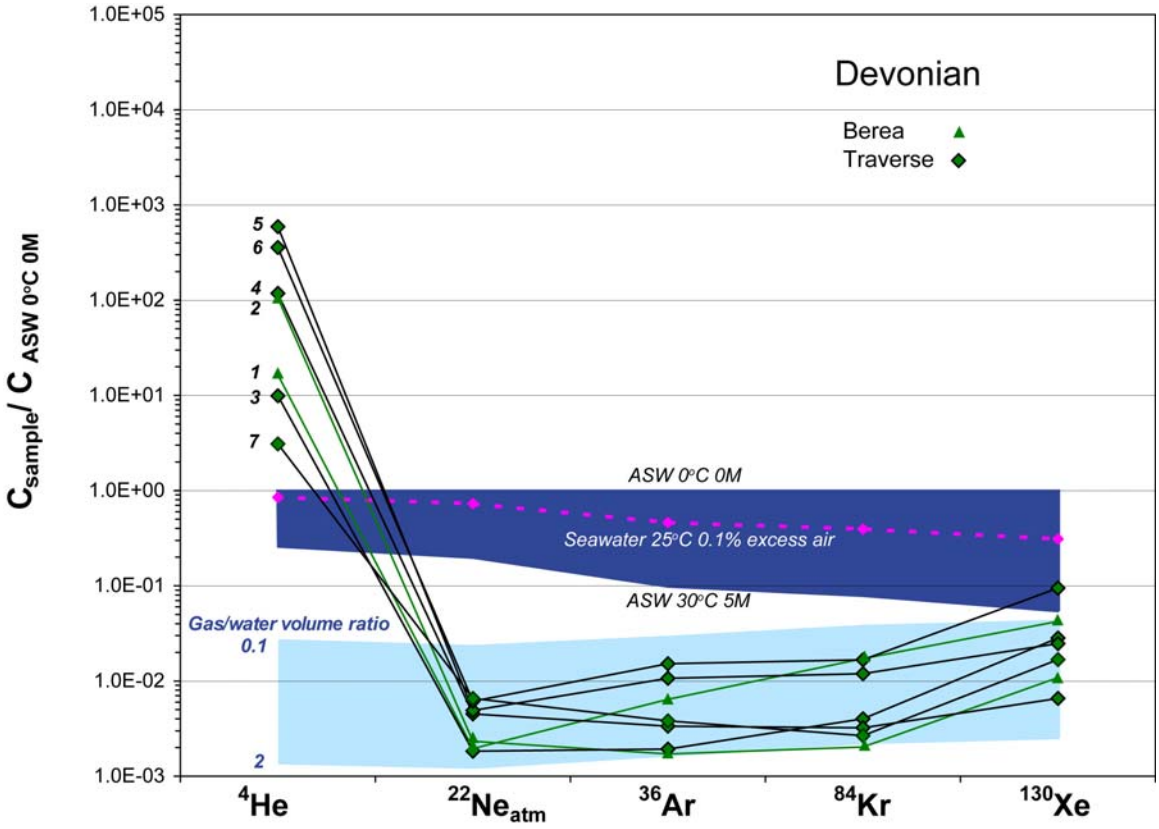

Figure 5.2.a) Berea and Traverse formations; Atmospheric noble gas concentrations in brines normalized to noble gas concentrations in air saturated water at 0°C and 0M. The dark blue area covers the ASW domain for temperatures varying from 0 to 30°C and water salinities varying between 0 and 5M, i.e., varying between 0°C and 0M (maximum value) and 30°C and 5M (minimum value). Air saturated seawater at 25°C with 0.1% excess air addition is indicated. The light blue area indicates the atmospheric noble gas depletion pattern in the residual waters following a gas-water phase interaction with initial seawater at 25°C with 0.1% excess air. Noble gas concentrations corresponding to gas-water volume ratios varying between 0.1 and 2 are indicated. Sample numbers are in bold.

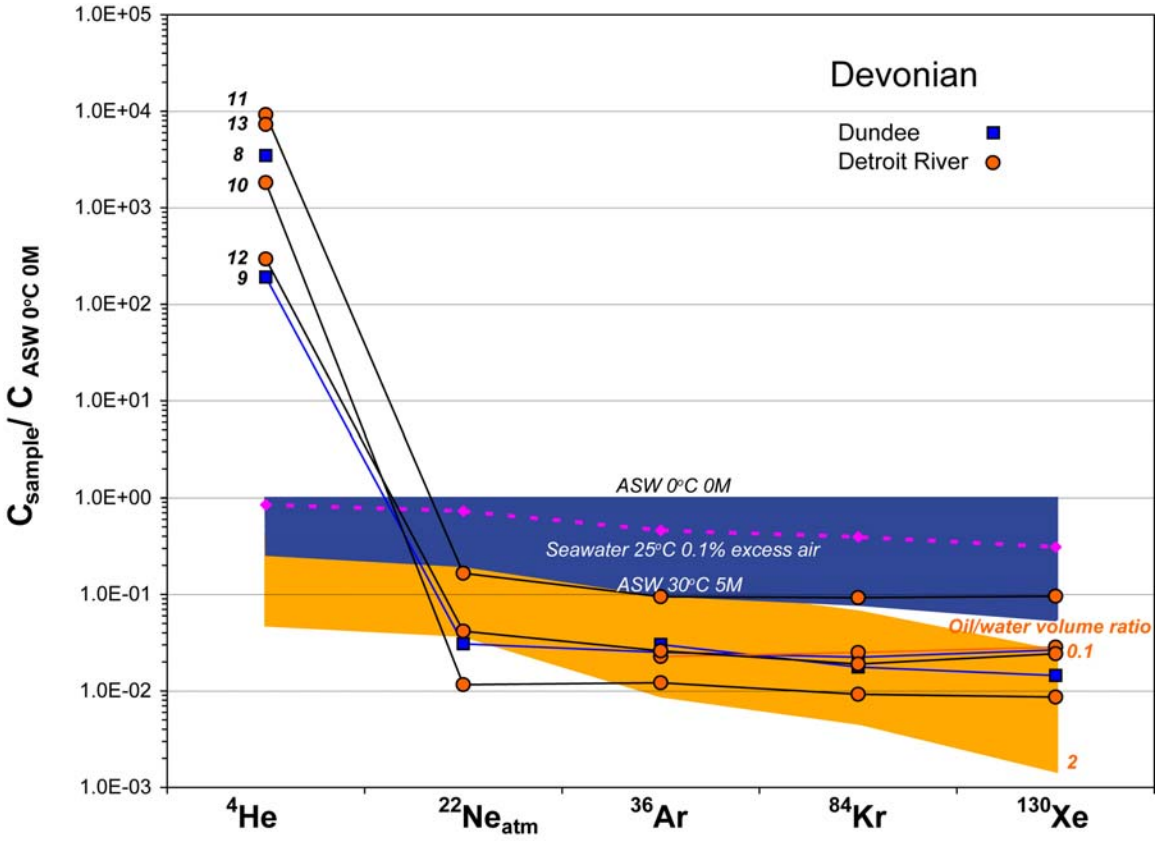

Figure 5.2.b) Dundee and Detroit River formations; Atmospheric noble gas concentrations in brines normalized to noble gas concentrations in air saturated water at 0°C and 0M. The dark blue area covers the ASW domain for temperatures varying from 0 to 30°C and water salinities varying between 0 and 5M, i.e., varying between 0°C and 0M (maximum value) and 30°C and 5M (minimum value). Air saturated seawater at 25°C with 0.1% excess air addition is indicated. The yellow area indicates the atmospheric noble gas depletion pattern in the residual waters after an oil-water phase interaction; noble gas concentrations corresponding to oil-water volume ratios varying between 0.1 and 2 are indicated. Sample numbers are in bold.

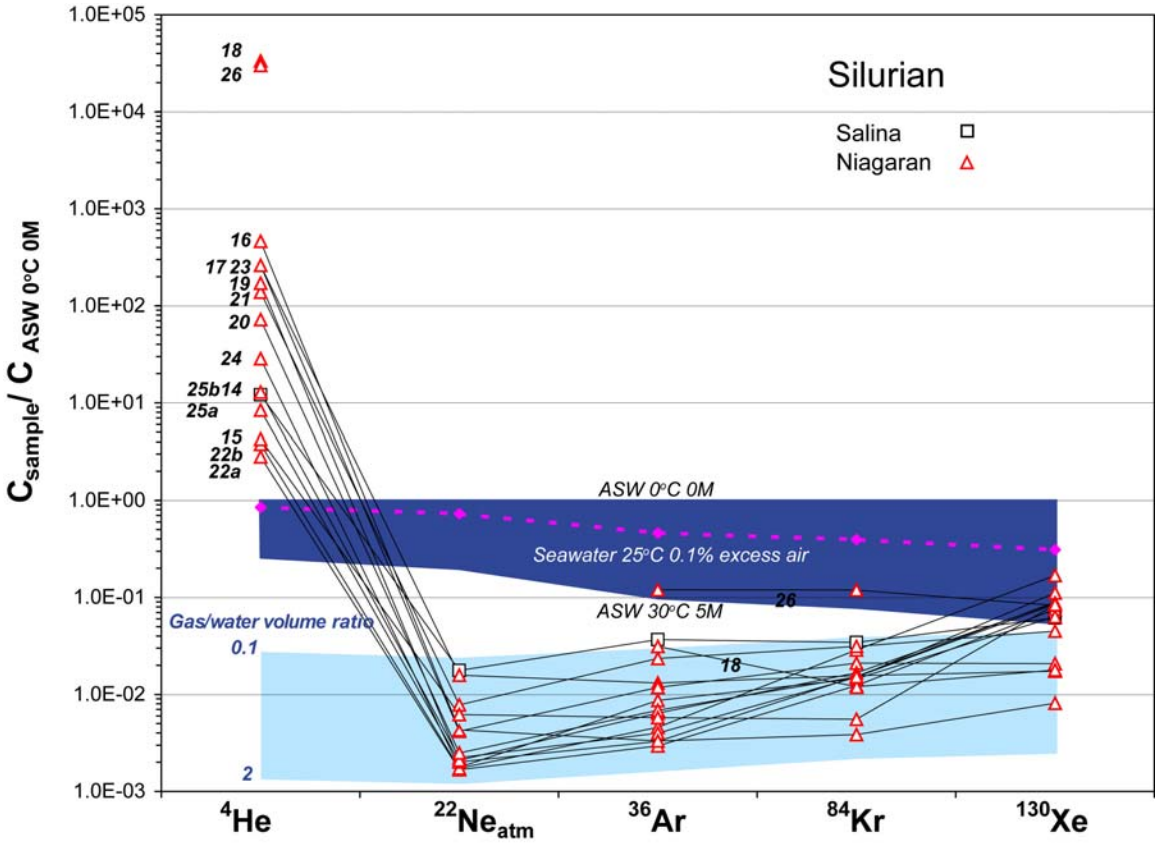

Figure 5.2.c) Salina and Niagaran formations; Atmospheric noble gas concentrations in brines normalized to noble gas concentrations in air saturated water at 0°C and 0M. The dark blue area covers the ASW domain for temperatures varying from 0 to 30°C and water salinities varying between 0 and 5M, i.e., varying between 0°C and 0M (maximum value) and 30°C and 5M (minimum value). Air saturated seawater at 25°C with 0.1% excess air addition is indicated. The light blue area indicates the atmospheric noble gas depletion pattern in the residual waters following a gas-water phase interaction with initial seawater at 25°C with 0.1% excess air. Noble gas concentrations corresponding to gas-water volume ratios varying between 0.1 and 2 are indicated. Sample numbers are in bold.

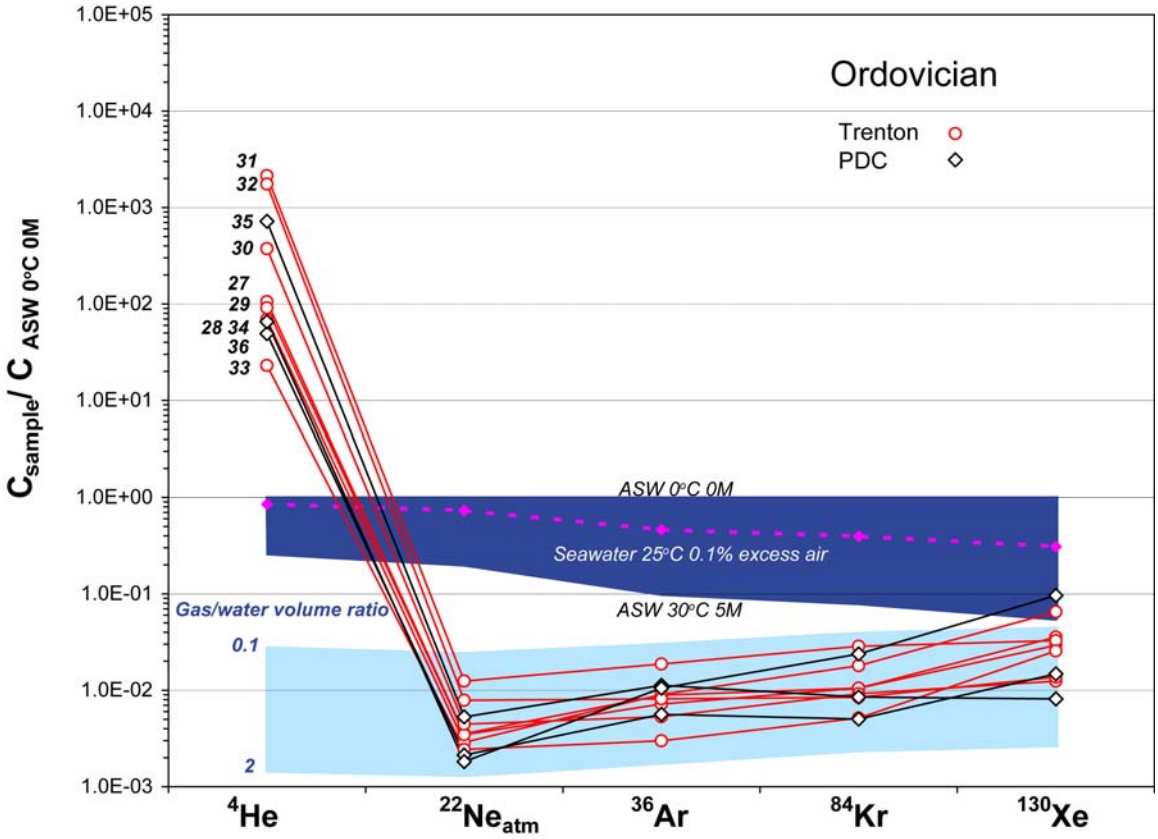

Figure 5.2.d) Trenton and PDC formations; Atmospheric noble gas concentrations in brines normalized to noble gas concentrations in air saturated water at 0°C and 0M. The dark blue area covers the ASW domain for temperatures varying from 0 to 30°C and water salinities varying between 0 and 5M, i.e., varying between 0°C and 0M (maximum value) and 30°C and 5M (minimum value). Air saturated seawater at 25°C with 0.1% excess air addition is indicated. The light blue area indicates the atmospheric noble gas depletion pattern in the residual waters following a gas-water phase interaction with initial seawater at 25°C with 0.1% excess air. Noble gas concentrations corresponding to gas-water volume ratios varying between 0.1 and 2 are indicated. Sample numbers are in bold.

contribution of atmospheric ^{36}Ar, ^{84}Kr, and ^{130}Xe with respect to total measured concentrations for these isotopes and for all samples.

Except for samples 11 (Detroit River) and 26 (Niagaran) which display near ASW values, concentrations of atmospheric noble gases in all samples are strongly depleted relative to those of ASW (Table 5.1, Fig. 5.2). On average, total measured atmospheric ^{22}Ne, ^{36}Ar, ^{84}Kr, and ^{130}Xe concentrations represent 1.2%, 1.6%, 1.9%, and 4.7% of those of ASW at 0°C, 0M, respectively. The depletion of lighter noble gases (^{22}Ne and ^{36}Ar) is thus stronger than that of heavier ones (^{84}Kr and ^{130}Xe). Most of our brine samples show large degrees of depletion even with respect to the lowest noble gas concentrations possible under reasonable temperature and salinity conditions for these reservoirs, i.e., ASW at 30°C and 5 M NaCl solution (Table 5.1, Fig. 5.2). While both ^{22}Ne and ^{84}Kr concentrations show a strong linear positive correlation (R^2=0.89 and R^2=0.90, respectively) with measured ^{36}Ar concentrations, no particular correlation is observed between measured ^{130}Xe and ^{36}Ar concentrations. These overall general patterns are discussed and analyzed below.

5.4.2 Loss of atmospheric noble gases - elemental partitioning between oil-water and gas-water phases

5.4.2.1. Introduction

Atmospheric noble gases in groundwaters/brines are expected to initially have an ASW-like abundance pattern as they originate from water in solubility equilibrium with the atmosphere [e.g., *Mazor and Bosch*, 1987]. It is commonly suggested that the depletion of atmospheric noble gases results from contact with other subsurface fluid phases, in particular, an oil or natural gas phase which is originally free of atmospheric

noble gases [*Zartman et al.*, 1961; *Bosch and Mazor*, 1988; *Zaikowski and Spangler*, 1990]. Because the partitioning of noble gases between a gas-water or oil-water phase results in specific elemental fractionation patterns, atmospheric noble gases in groundwaters/brines can be used to identify and quantify the occurrence of oil-water and gas-water phase interactions [e.g., *Ballentine et al.*, 1991; *Pinti and Marty*, 1995; *Battani et al.*, 2000; *Brennwald et al.*, 2005; *Zhou et al.*, 2005]. Below, it is evaluated that whether such mechanisms can be responsible for the observed depletion patterns in these samples of Michigan Basin brines.

5.4.2.2 Oil-water and gas-water phase interactions models

The concentrations of atmospheric noble gases in residual water following oil-water and gas-water phase interactions were calculated following partitioning models developed by *Bosch and Mazor* [1988], and assuming an original noble gas concentration corresponding to that of seawater at 25°C with 0.1% excess air (Table 5.1, Fig. 5.2). Such a composition is assumed to be representative of the original Michigan Basin brines seawater [e.g., *Wilson and Long*, 1993a, b]. A temperature of 40°C and a salinity of 4.4 M NaCl which closely reflects overall present reservoir conditions were adopted for modeling purposes (Table 5.2). Solubility data (Henry's Law constants) for all noble gases are given in Table 5.2.

Because noble gas solubility in oil increases markedly with increasing atomic mass, interaction of water with an oil phase will lead to a residual water phase (Fig. 5.2.b., yellow area) displaying a stronger depletion in heavy noble gases (e.g., ^{130}Xe and ^{84}Kr) compared to light ones (e.g., ^{36}Ar and ^{22}Ne). Such pattern is precisely the opposite of that

Table 5.2. Reservoir conditions used in models

Reservoir	Average Depth [(a)] (m)	Temperature [(b)] (°C)	Salinity [(c)] (M NaCl solution)	K He [(d)] (atm Kg mol^{-1})	K Ne [(d)] (atm Kg mol^{-1})	K Ar [(d)] (atm Kg mol^{-1})	K Kr [(d)] (atm Kg mol^{-1})	K Xe [(d)] (atm Kg mol^{-1})
Berea	911	32	5.5	9.7E+03	9.8E+03	4.7E+03	3.0E+03	2.1E+03
Traverse	893	32	4.9	8.4E+03	8.4E+03	3.9E+03	2.4E+03	1.7E+03
Dundee	1063	35	4.8	8.2E+03	8.1E+03	3.9E+03	2.4E+03	1.7E+03
Detroit River	1125	36	5.7	1.0E+04	1.0E+04	5.2E+03	3.3E+03	2.3E+03
Salina	699	28	5.6	1.0E+04	1.0E+04	4.8E+03	3.0E+03	2.0E+03
Niagaran	1019	34	5.6	9.9E+03	1.0E+04	5.0E+03	3.1E+03	2.2E+03
Trenton	1298	39	3.6	6.1E+03	5.9E+03	2.7E+03	1.7E+03	1.1E+03
PDC	3471	81	3.6	6.0E+03	5.7E+03	3.4E+03	2.3E+03	1.8E+03
Gas-Water Model		40	4.4	7.4E+03	7.2E+03	3.5E+03	2.2E+03	1.5E+03
Boiling Model		260	0	4.5E+02	6.3E+02	4.1E+02	4.0E+02	3.2E+02
Oil-Water Model		40		7.2E+02	6.1E+02	1.1E+02	3.9E+01	1.1E+01

a. Average depths for sampled wells in the Michigan Basin
b. Calculated after geothermal gradient T(°C)=14.5(°C)+0.0192(°C/m)×depth(m) [*Vugrinovich*, 1989].
c. After *Wilson and Long* [1993a,b].
d. Henry's Law constants for He, Ne, Ar, Kr, and Xe in water calculated after *Crovetto et al.* [1982], *Smith* [1985], *Smith and Kennedy* [1983] and in oil calcalated after *Kharaka and Specht* [1987].

displayed by most of our samples, specifically, samples from Berea, Traverse (Fig. 5.2.a), Salina, Niagaran (Fig. 5.2.c), Trenton and PDC (Fig. 5.2.d). Thus, the depletion of atmospheric noble gases in these samples due to interaction with an oil phase is highly unlikely. Similarly, the absence of a preferential pattern in samples from Dundee and Detroit River (Fig. 5.2.b) as well as in samples 18 and 26 from the Niagaran formation (Fig. 5.2.c) also renders highly unlikely interaction with an oil phase as the cause of such depletion for these samples (Fig. 5.2.b., yellow area).

By contrast, interaction between water and a gas phase (e.g., natural gases or CO_2) would lead to stronger depletion of the lighter noble gases (^{22}Ne and ^{36}Ar) compared to the heavier ones (e.g., ^{130}Xe and ^{84}Kr) in the residual water phase (brines). With the exception of the samples from Dundee and Detroit River (Fig. 5.2.b., yellow area), as well as the samples 18 and 26 from the Niagaran formation mentioned above, this general trend is precisely what is observed in most of our brine samples. Thus, to a first approximation, such a pattern would favor an interaction between water and a gas phase as the mechanism responsible for the observed atmospheric noble gas depletion. However, one must assess whether or not the relative volumes of gas and water involved in these interactions are reasonable, taking into account current reservoir conditions in place. Indeed, the degree of noble gas depletion in residual waters increases with increasing volume of gas (V_g) to volume of water (V_w), i.e., with increasing V_g/V_w ratios. The slope/curvature of such noble gas depletion patterns in a plot of ^{22}Ne versus ^{36}Ar will depend on whether such a process takes place in a closed (CS) or open (OS) system (Fig. 5.3). A closed-system process implies that the water and gas (or oil) phases remain in continuous contact as the system evolves, while an open system implies that the gas (or

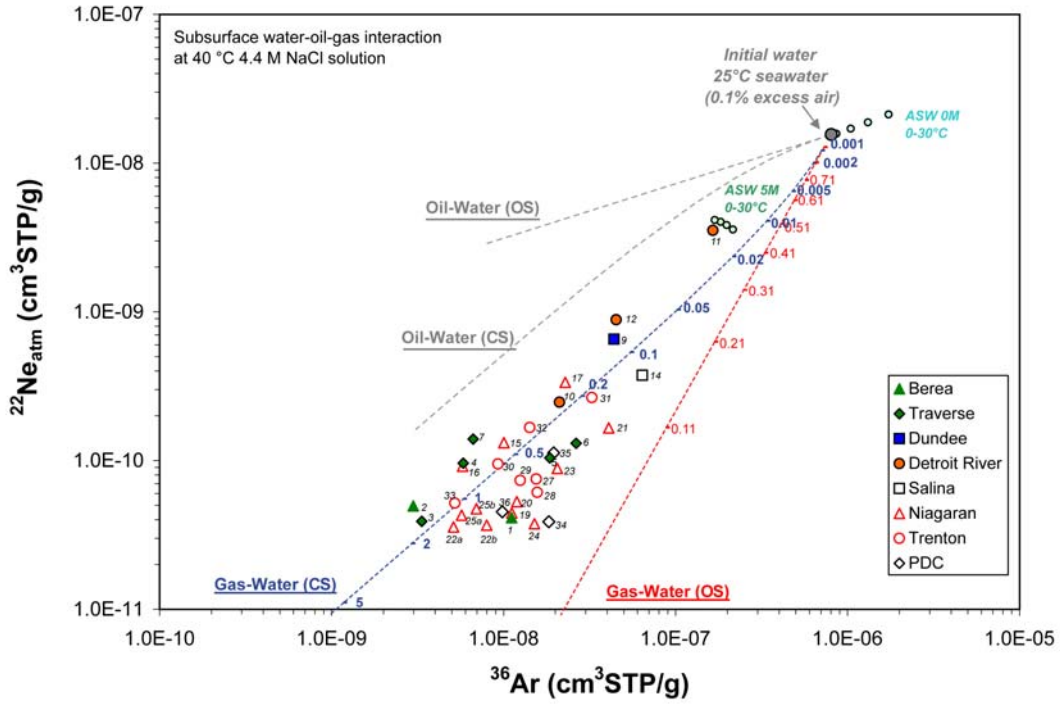

Figure 5.3. Calculated ^{22}Ne and ^{36}Ar concentrations in the residual water (brine) from an initial water composition corresponding to seawater (0.6M) at 25^{o}C with the addition of 0.1% excess air, following oil-water and gas-water interaction models for a open (OS) and closed (CS) system as these interactions proceed. Atmospheric ^{22}Ne and ^{36}Ar concentrations in our Michigan Basin brines are also plotted and identified by their sample numbers. ASW at 0-30°C for both 0M and 5M NaCl solutions are indicated for reference. Depletion curves were calculated for a reservoir temperature at 40°C and a salinity of 4.4M. Numbers (in blue) along the depletion curve indicate the volume of gas (V_g) to the volume of water (V_w) ratio, i.e., V_g/V_w. Numbers along the open system curve (in red) indicate the residual Ar concentration as a fraction of the initial concentration.

oil) phase is continuously removed from the residual water phase as the interaction proceeds (Fig. 5.3). While most samples (Berea, Traverse, Fig. 5.2a; Salina, Niagaran, Fig. 5.2c; Trenton, and PDC formation, Fig. 5.2d) mimic the abundance pattern of a residual water phase following gas-water phase interaction in a closed system (Fig. 5.3), the V_g/V_w ratios required (~0.1-2) if such an interaction had occurred are orders of magnitude greater than expected under reasonable subsurface reservoir conditions, and under those of our Michigan Basin brines in particular. Indeed, available oil and gas inventories in the sampled reservoirs point to a maximum V_g/V_w volume ratio of up to but not exceeding ~5.5×10^{-3} [*Dolton*, 1995], a value far smaller than the lowest V_g/V_w ratios of ~0.1 (samples 9,14,12) if a gas-water interaction was responsible for the observed noble gas depletion. Previous noble gas studies in hydrocarbon reservoirs of the Pakistan Indus Basin, the Pannonian Basin in Hungary as well as the Hugoton-Panhandle giant gas field in the USA revealed equally low V_g/V_w values of ~10^{-3}-10^{-2} [*Ballentine et al.*, 1991; *Battani et al.*, 2000; *Ballentine and Lollar*, 2002].

The impact of varying initial seawater and reservoir temperatures on estimated V_g/V_w ratios is negligible, with the most critical factor affecting this ratio being the original salinity value. If, instead of seawater composition (0.6M), one assumes an initial water composition corresponding to that of evaporated brines under direct contact with the atmosphere with extremely high salinities comparable to that of our present brines (e.g., mean salinity of 4.4 M NaCl), the result is a V_g/V_w ratio up to ~0.5. This value is still orders of magnitude greater than the one directly obtained from gas inventories in the Michigan Basin (~5.5×10^{-3}). It is therefore apparent that even extreme and unrealistic

initial conditions are unable to account for acceptable V_g/V_w values in the event of a possible gas-water interaction.

The depletion of atmospheric noble gases as a result of degassing during sampling due to low wellhead pressures can also be excluded. Indeed, if a gas phase had exsolved from the brine due to a pressure drop at the wellhead, the observed noble gas depletion would display a inverse correlation with well head pressures (i.e., greater degree of depletion associated with lower pressures), which is not observed. In addition, if one would consider reservoir conditions in our brines (e.g., 40°C, 1Km depth), these can be saturated with ~21mM/Kg CH_4 [*Haas*, 1978]. Degassing of CH_4 during sampling at a low well head pressures (e.g., 5atms) would lead at most to a V_g/V_w ratio of 0.098, a value that is over a order of magnitude lower than that required for our brines if depletion had resulted from a gas-water phase interaction.

Overall, the extremely high V_g/V_w ratios required considering a gas-water phase interaction model as a mechanism to explain the observed atmospheric noble gas depletion pattern cannot be easily reconciled with realistic reservoir conditions in the Michigan Basin. This leads to the consideration of alternative processes and, in particular, boiling and steam separation, as an explanation of the observed noble gas depletion pattern in these brines under Michigan Basin reservoir conditions.

5.4.3 Boiling and phase separation - implication for a past thermal event in the Michigan Basin

5.4.3.1 Introduction

Boiling and steam separation have been identified as basic processes occurring in hydrothermal systems in both oceanic and hydrothermal systems. Juan de Fuca Ridge

[*Butterfield et al.*, 1990], East Pacific Rise [*Oosting and Von Damm*, 1996], North Fiji Basin Ridge [*Ishibashi et al.*, 1994], Red Sea Basin [*Winckler et al.*, 2000], Yellowstone in the USA [*Mazor and Fournier*, 1973] and Cerro Prieto in Mexico [*Mazor and Truesdell*, 1984] were among the hydrothermal systems that received particular attention. Hot fluids boil as a result of decreasing pressure during ascent and separate into a steam (water vapor) phase and a residual liquid water phase, both of which have been documented in natural hydrothermal systems [see, e.g., *Butterfield et al.*, 1990]. During phase separation, non-volatile components such as Cl^- and Br^- are concentrated in the residual water phase resulting in hydrothermal waters with high salinity values. In contrast, because of their low solubility in liquid water, noble gases preferentially enter the steam phase, leaving a residual liquid that is highly depleted in noble gases [*Mazor and Truesdell*, 1984; *Mazor and Bosch*, 1987; *Kennedy*, 1988; *Winckler et al.*, 2000]. This characteristic, together with their conservative nature, renders atmospheric noble gases particularly useful in detecting the occurrence (past or present) of hydrothermal events in a particular region.

A wealth of thermal studies in the Michigan Basin based on a diversity of proxies (e.g., organic maturity data, stable isotopes, fluid inclusions, authigenic clay minerals, apatite fission track ages) all point to the occurrence of high temperatures (~80-260°C) in the past [*Cercone and Lohmann*, 1987; *Cercone and Pollack*, 1991; *Crowley*, 1991; *Coniglio et al.*, 1994; *Girard and Barnes*, 1995; *Luczaj et al.*, 2006]. Of particular significance, a minimum temperature range of up to 220-260°C was recorded in fluid inclusions from Ordovician carbonates at very shallow depths in the Michigan Basin [*Allen and Wiggins*, 1993; *Coniglio et al.*, 1994]. The transport of hot fluids from deep to

shallow portions of the basin along major faults and fracture zones connected to structures in the Precambrian basement was previously suggested to account for these high temperatures, which point to the presence of hydrothermal events in the past [*Sanford et al.*, 1985; *Budai and Wilson*, 1991; *Coniglio et al.*, 1994; *Girard and Barnes*, 1995; *Luczaj et al.*, 2006]. Below, it is proposed that the observed atmospheric noble gas depletion in the Michigan Basin brines is the result of boiling and steam separation similar to that observed in active hydrothermal systems and that it is associated with a past thermal event in the basin. To evaluate such an hypothesis, atmospheric noble gas concentrations were reconstructed in the residual water phase (brines) following a boiling and steam separation conceptual model originally developed by *Mazor and Truesdell* [1984].

5.4.3.2 The boiling model

The boiling model by *Mazor and Truesdell* [1984] describes the partitioning of noble gases between the water and steam phases according to Henry's Law. In a closed system, the concentration of noble gases in the residual water phase is given by [*Mazor and Truesdell*, 1984]:

$$\frac{C}{C_0} = \frac{1}{F + \frac{1-F}{A}} \qquad (5.1)$$

while in a open system, this concentration is given by:

$$\frac{C}{C_0} = F^{(1/A-1)} \tag{5.2}$$

where C and C_0 are the noble gas concentrations (e.g., ^{22}Ne, ^{36}Ar) in the residual and initial water respectively, F is the fraction of residual water after boiling, and A is the distribution coefficient of noble gases between water and steam phases. 1-F represents the fraction of vapor phase (steam) and is referred to as the degree of boiling. The distribution coefficient A can be calculated by:

$$A = \frac{RT}{K_h V_{sp}} \tag{5.3}$$

where R is the ideal gas constant (8.206×10^{-5} atm $m^3mol^{-1}K^{-1}$), T the boiling temperature (K), K_h the Henry's Law constant (atm kg mol^{-1}) for a particular noble gas and V_{sp} the specific volume of steam (kg m^{-3}) for a particular boiling temperature. These equations are valid for isothermal systems.

5.4.3.3 Results and discussion - boiling and phase separation

In an approach similar to that followed for the oil-water and gas-water models, an original noble gas concentration corresponding to that of seawater at 25°C with 0.1% excess air was adopted (Table 5.1). To reconstruct noble gas concentrations in our brines that would result from boiling and steam separation, a boiling temperature of 260°C was used, consistent with fluid inclusion data in Ordovician rocks in the Michigan Basin [*Coniglio et al.*, 1994]. The boiling model by *Mazor and Truesdell* [1984] requires the knowledge of noble gas solubilities in water. Solubility values for noble gases in fresh

water are well established for the temperature range of 30-330°C [*Crovette et al.*, 1982; *Smith*, 1985]. However, the solubilities of noble gases in seawater and brines (with salinities up to 5.2M NaCl) are only known for temperatures up to 65°C [*Smith and Kennedy*, 1983]. Due to a lack of solubility data for high temperatures and salinities, we used solubility data for high temperatures without considering the effects of salinity, an approach similar to that undertaken by *Winkler et al.* [2000] for the study of Red Sea brines.

Fig. 5.4 shows the evolution of ^{22}Ne and ^{36}Ar concentrations from the original seawater composition for both a closed and open system as boiling proceeds and as more and more noble gas leaves the residual phase (brine) and enters the steam. It is apparent that such a boiling and steam separation process for both closed and open systems leads to a dramatic decrease of atmospheric noble gas concentrations with respect to the initial seawater composition (Fig. 5.4). It is also apparent that our brines follow the general trend of these boiling curves remarkably closely. While 15 brine samples plot along or close to the closed system boiling curve, a small subset of samples (14, 34, 21, 24) plots along the open system boiling curve, indicating a dynamic process for loss of steam in these samples. In addition, half of the samples plot within the area bounded by these two hypothetical boiling curves. These samples might represent either a combination of both processes occurring at the same location but spaced in time, or simply be due to the mixing of brines whose composition resulted from a closed and open system boiling and steam separation, respectively. Brine samples along the boiling curves show various degrees of depletion of noble gases, possibly due to either different degrees of boiling or post boiling mixing with normal ASW.

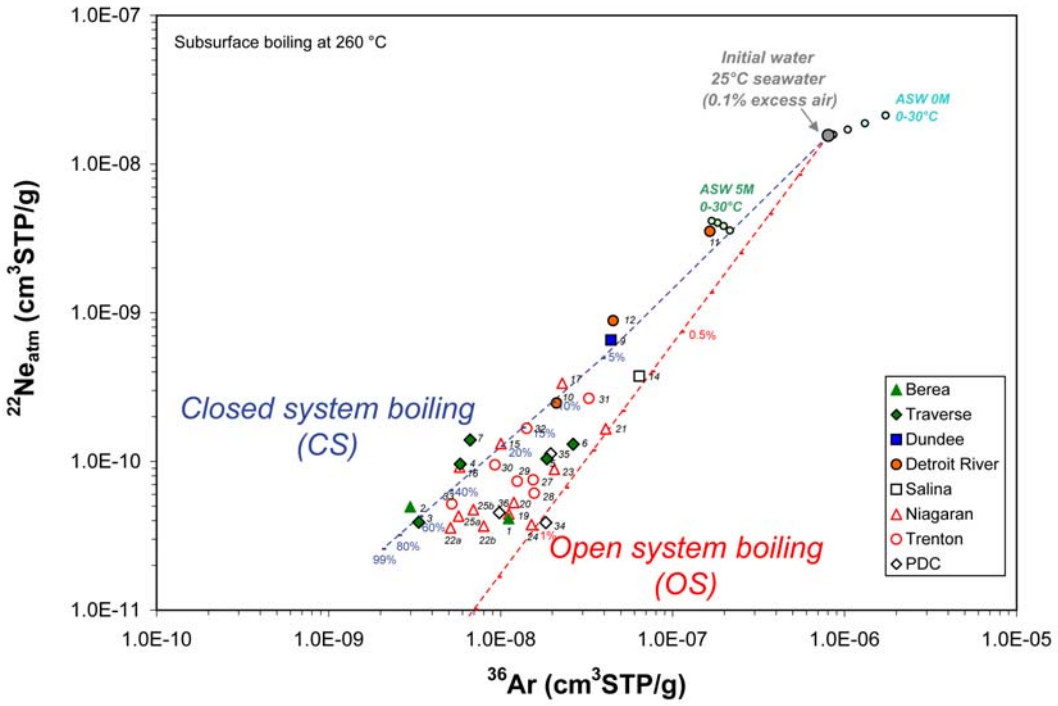

Figure 5.4. Calculated ^{22}Ne and ^{36}Ar concentrations in the residual water (brine) from an initial water composition corresponding to seawater (0.6M) at 25^{o}C with the addition of 0.1% excess air, and a reservoir temperature of 260°C, following a boiling and steam separation process for a open (OS) and closed (CS) system as these interactions proceed. Atmospheric ^{22}Ne and ^{36}Ar concentrations in our Michigan Basin brines are also plotted and identified by their sample numbers. ASW at 0-30°C for both 0M and 5M NaCl solutions are indicated for reference. Numbers along the depletion curve indicate the degree of steam loss for the closed system. Numbers along the depletion curves indicate the degree of steam loss for each one of the systems.

Analysis of the closed system boiling and steam phase separation process reveals a minimum and maximum steam loss of ~5% (sample 12) and ~60% (sample 2 and 3), respectively (Fig. 5.4). Such a degree of boiling is comparable to the 15-20% boiling suggested for oceanic hydrothermal fields at the Juan de Fuca Ridge [*Butterfield et al.*, 1990]. By contrast, boiling displayed in the Michigan Basin brines is greater than the ~3% level observed at an early stage of boiling in Cerro Pietro, Mexico [*Mazor and Truesdell*, 1984], as well as that of Red Sea brines [*Winckler et al.*, 2000]. The higher degree of boiling estimated for our brines as compared to Cerro Pietro and the Red Sea indicates that most of the original seawater in the Michigan Basin was converted into steam leading to a residual phase (brine) with very high salinities. This is precisely what we observe, with TDS values of up to 5.7M recorded in the basin [*Wilson and Long*, 1993a,b]. If the original ancient seawater in the Michigan Basin had a chemical composition similar to modern seawater and if the non-volatile components are assumed to be conservative during brine evolution, it is possible to estimate the degree of water loss independently, solely based on Cl^- and Br^- concentrations. Such estimation leads to a degree of water loss for Cl^- and Br^- varying between 74-92% and 79-98%, respectively [*Wilson and Long*, 1993a, b]. Differences between estimations based on atmospheric noble gases and major elements might be due to the fact that Cl^- and Br^- are not ideal conservative tracers during brine evolution. Indeed, interaction with evaporites (e.g., halite) and organic matter (e.g., in shale or carbonates) can potentially increase Cl^- and Br^- concentrations in brines [*Kharaka and Hanor*, 2003], thus leading to an overestimation of water loss. Evaporites, shale, and carbonates are present in the Michigan Basin and such water-rock interactions have been documented [*Wilson and*

Long, 1993a, b; *McIntosh et al.*, 2004]. Therefore, taking into account simplifications made in both calculations, the maximum degree of boiling (~60%) estimated from atmospheric noble gas concentrations is more likely and consistent with the degree based on major element data, which, independently, suggests a high degree of boiling in the basin.

In a hydrothermal system, the temperature and depth required for the initial boiling to occur can be estimated by using boiling point curves, which represent the vapor-liquid phase boundary in pressure-temperature space (Fig. 5.5). When a hot fluid encounters the boiling point curve, the result is boiling and phase separation, and formation of nearly pure water vapor from saline liquids [e.g., *Butterfield et al.*, 1990; *Ingebritsen and Sanford*, 1998]. Based on the boiling point curve for seawater (Fig. 5.5), the estimated boiling temperatures for most Michigan Basin brines vary between ~260°C and 340°C (see geothermal gradient, Fig. 5.5). These temperatures are slightly higher than the model boiling temperature used (260°C) which represents a fluid inclusion temperature from the outcrop area of the Ordovician carbonates [*Coniglio et al.*, 1994] likely following boiling and cooling and not a peak temperature of these boiled fluids. Indeed, in active hydrothermal systems, observed fluids temperatures are similarly lower than the required boiling temperatures by ~20-70°C, most likely due to conductive cooling with surrounding rocks or mixing with cold waters after boiling [*Butterfield et al.*, 1990; *Ishibashi et al.*, 1994; *Oosting and Von Damm*, 1996]. Alternatively, the presence of dissolved gases such as CO_2 or CH_4 which are commonly observed in subsurface fluids could greatly affect the shape of the boiling point curves [*Hanor*, 1980; *Butterfield et al.*, 1990; *Duan et al.*, 1992; *Duan et al.*, 1995] and substantially lower the boiling

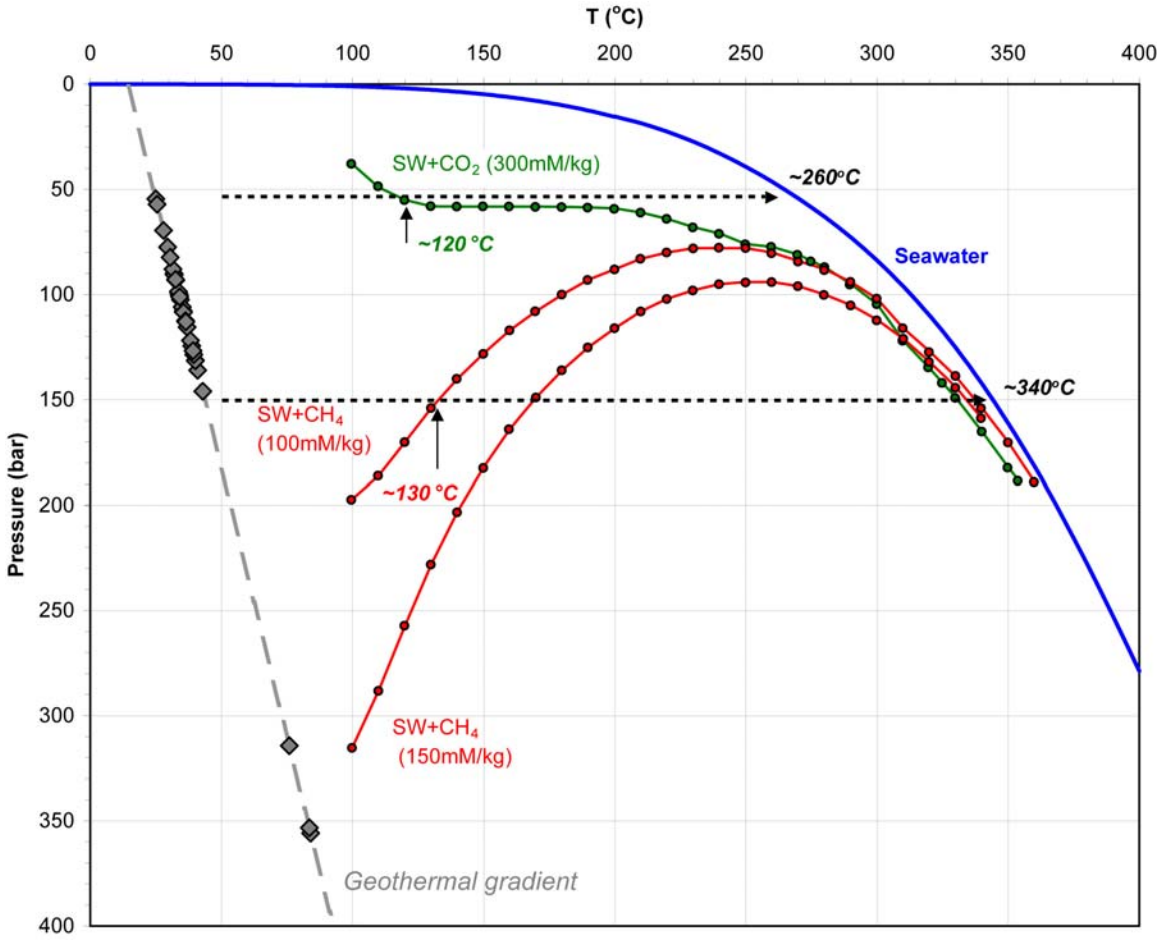

Figure 5.5. Boiling point curves for seawater [from *Bischoff and Rosenbauer*, 1988], seawater + 300mM/kg dissolved CO_2 [from *Butterfield et al.*, 1990; *Duan et al.*, 1992], and seawater+100mM and 150mM dissolved CH_4 [from *Haas*, 1978; *Hanor*, 1980; *Duan et al.*, 1995]. Diamonds represent Michigan Basin samples with temperatures assuming a current geothermal gradient of 19°C/km [*Vugrinovich*, 1989]. Arrows represent the temperatures (~260 and ~340°C) at which most of our brine samples would go through boiling and steam separation under these particular reservoir conditions.

point of Michigan Basin brines. For example, the boiling point could be greatly lowered from 260°C to 120°C with addition of CO_2 (Fig. 5.5) [*Butterfield et al.*, 1990]. The presence of CH_4 in the fluids could affect the boiling curves to an even greater extent [*Hanor*, 1980]. Indeed, if the seawater is saturated with CH_4 at reservoir conditions [*Haas*, 1978], the boiling point can be significantly lowered from 340°C to 130°C (Fig. 5.5), well within the range of the observed high paleo-temperatures in the Michigan Basin (~80-260°C).

Overall, the observed noble gas concentrations of Michigan Basin brines are remarkably similar to the results from a simple boiling and steam separation model under reasonably well constrained parameters, despite uncertainties of noble gas solubility data in brines. This consistency strongly suggests that the occurrence of an ancient thermal event is most likely responsible for the atmospheric noble gas depletion observed in these brines.

5.4.3.4 An ancient thermal event in the Michigan Basin

The depletion of atmospheric noble gases in Michigan Basin brines strongly points to the occurrence of an ancient thermal event in the basin, during which fluids and heat were transported from deeper portions of the basin along major fault and fracture zones (Fig. 5.1). It also suggests the subsequent occurrence of boiling and phase separation at shallower depths, which ultimately would have led to the extreme depletion of atmospheric noble gases in the residual brines. A reactivation of Precambrian basement structures is likely at the origin of such an event. Indeed, a reactivation of the mid-continental rift (MCR) system during the Late Devonian-Mississippian (370-323Ma)

period was previously suggested based on the formation of authigenic illite, which yields the youngest ages (323 Ma) and highest temperature estimates (~170°C) in the vicinity of the MCR [*Girard and Barnes*, 1995]. Apatite fission-track ages from drilled basement samples further indicate two additional, more recent periods of thermal activity, during the Triassic (~224Ma) and Cretaceous (~111-159Ma), respectively [*Crowley*, 1991]. Repeated movements along major faults prevailed throughout the early part of the Paleozoic and major uplift of the basin fault blocks occurred at the end of the Mississippian period [*Fisher et al.*, 1988]. The reactivation of deep-seated faults and fractures in the basement of both southeastern and northeastern Michigan Basin has been suggested to account for the circulation of hot fluids (e.g., 220-260°C) and formation of hydrothermal dolomite reservoirs [*Sanford et al.*, 1985; *Coniglio et al.*, 1994]. In addition, higher temperatures (~300-400°C) were also inferred from the studies of meta-gabbro and spilitic rocks from the deeply buried rift (~5Km), showing a signature of hydrothermal alteration similar to those altered by seawater at mid-ocean ridges [*McCallister et al.*, 1978; *Stakes*, 1978]. Numerical model simulations have also shown that hydrothermal processes originating from the ancient buried rift could generate hot fluid circulation at the base of the sedimentary sequence and be responsible for the high basin temperatures (200-300°C) in the past [*Nunn*, 1994; *Schoofs et al.*, 2000].

The reactivated rift and other basement structures of the Michigan basin could also affect the major element data of the sedimentary brines [*Wilson and Long*, 1993a, b; *Davisson and Criss*, 1996; *Martini*, 1997]. For example, the presence of Ca excess and Na deficit in deep Michigan Basin brines has been interpreted as evidence for albitization of Ca-plagioclase, an indication of interactions between deep hot fluids and basement

rocks [*Davisson and Criss*, 1996; *Schoofs et al.*, 2000]. The presence of unusually high ^{4}He excesses, high ^{4}He/heat flux ratios as well as high salinity waters at shallow depths of the basin has also suggested the upward movement of heat, He and major elements [*Castro et al.*, 2005; *Ma et al.*, 2005; *Castro et al.*, 2007].

Of greater relevance is the presence of a primordial solar-like mantle He and Ne signature in these brines [*Castro et al.*, 2008]. In addition to providing new insights into mantle convection theories, the discovery of a highly primordial signature in the stable intracratonic Michigan Basin points also to the mantle origin of such a hydrothermal event. Deep-seated active faults have been documented as fluid conduits for the release of mantle fluids into the shallow crust, especially in regions without substantial magmatism such as the Basin and Range province and along the San Andreas Fault [*Kennedy et al.*, 1997; *Kulongoski et al.*, 2005; *Kennedy and van Soest*, 2007]. Similar mechanisms may have played a role during a reactivation of the ancient basement structures in the Michigan Basin in late Paleozoic or even later periods [*Sanford et al.*, 1985; *Fisher et al.*, 1988; *Crowley*, 1991; *Girard and Barnes*, 1995]. While heat may have escaped quickly from the basin, such a thermal event can be still traced by the presence of both mantle He and Ne signatures and the depleted atmospheric noble gases in these brines.

5.4.4 Relative enrichment of Kr and Xe with respect to Ar

Concentrations of ^{84}Kr and ^{130}Xe in residual waters after subsurface boiling and steam separation were also calculated using the conceptual boiling model developed by *Mazor and Truesdell* [1984] and compared to the measured concentrations of brine samples (Fig. 5.6a, b). The parameters used and assumptions made are those previously

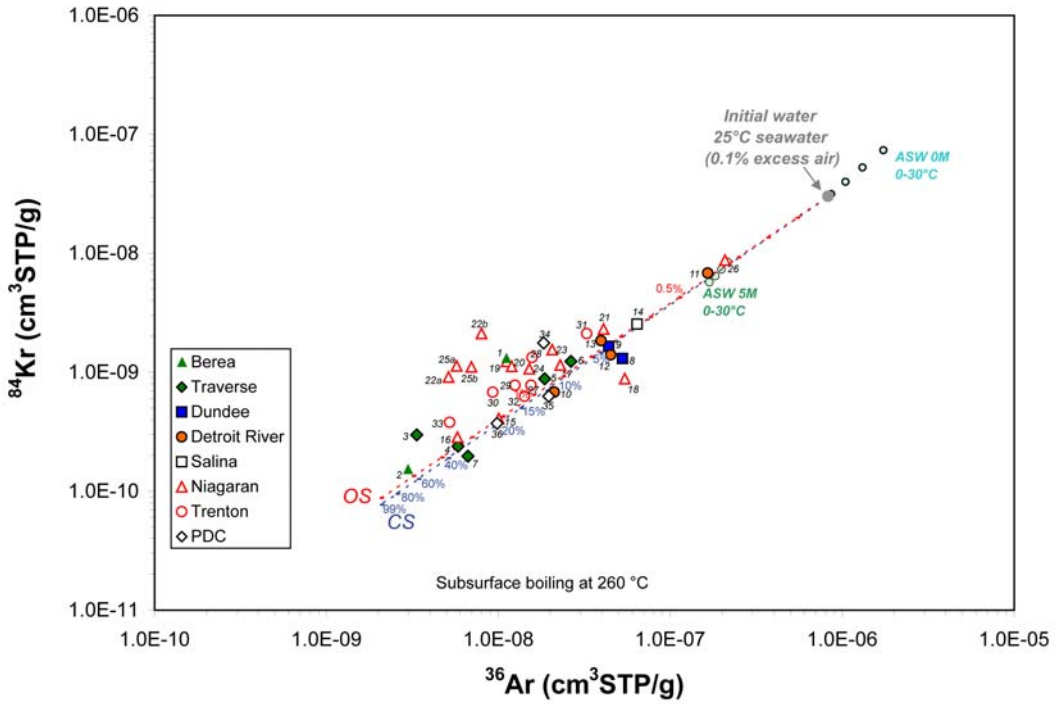

Figure 5.6. a) Atmospheric ^{84}Kr vs. ^{36}Ar concentrations in our brine samples; The boiling depletion curves for a closed (CS) and open (OS) system are indicated using similar parameters to those for Fig. 5.4. ASW at 0-30°C for both 0M and 5M NaCl solutions are indicated for reference as well as the identification number for each sample.

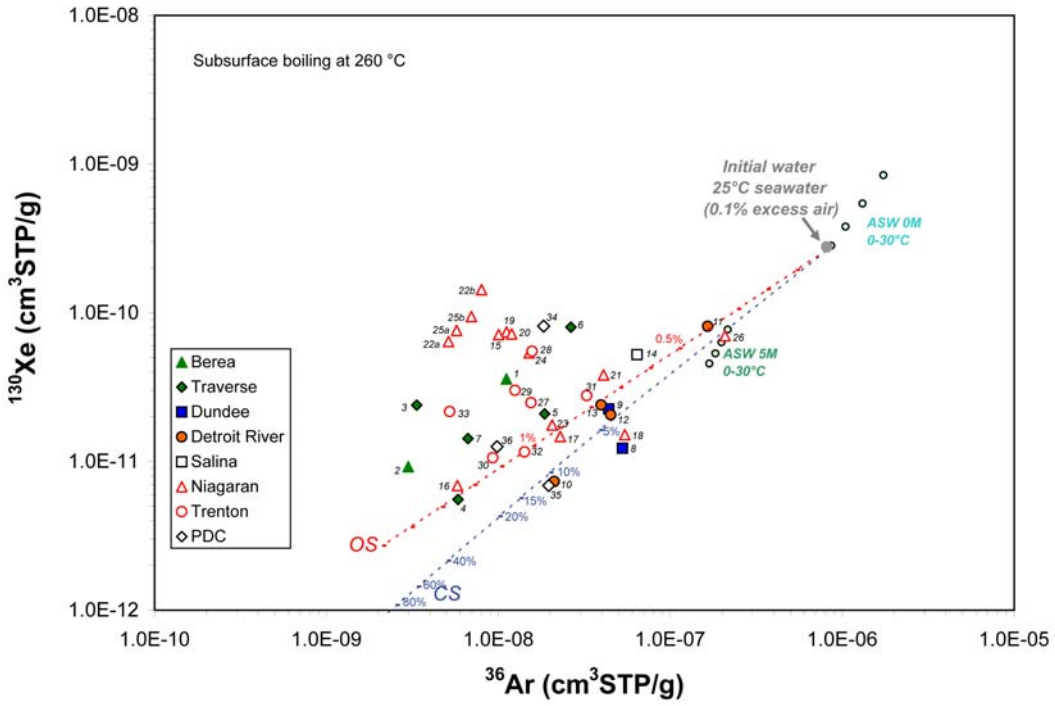

Figure 5.6.b) Atmospheric ^{130}Xe vs. ^{36}Ar concentrations in our brine samples; The boiling depletion curves for a closed (CS) and open (OS) system are indicated using similar parameters to those of Fig. 5.4. ASW at 0-30°C for both 0M and 5M NaCl solutions are indicated for reference as well as the identification number for each sample.

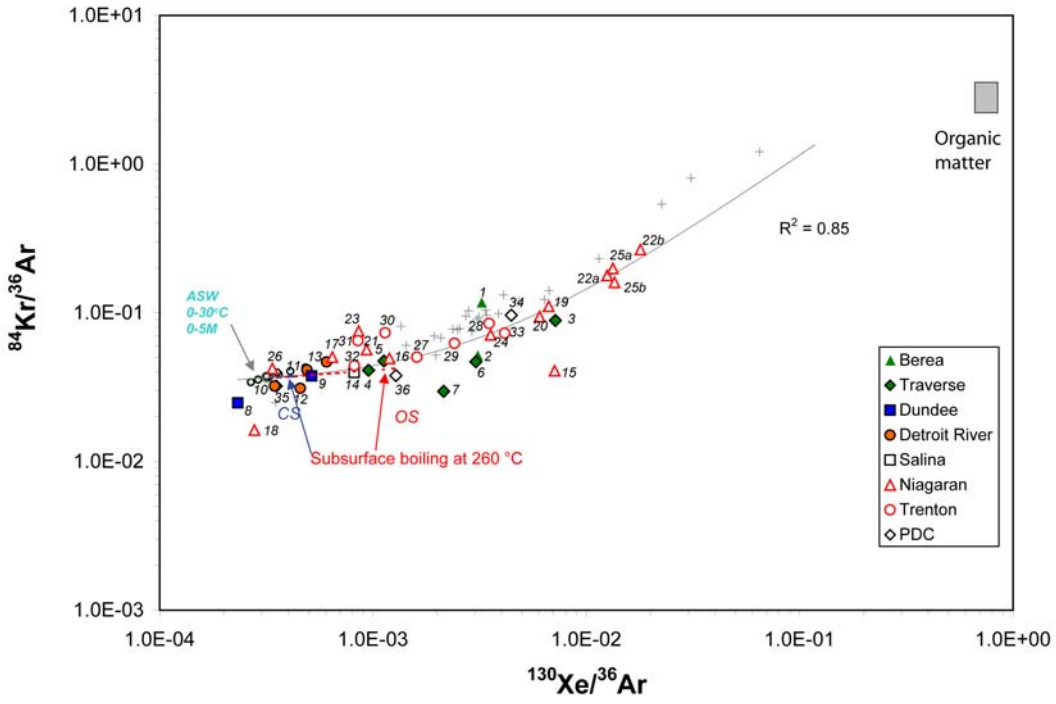

Figure 5.6. c) Atmospheric $^{84}Kr/^{36}Ar$ vs. $^{130}Xe/^{36}Ar$ ratios. The boiling depletion curves for a closed (CS) and open (OS) system are indicated using similar parameters to those of Fig. 5.4. ASW at 0-30°C for both 0M and 5M NaCl solutions are indicated for reference as well as the identification number for each sample. Grey crosses and grey block show composition of gas samples from the Elk Hills oil field [*Torgersen and Kennedy*, 1999] and organic matter composition [*Frick and Chang*, 1977]. Correlation between $^{84}Kr/^{36}Ar$ and $^{130}Xe/^{36}Ar$ ratios in our brine samples is also shown (grey line, with R^2=0.85; the linear relationship appears curved due to the logarithmic scales).

described (see section 5.4.3.3) for ^{22}Ne and ^{36}Ar. From Fig. 5.6, it is clear that although a subset of brine samples follows closely the predicted boiling depletion curves, most samples show measured ^{84}Kr and ^{130}Xe concentrations higher than those predicted by the boiling model, displaying an apparent enrichment of ^{84}Kr and ^{130}Xe relative to ^{36}Ar. Such enrichment is also apparent in Fig. 5.6.c in which $^{84}Kr/^{36}Ar$ is plotted against $^{130}Xe/^{36}Ar$. These samples also have $^{84}Kr/^{36}Ar$ and $^{130}Xe/^{36}Ar$ ratios that are greater than those of ASW (0-30°C; 0-5M, Fig. 5.6.c), reaching values up to ~6 and 37 times that of ASW (0°C, 0M; e.g., sample 22b), respectively. Such high $^{84}Kr/^{36}Ar$ and $^{130}Xe/^{36}Ar$ ratios are beyond the limits of the boiling model and strongly suggest additional sources for ^{84}Kr and ^{130}Xe. In addition, the $^{84}Kr/^{36}Ar$ and $^{130}Xe/^{36}Ar$ ratios of all brine samples show a strong positive linear correlation ($R^2 = 0.85$), and display a trend that is particularly distinct from that of the boiling curve (Fig. 5.6c).

High Kr/Ar and Xe/Ar ratios have also been previously identified in hydrocarbon-related samples [e.g., *Torgersen and Kennedy*, 1999; *Zhou et al.*, 2005] and have been interpreted as reflecting the release of sedimentary Kr and Xe from organic matter (e.g., shale) as previously suggested by *Frick and Chang* [1977] and *Podosek et al.* [1980]. *Torgersen et al.* [2004] suggested that this Kr and Xe characteristic signature is present in organic matter in sedimentary rocks, in which a relative enrichment with respect to Ar is observed and is thought to be due to a diffusion-controlled fractionation process. Such relative Kr and Xe enrichment was previously found in Elk Hills oil field gases in California (Fig. 5.6c, grey crosses) [cf., *Torgersen and Kennedy*, 1999], and was interpreted as a mixing between an ASW-like source (e.g., groundwater) and that of organic matter (e.g., shale, Fig. 5.6.c). Relative Kr and Xe enrichment in the Michigan

Basin brines mimics closely that previously observed in Elk Hills and suggests the influence of hydrocarbons on these basinal brines. Under this scenario, the original ASW-like signature for heavy noble gases would have been modified by boiling and steam separation, prior to the addition of Kr and Xe enriched signatures, possibly during hydrocarbon generation and/or hydrocarbon migration and accumulation in the oil and gas reservoirs. The close relationship between the deep basinal brines and hydrocarbons is thus revealed by the characteristic heavy noble gas signatures in these brines.

5.5. Conclusions

We present noble gas concentrations in 38 deep brines (~0.5-3.6km) from the Michigan Basin. The atmospheric noble gas components (^{22}Ne, ^{36}Ar, ^{84}Kr, and ^{130}Xe) show a strong depletion pattern with respect to ASW with depletion of lighter gases (^{22}Ne and ^{36}Ar) being stronger compared to heavier ones (^{84}Kr and ^{130}Xe). To understand the mechanisms responsible for this overall atmospheric noble gas depletion, phase interaction models were tested. While oil-water and gas-water interaction models could not, under reasonable assumptions, explain both the extent and the observed atmospheric noble gas depletion pattern, the opposite is true with a model involving subsurface boiling and steam separation. Indeed, the latter not only explains the overall observed atmospheric noble gas depletion pattern, it also points strongly to the presence of a past hydrothermal event. This finding is consistent with the presence of primordial solar-like He and Ne signatures in the basin previously identified in these same brines [*Castro et al.*, 2008], and suggests a mantle origin for the occurrence of this thermal event. Such a boiling and steam separation model is also consistent with the presence of past elevated

temperatures in the Michigan Basin (e.g., ~80-260°C) at shallow depths as suggested by numerous previous studies in the basin. It is suggested here that a recent reactivation of the ancient mid-continent rift (MCR) system underneath the Michigan Basin is likely responsible for the release of both heat and mantle noble gases into the basin via deep-seated faults and fracture zones. While the heat has already escaped the system, such a thermal event can still be traced by the presence of the observed atmospheric noble gas depletion in addition to the previously identified high ^{4}He/heat flux ratio at shallow depths in the basin [*Castro et al.*, 2005; 2007].

An enrichment of atmospheric Kr and Xe relative to Ar is also observed in these brines, an enrichment that cannot easily be solely accounted for by the boiling and steam separation model. This relative enrichment is interpreted as reflecting the addition of sedimentary Kr and Xe from associated hydrocarbons, probably during hydrocarbon generation and/or hydrocarbon migration and accumulation. Such enrichment would have occurred following the hydrothermal event that led to the boiling and steam separation of atmospheric noble gases and consequently, their depletion with respect to ASW.

This study pioneers the use of atmospheric noble gases in subsurface fluids to trace the thermal history of stable tectonic regions.

References

Allan, J.R., Wiggins, W.D., 1993. *Dolomite reservoirs: geochemical techniques for evaluating origin and distribution*, AAPG Continuing Education Course Note Series #36, AAPG, Tulsa.

Ballentine, C.J., O'Nions, R.K., Oxburgh, E.R., Horvath, F., Deak, J., 1991. Rare gas constraints on hydrocarbon accumulation, crustal degassing and groundwater flow in the Pannonian Basin, *Earth and Planetary Science Letters* 105, 229-246.

Ballentine, C.J., Lollar, B.S., 2002. Regional groundwater focusing of nitrogen and noble gases into the Hugoton-Panhandle giant gas field, USA, *Geochimica et Cosmochimica Acta* 66, 2483-2497.

Battani, A., Sarda, P., Prinzhofer, A., 2000. Basin scale natural gas source, migration and trapping traced by noble gases and major elements : the Pakistan Indus Basin, *Earth and Planetary Science Letters* 181, 229-249.

Bischoff, J.L., Rosenbauer, R.J., 1988. Liquid-vapor relations in the critical region of the system NaCl-H2O from 380 to 415C: a refined determination of the critical point and two-phase boundary of seawater, *Geochimica et Cosmochimica Acta* 52, 2121-2126.

Bosch, A., Mazor, E., 1988. Natural gas association with water and oil as depicted by atmospheric noble gases: case studies from the southeastern Mediterranean Coastal Plain, *Earth and Planetary Science Letters* 87, 338-346.

Brennwald, M.S., Kipfer, R., Imboden, D.M., 2005. Release of gas bubbles from lake sediment traced by noble gas isotopes in the sediment pore water, *Earth and Planetary Science Letters* 235, 31-44.

Budai, J.M., Wilson, J. L., 1991. Diagenesis history of the Trenton and Black River formations in the Michigan Basin. In: Catacosinos, P.A., Daniels, P.A. Jr. (Eds.), *Early sedimentary evolution of the Michigan Basin*, GSA Special Paper, vol. 256, pp. 73-88.

Butterfield, D.A., Massoth, G.J., McDuff, R.E., Lupton, J.E., Lilley, M.D., 1990. Geochemistry of hydrothermal fluids from Axial Seamount Hydrothermal Emissions Study Vent Field, Juan de Fuca Ridge: subseafloor boiling and subsequent fluid-rock interaction, *Journal of Geophysical Research* 95, 12895-12921.

Castro, M.C., Jambon, A., de Marsily, G., Schlosser, P., 1998a. Noble gases as natural tracers of water circulation in the Paris Basin 1. Measurements and discussion of their origin and mechanisms of vertical transport in the basin, *Water Resources Research* 34, 2443-2466.

Castro, M.C., Goblet, P., Ledoux, E., Violette, S., de Marsily, G., 1998b. Noble gases as

natural tracers of water circulation in the Paris Basin 2. Calibration of a groundwater flow model using noble gas isotope data, *Water Resources Research* 34, 2467-2483.

Castro, M.C., Stute, M., Schlosser, P., 2000. Comparison of ^{4}He ages and ^{14}C ages in simple aquifer systems: implications for groundwater flow and chronologies, *Applied Geochemistry* 15, 1137-1167.

Castro, M.C., Goblet, P., 2003. Calibration of regional groundwater flow models: working toward a better understanding of site-specific systems, *Water Resources Research* 39, 1172, doi:10.1029/2002WR001653.

Castro, M.C., Patriarche, D., Goblet, P., 2005. 2-D numerical simulations of groundwater flow, heat transfer and ^{4}He transport – implications for the He terrestrial budget and the mantle helium-heat imbalance, *Earth and Planetary Science Letters* 237, 893-910.

Castro, M.C., Patriarche, D., Goblet, P., Ma, L., Hall, C.M., 2007. ^{4}He/heat flux ratios as new indicators of past thermal and tectonic events – new constrains on the tectonothermal history of the Michigan Basin, *the 4th Mini Conference on Noble Gases in the Hydrosphere and in Natural Gas Reservoirs*, GFZ Potsdam.

Castro, M.C., Ma, L., Hall, C.M., 2008. A Primordial, solar He-Ne signature in crustal fluids of a stable continental region, in review.

Catacosinos, P.A., Daniel, P.A. Jr., Harrison, W.B. III, 1991. Structure, stratigraphy, and petroleum geology of the Michigan Basin. In: Leighton, M.W., Kolata, D.R., Oltz, D.F., Eidel, J.J. (Eds.), *Interior cratonic basins*, AAPG Memoir, vol. 51, pp. 561-601.

Cercone, K.R., 1984. Thermal history of Michigan Basin, *AAPG Bulletin* 68, 130-136.

Cercone, K.R., Lohmann, K.C., 1987.Late burial diagenesis of Niagaran (middle Silurian) pinnacle reefs in Michigan Basin, *AAPG Bulletin* 71, 156-166.

Cercone, K.R., Pollack, H.N., 1991. Thermal maturity of the Michigan Basin. In: Catacosinos, P.A., Daniels, P.A. Jr. (Eds.), *Early sedimentary evolution of the Michigan Basin*, GSA Special Paper, vol. 256, pp. 1-11.

Coniglio, M., Sherlock, R., Williams-Jones, A.E., Middleton, K., Frape, S.K., 1994. Burial and hydrothermal diagenesis of Ordovician carbonates from the Michigan Basin, Ontario, Canada, *Spec. Publs. Int. Ass. Sediment.* 21, 231-254.

Crovetto, R. Fernandez-Prini, R., Japas, M.L., 1982. Solubilities of inert gases and methane in H_2O and in D_2O in the temperature range of 300 to 600K, *J. Chem. Phys.* 76, 1077-1086.

Crowley, K.D., 1991. Thermal history of Michigan Basin and southern Canadian Shield

from apatite fission track analysis, *Journal of Geophysical Research* 96, 697-711.

Davisson, M.L., Criss, R.E., 1996. Na-Ca-Cl relations in basinal fluids, *Geochimica et Cosmochimica Acta* 60, 2743-2752.

Dolton, G.L., 1995. Michigan Basin Province (063). In: Gautier, D.L., Dolton, G.L., Takahashi, K.I., Varnes, K.L. (Eds.), *1995 National assessment of United States oil and gas resources: results, methodology, and supporting data*, U.S. Geological Survey, GS-30.

Dorr, J.A. Jr., Eschman, D.F., 1970. *Geology of Michigan*, first ed. Univ. of Michigan Press, Ann Arbor, Michigan.

Duan, Z., Moller, N., Weare, J.H., 1992. An equation of state for the CH_4-CO_2-H_2O system: II. Mixtures from 50 to 1000°C and 0 to 1000 bar, *Geochimica et Cosmochimica Acta* 56, 2619-2631.

Duan, Z., Moller, N., Weare, J.H., 1995. Equation of state for the NaCl-H_2O-CO_2 system: prediction of phase equilibria and volumetric properties, *Geochimica et Cosmochimica Acta* 59, 2869-2882.

Fisher, J.H., Barratt, M.W., Droste, J.B., Shaver, R.H., 1988. Michigan Basin. In: Sloss, L.L. (Ed.), *Sedimentary Cover – North America Craton*, Geological Society of America, vol. D-2, pp. 361-382.

Frick, U., Chang, S., 1977. Ancient carbon and noble gas fractionation, *Proc. Lunar. Sci. Conf.* 8, 263-272.

Girard, J.-P., Barnes, D.A., 1995. Illitization and paleothermal regimes in the middle Ordovician St. Peter sandstone, central Michigan Basin: K-Ar, oxygen isotope, and fluid inclusion data, *AAPG Bulletin* 79, 49-69.

Haas, J.L. Jr., 1978. *An empirical equation with tables of smoothed solubilities of methane in water and aqueous sodium chloride solutions up to 25 weight percent, 360°C, and 138MPa*, Open-File Report 78-1004, U.S. Geological Survey, Reston.

Hanor, J.S., 1980. Dissolved methane in sedimentary brines: potential effect on the PVT properties of fluid inclusions, *Economic Geology* 75, 603-617.

Hinze, W.J., Kellogg, R.L., O'Hara, N.W., 1975. Geophysical studies of basement geology of Southern Peninsula of Michigan, *AAPG Bulletin* 59, 1562-1584.

Ingebritsen, S.E., Sanford, W.E., 1998. *Groundwater in geologic processes*, first ed. Cambridge University Press, New York.

Ishibashi, J.-I., Grimaud, D., Nojiri, Y., Auzende, J.-M., Urabe, T., 1994. Fluctuation of chemical compositions of the phase-separated hydrothermal fluids from the North Fiji Basin Ridge, *Marine Geology* 116, 215-226.

Kennedy, B.M., 1988. Noble gases in vent water from the Juan de Fuca Ridge, *Geochimica et Cosmochimica Acta* 52, 1929-1935.

Kennedy, B.M., Kharaka, Y.K., Evans, W.C., Ellwood, A., DePaolo, D.J., Thordsen, J., Ambats, G., Mariner, R.H., 1997. Mantle fluids in the San Andreas Fault system, California, *Science* 278, 1278-1281.

Kennedy, B.M., van Soest, M.C., 2007. Flow of mantle fluids through the ductile lower crust: helium isotope trends, *Science* 318, 1433-1436.

Kharaka, Y.K., Specht, D.J., 1988. The solubility of noble gases in crude oil at 25-100°C, *Applied Geochemistry* 3, 137-144.

Kharaka, Y.K., Hanor, J.S., 2003. Deep fluids in the continents: I. sedimentary basins. In: Drever, J.I. (Ed.), *Surface and ground water, weathering, and soils*, Treatise on Geochemistry, vol. 5, pp. 499-540.

Kulongoski, J.T., Hilton, D.R., Izbicki, J.A., 2005. Source and movement of helium in the eastern Morongo groundwater Basin: the influence of regional tectonics on crustal and mantle helium fluxes, *Geochimica et Cosmochimica Acta* 69, 3857-3872.

Lippmann, J., Stute, M., Torgersen, T., Moser, D.P., Hall, J.A., Lin, L., Borcsik, M., Bellamy, R.E.S., Onstott, T.C., 2003. Dating ultra-deep mine waters with noble gases and ^{36}Cl, Witwatersrand Basin, South Africa, *Geochimica et Cosmochimica Acta* 67, 4597-4619.

Long, D.T., Wilson, T.P., Takacs, M.J., Rezabek, D.H., 1988. Stable-isotope geochemistry of saline near-surface ground water: east-central Michigan Basin, *Geo. Soc. Am. Bull.* 100, 1568-1577.

Luczaj, J.A., Harrison, W.B. III, Williams, N.S., 2006. Fractured hydrothermal dolomite reservoirs in the Devonian Dundee formation of the central Michigan Basin, *AAPG Bulletin* 90, 1787-1801.

Ma, L., Castro, M.C., Hall, C.M., 2004. A late Pleistocene-Holocene noble gas paleotemperature record in southern Michigan, *Geophysical Research Letters* 31, L23204, doi:10.1029/2004GL021766.

Ma, L., Castro, M.C., Hall, C.M., Walter, L.M., 2005. Cross-formational flow and salinity sources inferred from a combined study of helium concentrations, isotopic ratios, and major elements in the Marshall aquifer, southern Michigan, *Geochemistry Geophysics Geosystems* 6, Q10004, doi:10.1029/2005GC001010.

Martini, A.M., 1997. *Hydrogeochemistry of saline fluids and associated water and gas*, Ph.D. dissertation, Univ. of Michigan, Ann Arbor.

Mazor, E., Fournier, R.O., 1973. More on noble gases in Yellowstone National Park hot

waters, *Geochimica et Cosmochimica Acta* 37, 515-525.

Mazor, E., Truesdell, A.H., 1984. Dynamics of a geothermal field traced by noble gases: Cerro Prieto, Mexico, *Geothermics* 13, 91-102.

Mazor, E., Bosch, A., 1987. Noble gases in formation fluids from deep sedimentary basins: a review, *Applied Geochemistry* 2, 621-627.

McCallister, R.H., Boctor, N.Z., Hinze, W.J., 1978. Petrology of the spilitic rocks from the Michigan Basin deep drill hole, *Journal of Geophysical Research* 83, 5825-5831.

McIntosh, J.C., Walter, L.M., Martini, A.M., 2004. Extensive microbial modification of formation water geochemistry: Case study from a mid-continent sedimentary basin, United States, *Geo. Soc. Am. Bull.* 116, 743-759.

Nunn, J.A., 1994. Free thermal convection beneath intracratonic basins: thermal and subsidence effects, *Basin Research* 6, 115-130.

Oosting, S.E., Von Damm, K.L., 1996. Bromide/chloride fractionation in seafloor hydrothermal fluids from 9-10°N East Pacific Rise, *Earth and Planetary Science Letters* 144, 133-145.

Ozima, M., Podosek, F.A., 2002. *Noble gas geochemistry*, second ed. Cambridge University Press, New York.

Patriarche, D., Castro, M.C., Goblet, P., 2004. Large-scale hydraulic conductivities inferred from three-dimensional groundwater flow and 4He transport modeling in the Carrizo aquifer, Texas, *Journal of Geophysical Research* 109, B11202, doi: 10.1029/2004JB003173.

Pinti, D.L., Marty, B., 1995. Noble gases in crude oils from the Paris Basin, France: implications for the origin of fluids and constraints on oil-water-gas interactions, *Geochimica et Cosmochimica Acta* 59, 3389-3404.

Podosek, F.A., Honda, M., Ozima, M., 1980. Sedimentary noble gases, *Geochimica et Cosmochimica Acta* 44, 1875-1884.

Prinzhofer, A., Battani, A., 2003. Gas isotopes tracing: an important tool for hydrocarbons exploration, *Oil & Gas Science and Technology-Rev. IFP* 58, 299-311.

Saar, M.O., Castro, M.C., Hall, C.M., Manga, M., Rose, T.P., 2005. Quantifying magmatic, crustal, and atmospheric helium contributions to volcanic aquifers using all stable noble gases: implications for magmatism and groundwater flow, *Geochemistry Geophysics Geosystems* 6, Q03008, doi:10.1029/2004GC000828.

Sanford, B.V., Thompson, F.J., McFall, G.H., 1985. Plate tectonics – a possible

controlling mechanism in the development of hydrocarbon traps in southwestern Ontario, *Bulletin of Canadian Petroleum Geology* 33, 52-71.

Schoofs, S., Trompert, R.A., Hansen, U., 2000. Thermochemical convection in and beneath intracratonic basins: onset and effects, *Journal of Geophysical Research* 105, 25567-25585.

Smith, S.P., Kennedy, B.M., 1983. The solubility of noble gases in water and in NaCl brine, *Geochimica et Cosmochimica Acta* 47, 503-515.

Smith, S.P., 1985. Noble gas solubility in water at high temperatures, *Eos Trans. AGU* 66, 397.

Stakes, D.S., 1978. Mineralogy and geochemistry of the Michigan deep hole metagabbro compared to seawater hydrothermal alteration, *Journal of Geophysical Research* 83, 5820-5824.

Torgersen, T., Clarke, W.B., 1985. Helium accumulation in groundwater, I: An evaluation of sources and the continental flux of crustal 4He in the Great Artesian Basin, Australia, *Geochimica et Cosmochimica Acta* 49, 1211-1218.

Torgersen, T., Kennedy, B.M., 1999. Air-Xe enrichments in Elk Hills oil field gases: role of water in migration and storage, *Earth and Planetary Science Letters* 167, 239-253.

Torgersen, T., Kennedy, B.M., van Soest, M.C., 2004. Diffusive separation of noble gases and noble gas abundance patterns in sedimentary rocks, *Earth and Planetary Science Letters* 226, 477-489.

Van Schmus, W.R., 1992. Tectonic setting of the Midcontinent Rift system, *Tectonophysics* 213, 1-15.

Vugrinovich, R., 1986. *Patterns of regional subsurface fluid movement in the Michigan Basin*, Open File Rep. 86-6, Geol. Surv. Div. Mich. Dep. of Nat. Resour., Lansing.

Vugrinovich, R., 1988. Shale compaction in the Michigan Basin: estimates of former depth of burial and implications for paleogeothermal gradients, *Bulletin of Canadian Petroleum Geology* 36, 1-8.

Vugrinovich, R., 1989. Subsurface temperatures and surface heat flow in the Michigan Basin and their relationships to regional subsurface fluid movement. *Marine and Petroleum Geology* 6, 60-70.

Weiss, R.F., 1968. Piggyback sampler for dissolved gas studies on sealed water samples, *Deep Sea Res. Oceanogr. Abstr.* 15, 695-699.

Wilson, T.P., Long, D.T., 1993a. Geochemistry and isotope chemistry of Michigan Basin brines: Devonian formations, *Applied Geochemistry* 8, 81-100.

Wilson, T.P., Long, D.T., 1993b. Geochemistry and isotope chemistry of Ca-Na-Cl brines in Silurian strata, Michigan Basin, *Applied Geochemistry* 8, 507-524.

Winckler, G., Kipfer, R., Aeschbach-Hertig, W., Botz, R., Schmidt, M., Schuler, S., Bayer, R., 2000. Sub sea floor boiling of Red Sea brines: new indication from noble gas data, *Geochimica et Cosmochimica Acta* 64, 1567-1575.

Zaikowski, A., Spangler, R.R., 1990. Noble gas methane partitioning from ground water: an aid to natural gas exploration and reservoir evaluation, *Geology* 18, 72-74.

Zartman, R.E., Wasserburg, G.J., Reynolds, J.H., 1961. Helium, argon, and carbon in some natural gases, *Journal of Geophysical Research* 66, 277-306.

Zhou, Z., Ballentine, C.J., Kipfer, R., Schoell, M., Thibodeaux, S., 2005. Noble gas tracing of groundwater/coalbed methane interaction in the San Juan Basin, USA, *Geochimica et Cosmochimica Acta* 69, 5413-5428.

CHAPTER 6

CRUSTAL NOBLE GASES IN DEEP BRINES AS NATURAL TRACERS OF VERTICAL TRANSPORT PROCESSES IN THE MICHIGAN BASIN

Abstract

Noble gas concentrations and isotopic ratios are presented for 38 deep (~0.5-3.6km) brine samples in the Michigan Basin. These brine samples clearly show the presence of an important crustal component of ^{4}He, ^{21}Ne, ^{40}Ar, and ^{136}Xe. Both $^{40}Ar_{crust}$ and $^{136}Xe_{crust}$ display the presence of a strong vertical gradient along the sedimentary strata of the basin. The in-situ production for these two gases within the sedimentary strata is insufficient to account for the observed crustal component in the Michigan brines. These point to the presence of a deep, external source for crustal noble gases, likely the Precambrian crystalline basement beneath the Michigan Basin. Furthermore, observed elemental ratios of crustal noble gases ($^{4}He/^{40}Ar$, $^{21}Ne/^{40}Ar$, $^{4}He/^{136}Xe$, and $^{21}Ne/^{136}Xe$) in these brines vary over several orders of magnitude with respect to the expected production ratios from the crystalline basement rocks and display a systematic pattern within the basin. Specifically, samples above the Salina Group (shallow formations) are enriched in $^{4}He_{crust}$ and $^{21}Ne_{crust}$ with respect to $^{40}Ar_{crust}$ and $^{136}Xe_{crust}$, as opposed to those below the massive Salina evaporite layer (deeper formations) which exhibit complementary patterns, i.e., depleted in $^{4}He_{crust}$ and $^{21}Ne_{crust}$ with respect to $^{40}Ar_{crust}$ and $^{136}Xe_{crust}$. It is shown that such a general trend is best explained by a Rayleigh-type

elemental fractionation model involving upward transport of crustal noble gases and associated elemental fractionation processes, controlled by both diffusion- and solubility-related mechanisms. As previously indicated by the mantle and atmospheric noble gas signatures in these same Michigan brine samples, the release of deep crustal noble gases into the basin is yet another independent indicator pointing to the occurrence of a past thermal event in the basin. It is suggested here that a recent reactivation of the ancient mid-continent rift (MCR) system underneath the Michigan Basin is likely responsible for the upward transport of heat and loss of the atmospheric noble gas component, as well as a release of crustal (still ongoing) and mantle noble gases into the basin via deep-seated faults and fracture zones. Such a model also supports the hypothesis of an internal heat source as being largely responsible for the existence of past high temperatures in the basin without an involvement of large-scale brine migration from peripheral forming orogenic foldbelts.

6.1. Introduction

Because of their conservative nature and because of their specific characteristics depending on their origin (atmosphere, crust, mantle), noble gases (He, Ne, Ar, Kr, Xe) are a powerful tool to investigate the origin and evolution of crustal fluids in sedimentary basins [e.g., *Oxburgh et al.*, 1986; *Hiyagon and Kennedy*, 1992; *O'Nions and Ballentine*, 1993; *Pinti and Marty*, 1995; *Castro et al.*, 1998a, b; *Patriarche et al.*, 2004; *Kulongoski et al.*, 2005]. In particular, the concentrations of certain noble gases in deep groundwaters frequently exceed those expected for water in solubility equilibrium with the atmosphere (Air Saturated Water - ASW). Although mantle noble gases are commonly present in

subsurface fluids [e.g., *Oxburgh et al.*, 1986], these excesses result mainly from crustal production of: a) ^{4}He and ^{40}Ar from radioactive decay of U/Th and ^{40}K, respectively; b) ^{21}Ne from secondary α or n-reactions on target elements such as O and Mg, and: c) $^{136, 134, 132, 131}Xe$ isotopes from the spontaneous fission of U [e.g., *Wetherill ,* 1953,1954; *Ballentine and Burnard*, 2002]. Crustal noble gases may be produced inside an aquifer (in-situ production) or in deeper layers (external production). Noble gases will be subsequently transported to shallower levels by advection, dispersion and/or diffusion or by a combination of these processes [e.g., *Castro et al.*, 1998a,b; *Castro and Goblet*, 2003]. Although chemically inert and stable, noble gases display contrasting physical properties due to their large differences in atomic numbers. In particular, their solubilities in water vary by over an order of magnitude [*Ozima and Podosek*, 2002], while molecular diffusivities, from He to Xe, vary by a factor of 7 at a temperature of 0ºC [*Jahne et al.*, 1987]. Thus, noble gases are differently transported in the subsurface, and, as a result, their concentrations and elemental ratios have been widely used as geochemical tracers of subsurface fluid movement in major sedimentary systems around the world (e.g., the Great Artesian Basin in Australia [*Torgersen and Clarke*, 1985; *Torgersen et al.*, 1989], the Pannonian Basin in Hungary [*Ballentine et al.*, 1991], the Paris Basin in France [*Pinti and Marty*, 1995; *Castro et al.*, 1998a, b], and the Gulf Coast Basin in the USA [*Castro et al.*, 2005]).

In addition, when combined with heat flow, the study of ^{4}He in crustal fluids allows for the reconstruction of the thermal and tectonic history of continental regions [*Castro et al.*, 2005]. More specifically, *Castro et al.* [2005] have shown that the occurrence of a ^{4}He/heat flux ratio greater than the radiogenic production ratio can only

result from a past thermal event of mantle origin in which most of the heat has already escaped while He is slowly making its way toward the surface. Such a high ^{4}He/heat flux ratio was recently identified in shallow (<100 m) groundwaters of the Marshall aquifer in the Michigan Basin [*Ma et al.*, 2005; *Castro et al.*, 2007]. To confirm the occurrence of such a thermal event and to clarify its origin, 38 deep (0.5-3.6Km) brine samples were collected in the Michigan Basin and analyzed for noble gas concentrations and isotopic ratios [*Castro et al.*, 2008; *Ma et al.*, 2008; *this study*]. While both the He and Ne isotopic ratios clearly indicate the presence of a mantle component, Ne isotopic compositions point unequivocally to the presence of a primordial, solar-like signature in this continental region, thus, confirming the mantle origin of this past thermal event [*Castro et al.*, 2008]. In addition, depletion of atmospheric noble gases in these brines is also observed and is best explained by a model involving subsurface boiling and steam separation. The atmospheric component of noble gases provides thus an additional independent indicator of the occurrence of a past thermal event in this system [*Ma et al.*, 2008].

Here, we present a companion study that focuses on the crustally produced noble gases ($^{4}He_{crust}$, $^{21}Ne_{crust}$, $^{40}Ar_{crust}$ and $^{136}Xe_{crust}$) present in the Michigan Basin brines. Specifically, it is shown that the crustal noble gas component in these brines originated mainly from the Precambrian basement underneath the Michigan Basin and that its distribution pattern can be best explained by a model involving vertical upward transport and associated elemental fractionation during both diffusion- and solubility-controlled processes. The release of these deep crustal noble gases into the basin also points to the occurrence of a past thermal event in the basin, as previously suggested by the release of

both heat and mantle noble gases [*Castro et al.*, 2008; *Ma et al.*, 2008]. Such a release is most likely related to the recent reactivation of the Mid Continent Rift (MCR) system underneath the Michigan Basin and highlights the impact of tectonic activity in deep crustal degassing processes. Our study highlights the use of crustally produced noble gases to trace subsurface fluid movement and to study the thermal history of currently stable regions.

6.2. Geological and Hydrogeologic Background

The Michigan Basin is a concentric intracratonic depression floored by crystalline Precambrian basement, and consists of a succession of sedimentary rocks with ages from Precambrian to Jurassic that reaches depths over 5Km (Fig. 6.1) [*Dorr and Eschman*, 1970; *Catacosinos et al.*, 1991]. The entire sedimentary strata are composed mainly of evaporites, carbonates, shale, and sandstone underneath a thick layer of Pleistocene glacial deposits (Fig. 6.1b). Depending on their nature, these sedimentary rocks constitute either aquitards (e.g., shale, evaporites) or aquifers (mostly sandstones and reefal and dolomitized limestones), giving rise to a multi-layered aquifer system [*Vugrinovich*, 1986].

Major tectonic structures such as the Albion-Scipio Fault, the Lucas Fault, and the Howell Anticline are present in southern Michigan and penetrate the crystalline basement, which is mainly composed of Precambrian (~1.1->2.5Ga) igneous-metamorphic rocks (Fig. 6.1a). The basement is believed to have a well-developed pattern of jointing and faulting, similar to the highly fractured neighboring Canadian Shield outcrop [*Sanford et al.*, 1985; *Fisher et al.*, 1988]. A rift zone that formed during an episode of crustal

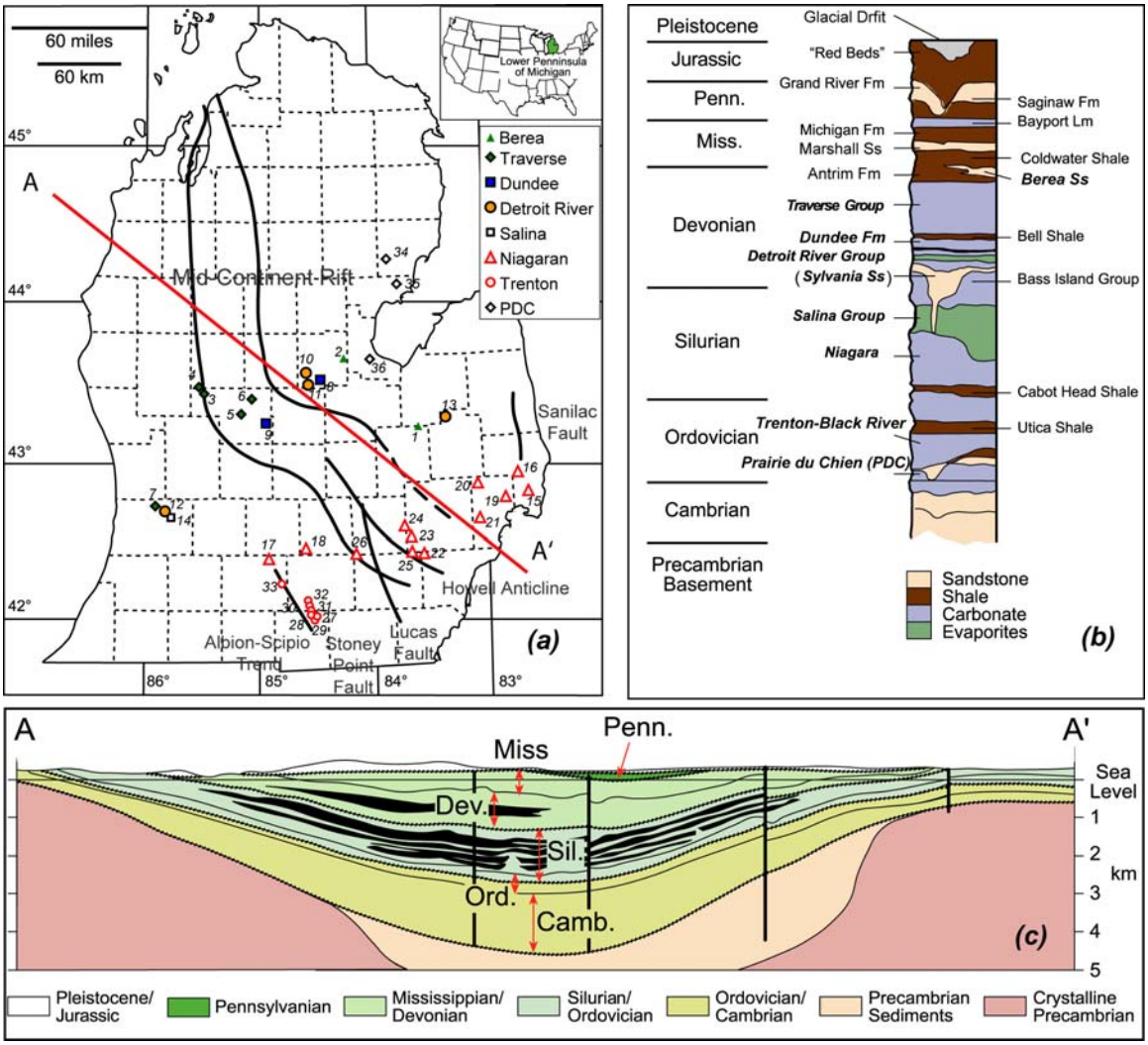

Figure 6.1. a) Central portion of the Michigan Basin (Lower Peninsula of Michigan). Major tectonic structures (e.g., Mid Continental Rift) and sample locations are indicated [*after Dorr and Eschman*, 1970; *Fisher et al.*, 1988; *Catacosinos et al.*, 1991]; **b)** Stratigraphic succession of the Michigan Basin. Major lithologies present in the basin are identified; units for which formation brines were sampled in this study are highlighted in bold; **c)** General schematic geological representation along cross section A-A'.

extension at ~1.1 Ga transects the entire crystalline basement of the Michigan Basin (Fig. 6.1a), and is believed to be part of the MCR system [*Hinze et al.*, 1975; *Van Schmus*, 1992]. Repeated movements along major faults in southern Michigan prevailed throughout the early part of the Paleozoic and major uplift of most of the basin fault blocks occurred at the end of the Mississippian Period (~320 Ma) [*Fisher et al.*, 1988].

Despite the current low geothermal gradient in the basin (~19°C/Km) [*Vugrinovich*, 1989], oil and natural gas reservoirs in southern Michigan are abundant and ubiquitously distributed within the sedimentary sequence, from the deep Ordovician to the shallow Mississipian (Fig. 6.1b) [*Dorr and Eschman*, 1970; *Catacosinos et al.*, 1991], indicating the occurrence of higher temperatures in the past. A wealth of thermal studies in the basin based on a diversity of proxies (e.g., organic maturity data, stable isotopes, fluid inclusions, authigenic clay minerals, apatite fission track ages) point to the occurrence of high temperatures (up to 260°C) in the past [*Cercone and Lohmann*, 1987; *Cercone and Pollack*, 1991; *Crowley*, 1991; *Coniglio et al.*, 1994; *Girard and Barnes*, 1995; *Luczaj et al.*, 2006]. The origin and thermal history of such reservoirs, however, remain uncertain. Because these high temperatures cannot be easily explained by long-term deep burial [e.g, *Cercone*, 1984; *Vugrinovich*, 1988; *Luczaj et al.*, 2006], models involving transport of heat and fluids from deeper parts of the basin along major faults and fracture zones connected to the Precambrian basement structures were proposed [*Sanford et al.*, 1985; *Budai and Wilson*, 1991; *Coniglio et al.*, 1994; *Girard and Barnes*, 1995; *Luczaj et al.*, 2006].

In addition to oil and natural gas, formation waters (brines) with very high salinities (e.g., total dissolved solids>450g/L) distributed throughout the basin have also

been documented [*Long et al.*, 1988; *Wilson and Long*, 1993a, b; *Martini*, 1997; *McIntosh et al.*, 2004]. Studies of major elements and stable isotopes suggest that these deep basinal brines originated from ancient seawater and have a complex evolution history involving intensive water-rock interactions, dissolution of evaporites, as well as mixing with meteoric and seawater [*Long et al.*, 1988; *Wilson and Long*, 1993a, b; *Davisson and Criss*, 1996; *Martini*, 1997; *McIntosh et al.*, 2004]. The upward transport of fluids was also suggested to account for the presence of extremely high salinity waters [*Long et al.*, 1988] as well as of unusually high ^{4}He excesses and fluxes at shallow depths [*Ma et al.*, 2005].

6.3. Sampling Techniques and Experimental Methods

A total of 38 brine samples were collected from eight formations in the Michigan Basin for noble gas analysis (Figs. 6.1a,b). Brines were sampled from actively pumping wells in copper tubes (i.e. standard refrigeration grade 3/8" Cu tubing) that were sealed by stainless steel pinch-off clamps [*Weiss*, 1968] at well head pressures after water was allowed to flow for ~10 minutes to avoid atmospheric contamination and to ensure that water temperature had reached equilibrium. Elemental and isotopic noble gas measurements were performed at the University of Michigan as described briefly below and in detail elsewhere [*Ma et al.*, 2004; *Saar et al.*, 2005].

Brine samples (~14 ml) were attached to a vacuum extraction system and noble gases were quantitatively extracted for inletting into a MAP-215 mass spectrometer. Noble gases were transported using water vapor as a carrier gas through two constrictions in the vacuum system, purified by two Ti sponge getters, and sequentially allowed to

enter a MAP-215 mass spectrometer using a cryo-separator. The cryo-separator temperatures were set at 30, 60, 180, 215, and 270K for analysis of He, Ne, Ar, Kr, and Xe, respectively. ^{4}He, ^{20}Ne, and ^{40}Ar isotopes were measured using a Faraday detector and ^{3}He, $^{21, 22}Ne$, $^{38,36}Ar$, as well as $^{86,84,83,82,80}Kr$ and $^{136,134,132,131,130,129,128}Xe$ isotopes were measured using an electron multiplier in ion counting mode. During neon isotope analysis, a liquid N_2 cold trap was applied to minimize peak interferences and appropriate mass peaks were monitored to correct for interferences of $^{40}Ar^{2+}$ on ^{20}Ne, CO_2^{2+} on ^{22}Ne and $H_2{}^{18}O^{+}$ on ^{20}Ne. The interference corrections for ^{20}Ne and ^{22}Ne were typically ~1.1% and 0.17%, respectively. Before each sample analysis, a calibrated amount of air standard and a procedural blank were performed following the same procedure of the sample measurement. The blank correction was applied to all measured peaks. ^{4}He, ^{22}Ne, ^{36}Ar, ^{84}Kr, and ^{130}Xe elemental abundances and their respective isotopic ratios for each sample were normalized to the air standard after blank correction. Blank correction for ^{4}He, ^{36}Ar, ^{84}Kr, and ^{130}Xe is negligible. The average measured sample/blank signal size ratio for ^{22}Ne is about 15. ^{4}He, ^{22}Ne, ^{36}Ar, ^{84}Kr, and ^{130}Xe abundances have typical uncertainties of 1.5, 1.3, 1.3, 1.5 and 2.2%, respectively. All uncertainties are at $\pm 1\sigma$ level of confidence. The whole procedure was tested and calibrated with synthetic laboratory fresh water samples produced at a known temperature.

6.4. Results

Noble gas concentrations and isotopic ratios, sample numbers, formation, lithology as well as sample depths are reported in Tables 6.1 and 6.2. Noble gas concentrations in air saturated seawater (0.6M NaCl solution) as well as atmospheric

Table 6.1. He, Ne, Ar, Kr, and Xe elemental concentrations with sample number, formation, lithology, and depth.

Sample Number	Formation	Lithology	Depth (m)	^{4}He [(a)] (cm^3STP/g)	^{22}Ne (cm^3STP/g)	^{36}Ar (cm^3STP/g)	^{84}Kr (cm^3STP/g)	^{130}Xe (cm^3STP/g)
	Devonian							
1	Berea	Sandstone	1005	8.37E-07	4.50E-11	1.11E-08	1.27E-09	3.59E-11
2	Berea	Sandstone	780	5.35E-06	5.17E-11	2.98E-09	1.50E-10	9.20E-12
3	Traverse	Carbonate	1014	5.03E-07	4.68E-11	3.34E-09	2.97E-10	2.40E-11
4	Traverse	Carbonate	1015	5.99E-06	1.05E-10	5.82E-09	2.38E-10	5.54E-12
5	Traverse	Carbonate	909	3.00E-05	1.24E-10	1.86E-08	8.80E-10	2.09E-11
6	Traverse	Carbonate	1072	1.82E-05	1.56E-10	2.64E-08	1.23E-09	8.01E-11
7	Traverse	Carbonate	546	1.57E-07	1.48E-10	6.65E-09	1.97E-10	1.42E-11
8	Dundee	Carbonate	1036	1.76E-04	2.90E-09	5.27E-08	1.30E-09	1.23E-11
9	Dundee	Carbonate	1090	9.68E-06	6.74E-10	4.38E-08	1.65E-09	2.26E-11
10	Detroit River	Carbonate	1378	9.26E-05	2.85E-10	2.12E-08	6.80E-10	7.32E-12
11	Detroit River	Sandstone	1480	4.69E-04	3.68E-09	1.65E-07	6.82E-09	8.09E-11
12	Detroit River	Carbonate	572	1.49E-05	9.14E-10	4.51E-08	1.40E-09	2.06E-11
13	Detroit River	Carbonate	1070	3.72E-04	9.25E-10	3.96E-08	1.84E-09	2.40E-11
	Silurian							
14	Salina	Carbonate	699	6.13E-07	4.04E-10	6.40E-08	2.53E-09	5.22E-11
15	Niagaran	Carbonate	830	2.16E-07	1.63E-10	1.00E-08	4.09E-10	7.12E-11
16	Niagaran	Carbonate	1022	2.35E-05	9.92E-11	5.77E-09	2.85E-10	6.89E-12
17	Niagaran	Carbonate	1096	1.33E-05	3.52E-10	2.28E-08	1.15E-09	1.47E-11
18	Niagaran	Carbonate	1168	1.70E-03	3.57E-09	5.44E-08	8.85E-10	1.51E-11
19	Niagaran	Carbonate	887	8.67E-06	5.24E-11	1.12E-08	1.23E-09	7.42E-11
20	Niagaran	Carbonate	1143	3.66E-06	5.48E-11	1.19E-08	1.12E-09	7.20E-11
21	Niagaran	Carbonate	915	7.01E-06	2.04E-10	4.09E-08	2.31E-09	3.81E-11
22a	Niagaran	Carbonate	941	1.42E-07	4.68E-11	5.12E-09	9.12E-10	6.41E-11
22b	Niagaran	Carbonate	941	1.92E-07	4.91E-11	7.97E-09	2.12E-09	1.43E-10
23	Niagaran	Carbonate	1138	1.33E-05	1.08E-10	2.05E-08	1.55E-09	1.76E-11
24	Niagaran	Carbonate	1259	1.45E-06	4.44E-11	1.51E-08	1.07E-09	5.37E-11
25a	Niagaran	Carbonate	996	4.27E-07	5.63E-11	5.70E-09	1.13E-09	7.60E-11
25b	Niagaran	Carbonate	996	6.55E-07	6.19E-11	6.95E-09	1.11E-09	9.42E-11
26	Niagaran	Carbonate	937	1.53E-03	5.83E-09	2.08E-07	8.78E-09	7.03E-11
	Ordovician							
27	Trenton	Carbonate	1330	5.39E-06	8.67E-11	1.55E-08	7.78E-10	2.48E-11
28	Trenton	Carbonate	1332	3.53E-06	7.49E-11	1.57E-08	1.33E-09	5.51E-11
29	Trenton	Carbonate	1301	4.62E-06	8.24E-11	1.25E-08	7.78E-10	3.01E-11
30	Trenton	Carbonate	1302	1.91E-05	1.09E-10	9.28E-09	6.81E-10	1.06E-11
31	Trenton	Carbonate	1302	1.09E-04	3.01E-10	3.26E-08	2.11E-09	2.77E-11
32	Trenton	Carbonate	1233	8.87E-05	1.94E-10	1.42E-08	6.26E-10	1.16E-11
33	Trenton	Carbonate	1283	1.17E-06	5.95E-11	5.21E-09	3.79E-10	2.16E-11
34	PDC	Carbonate	3595	3.33E-06	5.03E-11	1.83E-08	1.76E-09	8.14E-11
35	PDC	Carbonate	3621	3.66E-05	1.29E-10	1.96E-08	6.28E-10	6.88E-12
36	PDC	Carbonate	3196	2.50E-06	5.55E-11	9.81E-09	3.71E-10	1.26E-11
Seawater (0.6MNaCl solution) at 25°C[(b)]				3.8E-08	1.4E-08	7.7E-07	2.9E-08	2.6E-10

a. ^{4}He, ^{22}Ne, ^{36}Ar, ^{84}Kr, and ^{130}Xe abundances have typical uncertainties (±1σ) of 1.5%, 1.3%, 1.3%, 1.5%, and 2.2%, respectively.

b. ASW concentrations calculated from *Crovetto et al.* [1982], *Smith* [1985] and *Smith and Kennedy* [1983].

Table 6.2. Noble gas isotopic ratios in Michigan Basin brines (with ±1σ uncertainties).

Sample Number	$^{40}Ar/^{36}Ar$	+/-	$^{86}Kr/^{84}Kr$	+/-	$^{129}Xe/^{130}Xe$	+/-	$^{131}Xe/^{130}Xe$	+/-	$^{132}Xe/^{130}Xe$	+/-	$^{134}Xe/^{130}Xe$	+/-	$^{136}Xe/^{130}Xe$	+/-
Devonian														
1	367.9	2.9	0.3034	0.0022	6.435	0.025	5.173	0.024	6.576	0.027	2.548	0.011	2.168	0.012
2	335.4	2.6	0.3005	0.0030	6.528	0.035	5.220	0.028	6.647	0.036	2.558	0.015	2.194	0.013
3	363.3	1.6	0.3028	0.0050	6.414	0.059	5.187	0.045	6.591	0.057	2.562	0.024	2.178	0.019
4	332.8	1.3	0.3037	0.0029	6.484	0.052	5.202	0.043	6.590	0.051	2.550	0.020	2.178	0.019
5	385.7	1.3	0.3058	0.0024	6.533	0.057	5.249	0.046	6.665	0.056	2.580	0.022	2.199	0.018
6	326.0	0.8	0.3064	0.0031	6.527	0.039	5.228	0.032	6.636	0.039	2.581	0.016	2.191	0.014
7	313.2	2.7	0.3021	0.0028	6.458	0.042	5.196	0.033	6.587	0.041	2.566	0.018	2.167	0.016
8	326.5	2.1	0.3009	0.0024	6.511	0.041	5.212	0.036	6.625	0.043	2.575	0.019	2.193	0.016
9	328.8	0.8	0.3049	0.0033	6.494	0.065	5.225	0.056	6.615	0.070	2.570	0.029	2.196	0.023
10	372.8	1.2	0.3042	0.0028	6.478	0.043	5.220	0.037	6.594	0.045	2.559	0.019	2.183	0.017
11	376.9	6.9	0.3069	0.0031	6.483	0.091	5.210	0.074	6.597	0.093	2.579	0.037	2.184	0.030
12	299.8	1.9	0.3041	0.0021	6.465	0.027	5.205	0.025	6.556	0.030	2.552	0.013	2.151	0.009
13	358.3	2.0	0.3017	0.0024	6.528	0.042	5.267	0.036	6.644	0.043	2.584	0.017	2.188	0.014
Silurian														
14	309.4	1.3	0.3035	0.0033	6.530	0.063	5.271	0.052	6.641	0.066	2.602	0.027	2.201	0.025
15	376.1	2.3	0.3020	0.0033	6.488	0.039	5.194	0.030	6.581	0.039	2.555	0.017	2.160	0.014
16	671.3	3.3	0.3011	0.0022	6.521	0.046	5.194	0.036	6.587	0.048	2.544	0.019	2.165	0.015
17	656.1	1.2	0.3057	0.0030	6.439	0.071	5.200	0.056	6.569	0.069	2.571	0.026	2.140	0.029
18	437.6	3.0	0.3003	0.0053	6.477	0.052	5.171	0.040	6.578	0.054	2.550	0.024	2.193	0.021
19	827.1	6.1	0.3028	0.0027	6.446	0.021	5.156	0.018	6.548	0.023	2.544	0.010	2.168	0.008
20	591.3	3.0	0.3052	0.0027	6.404	0.024	5.167	0.022	6.520	0.023	2.543	0.011	2.153	0.011
21	782.0	3.3	0.3047	0.0030	6.468	0.095	5.176	0.076	6.562	0.099	2.561	0.043	2.150	0.033
22a	655.8	3.5	0.3070	0.0032	6.500	0.057	5.217	0.048	6.623	0.060	2.580	0.024	2.192	0.019
22b	789.4	2.9	0.3043	0.0020	6.484	0.066	5.244	0.054	6.613	0.068	2.598	0.028	2.193	0.023
23	606.7	2.5	0.3060	0.0027	6.527	0.067	5.250	0.055	6.647	0.072	2.583	0.026	2.191	0.023
24	425.4	0.8	0.3070	0.0028	6.498	0.046	5.205	0.039	6.607	0.046	2.565	0.019	2.173	0.016
25a	1044.6	5.1	0.3069	0.0018	6.474	0.039	5.204	0.034	6.623	0.039	2.593	0.017	2.212	0.014
25b	1010.1	5.1	0.3047	0.0023	6.455	0.077	5.196	0.063	6.606	0.075	2.597	0.029	2.216	0.027
26	411.6	1.3	0.3013	0.0044	6.527	0.063	5.221	0.047	6.648	0.063	2.571	0.026	2.167	0.022
Ordovician														
27	597.1	1.7	0.3038	0.0032	6.539	0.070	5.273	0.057	6.689	0.071	2.641	0.031	2.273	0.026
28	715.4	2.5	0.3045	0.0026	6.476	0.063	5.213	0.051	6.636	0.069	2.634	0.026	2.265	0.023
29	611.4	1.9	0.3053	0.0022	6.489	0.064	5.222	0.056	6.688	0.071	2.618	0.028	2.261	0.025
30	1152.0	5.6	0.3066	0.0026	6.493	0.042	5.218	0.032	6.642	0.039	2.628	0.016	2.248	0.015
31	1221.6	7.7	0.3060	0.0027	6.483	0.044	5.237	0.036	6.677	0.047	2.643	0.020	2.263	0.017
32	1166.4	6.7	0.3041	0.0031	6.463	0.054	5.227	0.045	6.635	0.059	2.618	0.024	2.237	0.021
33	1037.7	6.1	0.3037	0.0032	6.532	0.111	5.213	0.084	6.591	0.109	2.608	0.039	2.226	0.036
34	2863.1	55.5	0.3014	0.0021	6.408	0.031	5.196	0.025	6.652	0.032	2.709	0.012	2.365	0.012
35	2610.0	25.9	0.3096	0.0043	6.527	0.076	5.242	0.063	6.704	0.083	2.681	0.034	2.328	0.028
36	1559.7	5.8	0.3095	0.0043	6.506	0.068	5.238	0.056	6.727	0.070	2.734	0.031	2.359	0.025
Air[(a)]	295.5	0.5	0.3052	0.0003	6.496	0.009	5.213	0.008	6.607	0.005	2.563	0.004	2.176	0.003

a. after *Ozima and Podosek* [2002]

isotopic ratios are also listed for reference. The He and Ne isotopic ratios, as well as the atmospheric noble gas components of these brine samples have been reported and discussed elsewhere [*Castro et al.*, 2008; *Ma et al.*, 2008].

6.4.1. Isotopic ratios of noble gases in Michigan Basin brines

$^{3}He/^{4}He$ (R) ratios in Michigan Basin brines vary from 0.053±0.009 times the atmospheric ratio Ra, a typical crustal production value (~0.01-0.05) [e.g., *Oxburgh et al.*, 1986], to 1.29±0.27 (Fig. 6.2a). Because the atmospheric He contribution is negligible in these brines [*Castro et al.*, 2008], the measured R/Ra ratios represent a mixture of only crustal and mantle He components. Typical crustal R/Ra production values are 0.01-0.05 [e.g., *Oxburgh et al.*, 1986] because of the dominant production of ^{4}He from U and Th decay; mantle R/Ra ratios are much greater due to the presence of primordial ^{3}He in the mantle, e.g., ~8 in the mantle MORB source region and ~35 in the OIB source regions [e.g., *Graham*, 2002]. Measured R/Ra ratios in these brine samples are greater than typical crustal values (Fig. 6.2a), strongly pointing to the presence of a mantle He component. Using a mantle R/Ra value of 8 and a crustal production value of 0.05, crustal ^{4}He contributions in these samples vary between 84.4% and 100% of total measured ^{4}He, with a mantle ^{4}He contribution of up to ~15.6%.

Measured $^{20}Ne/^{22}Ne$ ratios are greater than the air value (9.8) and suggest the presence of mantle Ne in these samples [*Castro et al.*, 2008]. $^{21}Ne/^{22}Ne$ ratios range from 0.0290±0.0002 to 0.0432±0.0004 (Fig. 6.2b), reflecting the addition of crustally produced ^{21}Ne through the nuclear reactions of $^{18}O(\alpha, n)^{21}Ne$ and $^{24}Mg(n,\alpha)^{21}Ne$ [*Wetherill*, 1954]. The simultaneous analysis of both $^{20}Ne/^{22}Ne$ and $^{21}Ne/^{22}Ne$ ratios allows separation of the

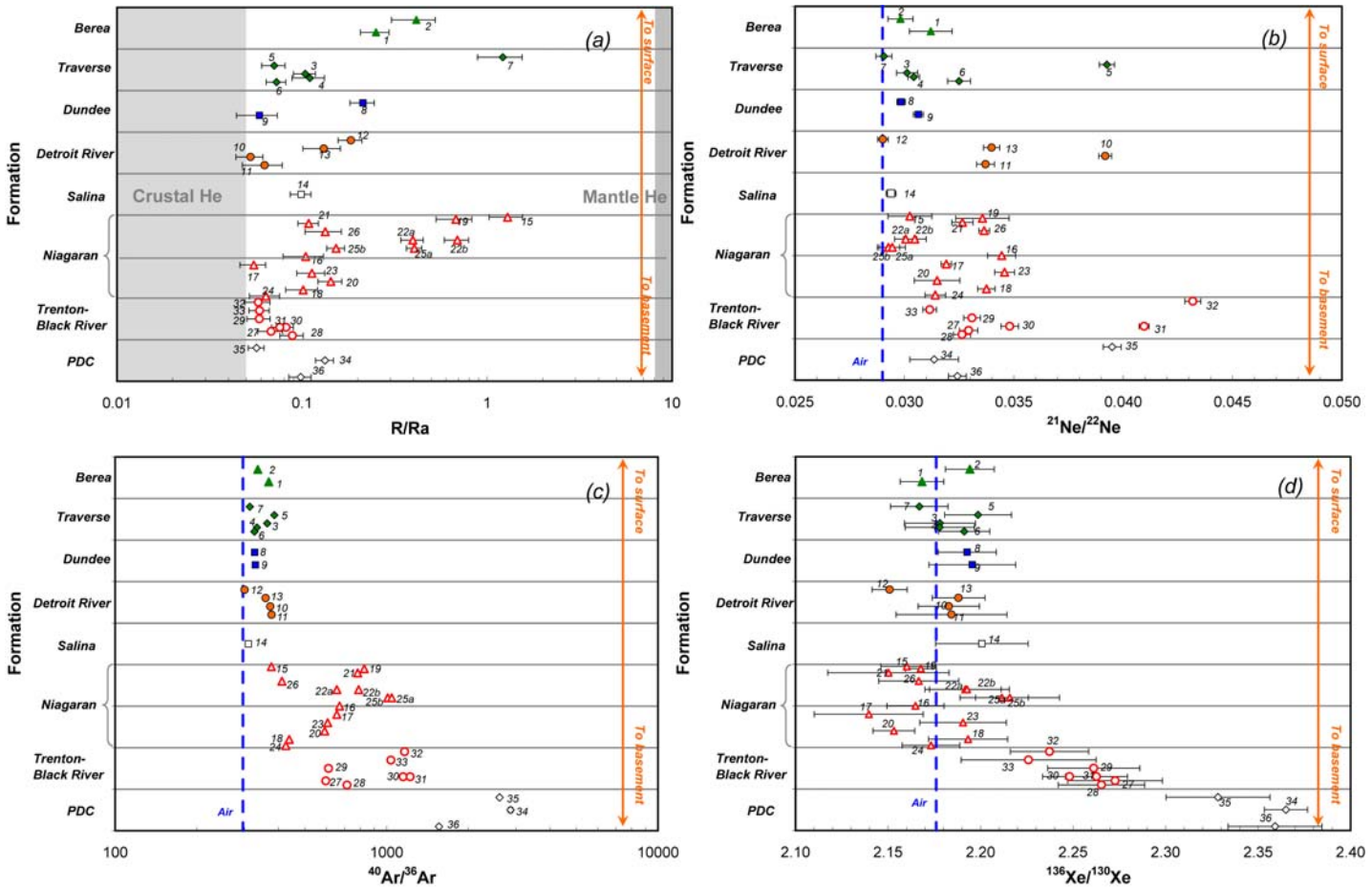

Figure 6.2. Noble gas isotopic ratios of Michigan Basin brines in the sedimentary sequence; **a)** R/Ra ratios; grey areas indicate the typical crustal R/Ra values (~0.01-0.05) [*Oxburgh* et al., 1986] and mantle (Mid Ocean Ridge Basalts – MORB) R/Ra values (>~8; [*Graham*, 2002]); **b)** $^{21}Ne/^{22}Ne$ ratios; **c)** $^{40}Ar/^{36}Ar$ ratios; **d)** $^{136}Xe/^{130}Xe$ ratios; The isotopic ratios of air (blue dashed lines) are shown [*Ozima and Podesek*, 2002] for all ratios except for R/Ra as He atmospheric contributions are negligible in these samples.

atmospheric, crustal, and mantle Ne components as the three sources all have distinct end-member values [*Castro et al.*, 2008]. Analysis of Ne isotopic ratios in these brines indicates an atmospheric ^{21}Ne contribution varying from 57.7% to 96.9% of total measured ^{21}Ne, a crustal ^{21}Ne contribution varying between 0.5% and 35.1%, and a mantle ^{21}Ne contribution ranging from 2.6% to 26.9% [*Castro et al.*, 2008].

The ^{40}Ar/^{36}Ar ratios of these brine samples are all above the atmospheric value (295.5) and reflect the addition of radiogenic ^{40}Ar. These ratios vary between 299.8±1.9 and 2863.1±55.5, the higher values being found in the deeper formations (Niagaran, Trenton, and PDC; Table 6.2; Fig. 6.2c). This ratio increases rapidly with depth and displays a marked isotopic gradient along the sedimentary sequence (Fig. 6.2c), pointing to a deeper source of radiogenic ^{40}Ar. Similar to ^{4}He, excesses of ^{40}Ar are commonly observed in old crustal fluids due to natural decay of ^{40}K. Unfortunately, the exact crustal and mantle contributions of ^{40}Ar cannot be effectively separated due to current uncertainties of both ^{40}Ar/^{36}Ar and ^{38}Ar/^{36}Ar end-member values. As inferred from the He isotopic analysis in these brines, excess ^{40}Ar results mostly from crustally produced ^{40}Ar, although the presence of a small mantle ^{40}Ar contribution (≤16%) cannot be completely ruled out. The likely presence of a dominant crustal ^{40}Ar component in these samples is further discussed below.

Kr isotopic ratios (e.g, ^{86}Kr/^{84}Kr; Table 6.2) are all indistinguishable from the atmospheric value (Table 6.2), and point to the absence of components other than atmospheric. Kr will thus not be the object of further discussion in the present document.

^{136}Xe/^{130}Xe ratios of Michigan brines show values above the atmospheric ratio (2.176), up to 2.365±0.012 in the deepest PDC formation, clearly showing the presence

of excess ^{136}Xe (Table 6.2, Fig. 6.2d). Similar to $^{40}Ar/^{36}Ar$ ratios, $^{136}Xe/^{130}Xe$ ratios also display a strong vertical gradient along the sedimentary strata, suggesting a deeper source for this excess ^{136}Xe (Fig. 6.2d). Similar gradients are also observed with $^{134}Xe/^{130}Xe$ and $^{132}Xe/^{130}Xe$ ratios (Table 6.2). These high Xe isotopic ratios suggest the presence of crustal and/or mantle Xe components in these brines, in addition to the atmospheric component. The presence of mantle Xe can be readily identified through a positive correlation between $^{136}Xe/^{130}Xe$ and $^{129}Xe/^{130}Xe$ ratios (e.g., blue line, Fig. 6.3a) [after *Ozima and Podosek*, 2002]. However, most of our Michigan brines do not display such a correlation and plot instead on the crustally produced Xe line (red line, Fig. 6.3a). This suggests that Xe excesses originate largely from a crustal Xe source. Indeed, $^{136}Xe/^{130}Xe$ and $^{134}Xe/^{130}Xe$ ratios of Michigan brines display a strong linear correlation with a slope of 1.2 (Fig. 6.3b), a value that is consistent with the expected $^{136}Xe/^{134}Xe$ production value from ^{238}U spontaneous fission [e.g., *Wetherill*, 1953; *Eikenberg et al.*, 1993]. Linear correlations are similarly observed between $^{136}Xe/^{130}Xe$ and $^{132}Xe/^{130}Xe$ as well as $^{136}Xe/^{130}Xe$ and $^{131}Xe/^{130}Xe$ ratios, with slopes that are consistent with the respective expected production ratios from ^{238}U spontaneous fission [e.g., *Wetherill*, 1953; *Eikenberg et al.*, 1993]. Based on the above observations, Xe excesses in the Michigan Basin brines have a largely crustal Xe contribution. The positive correlation observed between $^{136}Xe/^{130}Xe$ and $^{40}Ar/^{36}Ar$ ratios in these brines (Figs. 6.2c,d) further reinforces the notion that a crustal source is also largely responsible for the observed ^{40}Ar excesses.

It is relevant to note upfront that, unlike Ar and Xe isotopic ratios (Figs. 6.2c,d), neither R/Ra nor $^{21}Ne/^{22}Ne$ ratios of Michigan Basin brines display the presence of a vertical gradient along the sedimentary strata (Figs. 6.2a,b).

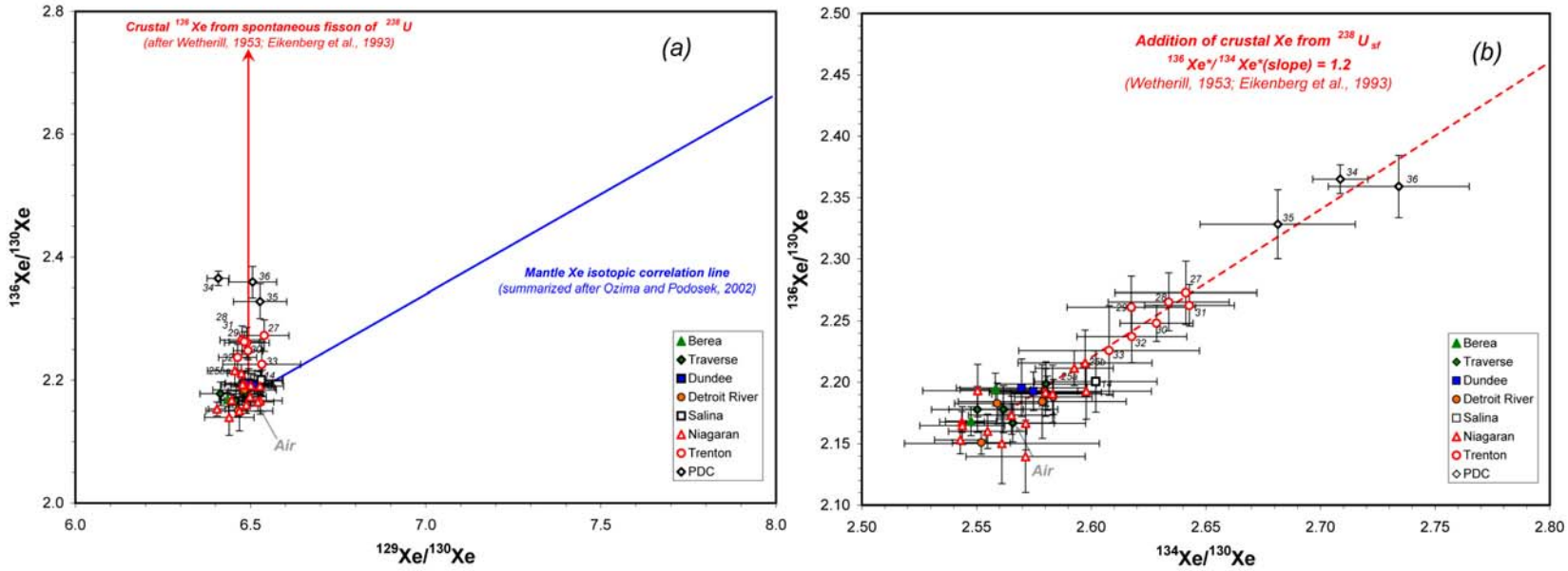

Figure 6.3. Xe isotopic ratios in Michigan Basin brines. **a)** $^{136}Xe/^{130}Xe$ versus $^{129}Xe/^{130}Xe$; **b)** $^{136}Xe/^{130}Xe$ versus $^{134}Xe/^{130}Xe$; the mantle Xe isotopic correlation line [after *Ozima and Podesek*, 2002] is indicated in a) (blue line); crustal Xe isotopic lines from spontaneous fission of U [after *Wetherill*, 1953; *Eikenberg* et al., 1993] are shown (red lines). The air Xe isotopic composition is indicated.

6.4.2. Separation of crustal noble gas components in Michigan brines

Concentrations and elemental ratios of crustally produced noble gases in Michigan Basin brines are reported in Table 6.3. Crustal He concentrations ($^4He_{crust}$) in these brines were estimated by using the He isotopic ratios as discussed in the previous section. Similarly, crustal ^{21}Ne contributions ($^{21}Ne_{crust}$) were obtained from the analysis of Ne isotopic ratios [see *Castro et al.*, 2008]. Because crustal Ar and Xe excesses are largely dominant and their mantle end-members ill-defined, it is considered in this study that addition of both ^{40}Ar and ^{136}Xe results entirely from crustal production. Crustal Ar and Xe contributions ($^{40}Ar_{crust}$ and $^{136}Xe_{crust}$) were thus estimated as follows:

$$(^{40}Ar_{crust}) = (^{36}Ar)_{measured} \times \left(\left(\frac{^{40}Ar}{^{36}Ar} \right)_{measured} - \left(\frac{^{40}Ar}{^{36}Ar} \right)_{air} \right) \qquad (6.1)$$

$$(^{136}Xe_{crust}) = (^{130}Xe)_{measured} \times \left(\left(\frac{^{136}Xe}{^{130}Xe} \right)_{measured} - \left(\frac{^{136}Xe}{^{130}Xe} \right)_{air} \right) \qquad (6.2)$$

where $(^{40}Ar/^{36}Ar)_{air} = 295.5$ and $(^{136}Xe/^{130}Xe)_{air} = 2.176$ [*Ozima and Podosek*, 2002]. Neglecting the presence of a potentially small mantle Ar and/or Xe contribution would not affect the discussion and conclusions that follow.

Both $^4He_{crust}$ and $^{21}Ne_{crust}$ concentrations vary over several orders of magnitude, from 1.34×10^{-7} to 1.69×10^{-3} cm^3STP/g and from 1.03×10^{-14} to 2.97×10^{-11} cm^3STP/g, respectively and they display an absence of vertical concentration gradients along the sedimentary strata (Table 6.3). By contrast, the presence of a vertical gradient for $^{40}Ar_{crust}$ and $^{136}Xe_{crust}$ concentrations in the Michigan brines, which range from 1.18×10^{-7} to 4.70×10^{-5} cm^3STP/g and 1.09×10^{-14} to 1.54×10^{-11} cm^3STP/g, respectively (Table 6.3) is

Table 6.3. Concentrations and elemental ratios of crustal noble gases in Michigan brine samples.

Sample Number	$^{4}He_{crust}$ (cm^3STP/g)	+/-	$^{21}Ne_{crust}$ (cm^3STP/g)	+/-	$^{40}Ar_{crust}$ (cm^3STP/g)	+/-	$^{136}Xe_{crust}$ (cm^3STP/g)	+/-
Devonian								
1	8.16E-07	1.22E-08	9.45E-14	4.94E-14	8.07E-07	3.42E-08		
2	5.11E-06	7.66E-08	3.67E-14	3.41E-14	1.19E-07	7.78E-09	1.68E-13	1.21E-13
3	4.99E-07	7.49E-09	2.40E-14	2.54E-14	2.27E-07	6.21E-09	4.95E-14	4.59E-13
4	5.95E-06	9.72E-07	1.27E-13	3.40E-14	2.17E-07	8.31E-09	1.09E-14	1.04E-13
5	3.00E-05	4.50E-07	1.33E-12	4.37E-14	1.68E-06	3.28E-08	4.74E-13	3.78E-13
6	1.81E-05	2.72E-07	4.99E-13	8.48E-14	8.06E-07	2.30E-08	1.22E-12	1.11E-12
7	1.34E-07	2.01E-09			1.18E-07	1.78E-08		
8	1.73E-04	2.59E-06	3.25E-12	6.43E-13	1.63E-06	1.12E-07	2.05E-13	1.92E-13
9	9.67E-06	1.45E-07	1.11E-12	1.48E-13	1.46E-06	4.00E-08	4.41E-13	5.30E-13
10	9.26E-05	1.39E-06	3.07E-12	1.00E-13	1.64E-06	3.37E-08	5.02E-14	1.21E-13
11	4.68E-04	7.02E-06	1.86E-11	1.61E-12	1.34E-05	1.15E-06	6.74E-13	2.42E-12
12	1.46E-05	2.20E-07			1.92E-07	8.74E-08		
13	3.68E-04	5.52E-06	5.02E-12	4.06E-13	2.49E-06	8.62E-08	2.91E-13	3.43E-13
Silurian								
14	6.10E-07	9.15E-09	5.35E-14	8.94E-14	8.91E-07	8.57E-08	1.29E-12	1.31E-12
15	1.82E-07	2.74E-09	1.04E-13	1.77E-13	8.09E-07	2.56E-08		
16	2.34E-05	3.50E-07	5.62E-13	6.58E-14	2.17E-06	3.40E-08		
17	1.33E-05	1.99E-07	1.07E-12	7.83E-14	8.24E-06	1.10E-07		
18	1.69E-03	2.54E-05	1.90E-11	1.56E-12	7.72E-06	1.94E-07	2.61E-13	3.23E-13
19	7.98E-06	1.20E-07	2.34E-13	6.86E-14	5.93E-06	1.03E-07		
20	3.61E-06	5.42E-08	1.44E-13	6.07E-14	3.53E-06	5.81E-08		
21	6.96E-06	1.04E-07	6.76E-13	1.11E-13	1.99E-05	2.91E-07		
22a	1.36E-07	2.04E-09	1.03E-14	2.57E-14	1.84E-06	2.99E-08	1.01E-12	1.24E-12
22b	1.77E-07	2.65E-09	2.97E-14	2.68E-14	3.94E-06	5.63E-08	2.39E-12	3.25E-12
23	1.32E-05	1.98E-07	5.88E-13	5.86E-14	6.39E-06	9.74E-08	2.55E-13	4.11E-13
24	1.44E-06	2.17E-08	8.96E-14	2.44E-14	1.96E-06	2.85E-08		
25a	4.08E-07	6.12E-09			4.27E-06	6.27E-08	2.70E-12	1.08E-12
25b	6.46E-07	9.69E-09			4.97E-06	7.36E-08	3.75E-12	2.53E-12
26	1.51E-03	2.27E-05	2.97E-11	1.35E-12	2.41E-05	4.16E-07		
Ordovician								
27	5.38E-06	8.06E-08	3.27E-13	3.75E-14	4.67E-06	6.60E-08	2.40E-12	6.38E-13
28	3.51E-06	5.26E-08	2.42E-13	3.26E-14	6.60E-06	9.42E-08	4.92E-12	1.29E-12
29	4.61E-06	6.92E-08	3.38E-13	3.58E-14	3.95E-06	5.63E-08	2.56E-12	7.52E-13
30	1.90E-05	2.85E-07	6.41E-13	4.78E-14	7.95E-06	1.16E-07	7.62E-13	1.55E-13
31	1.08E-04	1.63E-06	3.86E-12	8.23E-14	3.02E-05	4.67E-07	2.40E-12	4.67E-13
32	8.86E-05	1.33E-06	2.94E-12	9.18E-14	1.24E-05	1.87E-07	7.11E-13	2.46E-13
33	1.17E-06	1.75E-08	1.13E-13	1.98E-14	3.87E-06	5.94E-08	1.08E-12	7.89E-13
34	3.29E-06	4.94E-08	8.53E-14	6.38E-14	4.70E-05	1.36E-06	1.54E-11	1.01E-12
35	3.66E-05	5.49E-07	1.43E-12	5.89E-14	4.53E-05	7.77E-07	1.05E-12	1.95E-13
36	2.48E-06	3.72E-08	1.66E-13	2.44E-14	1.24E-05	1.71E-07	2.30E-12	3.22E-13

Table 6.3. (continued)

Sample Number	$(^4He/^{40}Ar)_{crust}$	+/-	$(^{21}Ne/^{40}Ar)_{crust}$	+/-	$(^4He/^{136}Xe)_{crust}$	+/-	$(^{21}Ne/^{136}Xe)_{crust}$	+/-
Devonian								
1	1.01	0.05	1.17E-07	6.14E-08				
2	43.0	2.9	3.09E-07	2.87E-07	3.04E+07	2.20E+07	2.19E-01	2.57E-01
3	2.20	0.07	1.06E-07	1.12E-07	1.01E+07	9.37E+07	4.86E-01	4.54E+00
4	27.4	4.6	5.85E-07	1.58E-07	5.45E+08	5.18E+09	1.16E+01	1.10E+02
5	17.9	0.4	7.96E-07	3.04E-08	6.33E+07	5.05E+07	2.82E+00	2.25E+00
6	22.5	0.7	6.20E-07	1.07E-07	1.49E+07	1.36E+07	4.10E-01	3.80E-01
7	1.1	0.2						
8	105.7	7.4	1.99E-06	4.17E-07	8.41E+08	7.87E+08	1.58E+01	1.51E+01
9	6.6	0.2	7.63E-07	1.04E-07	2.19E+07	2.63E+07	2.53E+00	3.05E+00
10	56.6	1.4	1.87E-06	7.23E-08	1.85E+09	4.46E+09	6.11E+01	1.48E+02
11	34.8	3.0	1.38E-06	1.69E-07	6.95E+08	2.50E+09	2.75E+01	9.90E+01
12	76.2	34.7						
13	147.9	5.6	2.02E-06	1.78E-07	1.26E+09	1.49E+09	1.72E+01	2.03E+01
Silurian								
14	0.68	0.07	6.01E-08	1.01E-07	4.73E+05	4.78E+05	4.15E-02	8.10E-02
15	0.23	0.01	1.28E-07	2.18E-07				
16	10.8	0.2	2.59E-07	3.06E-08				
17	1.61	0.03	1.29E-07	9.66E-09				
18	218.9	6.4	2.46E-06	2.11E-07	6.47E+09	8.00E+09	7.27E+01	9.00E+01
19	1.35	0.03	3.94E-08	1.16E-08				
20	1.02	0.02	4.09E-08	1.72E-08				
21	0.35	0.01	3.40E-08	5.62E-09				
22a	0.074	0.002	5.59E-09	1.39E-08	1.35E+05	1.66E+05	1.02E-02	2.84E-02
22b	0.045	0.001	7.55E-09	6.81E-09	7.40E+04	1.01E+05	1.25E-02	2.03E-02
23	2.06	0.04	9.21E-08	9.29E-09	5.16E+07	8.31E+07	2.30E+00	3.71E+00
24	0.74	0.02	4.57E-08	1.25E-08				
25a	0.095	0.002			1.51E+05	6.05E+04		
25b	0.130	0.003			1.72E+05	1.16E+05		
26	62.7	1.4	1.23E-06	5.97E-08				
Ordovician								
27	1.15	0.02	7.00E-08	8.10E-09	2.24E+06	5.94E+05	1.36E-01	3.93E-02
28	0.53	0.01	3.66E-08	4.97E-09	7.13E+05	1.87E+05	4.91E-02	1.45E-02
29	1.17	0.02	8.56E-08	9.16E-09	1.80E+06	5.29E+05	1.32E-01	4.11E-02
30	2.39	0.05	8.07E-08	6.13E-09	2.49E+07	5.09E+06	8.41E-01	1.83E-01
31	3.59	0.08	1.28E-07	3.37E-09	4.51E+07	8.80E+06	1.61E+00	3.14E-01
32	7.2	0.2	2.38E-07	8.26E-09	1.25E+08	4.33E+07	4.14E+00	1.44E+00
33	0.30	0.01	2.92E-08	5.14E-09	1.08E+06	7.90E+05	1.04E-01	7.85E-02
34	0.070	0.002	1.81E-09	1.36E-09	2.14E+05	1.44E+04	5.54E-03	4.16E-03
35	0.81	0.02	3.17E-08	1.41E-09	3.49E+07	6.49E+06	1.37E+00	2.60E-01
36	0.200	0.004	1.34E-08	1.97E-09	1.08E+06	1.52E+05	7.22E-02	1.47E-02

apparent. Light (^{4}He and ^{21}Ne) and heavy (e.g, ^{40}Ar and ^{136}Xe) noble gases thus display fundamentally different patterns within the basin.

6.5. Discussion

In the previous section it has been clearly shown the occurrence of crustal noble gases in all Michigan brines. It has also been shown that unlike $^{4}He_{crust}$ and $^{21}Ne_{crust}$, both $^{40}Ar_{crust}$ and $^{136}Xe_{crust}$ display the presence of a strong vertical gradient along the sedimentary sequence, pointing to their deep origin (Fig. 6.2). Here, we will first show that most crustally produced noble gases likely originate in the Precambrian basement rocks. We will then discuss the observed distribution patterns of elemental ratios along the sedimentary strata and potential mechanisms of upward vertical transport within the basin through a simple Rayleigh-type fractionation model. Finally we will discuss the implications for the thermal evolution history in this currently stable region.

6.5.1. Precambrian basement rocks as an external source for crustally produced noble gases in Michigan Basin brines

The amount of crustally produced noble gases released into groundwater depends mainly on three factors: (1) production rate in the crustal rock; (2) efficiency of the isotope released from the rock into the water, and; (3) duration of the rock-fluid contact. Concentration of crustal noble gases into the water can thus be estimated following:

$$[C_i]_{H_2O} = P_i \times \rho \times \Lambda \times ((1-\omega)/\omega) \times t \qquad (6.3)$$

where $[C_i]_{H2O}$ is the concentration of the isotope *i* accumulated in the water (cm^3STPg^{-1} H_2O); P_i is the crustal production rate of isotope *i* in the reservoir rock ($cm^3STPg^{-1}_{rock}yr^{-1}$), ρ is the density of the rock (gcm^{-3}), Λ is the release efficiency from the rock matrix into

water (normally assumed to be unity), ω is the porosity of the reservoir rock (volume ratio), and t is the residence time of the water (year).

Crustal noble gas production rates (P_i) can be estimated from U, Th, K, and major element concentrations of reservoir rocks as summarized by *Ballentine and Burnard* [2002]. Production rates of individual sampled formations in this study (Fig. 6.1b), the underlying Precambrian crystalline basement, as well as the average upper crust were calculated and are listed in Table 6.4.

The existence of an external source for the crustal noble gases in these brines can be demonstrated by using a simple first-order calculation of $^{40}Ar/^{36}Ar$ and $^{136}Xe/^{130}Xe$ ratios in the water phase using ^{40}Ar and ^{136}Xe production rates (Table 6.4). In this study, Ordovician PDC carbonates are the deepest and the oldest formation (~10% porosity; Fig. 6.1b). Assuming that in-situ produced ^{40}Ar and ^{136}Xe in the 480 Ma carbonates were entirely released into the water phase (with initial noble gas concentrations corresponding to that of sea water at 25ºC; Table 6.1), the resultant $^{40}Ar/^{36}Ar$ and $^{136}Xe/^{130}Xe$ ratios in the water phase would be 448 and 2.235, respectively, both significantly lower than the measured $^{40}Ar/^{36}Ar$ and $^{136}Xe/^{130}Xe$ ratios in the PDC brines (up to 2863.1±55.5 and 2.365±0.012, respectively; Table 6.2). In fact, the total in-situ produced ^{40}Ar and ^{136}Xe within the 480Ma carbonates can only account for about 6% and 30% of the total observed ^{40}Ar and ^{136}Xe excesses, respectively. Therefore, the above calculation strongly suggests that these brines received crustal noble gases from a source external to their sedimentary reservoirs, most likely from the underlying Precambrian crystalline basement, which is capable of producing significant amounts of crustal noble gases because of its much greater age (~1.1 to greater than 2.5Ga) and high U, Th, and K

Table 6.4. Calculated production rates and elemental ratios of crustally produced noble gases in the Michigan Basin as well as in the crystalline basement.

Formation	Lithology	U (ppm)	Th (ppm)	K (ppm)	O (%)	Mg (%)	$P[^4He]$ [e] ($cm^3STPg^{-1}_{rock}yr^{-1}$)	$P[^{21}Ne]$ ($cm^3STPg^{-1}_{rock}yr^{-1}$)	$P[^{40}Ar]$ ($cm^3STPg^{-1}_{rock}yr^{-1}$)	$P[^{136}Xe]$ ($cm^3STPg^{-1}_{rock}yr^{-1}$)	$(^4He/^{40}Ar)_{crust}$	$(^{21}Ne/^{40}Ar)_{crust}$	$(^4He/^{136}Xe)_{crust}$	$(^{21}Ne/^{136}Xe)_{crust}$
Berea [a]	Carbonate	2.2	1.7	2700	48	4.7	3.1E-13	1.7E-20	1.0E-14	1.4E-21	30.6	1.7E-06	2.2E+08	12.3
Traverse	Carbonate	2.2	1.7	2700	48	4.7	3.1E-13	1.7E-20	1.0E-14	1.4E-21	30.6	1.7E-06	2.2E+08	12.3
Dundee	Carbonate	2.2	1.7	2700	48	4.7	3.1E-13	1.7E-20	1.0E-14	1.4E-21	30.6	1.7E-06	2.2E+08	12.3
Detroit River	Carbonate	2.2	1.7	2700	48	4.7	3.1E-13	1.7E-20	1.0E-14	1.4E-21	30.6	1.7E-06	2.2E+08	12.3
	Sandstone	0.45	1.7	10700	53.3	0.7	1.0E-13	5.2E-21	4.1E-14	2.9E-22	2.5	1.3E-07	3.6E+08	18.3
Salina	Carbonate	2.2	1.7	2700	48	4.7	3.1E-13	1.7E-20	1.0E-14	1.4E-21	30.6	1.7E-06	2.2E+08	12.3
Niagaran	Carbonate	2.2	1.7	2700	48	4.7	3.1E-13	1.7E-20	1.0E-14	1.4E-21	30.6	1.7E-06	2.2E+08	12.3
Trenton	Carbonate	2.2	1.7	2700	48	4.7	3.1E-13	1.7E-20	1.0E-14	1.4E-21	30.6	1.7E-06	2.2E+08	12.3
PDC	Carbonate	2.2	1.7	2700	48	4.7	3.1E-13	1.7E-20	1.0E-14	1.4E-21	30.6	1.7E-06	2.2E+08	12.3
Precambrian crystalline basement [b]	Granite/Rhyolite	4	13.2	43834	47.5	0.13	8.6E-13	4.0E-20	1.7E-13	2.6E-21	5.2	2.4E-07	3.4E+08	15.6
Canadian Precambrian Shield [c]	Crystalline rocks	2.45	10.3	25800	47.5	1.33	5.9E-13	2.6E-20	9.8E-14	1.6E-21	6.0	2.7E-07	3.8E+08	16.9
Average upper crust [d]		2.8	10.7	28200	47.5	1.33	6.4E-13	2.9E-20	1.1E-13	1.8E-21	6.0	2.7E-07	3.6E+08	16.3

a. U, Th, K, O, and Mg estimated from average lithological composition after *Parker* [1967].
b. U, Th, K, O, and Mg estimated from outcrop area for the crystalline basement [*Menuge et al.*, 2002].
c. U, Th, K, O, and Mg estimated from outcrop area in the Canadian Shield [*Shaw*, 1967].
d. U, Th, K, O, and Mg estimated for average upper crust [*Rudnick and Fountain*, 1995].
e. Production rates for ^4He, ^{21}Ne, ^{40}Ar and ^{136}Xe calculated by using equations summarized by *Ballentine and Burnard* [2002].

content (Table 6.4). Indeed, the involvement of the Precambrian basement in the crustal noble gas mass balance is also supported by the observed high He excesses in the shallow Marshall aquifer, which requires an unusually high He flux from below, partly supplied by the sedimentary formations and partly from the deep Precambrian basement (Fig. 6.1b) [*Ma et al.*, 2005]. Deep external sources that account for crustal noble gas excesses have also been previously proposed [e.g., *Torgersen and Clarke*, 1985; *Zaikowski et al.*, 1987; *Torgersen et al.*, 1989; *Ballentine et al.*, 1996; *Castro et al.*, 1998a,b; *Kulongoski et al.*, 2005].

Temperatures required for the release of noble gases from rocks also strongly favor an external origin for most crustally produced noble gases in the Michigan Basin. Indeed, it is generally accepted that the release of crustal noble gases from individual minerals is dependent on their closure temperatures which are inversely correlated to the noble gas diffusivity in these minerals [*Dodson*, 1973]. For instance, while radiogenic ^{4}He is released from calcite at aquifer temperatures above 50-70°C [*Copeland et al.*, 2007], release temperatures for radiogenic ^{40}Ar in common K-bearing minerals (e.g., muscovite, K-feldspar) are much higher, above ~250-275°C [*Lippolt and Weigel*, 1988]. Although the release temperatures for Ne and Xe in these common minerals are currently uncertain, based on the fact that their diffusivity decreases with increasing atomic number [*Ozima and Podesek*, 2002], it is quite reasonable to assume that Ne release temperatures will fall between those of He and Ar (e.g., ~70-250°C), while Xe release temperatures are expected to be greater than those of Ar (e.g., >275°C). These assumptions are supported by the increasing release temperatures for ^{4}He, ^{21}Ne, ^{84}Kr, and ^{136}Xe from zircons [*Honda et al.*, 2004; *Gautheron et al.*, 2006], as well as the observed Xe release temperature in

meteorites, which was shown to be greater than that of Ar [*Burkland et al.*, 1995]. Due to its currently low geothermal gradient (~19°C/km) [*Vugrinovich*, 1989], fluid temperatures in most of formations sampled here in the Michigan Basin are ~40-80°C, far lower than release temperatures required for ^{40}Ar and ^{136}Xe. It is thus apparent that only the Precambrian crystalline basement can account for most of the measured crustally produced noble gases in the Michigan Basin.

The existence of an external source is further supported by the presence of mantle He and Ne previously identified in these same brines and released during a past thermal event [*Castro et al.*, 2008]. Such a mantle component also points to the presence of an upward transport process during which both crustal and mantle noble gases were released into the basin via deep-seated faults and fractures from the underlying basement and lithospheric mantle.

6.5.2. Elemental fractionation patterns of crustally produced noble gases in Michigan brines

Crustally produced noble gases released at great depths and high temperatures are expected to have elemental ratios close to their crustal production ratios, as frequently observed in deep fluids from many other sedimentary basins around the world, for example, the Paris Basin [*Pinti and Marty*, 1995; *Castro et al.*, 1998a], the Great Artesian Basin [*Torgersen et al.*, 1989], and the Pannonian Basin [*Ballentine et al.*, 1991]. In the Michigan Basin, ^{4}He/^{40}Ar production ratios within the crystalline basement are estimated to be ~5.2-6.0 (Table 6.4). These values are very similar to the average upper crustal production value (^{4}He/^{40}Ar: ~ 6.0; Table 6.4). $(^{4}He/^{40}Ar)_{crust}$ ratios in our brine samples vary over several orders of magnitude with values between ~0.045, far smaller than the

crustal production ratio and 218.9, much greater than crustal production ratio (Table 6.3). The $(^{21}Ne/^{40}Ar)_{crust}$ ratio also varies over several orders of magnitude with values between 1.81×10^{-9} and 2.46×10^{-6} (Table 6.3), as compared to the crustal production ratio (2.7×10^{-7}; Table 6.4). $(^{4}He/^{136}Xe)_{crust}$ and $(^{21}Ne/^{136}Xe)_{crust}$ elemental ratios also show a similar pattern, with values varying from 7.40×10^{4} to 6.47×10^{9} and 0.00554 to 72.7, respectively (Table 6.3), far different from their production ratios of 3.8×10^{8} and 16.9 (Table 6.4).

$(^{4}He/^{40}Ar)_{crust}$ and $(^{21}Ne/^{40}Ar)_{crust}$ ratios in these brines display a similar, very specific and interesting pattern (Figs. 6.4a,b), in addition to presenting a strong positive correlation (Fig. 6.5a). Indeed, with the exception of a few samples (e.g., samples 26 and 18), samples from the deeper formations (e.g., Salina, Niagaran, Trenton and PDC) display elemental ratios smaller than (or close to) the expected crystalline basement production ratios. In contrast, with the exception of samples 1, 3, and 7, all other samples in the shallower formations (i.e., Berea, Traverse, Dundee, and Detroit River) display ratios that are greater (or far greater) than the production ratios (Figs. 6.4.a,b). A general trend is thus apparent in which samples from the shallower formations display elemental ratios complementary to those of deep formations, lower than the production ratios, separated by the Salina formation (Fig. 6.1b), an extremely thick sequence composed mostly of massive evaporites [*Catacosinos et al.*, 1991]. Similar patterns are observed for $(^{4}He/^{136}Xe)_{crust}$ and $(^{21}Ne/^{136}Xe)_{crust}$ ratios (Table 6.4, Fig. 6.5b). These results show that samples above the Salina Group (shallow formations) are enriched (in some cases to a great extent) in $^{4}He_{crust}$ and $^{21}Ne_{crust}$ with respect to $^{40}Ar_{crust}$ and $^{136}Xe_{crust}$, as opposed to

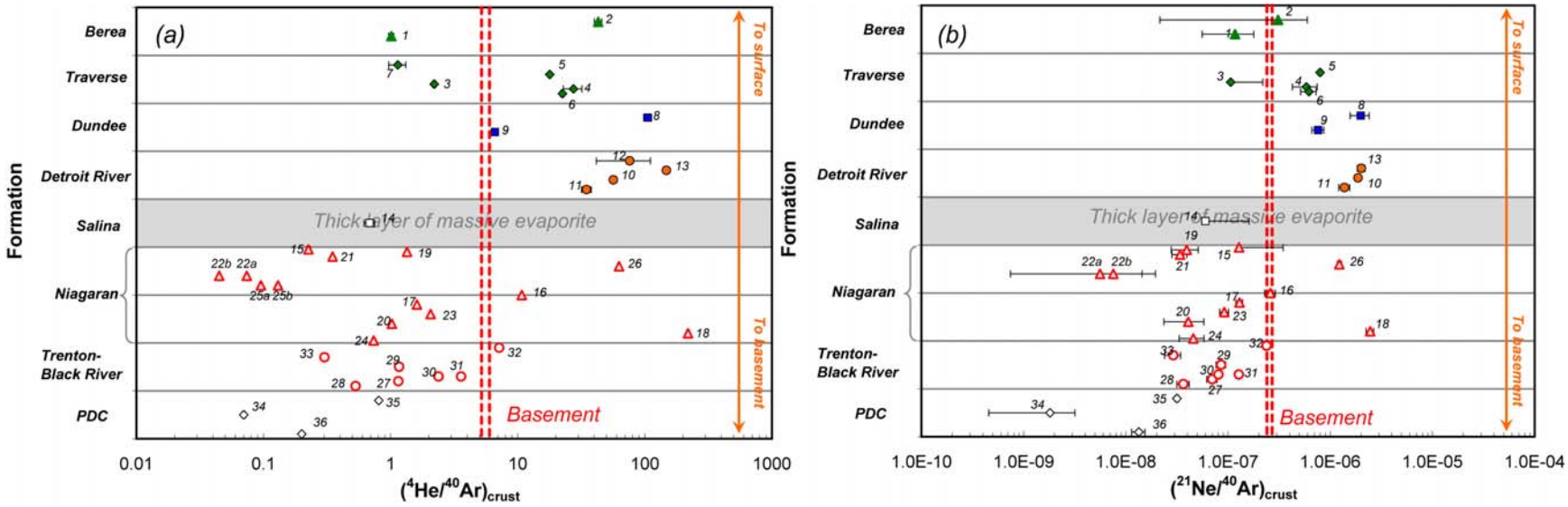

Figure 6.4. Elemental ratios of crustally produced noble gases in Michigan Basin brines in the sedimentary sequence. **a)** $(^{4}He/^{40}Ar)_{crust}$; **b)** $(^{21}Ne/^{40}Ar)_{crust}$; grey area indicates the Salina formation, a thick layer of massive evaporites in the Michigan Basin; production ratios from the Precambrian crystalline basement are shown (red dashed lines) [after *Shaw*, 1967; *Menuge et al.*, 2002].

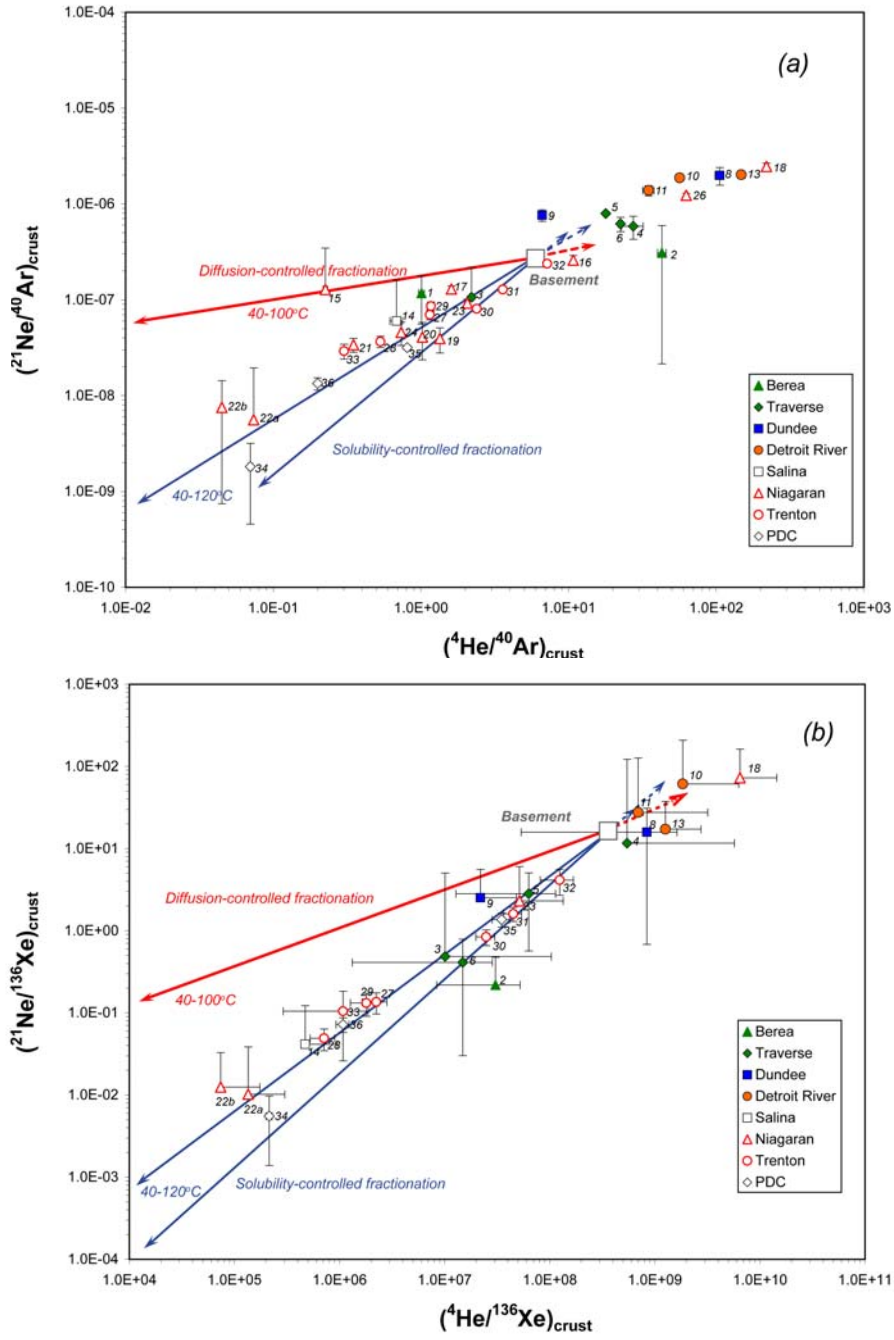

Figure 6.5. Elemental ratios of crustally produced noble gases in Michigan Basin brines. **a)** $(^{4}He/^{40}Ar)_{crust}$ and $(^{21}Ne/^{40}Ar)_{crust}$ ratios; **b)** $(^{4}He/^{136}Xe)_{crust}$ and $(^{21}Ne/^{136}Xe)_{crust}$ ratios; production ratios from the Precambrian crystalline basement are shown (open square) [after *Shaw*, 1967; *Menuge et al.*, 2002]. Elemental fractionation trends are calculated using a simple Rayleigh-type fractionation model, for a diffusion-controlled process (at 40-100°C) (red line) and a solubility-controlled process (at 40-120°C) (blue lines). Solid and dashed lines indicate the fractionated elemental ratios in the retained and escaped phases, respectively.

those below the massive evaporite layer (deeper formations) which exhibit complementary patterns (Figs. 6.4, 6.5).

It was previously suggested that crustal fluids released in a low-temperature environment (e.g., 50-250°C) may present $^{4}He/^{40}Ar$ ratios greater than the production ratio because of the different release temperatures of ^{4}He and ^{40}Ar [*O'Nion and Ballentine*, 1993]. However, such a low-temperature source cannot explain either the observed $(^{4}He/^{40}Ar)_{crust}$ ratios in these basin brines (much lower than the production ratio), or the observed systematic patterns within the sedimentary strata. Furthermore, it is apparent, as discussed above, that crustal noble gases in the Michigan Basin were not released in a low temperature environment. Various production ratios due to different lithologies in the basin (e.g., $^{4}He/^{40}Ar$ ratio ~2.5-30; Table 6.4) can also be ruled out as these production ratios cannot account for the observed extremely large range in the elemental ratios (Table 6.3). Alternatively, it has been shown that the preferential upward transport of He and Ne by diffusion in groundwater can lead to a relative enrichment of these gases with respect to Ar [*Castro et al.*, 1998a,b]. As *Castro et al.* [1998a,b] showed, such preferential transport and subsequent enrichment of He and Ne are due to their higher diffusion coefficients with respect to Ar [*Wise and Houghton*, 1966, 1968; *Ohsumi and Horibe*, 1984; *Jahne et al.*, 1987]. The extent of this enrichment will also greatly depend on the gas concentration gradients which are typically greater for He than for Ne, thus, leading to a greater level of He enrichment. Here, we suggest a possible mechanism, involving the upward transport of deep crustal noble gases from basement rocks toward the surface in which both high He and Ne diffusivities, combined with solubility-controlled processes that might occur when a gas phase (e.g., CO_2 or CH_4) is present

[*Zartman et al.*, 1961; *Bosch and Mazor*, 1988], for the observed fractionation between He, Ne and Ar, Xe. For elemental fractionation controlled by either diffusion or solubility processes, fluids in the upper portion of the sedimentary sequence are expected to be enriched in ^{4}He and ^{21}Ne as they are subjected to the additional input of ^{4}He and ^{21}Ne with respect to ^{40}Ar and ^{136}Xe from below, while the fluids in lower formations will show a relative enrichment of ^{40}Ar and ^{136}Xe resulting from a more marked loss of ^{4}He and ^{21}Ne. This pattern is precisely the one presented in these brine samples (Figs. 6.4 and 6.5). In the following section, a simple Rayleigh-type elemental fractionation model is used to test this hypothesis and to better constrain processes leading to the observed elemental fractionation during upward transport.

6.5.3. Mechanisms for the observed noble gas elemental fractionation – a Rayleigh-type elemental fractionation model

As previously discussed, the observed elemental fractionation might be due to either diffusion-controlled or solubility-controlled processes during the upward transport of crustal noble gases in the basin. To test this hypothesis, we use a simple model in which fractionated elemental ratios in the escaped phase (into the shallow formations) and in the retained phase (left in the deep formations) are simulated during upward transport using the Rayleigh Law as follows:

$$\left(\frac{^{4}He}{^{40}Ar}\right)_{retained} = \left(\frac{^{4}He}{^{40}Ar}\right)_{0} f^{(\alpha-1)} \qquad (6.4)$$

$$\left(\frac{^{4}He}{^{40}Ar}\right)_{escaped} = \left(\frac{^{4}He}{^{40}Ar}\right)_{0} \frac{1-f^{\alpha}}{1-f} \qquad (6.5)$$

where subscripts *0*, *retained*, and *escaped* stand for elemental ratios in the initial, retained, and escaped phases, respectively; *f* is the fraction of ^{40}Ar remaining in the retained phase after fractionation occurred. Similar models have been previously used by *Battani et al.* [2000] and *Brennwald et al.* [2005] to study noble gas elemental fractionation in natural gas and sediment pore waters, respectively. For a diffusion-controlled process, the exponent coefficient α is given by:

$$\alpha = \frac{D_{He}}{D_{Ar}} \tag{6.6}$$

where D_{He} and D_{Ar} are the noble gas diffusion coefficients in porous media, which can be in turn related to noble gas diffusion coefficients in water [*Ohsumi and Horibe*, 1984; *Jahne et al.*, 1987]. The exponent coefficient α for a solubility-controlled process is given by:

$$\alpha = \frac{K_{He}}{K_{Ar}} \tag{6.7}$$

where K_{He} and K_{Ar} are Henry's Law constants [*Crovetto et al.* 1982; *Smith*,1985; *Smith and Kennedy*,1983]. Similar sets of equations can be derived for ^{21}Ne/^{40}Ar, ^{4}He/^{136}Xe, and ^{40}Ar/^{136}Xe ratios, respectively. Diffusion coefficient values and Henry's Law constants used for all gases are given in Table 6.5. Both diffusion and solubility coefficients are highly dependent on temperature. However, when applied in the Rayleigh Law equations (Eqs. 6.4 and 6.5), the impact of temperature on the observed fractionation due to a diffusion controlled process almost vanishes due to the similar values for diffusion coefficients for He and Ne.

Elemental fractionation due to both diffusion- and solubility-controlled processes under reservoir temperatures of 40-100°C and 40-120°C, respectively, are shown in

Table 6.5. Diffusion coefficient values and Henry's Law constants used in the Rayleigh model.

	D at 40°C [(a)] ($cm^2\ s^{-1}$)	D at 100°C [(a)] ($cm^2\ s^{-1}$)	K at 40°C [(b)] (atm kg mol^{-1})	K at 120°C[(b)] (atm kg mol^{-1})
He	9.15E-05	1.88E-04	7.41E+03	1.71E+03
Ne	5.38E-05	1.35E-04	7.20E+03	1.88E+03
Ar	4.09E-05	1.19E-04	3.51E+03	1.10E+03
Kr	2.73E-05	9.51E-05	2.20E+03	7.82E+02
Xe	2.24E-05	8.50E-05	1.54E+03	5.69E+02
α(He/Ar)	2.24	1.58	2.11	1.56
α(Ne/Ar)	1.32	1.13	2.05	1.71
α(He/Xe)	4.08	2.22	4.82	3.01
α(Ne/Xe)	2.40	1.58	4.69	3.30

a) Diffusion coefficients in water calculated after *Jahne et al.* [1987].
b) Henry's Law constants for a 4.4M NaCl brine solution calculated after *Crovetto et al.* [1982], *Smith* [1985], and *Smith and Kennedy* [1983]. Due to a lack of solubility data for high temperatures and salinities, Henry's Law constants at 120°C are calculated for freshwater.

Figure 6.5. It is apparent that both processes are capable of producing a relative enrichment of light noble gases (^{4}He and ^{21}Ne) in the escaped phases (dashed lines) and complementary enrichment of heavy noble gases (^{40}Ar and ^{136}Xe) in the retained phases (solid lines). It is clear that except for a few samples (15, 1, 32, and 16) that follow the diffusion-controlled fractionation pattern (red line), many brine samples follow closely the solubility-controlled elemental fractionation pattern within a temperature range of 40-120°C (blue lines) (Fig. 6.5a). A subset of samples falls between the trends defined by the diffusion- and solubility-controlled fractionations. These samples might represent either a combination of both processes occurring at the same location but spaced in time, or simply a mixture between brines whose composition resulted from diffusion- and solubility-controlled fractionation, respectively. Similar patterns are also observed with $(^{4}He/^{136}Xe)_{crust}$ and $(^{21}Ne/^{136}Xe)_{crust}$ (Fig. 6.5b). We thus suggest that both solubility- and diffusion-controlled mechanisms are responsible for the observed elemental fractionation patterns in these brines. While high diffusivities and preferential concentration in the gas phase of He and Ne with respect to Ar and Xe lead to a relative enrichment of ^{4}He and ^{21}Ne above the Salina formation during upward transport, an enrichment of ^{40}Ar and ^{136}Xe is observed below this very low permeability formation, which severely slows upward movement of these two gases (Figs. 6.4, 6.5).

Few samples fall outside of this general pattern. For example, samples 26 and 18 in the deep Niagaran formation show signatures similar to those of the shallow formations (e.g., Fig. 6.5a). These samples may indicate that the escaped phase may sometimes be trapped below the Salina formation. In contrast, the retained phase may also be transported to the shallow formations at a later time and this phenomenon may

explain the unusual signatures of samples 1 and 3 (Fig. 6.5a). These exceptions reflect the complexity of the system considering the spatial scale of the study area and diversity of formations from which these brine samples are collected (Figs. 6.1a,b). Despite this, it is apparent that a highly simplified Rayleigh Law model is largely capable of explaining the observed general pattern of noble gases elemental fractionation.

6.5.4. Recent reactivation of the mid-continent rift: an internal heat source for Michigan Basin brines

Indicators of past high temperatures in uppermost Precambrian and Paleozoic formations occur widely in the North American Mid-continent, for example in the Appalachian and Illinois Basin [e.g., *Bethke and Marshak*, 1990]. These have been commonly linked to the Appalachian and Ouachita orogenic activities and subsequent large-scale brine migrations expelled from these orogenic foldbelts towards the cratonic interior [*Oliver*, 1986; *Bethke and Marshak*, 1990]. In the Michigan Basin, the occurrence of past high temperatures (up to 260°C) has been similarly identified in a wealth of thermal studies based on a diversity of proxies (e.g., organic maturity data, stable isotopes, fluid inclusions, authigenic clay minerals, apatite fission track ages; [*Cercone and Lohmann*, 1987; *Cercone and Pollack*, 1991; *Crowley*, 1991; *Coniglio et al.*, 1994; *Girard and Barnes*, 1995; *Luczaj et al.*, 2006]). However, until very recently it remained unclear whether such high past temperatures could be attributed to long-distance brine migration, and thus, to an external heat source or instead, to a local, internal source. Indeed, with its massive Late Silurian and Early Devonian evaporite formations (Salina group), the Michigan Basin is also a major potential source of such hot brines [e.g., *Hay et al.*, 1988; *Liu et al.*, 2003]. The transport of heat and fluids from deeper parts of the

basin along major faults and fracture zones connected to the Precambrian basement structures have been previously proposed to account for past high temperatures in the basin [*Budai and Wilson*, 1991; *Coniglio et al.*, 1994; *Girard and Barnes*, 1995; *Luczaj et al.*, 2006]. The occurrence of hot fluids flowing out of the Michigan Basin have also been suggested to account for the presence of hydrothermal dolomites in eastern Wisconsin [*Luczaj*, 2006] and northern Indiana [*Yoo et al.*, 2000]. All these studies suggest the presence of an internal heat source within the Michigan Basin as being responsible for the past high temperatures without the involvement of large-scale brine migration from peripheral forming orogenic foldbelts. In this study, the observed vertical elemental fractionation of crustal noble gases in Michigan brines strongly supports this hypothesis (Figs. 6.4 and 6.5). As previously indicated by the mantle [*Castro et al.*, 2008] and atmospheric [*Ma et al.*, 2008] noble gas signatures in Michigan Basin brines, the release of deep crustal noble gases into the basin (Fig. 6.6), which is likely still on-going, is yet another independent indicator for the occurrence of a past thermal event in the basin. A recent reactivation of Precambrian basement structures is likely the origin of such a thermal event and provides an internal heat source. Indeed, the reactivation of the ancient MCR system during the Late Devonian-Mississippian (370-323Ma) period was previously suggested based on the formation of authigenic illite, which yields the youngest ages (323 Ma) and highest temperature estimates (~170°C) in the vicinity of the MCR [*Girard and Barnes*, 1995]. Apatite fission-track ages from drilled basement samples further indicate two additional, more recent periods of thermal activity, during the Triassic (~224Ma) and Cretaceous (~111-159Ma) [*Crowley*, 1991]. Repeated movements along major faults prevailed throughout the early part of the Paleozoic and

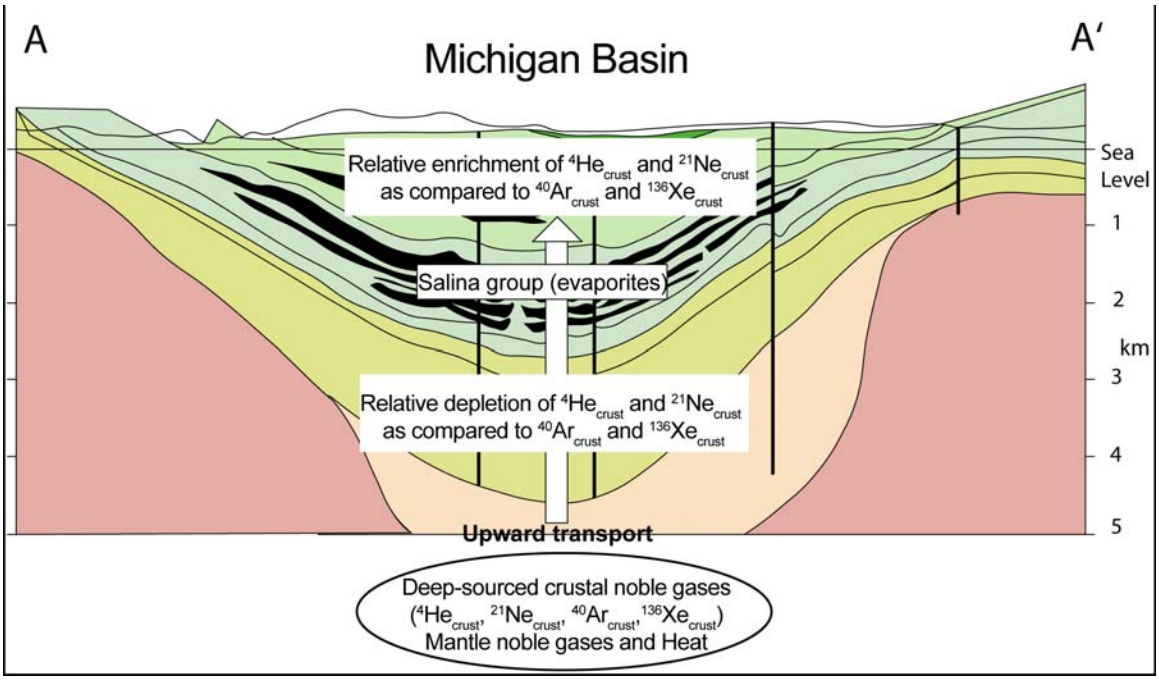

Figure 6.6. Schematic representation of a conceptual model for the release of the heat, mantle and crustal noble gases into the Michigan Basin due to the recent reactivation of the MCR underneath the Michigan Basin. Upward transport processes and associated elemental fractionation are responsible for the observed enrichment of $^{4}He_{crust}$ and $^{21}Ne_{crust}$ with respect to $^{40}Ar_{crust}$ and $^{136}Xe_{crust}$ in the shallow formations above the Salina group, as well as the complementary depletion of such components in deep formations. Figure legend of the cross-section is the same as that of Figure 6.1c.

major uplift of the basin fault blocks occurred at the end of the Mississippian period [*Fisher et al.*, 1988]. A reactivation of deep-seated faults and fractures in the basement of both southeastern and northeastern Michigan Basin has been suggested to account for the circulation of hot fluids (e.g., 220-260°C) and formation of hydrothermal dolomite reservoirs [*Sanford et al.*, 1985; *Coniglio et al.*, 1994].

Overall, our noble gas study of Michigan Basin brines [*Castro et al.*, 2008; *Ma et al.*, 2008; *this study*] shows that the upward transport of heat and loss of the atmospheric noble gas component, as well as the release of crustal and mantle noble gases are likely related to the recently reactivated MCR system, and supports the internal heat source hypothesis as being largely responsible for the existence of past high temperatures in the basin (Fig. 6.6).

6.6. Conclusions

We present noble gas concentrations and isotopic ratios from 38 deep brines (~0.5-3.6km) in the Michigan Basin. These brine samples clearly show the presence of an important crustal component of $^{4}He_{crust}$, $^{21}Ne_{crust}$, $^{40}Ar_{crust}$, and $^{136}Xe_{crust}$. Both $^{40}Ar_{crust}$ and $^{136}Xe_{crust}$ display the presence of a strong vertical gradient along the sedimentary strata of the Michigan Basin. It is clearly shown that the in-situ production for these two gases within the sedimentary strata is insufficient to account for the observed crustal components in the Michigan brines. These point to the presence of a deep, external source for crustal noble gases, likely the Precambrian crystalline basement beneath the Michigan Basin. Furthermore, the observed elemental ratios of crustal noble gases ($^{4}He/^{40}Ar$, $^{21}Ne/^{40}Ar$, $^{4}He/^{136}Xe$, and $^{21}Ne/^{136}Xe$) vary over several orders of magnitude

with respect to the expected production ratios of the crystalline basement rocks and display a systematic pattern within the basin. Specifically, samples above the Salina Group are enriched in $^{4}He_{crust}$ and $^{21}Ne_{crust}$ with respect to $^{40}Ar_{crust}$ and $^{136}Xe_{crust}$, as opposed to those below the massive Salina evaporite layer, which exhibit complementary patterns. It is shown that such a general trend is well explained by a Rayleigh-type elemental fractionation model involving the upward transport of crustal noble gases and associated elemental fractionation processes, controlled by both diffusion- and solubility-related mechanisms. As previously indicated by the mantle and atmospheric noble gas signatures in Michigan Basin brines [*Castro et al.*, 2008; *Ma et al.*, 2008], the release of deep crustal noble gases into the basin is yet another independent indicator for the occurrence of a past thermal event in the basin. It is suggested here that recent reactivation of the ancient mid-continent rift (MCR) system underneath the Michigan Basin is likely responsible for the upward transport of heat and loss of the atmospheric noble gas component, as well as release of crustal and mantle noble gases into the basin via deep-seated faults and fracture zones. Such a conceptual model also supports the hypothesis of an internal heat source as being largely responsible for the existence of past high temperatures in the basin, without the involvement of large-scale brine migration from peripheral forming orogenic foldbelts.

References

Ballentine, C.J., R.K. O'Nions, E.R. Oxburgh, F. Horvath, and J. Deak (1991), Rare gas constraints on hydrocarbon accumulation, crustal degassing and groundwater flow in the Pannonian Basin, *Earth Planet. Sci. Lett.*, *105*, 229-246.

Ballentine, C.J., R.K. O'Nions, and M.L. Coleman (1996), A Magnus opus: helium, neon, and argon isotopes in a North Sea oilfield, *Geochim. Cosmochim. Acta*, *60*, 831-849.

Ballentine, C.J., and P.G. Burnard (2002), Production, release and transport of noble gases in the continental crust, *Rev. Mineral. Geochem.*, *47*, 481-538.

Battani, A., P. Sarda, and A. Prinzhofer (2000), Basin scale natural gas source, migration and trapping traced by noble gases and major elements: the Pakistan Indus Basin, *Earth Planet. Sci. Lett.*, *181*, 229-249.

Bethke, C.M., and S. Marshak (1990), Brine migrations across North America – the plate tectonics of groundwater, *Annu. Rev. Earth Planet. Sci.*, *18*, 287-315.

Bosch, A., and E. Mazor (1988), Natural gas association with water and oil as depicted by atmospheric noble gases: case studies from the southeastern Mediterranean Coastal Plain, *Earth Planet. Sci. Lett.*, *87*, 338-346.

Brennwald, M.S., R. Kipfer, and D.M. Imboden (2005), Release of gas bubbles from lake sediment traced by noble gas isotopes in the sediment pore water, *Earth Planet. Sci. Lett.*, *235*, 31-44.

Budai, J.M., and J.L. Wilson (1991), Diagenesis history of the Trenton and Black River formations in the Michigan Basin, in *Early sedimentary evolution of the Michigan Basin*, edited by P.A. Catacosinos and P.A. Jr. Daniels, GSA Special Paper, *256*, pp. 73-88.

Burkland, M.K., T.D. Swindle, and S.L. Baldwin (1995), Isothermal heating experiments on Bjurbole: implications for the release mechanisms of radiogenic ^{129}Xe, *Geochim. Cosmochim. Acta*, *59*, 2085-2094.

Castro, M.C., A. Jambon, G. de Marsily, and P. Schlosser (1998a), Noble gases as natural tracers of water circulation in the Paris Basin 1. Measurements and discussion of their origin and mechanisms of vertical transport in the basin, *Water Resour. Res.*, *34*, 2443-2466.

Castro, M.C., P. Goblet, E. Ledoux, S. Violette, and G. de Marsily (1998b), Noble gases as natural tracers of water circulation in the Paris Basin 2. Calibration of a groundwater flow model using noble gas isotope data, *Water Resour. Res.*, *34*, 2467-2483.

Castro, M.C., and P. Goblet (2003), Calibration of regional groundwater flow models:

working toward a better understanding of site-specific systems, *Water Resour. Res.*, *39*, 1172, doi:10.1029/2002WR001653.

Castro, M.C., D. Patriarche, and P. Goblet (2005), 2-D numerical simulations of groundwater flow, heat transfer and ^{4}He transport – implications for the He terrestrial budget and the mantle helium-heat imbalance, *Earth Planet. Sci. Lett.*, *237*, 893-910.

Castro, M.C., D. Patriarche, P. Goblet, L. Ma, and C.M. Hall (2007), ^{4}He/heat flux ratios as new indicators of past thermal and tectonic events – new constrains on the tectonothermal history of the Michigan Basin, the 4th Mini Conference on Noble Gases in the Hydrosphere and in Natural Gas Reservoirs, GFZ Potsdam.

Castro, M.C., L. Ma, and C.M. Hall (2008), A primordial, solar He-Ne signature in crustal fluids of a stable continental region, in review.

Catacosinos, P.A., P.A. Jr. Daniel, and W.B. III Harrison (1991), Structure, stratigraphy, and petroleum geology of the Michigan Basin, in *Interior cratonic basins,* edited by M. W. Leighton et al., AAPG Memoir, *51*, pp. 561-601.

Cercone, K.R. (1984), Thermal history of Michigan Basin, *AAPG Bulletin*, *68*, 130-136.

Cercone, K.R., and H.N. Pollack (1991), Thermal maturity of the Michigan Basin, in *Early sedimentary evolution of the Michigan Basin*, edited by P.A. Catacosinos and P.A. Jr. Daniels, GSA Special Paper, *256*, pp. 1-11.

Cercone, K.R., and K.C. Lohmann (1987), Late burial diagenesis of Niagaran (middle Silurian) pinnacle reefs in Michigan Basin, *AAPG Bulletin*, *71*, 156-166.

Coniglio, M., R. Sherlock, A.E., Williams-Jones, K. Middleton, and S.K. Frape (1994), Burial and hydrothermal diagenesis of Ordovician carbonates from the Michigan Basin, Ontario, Canada, *Spec. Publs. Int. Ass. Sediment.*, *21*, 231-254.

Copeland, P., E.B. Watson, S.C. Urizar, D. Patterson, and T.J. Lapen (2007), Alpha thermochronology of carbonates, *Geochim. Cosmochim. Acta*, *71*, 4488-4511.

Crovetto, R., R. Fernandez-Prini, and M.L. Japas (1982), Solubilities of inert gases and methane in H_2O and in D_2O in the temperature range of 300 to 600K, *J. Chem. Phys.*, *76*, 1077-1086.

Crowley, K.D. (1991), Thermal history of Michigan Basin and southern Canadian Shield from apatite fission track analysis, *Journal of Geophysical Research*, *96*, 697-711.

Davisson, M.L., and R.E. Criss (1996), Na-Ca-Cl relations in basinal fluids, *Geochim. Cosmochim. Acta*, *60*, 2743-2752.

Dodson, M.H. (1973), Closure temperature in cooling geochronological and petrological systems, *Contr. Mineral. and Petrol.*, *40*, 259-274.

Dorr, J.A. Jr., and D.F. Eschman (1970), *Geology of Michigan*, 1st ed. Univ. of Michigan Press, Ann Arbor, Michigan.

Eikenberg, J., P. Signer, and R. Wieler (1993), U-Xe, U-Kr, and U-Pb systematics for dating uranium minerals and investigations of the production of nucleogenic neon and argon, *Geochim. Cosmochim. Acta*, *57*, 1053-1069.

Fisher, J.H., M.W. Barratt , J.B. Droste, and R.H. Shaver (1988), Michigan Basin, in *Sedimentary Cover – North America Craton*, edited by L.L. Sloss, Geological Society of America, *D-2*, pp. 361-382.

Gautheron, C.E., L. Tassan-Got, and K.A. Farley (2006), (U-Th)/Ne chronometry, *Earth Planet. Sci. Lett.*, *243*, 520-535.

Girard, J.-P., and D.A. Barnes (1995), Illitization and paleothermal regimes in the middle Ordovician St. Peter sandstone, central Michigan Basin: K-Ar, oxygen isotope, and fluid inclusion data, *AAPG Bulletin*, *79*, 49-69.

Graham, D.W. (2002), Noble gas isotope geochemistry of mid-ocean ridge and ocean island basalts: characterization of mantle source reservoirs, *Rev. Mineral. Geochem.*, *47*, 247-318.

Hay, R.L., M. Lee, D.R. Kolata, J.C. Matthews, and J.P. Morton (1988), Episodic potassic diagenesis of Ordovician tuffs in the Mississippi Valley area, *Geology*, *16*, 743-747.

Hinze, W.J., R.L. Kellogg, and N.W. O'Hara (1975), Geophysical studies of basement geology of Southern Peninsula of Michigan, *AAPG Bulletin*, *59*, 1562-1584.

Hiyagon, H., and B.M. Kennedy (1992), Noble gases in CH_4-rich gas fields, Alberta, Canada, *Geochim. Cosmochim. Acta*, *56*, 1569-1589.

Honda, M., Nutman, A.P., Bennett, V.C., and Yatsevich, I. (2004), Radiogenic, nucleogenic and fissiongenic noble gas compositions in early Archaean magmatic zircons from Greenland, *Geochemical Journal*, *38*, 265-269.

Jahne, B., G. Heinz, and W. Dietrich (1987), Measurement of the diffusion coefficients of sparingly soluble gases in water, *J. Geophys. Res.*, *92*, 10767-10776.

Kulongoski, J.T., D.R. Hilton, and J.A. Izbicki (2005), Source and movement of helium in the eastern Morongo groundwater Basin: the influence of regional tectonic on crustal and mantle helium fluxes, *Geochim. Cosmochim. Acta*, *69*, 3857-3872.

Lippolt, H.J., and Weigel, E. (1988), ^{4}He diffusion in ^{40}Ar-retentive minerals, *Geochim. Cosmochim. Acta*, *52*, 1449-1458.

Liu, J., R.L. Hay, A. Deino, and T.K. Kyser (2003), Age and origin of authigenic K-feldspar in uppermost Precambrian rocks in the North American Midcontinent,

GSA Bulletin, *115*, 422-433.

Long, D.T., T.P. Wilson, M.J. Takacs, and D.H. Rezabek (1988), Stable-isotope geochemistry of saline near-surface ground water: east-central Michigan Basin, *Geo. Soc. Am. Bull.*, *100*, 1568-1577.

Luczaj, J.A. (2006), Evidence against the Dorag (mixing-zone) model for dolomitization along the Wisconsin arch – a case for hydrothermal diagenesis, *AAPG Bulletin*, *90*, 1719-1738.

Luczaj, J.A., W.B. III Harrison, and N.S. Williams (2006), Fractured hydrothermal dolomite reservoirs in the Devonian Dundee formation of the central Michigan Basin, *AAPG Bulletin*, *90*, 1787-1801.

Ma, L., M.C. Castro, and C.M. Hall (2004), A late Pleistocene-Holocene noble gas paleotemperature record in southern Michigan, *Geophysical Research Letters*, *31*, L23204, doi:10.1029/2004GL021766.

Ma, L., M.C. Castro, C.M. Hall, and L.M. Walter (2005), Cross-formational flow and salinity sources inferred from a combined study of helium concentrations, isotopic ratios, and major elements in the Marshall aquifer, southern Michigan, *Geochem. Geophys. Geosyst.*, *6*, Q10004, doi:10.1029/2005GC001010.

Ma, L., M.C. Castro, and C.M. Hall (2008), Atmospheric noble gas signatures in deep Michigan Basin brines as indicators of a past thermal event, *Earth Planet. Sci. Lett.*, in press.

Martini, A.M. (1997), Hydrogeochemistry of saline fluids and associated water and gas, Ph.D. dissertation, Univ. of Michigan, Ann Arbor.

McIntosh, J.C., L.M. Walter, and A.M. Martini (2004), Extensive microbial modification of formation water geochemistry: Case study from a mid-continent sedimentary basin, United States, *Geo. Soc. Am. Bull.*, *116*, 743-759.

Menuge, J.F., T.S. Brewer, and C.M. Seeger (2002), Petrogenesis of metaluminous A-type rhyolites from the St Francois Mountains, Missouri and the Mesoproterozoic evolution of the southern Laurentian margin, *Precambrian Research*, *113*, 269-291.

O'Nions, R.K., and C.J. Ballentine (1993), Rare gas studies of basin scale fluid movement, *Phil. Trans. R. Soc. Lond. A*, *344*, 141-156.

Ohsumi, T., and Y. Horibe (1984), Diffusivity of He and Ar in deep-sea sediments, *Earth Planet. Sci. Lett.*, *70*, 61-68

Oliver, J.E. (1986), Fluids expelled tectonically from orogenic belts: their role in hydrocarbon migration and other geologic phenomena, *Geology*, *14*, 99-102.

Oxburgh, E.R., R.K. O'Nions, and R.I. Hill (1986), Helium isotopes in sedimentary basins, *Nature*, *324*, 632-635.

Ozima, M., and F.A. Podosek (2002), *Noble gas geochemistry*, 2nd ed., 286 pp., Cambridge University Press, New York.

Parker, R.L. (1967), Composition of Earth's crust, Data of Geochemistry, *U. S. Geol. Surv. Prof. Pap.*, *440-D*, pp. 1-19.

Patriarche, D., M.C. Castro, and P. Goblet (2004), Large-scale hydraulic conductivities inferred from three-dimensional groundwater flow and ^{4}He transport modeling in the Carrizo aquifer, Texas, *J. Geophys. Res.*, *109*, B11202, doi: 10.1029/2004JB003173.

Pinti, D.L., and B. Marty (1995), Noble gases in crude oils from the Paris Basin, France: implications for the origin of fluids and constraints on oil-water-gas interactions, *Geochim. Cosmochim. Acta*, *59*, 3389-3404.

Rudnick, R.L., and D.M. Fountain (1995), Nature and compostion of the continental crust: a lower crustal perspective, *Reviews of Geophysics*, 33, 267-309.

Saar, M.O., M.C. Castro, C.M. Hall, M. Manga, and T.P. Rose (2005), Quantifying magmatic, crustal, and atmospheric helium contributions to volcanic aquifers using all stable noble gases: implications for magmatism and groundwater flow, *Geochemistry Geophysics Geosystems*, *6*, Q03008, doi:10.1029/2004GC000828.

Sanford, B.V., F. J. Thompson, and G. H. McFall (1985), Plate tectonics – a possible controlling mechanism in the development of hydrocarbon traps in southwestern Ontario, *Bulletin of Canadian Petroleum Geology*, *33*, 52-71.

Shaw, D.M. (1967), U, Th and K in the Canadian Precambrian shield and possible mantle compositions, *Geochim. Cosmochim. Acta*, *31*, 1111-1113.

Smith, S.P. (1985), Noble gas solubility in water at high temperatures, *Eos Trans. AGU*, *66*, 397.

Smith, S.P., and B.M., Kennedy (1983), The solubility of noble gases in water and in NaCl brine, *Geochim. Cosmochim. Acta*, *47*, 503-515.

Torgersen, T., and W.B. Clarke (1985), Helium accumulation in groundwater; I. an evaluation of sources and the continental flux of crustal ^{4}He in the Great Artesian Basin, Australia, *Geochim. Cosmochim. Acta*, *49*, 2445-2452.

Torgersen, T., B.M. Kennedy, H. Hiyagon, K. Y. Chiou, J.H. Reynolds, and W.B. Clarke (1989), Argon accumulation and the crustal degassing flux of ^{40}Ar in the Great Artesian Basin, Australia, *Earth Planet. Sci. Lett.*, *92*, 43-56.

Van Schmus, W.R. (1992), Tectonic setting of the Midcontinent Rift system,

Tectonophysics, *213*, 1-15.

Vugrinovich, R. (1986), *Patterns of regional subsurface fluid movement in the Michigan Basin*, Open File Rep. 86-6, Geol. Surv. Div. Mich. Dep. of Nat. Resour., Lansing.

Vugrinovich, R. (1988), Shale compaction in the Michigan Basin: estimates of former depth of burial and implications for paleogeothermal gradients, *Bulletin of Canadian Petroleum Geology*, *36*, 1-8.

Vugrinovich, R. (1989), Subsurface temperatures and surface heat flow in the Michigan Basin and their relationships to regional subsurface fluid movement, *Marine and Petroleum Geology*, *6*, 60-70.

Weiss, R.F. (1968), Piggyback sampler for dissolved gas studies on sealed water samples, *Deep Sea Res. Oceanogr. Abstr.*, *15*, 695-699.

Wetherill, G.W. (1953), Spontaneous fission yields from uranium and thorium, *Physical Review*, *92*, 907-912.

Wetherill, G.W. (1954), Variations in the isotopic abundances of neon and argon extracted from radioactive minerals, *Physical Review*, *96*, 679-683.

Wilson, T.P., and D.T. Long, (1993a), Geochemistry and isotope chemistry of Michigan Basin brines: Devonian formations, *Applied Geochemistry*, *8*, 81-100.

Wilson, T.P., and D.T. Long (1993b), Geochemistry and isotope chemistry of Ca-Na-Cl brines in Silurian strata, Michigan Basin, *Applied Geochemistry*, *8*, 507-524.

Wise, D.L., and G. Houghton (1966), The diffusion coefficients of ten slightly soluble gases in water at 10-60°C, *Chem. Eng. Sci.*, *21*, 999-1010.

Wise, D.L., and G. Houghton (1968), Diffusion coefficients of neon, krypton, xenon, carbon monoxide and nitric oxide in water at 10-60°C, *Chem. Eng. Sci.*, *23*, 1211-1216.

Yoo, C.M., J.M. Gregg, and K.L. Shelton (2000), Dolomitization and dolomite neomorphism: Trenton and Black River limestones (middle Ordovician) northern Indiana, U.S.A., *Journal of Sedimentary Research*, *70*, 265-274.

Zaikowski, A., B.J. Kosanke, and N. Hubbard (1987), Noble gas composition of deep brines from the Palo Duro Basin, Texas, *Geochim. Cosmochim. Acta*, *51*, 73-84.

Zartman, R.E., G.J. Wasserburg, and J.H. Reynolds (1961), Helium, argon, and carbon in some natural gases, *J. Geophys. Res.*, *66*, 277-306.

CHAPTER 7

CONCLUSIONS

This dissertation has focused on the noble gases dissolved in groundwater from the Michigan Basin, combined with a diversity of other natural tracers including stable isotopes (δD, $\delta^{18}O$, and $\delta^{13}C$), radiocarbon (^{14}C), major elements and heat flow. This dissertation investigates 14 freshwater samples from a shallow groundwater aquifer and 38 brine samples from eight deep aquifers. The study of noble gases in the Michigan Basin has provided a powerful tool to reconstruct paleoclimatic records in the late Pleistocene and Holocene, to trace the origin and evolution of deep brines, to investigate the tectonic and thermal history of this stable region, as well as to place constraints on the mantle structure and convection models. This dissertation has important implications for the fields of paleoclimatology, hydrogeology, tectonics, and mantle geochemistry. The major topics in this dissertation are summarized in the schematic cross sections of the Michigan Basin (Fig. 7.1).

In Chapter 2, noble gas temperatures (NGTs) and ^{14}C derived ages in groundwater of the shallow Marshall aquifer revealed a ground temperature of ~1ºC toward the end of the Last Glacial Maximum (LGM), suggesting that groundwater recharge occurred under

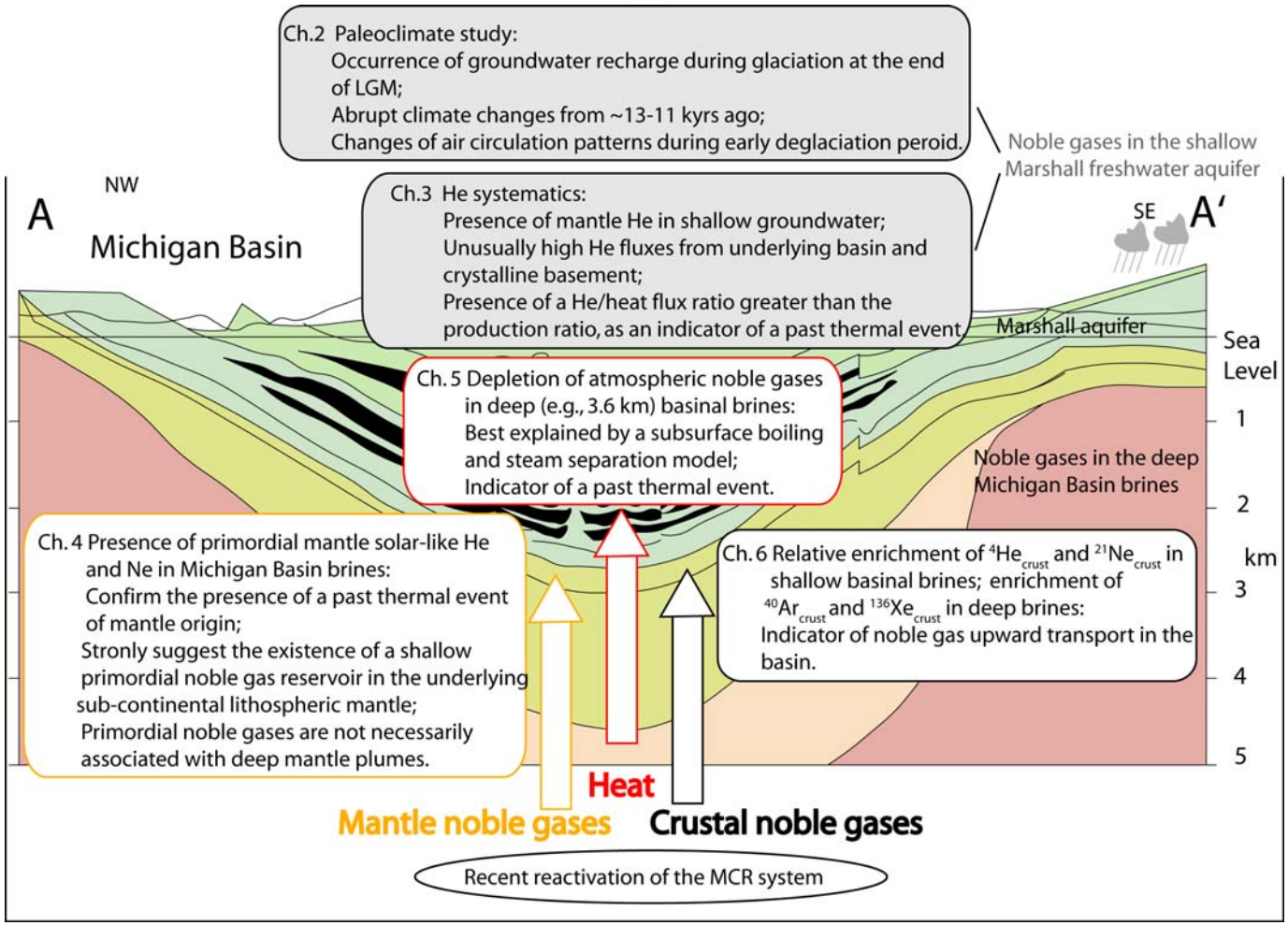

Figure 7.1. Schematic cross section of the Michigan Basin showing the main topics of this dissertation. Dissolved noble gases in a shallow freshwater aquifer (the Marshall aquifer) are discussed in Chapters 2 and 3. Arrows indicate the release of heat, mantle and crustal noble gases into the Michigan Basin due to recent reactivation of the MCR underneath the Michigan Basin. Noble gas signatures in the Michigan Basin brines from eight deep aquifers are discussed in Chapters 4, 5, and 6.

the Laurentide Ice Sheet (LIS) cover. In addition to the general warming observed since the LGM, the NGT record indicates an abrupt warming event between ~12.8 and 11.1kyrs BP, correlative to the Bølling-Allerød (BOA) warm phases. Ice-sheet-linked changes in freshwater delivery to the North Atlantic, together with changes in the North Atlantic Deep Water (NADW) circulation are possible a cause of such abrupt climate shifts in the northeastern US. Pleistocene waters yielding the lowest NGTs have the highest $\delta^{18}O$ and δD values, suggesting an atmospheric circulation pattern distinct from today, with a stronger moisture component from the Gulf of Mexico, possibly due to the presence of the LIS which weakened the Pacific westerly flow. NGT records from mid-high latitude areas thus hold great promise not only to ascertain whether or not groundwater recharge occurs under ice-covered regions, but also to identify major global climatic oscillations and changes in atmospheric circulation patterns.

Chapter 3 presents the accompanying helium data and major ion chemistry for the shallow Marshall aquifer. This data set is subsequently analyzed in conjunction with major element data sets from deeper and shallower water levels previously collected in this area. He excesses in old groundwater samples are mostly of crustal origin although the presence of a significant mantle He component in some samples cannot be ruled out. He excesses in the Marshall aquifer are unusually high for such shallow depths (≤300m), and reach over two and three orders of magnitude above those of air-saturated water (ASW) for ^{3}He and ^{4}He, respectively. These He excesses require a He source external to the aquifer, partly supplied by underlying formations within the sedimentary sequence, partly from the crystalline basement. To account for the He concentrations observed in the Marshall aquifer, He fluxes of 1×10^{-13} and 1.6×10^{-6} cm^3 STP $cm^{-2}yr^{-1}$ for ^{3}He and

^{4}He are require, respectively. The latter are far greater than the He fluxes reported in other sedimentary basins around the world (e.g., Paris Basin, Gulf Coast Basin) at similar and far greater depths. Such high He fluxes at such shallow depths within the Michigan Basin strongly suggest the presence of a dominant vertical water flow component, and further indicate that the impact of recharge water at depth is minor. An upward cross-formational flow is also likely responsible for the extremely high salinities present in the shallow sub-surface of the Michigan Basin. The occurrence of large-scale cross-formational flow is also consistent with the evolution displayed by the major ion chemistry throughout most of the sedimentary sequence, indicating that solutes from shallow levels carry the signature of deep formation brines. Of particular relevance, is the contrast observed between the high helium and low heat fluxes in the shallow Marshall aquifer, leading to helium/heat flux ratios greater than that of the radiogenic production ratio. Such high helium/heat flux ratios strongly suggest the occurrence of a major past thermal event in the basin.

To confirm the presence of such a thermal event and to clarify its origin, the second part of the dissertation (Chapters 4, 5, and 6) focused on the study of 38 deep brines from eight different formations beneath the Marshall aquifer of the Michigan Basin. More specifically, He and Ne data from these deep brines clearly reveal a primordial solar-like component in this stable continental region, where the presence of mantle plumes is highly unlikely (Chapter 4). This finding not only suggests that a deep primordial mantle reservoir is not required to explain the presence of such components, it also points to a very heterogeneous mantle as previously suggested. Consequently, the presence of a primordial noble gas signature does not necessarily indicate the existence of

a deep mantle plume. The SCLM underneath ancient cratons is a great candidate for hosting primitive ancient mantle reservoirs. This study provides a strong observational case for long-term primordial lithospheric storage of noble gases. It also provides new insights into the current debate of mantle structure and convection models.

Chapter 5 presents the atmospheric noble gases (e.g., ^{22}Ne, ^{36}Ar, ^{84}Kr, ^{130}Xe) of these deep brines. The atmospheric noble gas component shows a strong depletion pattern with respect to air saturated water. The depletion of lighter gases (^{22}Ne and ^{36}Ar) is stronger compared to the heavier ones (^{84}Kr and ^{130}Xe). To understand the mechanisms responsible for this overall atmospheric noble gas depletion, phase interaction models were tested. It is shown that this atmospheric noble gas depletion pattern is best explained by a model involving subsurface boiling and steam separation, and thus, is consistent with the occurrence of a past thermal event of mantle origin as previously indicated by both high ^{4}He/heat flux ratios and the presence of primordial mantle He and Ne signatures in the basin. Such a conceptual model is also consistent with the presence of past elevated temperatures in the Michigan Basin (e.g., ~80-260°C) at shallow depths as suggested by previous thermal studies in the basin. A relative enrichment of atmospheric Kr and Xe with respect to Ar is also observed, and is interpreted as reflecting the addition of sedimentary Kr and Xe from associated hydrocarbons following the hydrothermal event. This study pioneers the use of atmospheric noble gases in subsurface fluids to trace the thermal history of stable tectonic regions.

Chapter 6 discusses the accompanying crustal noble gases for the deep brine samples. These brine samples clearly show the presence of an important crustal component of ^{4}He, ^{21}Ne, ^{40}Ar, and ^{136}Xe. Both $^{40}Ar_{crust}$ and $^{136}Xe_{crust}$ display the presence

of a strong vertical gradient along the sedimentary strata of the basin. The in-situ production for these two gases within the sedimentary strata is insufficient to account for the observed crustal component in the Michigan brines. These observations point to the presence of a deep, external source for crustal noble gases, likely the Precambrian crystalline basement beneath the Michigan Basin. Furthermore, observed elemental ratios of crustal noble gases ($^{4}He/^{40}Ar$, $^{21}Ne/^{40}Ar$, $^{4}He/^{136}Xe$, and $^{21}Ne/^{136}Xe$) in these brines vary over several orders of magnitude with respect to the expected production ratios from the crystalline basement rocks and display a systematic pattern within the basin. It is shown that such a general trend is well explained by a Rayleigh-type elemental fractionation model involving upward transport of crustal noble gases and associated elemental fractionation processes, controlled by both diffusion- and solubility-related mechanisms. As previously indicated by the mantle (Chapter 4) and atmospheric noble gas signatures (Chapter 5) in these same Michigan Basin brine samples, the hypothesized release of deep crustal noble gases into the basin is yet another independent indicator pointing to the occurrence of a past thermal event in the basin. Such a model also supports the hypothesis of an internal heat source as being largely responsible for the existence of past high temperatures in the basin without the involvement of large-scale brine migration from peripheral forming orogenic foldbelts.

Most importantly, the findings from the mantle (Chapter 4), atmospheric (Chapter 5) and crustal (Chapter 6) noble gas components in these deep basin brines are remarkably consistent, all pointing to the presence of a past mantle thermal event in the basin, which is most likely related to the recent reactivation of the Mid Continent Rift (MCR) system underneath the Michigan Basin (Fig. 7.1). Noble gases in deep Michigan

basin brines thus provide new insights into the origin and evolution of deep brines, the thermal and tectonic history of this currently stable basin, as well as into the nature of the underlying lithospheric mantle.

This dissertation represents the first comprehensive application of noble gases as natural tracers in the groundwaters of the Michigan Basin.

APPENDIX

EXPERIMENTAL TECHNIQUES

Sample handling procedure

All water samples for noble gas analyses are collected in annealed, internally polished copper tubes (i.e. standard refrigeration grade 3/8" Cu tubing) that are sealed by stainless steel pinch-off clamps at well head pressures (Fig. A-1). The tubing is ~1cm in diameter and sample volumes are typically ~14ml of water. Samples are collected directly from the well heads after water is allowed to flow through for ~10 minutes to avoid atmospheric contamination and to ensure that temperature has reached equilibrium. The copper sample channels are mounted onto a noble gas extraction system in the Noble Gas Laboratory at the University of Michigan, which is designed to release water from clamped Cu tubes into a vacuum system and quantitatively extract the noble gases from the water in preparation for inletting into an MAP215 mass spectrometer.

Noble gas extraction and purification line

The extraction line consists of 4 zones (Fig. A-2): zone 1 consists of an attachment point for the Cu sample tube and a low-diffusion glass flask; zone 2 is connected to zone 1 via a 4 cm length of standard 1/16" stainless steel tubing and the zone has a stainless steel liquid nitrogen (LN_2) cold trap; zone 3 is connected to zone 2 through a 1 mm orifice and contains a canister of 3Å molecular sieve and a CuO/Ti

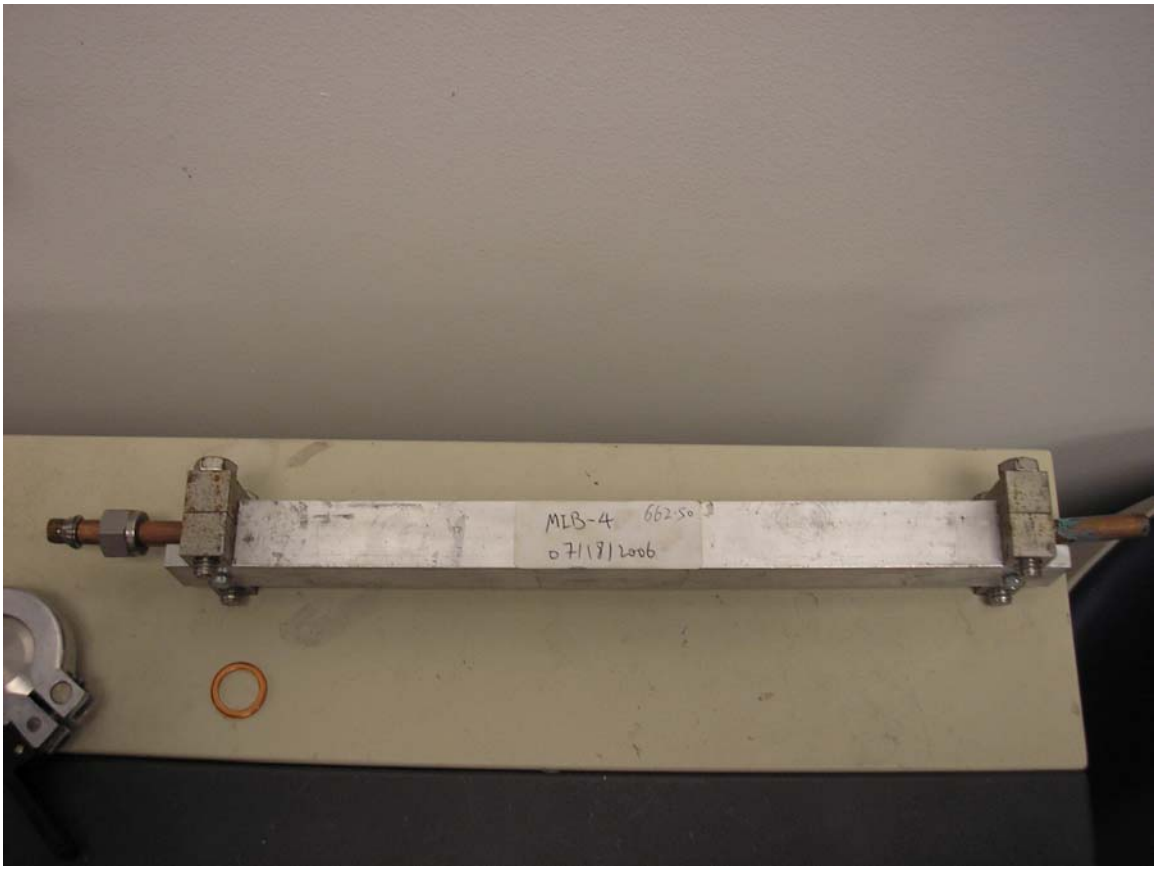

Fig. A-1: Noble gas sample tubes (standard refrigeration grade 3/8” Cu tubing) with stainless steel pinch-off clamps at either end.

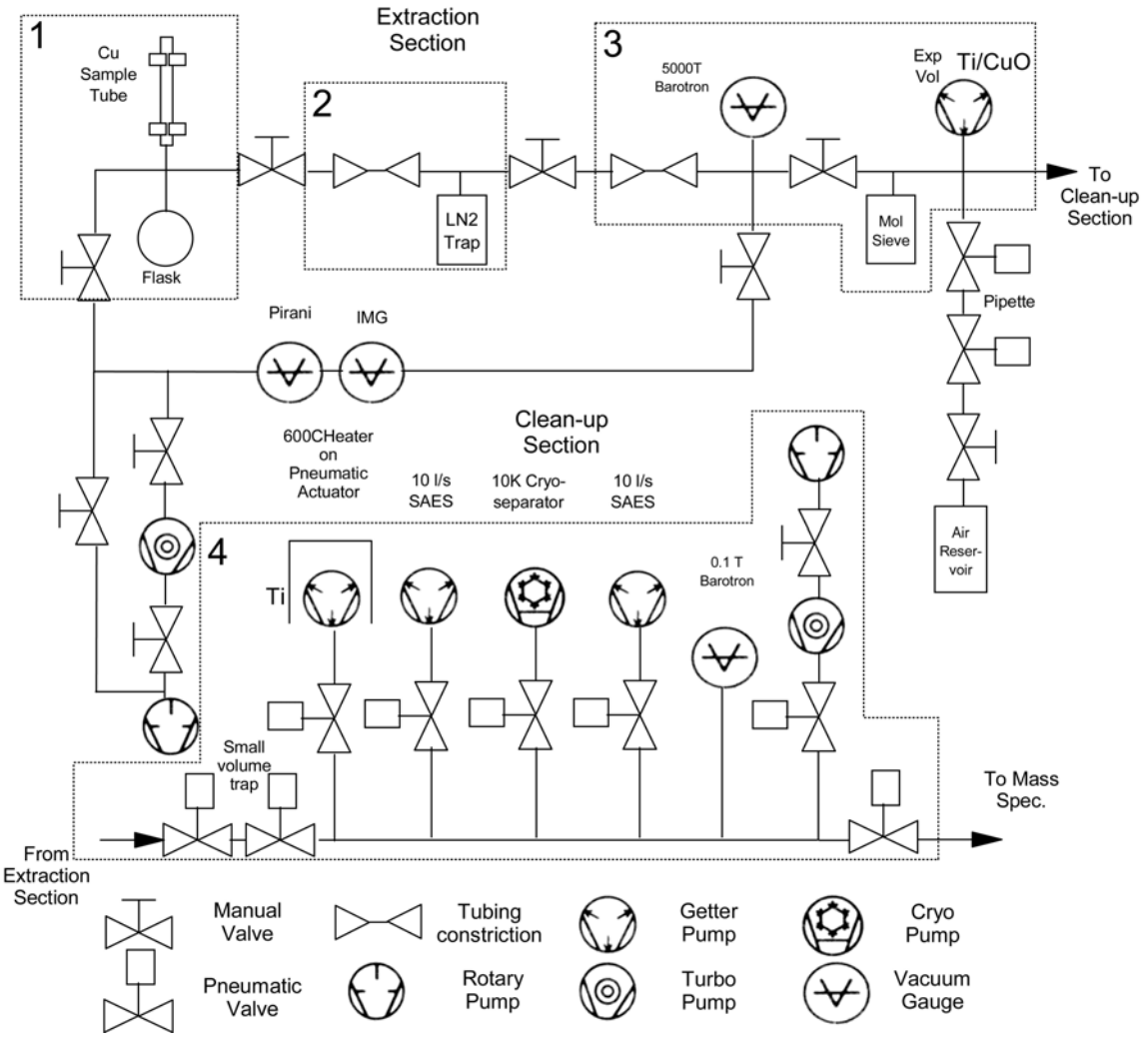

Fig. A-2: Schematic diagram of the noble gas extraction system. Areas surrounded by dashed lines are the four zones of the system described in the text.

sponge getter which also acts as a expansion volume; zone 4 is the main clean-up part of the system and has connections to a Ti sponge getter and an Air Products model CS202W cryo-separator whose temperature is controlled by a Scientific Instruments model 9700 controller. Temperature regulation for the cryo-separator at any point is at least within 0.05K and usually within 0.01K of the set point. Zones 1 through 3 share a common turbo pump vacuum system and are connected to each other with manually actuated Nupro 4BG bellows valves. An air pipette system is connected to zone 3. The air pipette and all of the valves in zone 4 use pneumatically actuated Nupro 4BG valves under computer control.

Noble gas measurement procedure

The noble gas measurement procedure comprises the analysis of an air standard, followed by a procedural blank, prior to the analysis of the water sample itself. The sample consists of a single 14ml water sample that is used to estimate the noble gas concentrations of He, Ne, Ar, Kr and Xe, as well as the isotope ratios of these elements, including the $^{3}He/^{4}He$ ratio. The noble gas concentrations are estimated by comparing the mass spectrometer signal strength for the sample with a standard air sample that can be introduced into zone 3 (Fig. A-2). The air pipette reservoir was loaded with outside air into a known volume. The air was subsequently dried with 3Å molecular sieve zeolite and its pressure was measured using a capacitive manometer. The depletion of the air reservoir is automatically monitored by the computer control software.

The measurement sequence starts with a complete set of isotope measurements of an air pipette aliquot that is introduced directly into zone 3. Approximately 2% of the

0.1882 ml air sample is trapped in a small volume between 2 valves connecting zones 3 and 4 (Fig. A-2). This volume is introduced into zone 4 and the remainder of the gas in zone 3 is pumped out. The air sample is gettered using Ti sponge at 600°C to remove active gases (e.g., N_2, CO_2, O_2) and a small portion of the cleaned noble gas is retained in the small volume between zones 3 and 4 for later measurement of the Ar isotopes. The majority of the sample is then pumped into the cryo-separator, which has been pre-cooled to a minimum T (below about 10K). At this T, all noble gases are trapped. And the cryo-separator is warmed up to an indicated T of 30K, at which only He is released (Fig. A-3). The He is then introduced into the mass spectrometer and its signal strength at mass 4 is determined. This He measurement is used strictly for the He volume estimate, as there is insufficient He at this stage for a measurement of ^{3}He.

The cryo-separator is then warmed to an indicated T of 60K and Ne is released into the mass spectrometer (Fig. A-3). Interference from doubly charged ^{40}Ar and CO_2 and singly charged H_2O is monitored by measurements at masses 40, 44, 18 as well as the Ne isotopes at masses 20, 21 and 22. During the Ne measurements, a liquid N_2 cold trap is placed in the mass spectrometry inlet to reduce the interference from Ar, CO_2 and H_2O. The correction factor for $^{40}Ar^{++}/^{40}Ar^{+}$ is 0.247, previously measured by cryo-separated Ar without the presence of Ne. The correction factor for $^{44}CO_2^{++}/^{44}CO_2^{+}$ is 0.007, measured with the presence of CO_2 in the mass spectrometer. The correction factor for $H_2{}^{18}O^{+}/H_2{}^{16}O^{+}$ is 0.002, the ^{18}O fraction in the oxygen isotopes. Correction for interferences at mass 20 (from $^{40}Ar^{++}$ and $H_2{}^{18}O^{+}$) ranges from 0.13%-4.38% of the total mass 20 signal for all water samples, typically averaging at 1.07%. Correction for interference at mass 22 (from $^{44}CO_2^{++}$) ranges from 0.01%-1.56% for all samples,

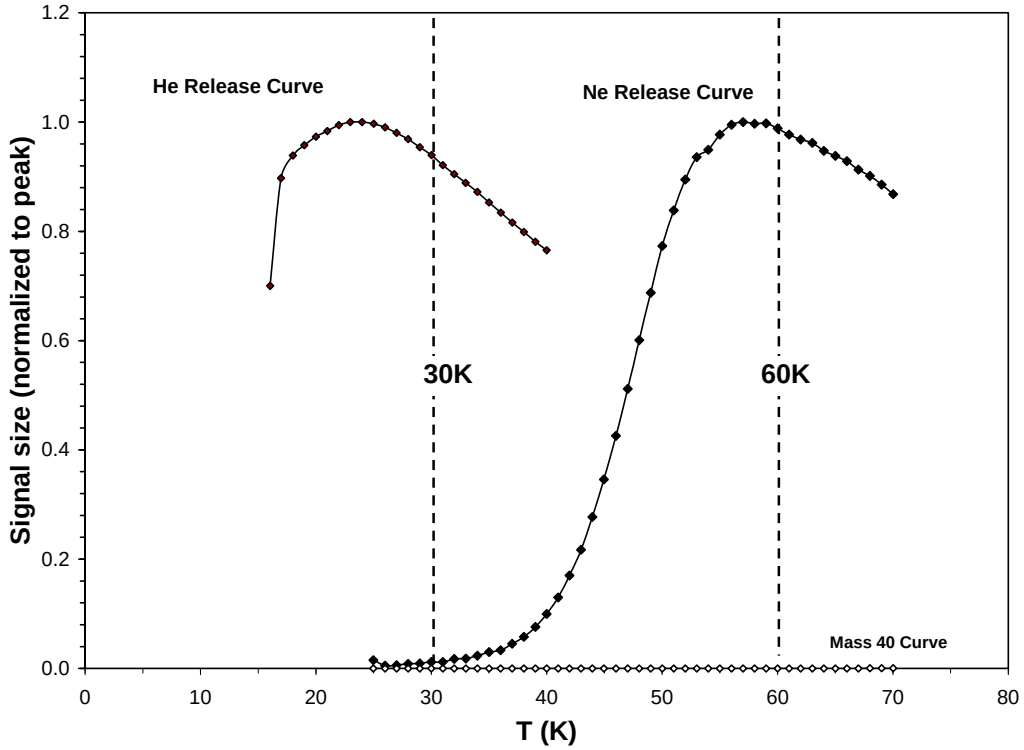

Fig. A-3: He and Ne release curve on the cryo-separator. Signal sizes are normalized to the peak during the measurement. He release temperature (30K) and Ne release temperature (60K) are indicated.

typically averaging at 0.17%. These corrections are small and very similar to other studies about mantle Ne isotopic ratios in rocks and crustal fluids [see, e.g., *Sarda et al.*, 1988, EPSL, 91, 73-88; *Honda et al.*, 1993, GCA, 57, 859-874].

The cryo-separator is also warmed further to 180K (Fig. A-4). The Ar measurement is made on the small amount of gas that is trapped between zones 3 and 4 (Fig. A-2). This gas is expanded into the zone 4 manifold, and only about 4% of this gas is inlet into the mass spectrometer. During the Ar measurements, the bulk of the original sample's Ar is pumped out of the cryo-separator at 180K. After the Ar is purged from the system, zone 4 is again isolated from its turbo-pump and allowed to warm to 215K, releasing the pipette sample's Kr (Fig. A-5). Xe is released in the T range of 215 to 270K, and the whole system is pumped out for 10 minutes with the cryo-separator held at 280K (Fig. A-5). Once cleaned out, the system is cooled again to below 10K in preparation for analyzing the procedure blank and water sample. ^{4}He, ^{20}Ne and ^{40}Ar isotopes are measured using a Faraday detector and ^{21}Ne, ^{22}Ne, ^{36}Ar, ^{38}Ar, as well as all Kr and Xe isotopes are measured using an electron multiplier in ion counting mode, except for the groundwater water study in the Marshall aquifer, where all Ne and Ar isotopes were measured using the Faraday detector.

The procedure blank is measured exactly in the same way as the water sample and air standard is measured. Typical procedural blanks for ^{4}He, ^{22}Ne, ^{36}Ar, ^{84}Kr, and ^{130}Xe are 1.8×10^{-8} cm^{3}STP, 2.8×10^{-10} cm^{3}STP, 2.5×10^{-9} cm^{3}STP, 2.3×10^{-11} cm^{3}STP, and 1.0×10^{-12} cm^{3}STP respectively.

While the procedure blank is being analyzed, the water sample is prepared in zones 1 through 3. Once the Cu tube is attached to zone 1, that zone is pumped down to

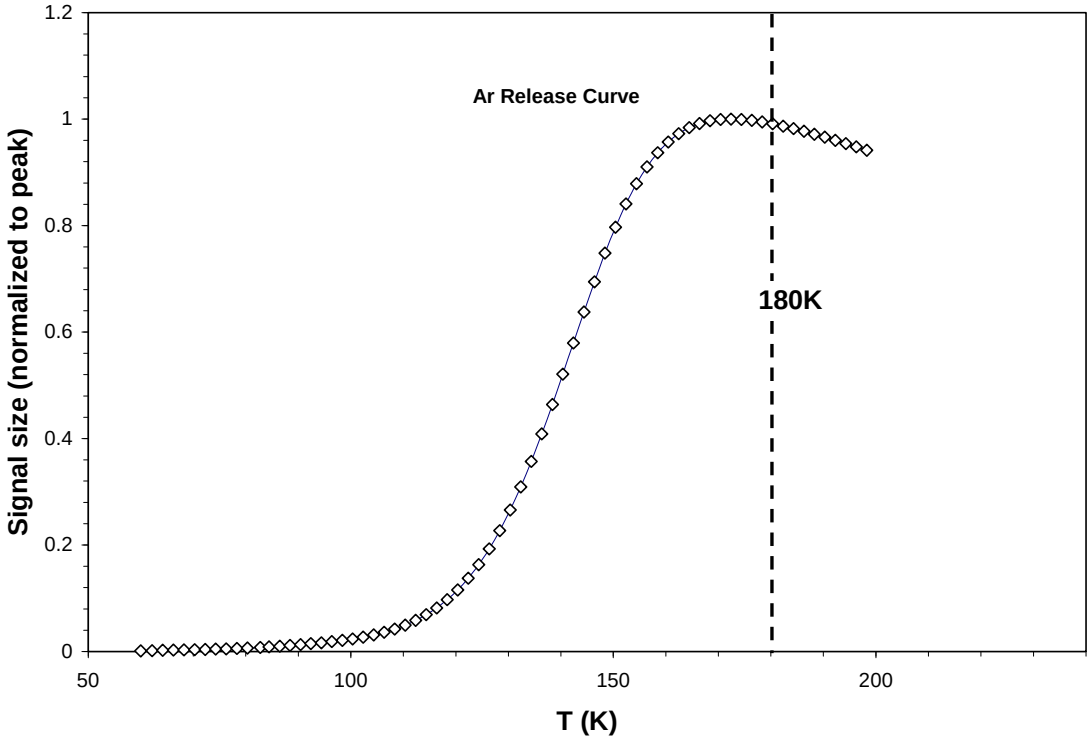

Fig. A-4: Ar release curve on the cryo-separator. Signal sizes are normalized to the peak during the measurement. Ar release temperature (180K) is indicated.

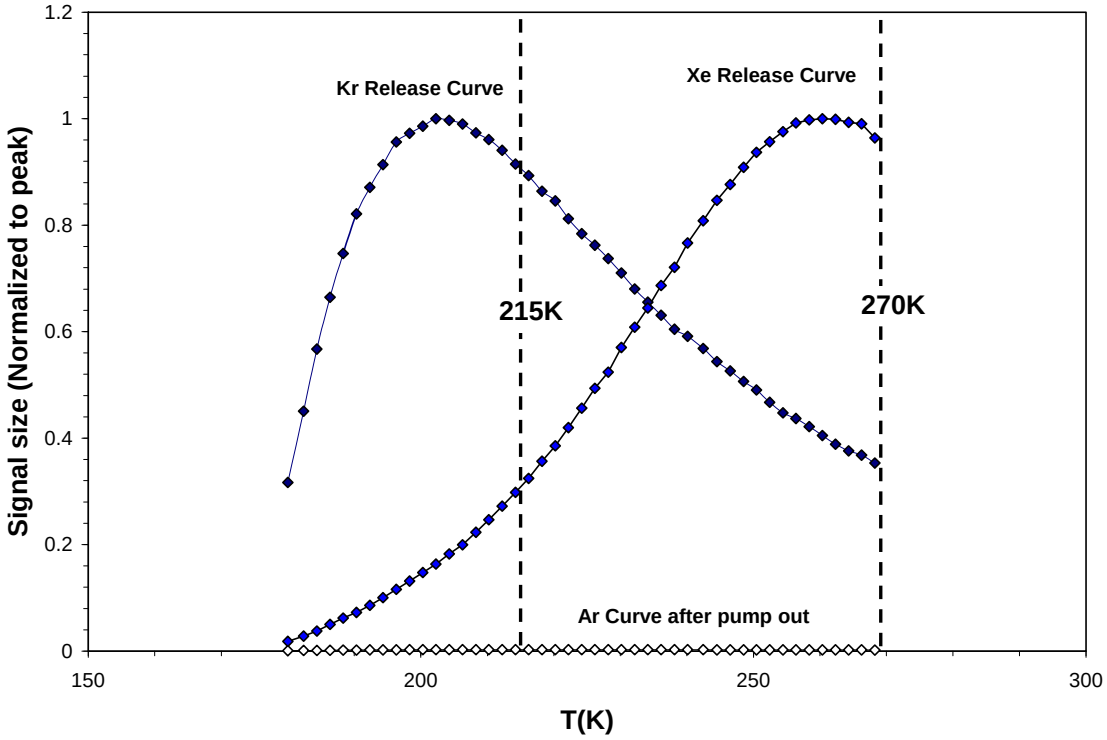

Fig. A-5: Kr and Xe release curve on the cryo-separator. Signal sizes are normalized to the peak during the measurement. Kr release temperature (215K) and Xe release temperature (270K) are indicated.

at least $1x10^{-3}$ Torr. Once this pressure is achieved, the lower clamp is released and the water sample is allowed to flow into the glass flask. The Cu tube is heated to make sure that all of the water is released from the tube. The water is stirred for 30 minutes and then the valve between zones 1 and 2 is opened, with liquid N_2 on the cold trap in zone 2. Noble gases and water vapor is pumped into the cold trap for 30 minutes. The capillary tube is equipped with a heater to avoid the possibility of gas transfer being blocked due to condensation of water in the capillary. After this transfer, the valve is closed and the cold trap is warmed to room T. Transfer of the noble gases to zone 3 is achieved by opening the valve between zones 2 and 3 for 5 seconds. This is sufficient time to evacuate all of the gas present in zone 2 to be pumped through the 1 mm orifice. This transfer procedure is repeated 4 more times to ensure that all noble gases are pumped by water vapor into zone 3. For the analysis of brine samples, the CuO/Ti sponge getter is heated up to 600°C by a torch to remove CH_4 and heavier hydrocarbons and is cooled down to room temperature. At this point, the water sample's noble gases are in the same volume and at the same T as the original air pipette sample. Once the procedure blank's mass spectrometer analyses are finished, and the cryo-separator has cooled again to below 10K, the same procedure is repeated for 2% of the water sample's noble gases.

Before the mass spectrometer runs can be started, the noble gas pressure in zone 4 is kept to within about 60% of that produced by the air pipette sample (about $4x10^{-3}$Torr). This pressure is monitored using a 0.1Torr full-scale capacitive manometer, and if necessary, about 46% of the gas is trapped in part of the system and the remainder pumped out. This is repeated as many times as necessary to reduce the pressure enough so that the sample's pressure is similar to that of the air pipette run. The ^{4}He, ^{22}Ne, ^{36}Ar,

^{84}Kr and ^{130}Xe volumes are estimated using the ratio of sample to pipette after blank correction at masses 4, 22, 36, 84 and 130, modified by whatever pressure reduction factor needed to get the sample near the same total pressure as the air pipette run. The isotopic ratios for all noble gases (except for $^{3}He/^{4}He$) are also determined using the ratio of sample to pipette after blank correction.

Only about 2% of the noble gas sample is introduced for the gas concentration measurement. The remaining 98% is retained in zone 3 for measurement of the $^{3}He/^{4}He$ ratio. The cryo-separator is cooled once again, this time to minimum T (below about 10K) at which point He is pumped. From the He concentration information in the first He measurement, an inlet strategy is determined to allow for a ^{4}He signal between about 1 and 3V on the Faraday detector. The ^{3}He and HD peaks are measured using the electron multiplier and the ^{4}He peak is measured using the Faraday detector. After the sample is inlet, zones 3 and 4 are pumped out, and readied for an air $^{3}He/^{4}He$ measurement on an air pipette sample. The R/R_a value is determined by the ratio of the apparent $^{3}He/^{4}He$ values for the sample and the air run.

During the sample mass spectrometer runs, the liquid water in zone 2 is returned to zone 1 by freezing the water back through the capillary into the glass flask. Once the flask is back at room T, the flask is removed from the system and the water is weighed. This mass value is used to estimate the noble gas concentrations.

Mass spectrometer characteristics

Noble gases are analyzed by using a MAP-215 mass spectrometer. Its resolving power is ~600, allowing separation of $^{3}He^{+}$ from HD^{+}. The mass spectrometer is

equipped with both a Faraday detector and an electron multiplier. The Faraday detector has a preamplifier with a $10^{11}\Omega$ resistor and the electron multiplier operates in ion counting mode. An adjustable width collector slit has been installed in front of the electron multiplier, which also aids the separation of the ^{3}He from the HD molecule. The ion source is a Nier type source operated typically at 500 mA electron trap current. The total internal volume of the MAP215 is ~1500cm^3 and ultra high vacuum is maintained with an ion pump. The magnetic field, switching between collectors and data acquisition is under computer control.

For the initial pipette analysis procedure described above, the typical signal sizes at masses 4, 20, and 40 are 0.08, 0.43, and 3.1 V on the Faraday detector. Kr and Xe are measured on the electron multiplier and their signal sizes have been scaled to the equivalent Faraday detector values (0.01 and 0.003 V for masses 84 and 132 respectively). When the $^{3}He/^{4}He$ ratio is measured, there is a signal of ~4.4 V on the Faraday detector at mass 4 and a signal of ~180 ions/s on the electron multiplier. The typical sensitivity for ^{4}He, ^{20}Ne, and ^{40}Ar on Faraday detector is ~8×10^{-5}, 1×10^{-4}, and 8×10^{-4} A/Torr, respectively. The sensitivity for ^{84}Kr and ^{132}Xe on the electron multiplier is ~ 1.6×10^{5} and 2.4×10^{4} atoms/cps, respectively, where cps is the ion counts per second.